Design and Testing of Prestressed Concrete Railway Deck Slabs

Nigel Peters

A Thesis

In

The Department of

Building, Civil and Environmental Engineering

Presented in Partial Fulfilment of the Requirements

for the Degree of Doctor of Philosophy at

Concordia University

Montreal, Quebec, Canada

September, 2004

Your file Votre référence
ISBN: 0-612-96954-1
Our file Notre référence
ISBN: 0-612-96954-1

ABSTRACT

Design and Testing of Prestressed Concrete Railway Deck Slabs

Nigel Peters
Concordia University 2004

Prestressed deck slabs fabricated from conventional strength concrete are frequently used in Railway bridge applications. The purpose of this research program was to assess the behaviour of precast, prestressed concrete railway deck slabs fabricated from high performance concrete (HPC). Six full scale slab specimens 3.7 m by 2.135 m, manufactured from concrete containing silica fume with compressive strengths of 80, 90 and 99 MPa , were tested to ultimate capacity.

A literature review was conducted on the mechanical properties and durability of high strength-high performance concrete. In addition, a laboratory test program was designed to determine the behaviour of the prestressed concrete slabs in flexural cracking, ultimate capacity, shear, ductility and bond development length of the strand.

The slabs were simply supported and a statically loaded at midspan, 3/8 span and ¼ span. Measurements of strain, deflection and applied loads were obtained.

The laboratory testing indicated that the concrete exhibited average positive cracking moments of about 92% of the theoretical cracking moment. The ultimate moment capacity was on average 98% of the theoretical ultimate value. The testing also indicated

that the slabs exhibited adequate post cracking ductility as evidenced by the average ultimate capacity of 2.5 times the cracking

The slabs very nearly reached their predicted full flexural strengths. This was in part due to the internal tied arch behaviour of the slabs. While inclined splitting was seen to occur, shear was not the mode of failure, but crushing of concrete in the compressive zone.

The tests also indicated that high strength-high performance concrete has bond development strengths nearly 30 % greater than that required by various codes (i.e. the length required to develop the strand is shorter than code length).

An economic analysis indicates that CN could realize savings of $752,000 Canadian annually primarily due to costs associated with train delays. This is based on current bridge lengths being re-decked.

As this is a joint Concordia University–CN research undertaking and the first time high strength-high performance concrete railway deck slabs have been tested, the results should not only be of interest to CN but to the railway industry in general.

The experimental slab design was for a 3.7 m wide slab. For other width slabs the test conclusion for negative moment and shear need to be adjusted by the reader accordingly.

ACKNOWLEDGEMENTS

The author wishes to express his sincere appreciation and gratitude to the following individuals and organizations whose contribution helped in the successful completion of this research work:

- Dr. Zenon A. Zielinski, Distinguished Professor Emeritus, Department of Building, Civil and Environmental Engineering, Concordia University for directing this research, for his friendship, patient tutelage, invaluable advice and constant encouragement throughout this research program. In particular, I wish to thank Dr. Zielinski for freely giving of his time in the guidance of this work.
- Dr. Robert Sweeney, Assistant Chief Engineer – Bridges and Structures, CN, (now retired) for his encouragement during much of this work and for his assistance during the laboratory testing. Also for his belief that this project has merit and for his forward thinking, that high performance concrete does have application to railway structures.
- Dr. Warren Kindzierski, Professor of Environmental Engineering, University of Alberta for his assistance, advice and encouragement.
- Mr James McLeod, UMA, for his assistance and advice on the preparation of the many figures contained in this work.
- Mr. Brian Abbott, Assistant Chief Engineer, CN for his assistance and encouragement in this work and particularly for his efforts in securing the necessary funding to carry out this work.
- Mr. Dennis Waller, Vice President of Engineering and Mechanical, (retired), CN, for believing in the merits of this work and for providing the funding.

- Mr. George Nowak, Senior Structural Engineer, CN, for his review of the load frame analysis and for his review and comments on the slab design.
- Mr. Frank Scott, Senior Research Engineer, CN, (now retired) for his assistance and advice on much of the strain gauge data.
- Dr. Adel Hanna, Professor of Civil Engineering, Concordia University, for his practical advice and guidance, especially through the experimental program.
- and lastly but not least to my wife Janice and children, Lyndsey, Andrew and Lauren, for their patience and understanding throughout this undertaking. Many were the times that activities with the family were forsaken in order to complete this work.

TABLE OF CONTENTS

TABLE OF CONTENTS

TABLE OF CONTENTS

TABLE OF CONTENTS

TABLE OF CONTENTS

TABLE OF CONTENTS

LIST OF FIGURES

Chapter 1

Chapter 2

Chapter 3

LIST OF FIGURES

Chapter 4

LIST OF FIGURES

LIST OF FIGURES

LIST OF TABLES

LIST OF TABLES

LIST OF NOTATIONS

a	depth of equivalent rectangular stress block
a	shear span length
b	width of slab
b	shear span length
d	depth of slab or effective depth of slab
d_b	diameter of bar or strand
d_1	distance from extreme compression fibre to the first level of tension zone reinforcement
d_2	distance from extreme compression fibre to the second level of tension zone reinforcement
e	eccentricity of design prestressing force parallel to the axis measured from the centroid of the slab
f_b	stress in bottom fibre of the slab
f_c	compressive stress in concrete
f'_c	specified compressive stress of concrete
f_i	initial prestress in strand
f_t	stress in top fibre of the slab
f_{pc}	compressive stress in concrete at the centroid of the cross section, after all prestress losses
f_{ps}	stress in prestressed reinforcement
$f_{ps(sup)}$	stress in prestressed reinforcement at support
f_{se}	effective prestress in strands after prestress losses

LIST OF NOTATIONS

f_{pu} ultimate tensile strength of prestressing tendon

f_r modulus of rupture (MOR) of concrete

f_{sp} tensile splitting strength of concrete

h overall height of slab

n modular ratio

w_{DL} distributed dead load

w_{win} wind loading

w_{LL} distributed live load

w_{LL+I} distributed live load plus impact load

A_c cross-sectional area of concrete

A_n net area

A_g gross area

A_{ps} area of prestressing steel

A_{ps1} area of prestressing reinforcement at depth d_1

A_{ps2} area of prestressing reinforcement at depth d_2

C centrifugal force

C compressive force due to concrete stress block

D degree of curve

D diameter of bar or strand

E actual superelevation on a curve

E_{28} modulus of elasticity of concrete at 28 day strength

E_a modulus of elasticity of aggregate

LIST OF NOTATIONS

E_c	modulus of elasticity of concrete
E_{ct}	tangent modulus of elasticity for concrete
E_p	modulus of elasticity of concrete paste
E_s	modulus of elasticity of presstress reinforcement
FS	factor of safety
I′	impact factor
I	moment of inertia
L	overall length of slab
L	span length
M	applied moment
M_{cr}	flexural cracking moment
M_{derail}	moment due to derailment load
M_{DL}	moment due to dead load
M_{LL}	moment due to live load
M_{LL+I}	moment due to live load and impact
M_{sup}	moment at support
M_{mid}	moment at midspan
M_U	ultimate moment capacity
M_y	moment at yielding of prestressing strand
N	number of cycles
P	prestressing force
P_i	initial prestressing force before losses

LIST OF NOTATIONS

P_{eff}	effective prestressing force after losses
P_f	final prestressing force after losses
P_U	applied load at ultimate capacity
R	support reaction
R_A	reaction at support A
R_B	reaction at support B
S_b	section modulus – bottom of slab
S_t	section modulus – top of slab
T_1	tensile force due to prestress reinforcement at depth d_1
T_2	tensile force due to prestress reinforcement at depth d_2
V	shear force
V_a	volume of aggregate
V_{ci}	flexural shear cracking load
V_{cw}	web shear cracking load
X	depth of stress block
X_{max}	maximum depth of stress block
Y	vertical displacement of the slab
Y_{max}	maximum vertical displacement of the slab
α_b	strength factor for aggregate
ε_b	strain at bottom fibre of the slab
ε_t	strain at top fibre of the slab
ε_{cu}	ultimate strain in concrete

LIST OF NOTATIONS

ε_{su} strain in prestressing steel when tendon reaches its ultimate tensile strength

ε_1 strain in prestressing steel at depth d_1

ε_2 strain in prestressing steel at depth d_2

ε_{max} maximum strain in concrete

ε_{ps} strain in prestressed concrete

$\mu\varepsilon$ microstrain

ρ_c mass density of concrete

σ stress

σ_b stress at bottom outer fibre of slab

σ_t stress at top outer fibre of slab

σ_x bursting stress in anchorage zone at point "x"

ρ steel area to concrete area ratio

φ capacity reduction factor

Δ deflection

Δ_{DL} deflection due to dead load

Δ_{LL+I} deflection due to live load and impact

Δ_{total} total deflection

Δ_{fp} stress range in prestress strand

CHAPTER 1

Introduction and Objectives

1.1 Background

Canadian National Railway (CN) has approximately 3916 bridges of various types and ages in Canada. Of these, some 737 are on its' mainline route between Halifax, Nova Scotia and Vancouver, British Columbia. Approximately 400 of these are deck plate girder (DPG) bridges with an open deck support system. These bridges are in relatively good condition. However, the open deck structure makes them difficult to maintain in today's heavy axle load traffic environment. The deck ties are usually 250 x 300 mm (10 x 12 in.) and cut from Douglas fir. Over time the wood under the tie plates crushes due to mechanical break down causing surface and alignment irregularities over the bridge. The Railway has therefore been converting these bridges to ballast deck bridges since the mid 1970's. The primary reason for this is because ballast deck bridges are easier to maintain, Murphy et al [1998]. Ballast deck bridges also offer improved resiliency to impact loading and greater flexibility in maintenance of the track

Figures 1.1 and 1.2 indicate the primary differences between an open deck and a ballast deck railway bridge. The conversion of an open deck bridge to a ballast deck bridge is accomplished by removing the wooden tie deck and placing a precast, prestressed concrete slab on the girders. This concrete deck slab is then filled with a layer of ballast upon which the track structure rests.

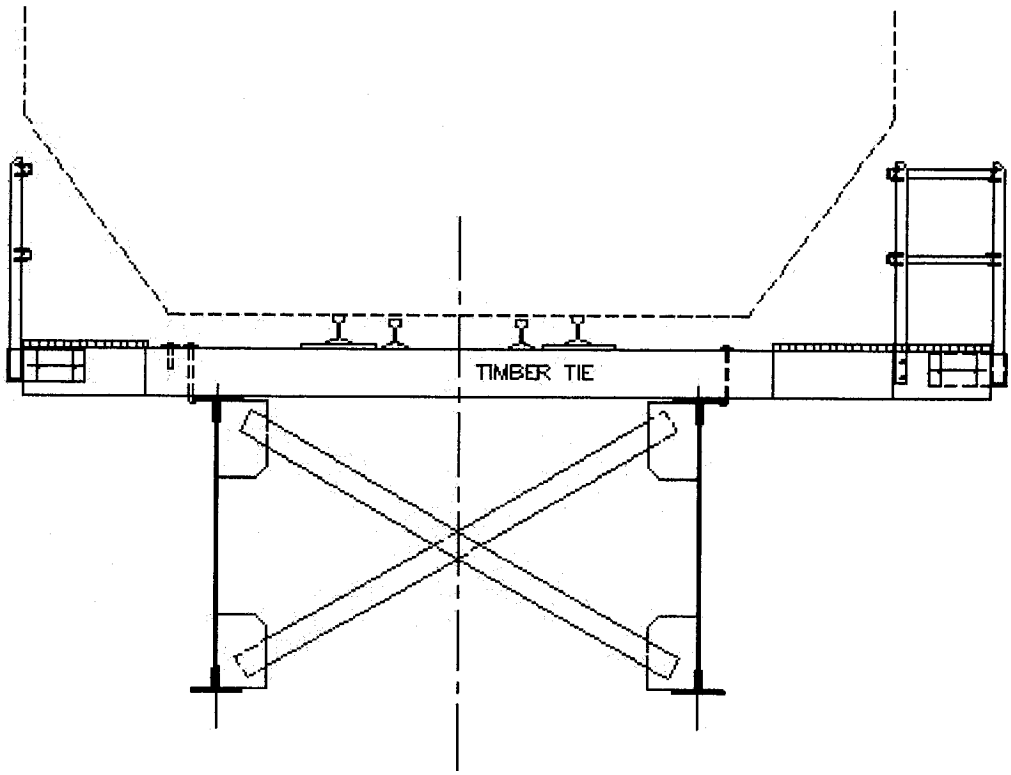

Figure 1.1 Cross section of a typical railway open deck bridge

In order to accomplish this work, a track closure called a work block is required. Such work blocks have a negative effect on the smooth movement of train traffic, with the result being the bunching of trains, both on line and in terminals, with subsequent train delays. Depending on the size of the bridge, such a bridge re-deck could take from 6 to 8 hours. This would include the work to remove the old wooden tie open deck, place the new concrete deck slabs and replace the new track structure. Figures 1.3 and 1.4 show such work being undertaken on a railway bridge. On a typical core main line, an average of 20 trains in each direction would be affected by such a work block.

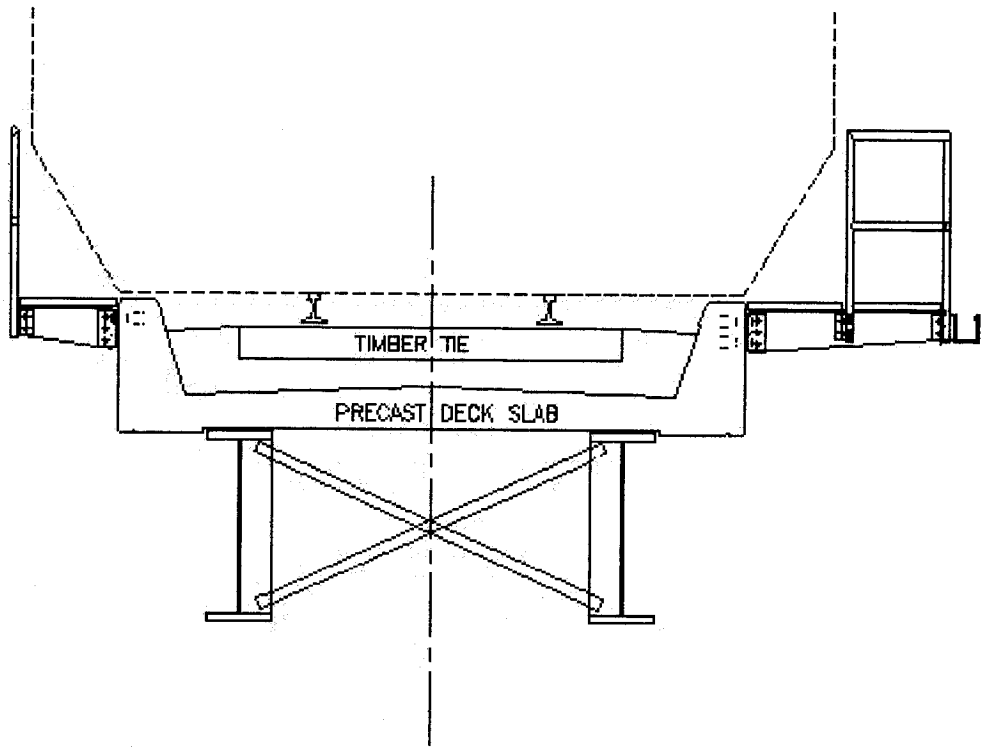

Figure 1.2. Cross section of a typical railway ballast deck bridge

It is estimated by CN's Costing Department that, for each train delayed by 1 hour, the cost to CN is $500.00 (Canadian). For each hour of work block, the cost to CN in train delay is $20,000.00. Therefore, there are significant savings involved in finding ways that shorten the time taken to convert a bridge from open deck to ballast deck.

To minimize delays to traffic, both Railways and Highway Departments are focusing on the use of precast, prestressed concrete deck panels to mainly shorten the time of reconstruction and bridge closure. The trend on both modes of surface transportation is to move towards rapid bridge deck replacement techniques due to intolerable extended

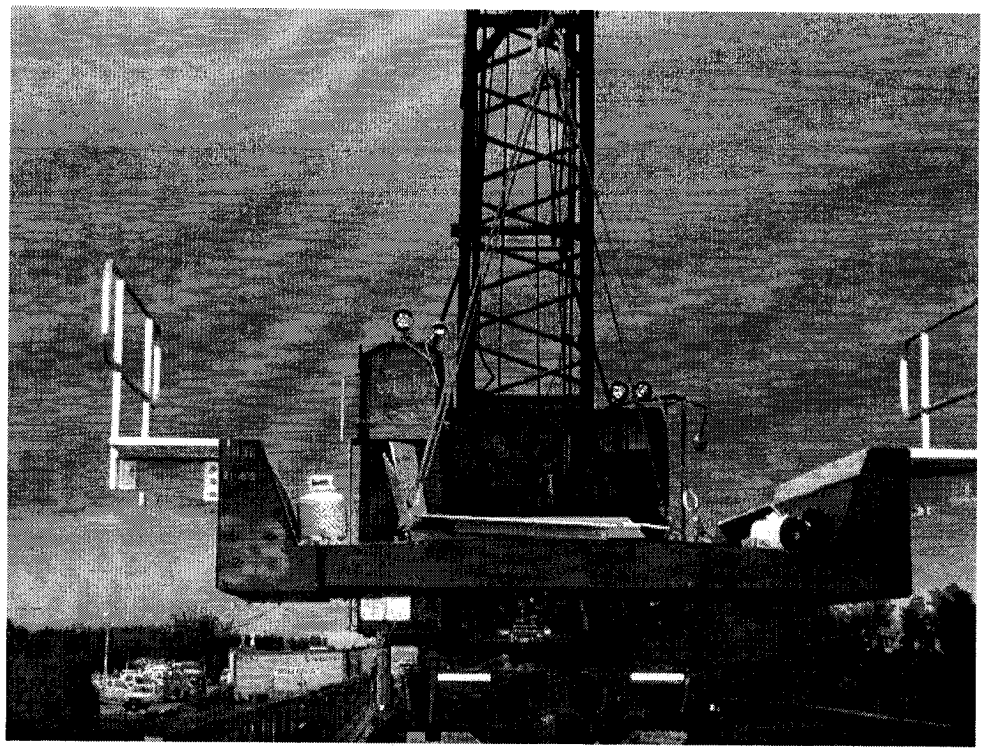

Figure 1.3 Precast slab being moved to position

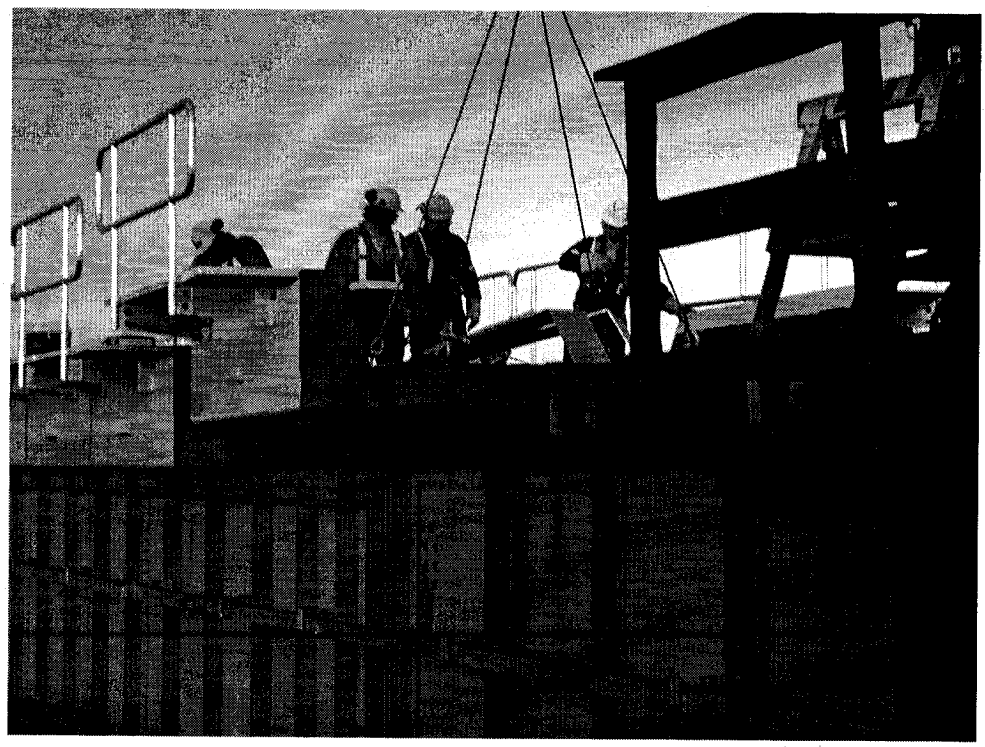

Figure 1.4 Pecast slab being positioned on bridge deck. Note existing open deck structure still in place on right.

bridge closures. Issa [2000] and Tadros and Mantu [1998], consider the trend towards prefabrication, such as the use of precast, prestressed concrete deck panels, as being able to significantly reduce both the cost of out of service time as well as reducing field labour.

The expanding and successful use of high performance concrete (HPC) on highway bridges indicates that it may have both practical and beneficial application on railway bridges. HPC in its simplistic mode is defined as "high strength concrete" (HSC) with a minimum compressive strength of 70 MPa (10,150 psi) with much improved mechanical and durability properties.

1.2 Purpose of the Research

The purpose of this research is to study the behaviour of a redesigned CN deck slab fabricated from high performance concrete (HPC). It is proposed to redesign the existing slab which currently utilizes 40 MPa (5,800 psi) concrete and replace it with HPC of 70 MPa (10,150 psi) compressive strength. The possible advantages of such a redesign are a thinner deck slab section and therefore reduced dead loading.

1.3 Objectives of the Research

Full scale testing of six optimized precast, prestressed concrete deck slabs will be conducted at Concordia University in order to evaluate the behavior of HPC deck slabs. These results will be compared to theoretical (predicted) values.

The results of the laboratory testing will be used by the Railway in order to make a determination on the future direction of the use of high performance concrete. If the

results are favorable the Railway intends to conduct further field-testing. An open deck bridge on the CN mainline between Montreal and Vancouver, will be selected as a candidate to be converted to a ballast deck bridge with this slab design and fabricated from high performance concrete. After conversion, the slabs and supporting substructure will be strain gauged and data relating to the response to impact and live loading from train traffic will be gathered. Specifically, field obtained dynamic strains will be compared against laboratory static strains and theoretical strains in order to assess the applicability of the concrete for future use. This portion of the work will not form a part of this thesis.

1.4 Broad Objectives

The broad objectives of this research project are to:

- conduct joint industry (CN) and University research on deck slabs constructed from HPC to gain a better understanding of their behavior;
- develop an appropriate laboratory test regime that will evaluate the slabs statically
- design a reduced thickness (275 to 250 mm) deck slab using HPC and evaluate its behavior

1.5 Specific Objectives

In order to accomplish the broader objectives of this research, specific objectives will be undertaken as follows:

1) Review recent domestic and international literature that deals with the state of the art of high performance concrete in regards to mechanical properties and long

term durability and make an assessment on its durability and applicability to railway use.

2) Develop and construct a deck slab design using HPC with a minimum compressive strength of 70 MPa (10,150 psi) in order to:
   - reduce dead loading by reducing the concrete thickness and therefore the weight per unit length
   - reduce the number of prestressed strands required
   - reduce the fabrication and erection costs.
3) Develop an appropriate laboratory test program to statically evaluate full scale prototype specimens
4) From the results of the laboratory test program:
   - evaluate the cracking capacity
   - evaluate the ultimate moment capacity
   - evaluate the shear capacity
   - evaluate the modes of failure
   - evaluate the ductility of the slab
   - evaluate the bond strength between the concrete and the strand
5) Improve productivity of slab installation and reduce disruptions to train traffic and costs associated with train delay.
6) Present recommendations to the Railway on whether or not this material is suitable for use in future Railway bridge structures.

Elements of this research and the above objectives will also address the concerns of CN as regards the following:

- Shear capacity of these slabs under increased loading and
- Bond length with HPC.

1.6 Thesis Organization

In addition to this chapter, there are 5 additional chapters and 6 appendices. In Chapter 2, the design of the deck slab test specimens is described. In Chapter 3, the test method and set up for each test is described in detail along with the specific instrumentation used. In Chapter 4, the failure mode of each slab is described, along with the results of the experimental program, which are then compared to the predicted values. In Chapter 5, an economic analysis is presented, which details the economics provided by the use of HPC deck slabs. In chapter 6, a summary of the research and the conclusions that can be drawn from this research are presented. Recommendations are also presented.

Appendix A is a literature review of the development and properties of HPC and is appended for completeness. Appendix B is a copy of the Excel© spreadsheet used to design the slab test specimens. Appendix C details the sample calculations for ultimate moment capacity. Appendix D details the sample calculations for first flexural cracking moment. Appendix E photographically documents the progression of test No. 5b. Appendix F is the raw test data and is appended for future reference and completeness.

CHAPTER 2

Slab Design

2.1 Design Reference

Using the American Railway Engineering and Maintenance of Way Association (AREMA) Manual [2000] Chapters 8 and 15 as a guide, full scale deck slabs for experimental laboratory testing were designed. Additional design criteria were specified by the CN Bridges and Structures Department.

2.2 Design Criteria

Due to certain laboratory restrictions (see chapter 3 for details) the slab size is restricted. The criteria for an initial design are as follows:

1 3700 mm (12 ft.-2 in.) wide

2 2135 (7 ft.) long

3 minimum f'c = 70 MPa (10,150 psi) at 28 days

4 15 mm prestressing strand with f_{pu} = 1860 MPa

5 initial prestress in strand = 185 kN

6 effective prestress in strand = 150 kN (0.7 f_{pu})

7 non-prestressed reinforcement f_y = 400 MPa

8 minimum cover 40 mm (1.5 in.) per AREMA Table 8-17.1

9 Live Loading = Coopers E-100

10 Impact Factor = 100%

11 Derailment Loading adopted from the Swiss Railway Code and located 0.18 m (7

in.) outside the centreline of support. See Section 2.4 for details.

2.3 Design Loads

2.3.1 Dead Load

As an initial design, the existing slab design dimensions will be used. The existing design has the following dimensions:

1 centerline thickness = 275 mm (10.83 in.)

2 edge thickness at curb = 225 mm (8.86 in.)

3 width of slab = 3700 (12 ft.-2 in.)

4 length of slab = 2135 (7 ft.)

5 span length (centre to centre of supports) = 2440 mm (8 ft.)

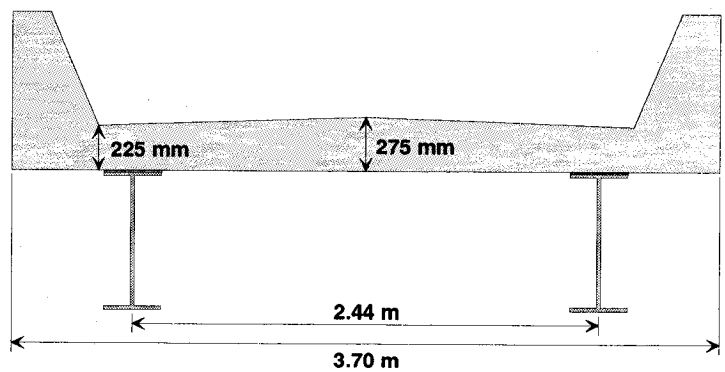

Figure 2.1 Cross-section of existing CN deck slab

For the purpose of calculating the dead load of the slab, ballast and track the following values will be used:

- concrete = 24.5 kN/m^3 (156 lb./ft.^{3})
- ballast = 20.0 kN/m^3 (127 lb./ft.^{3}) and 600 mm deep

- track (lump sum) = 3.6 kN/m (245 lb./ft.)

Note: due to a weight restriction on the laboratory crane (limited to 5 tonnes), both curbs were omitted from slab.

Dead Load:

concrete:	24.5 x 0.275 x 2.135	= 14.4 kN/m (988 lb./ft)
ballast:	20.0 x 0.6 x 2.135	= 25.6 kN/m (1,756 lb./ft.)
track:	3.6 x 2.135 /3.7	= 2.1 kN/m (144 lb./ft.)
Total Dead Load		= 42.1 kN/m (2,888 lb./ft.)

2.3.2 Live Load Configuration

Live load will be obtained by using Cooper's E loading from AREMA Chapter 15

Cooper's E – 80 axle loading is:

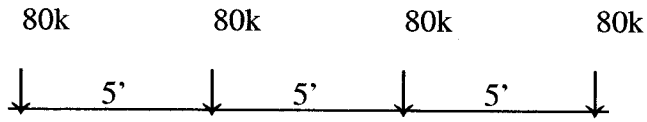

Multiply by 10/8 to obtain Cooper's E – 100 loading.

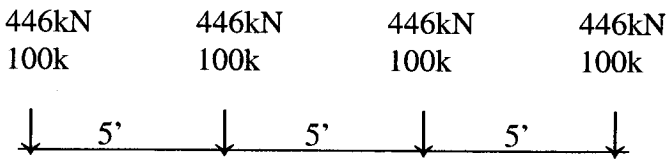

2.3.3 Live Load Distribution

Live load distribution is obtained from AREMA Chapter 8, Clause 2.2.3, which states that the load distribution is found from using the lesser of:

3' -0" (914 mm) plus 2 x effective depth of slab plus depth of ballast

or:

axle spacing 5 ft. (1524 mm)

914 + 600 + (2 x 250) = 2,014 mm

1524 mm < 2014 mm

therefore use 1524 mm (5 ft.)

2.3.4 Effective Width

The effective width is based on a 400 mm (15.75 in.) ballast depth with a 60° (from the vertical) distribution of load as shown below.

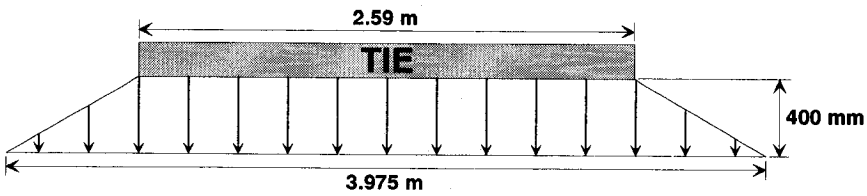

Figure 2.2 Load distribution from tie through ballast

Standard length tie = 2590 mm (8.5 ft.)

The minimum depth of ballast = 400 mm (16 in.)

400 tan 60 = 692 mm (27 in.)

2590 + 2(692) = 3975 mm (13 ft.)

3975 mm is greater than the slab width.

3975 > slab width = 3700 (13 ft. > 12 ft.-2 in.)

Therefore use an effective width of 3700 mm (12 ft.–2 in.)

2.3.5 Live Load

Note the number of 100 kip (446 kN) axles spaced at 1.524m (5 ft.) that can be applied to a 2.135 m (7 ft.) slab is 2. Therefore:

$$W_{LL} = \frac{446 \times 2}{3.7} = 241 \text{ kN/m (16,532 lb./ft.)}$$

2.3.6 Impact Load

CN uses 100% impact factor on its slabs.

Therefore I = 100

2.3.7 Centrifugal Force

The centrifugal force is given by:

$$C = 0.00117\, S^2 D \qquad 2.1$$

Where: C = centrifugal force as a percentage of live load

D = degree of curve

S = permissible speed in mph and

$$S = \sqrt{\frac{E+2}{0.0007D}} \qquad 2.2$$

Where: E = actual superelevation in inches (on CN maximum E = 5 in. (127 mm))

Substituting for $S = \sqrt{\frac{E+2}{0.0007D}}$ and E = 5 in. into $C = 0.00117\, S^2 D$ yields:

$$C = 0.00117\left(\frac{E+2}{0.0007}\right) = 0.00117\left(\frac{7}{0.0007}\right) = 11.7$$

Say C = 12% to be applied at 1836 mm (6 ft.) above the top of rail

2.3.8 Wind Loading

AREMA specifies the use of 300 lb./lin.ft. (4.4 kN/m) applied 2440 mm (8 ft.) above the top of rail. For a 2135 mm (7 ft.) long slab

wind = 4.4 x 2.135 = 9.4 kN

wind loading on slab is negligible and can be ignored.

2.3.9 Longitudinal force from live loading:

Longitudinal force = $\frac{100}{80}(200 + 17.5 \times 2.135) = 295.4\,\text{kN}$ (66.5 kips), applied 2440 mm (8 ft.) above top of rail elevation.

Traction force = $\frac{100}{80}\left(200\sqrt{2.135}\right) =$ 365.3 kN (82.1 kips) applied 915 mm (3 ft.) above top of rail elevation.

2.3.10 Summary of Loads

Live Load $W_{LL} = 241$ kN/m

Live load and Impact: $W_{LL+I} = 241 \times 2 = 482$ kN/m

Dead Load: $W_{DL} = 42.1$ kN/m

Wind Load: $W_{WL} = 4.36$ kN/m applied 2.44 m (8 ft.) above top of rail elevation

Centrifugal force: $W_C = 0.12 \times 241 = 28.9$ kN/m applied 1.38 m (4 ft.-6 in.) above top of rail elevation

Longitudinal force: $W_{long} = 295.4$ kN (66.5 kips), applied 2440 mm (8 ft.) above top of rail elevation.

$W_{tract} = 365.3$ kN (82.1 kips) applied 915 mm (3 ft.) above top of

rail elevation.

The group load combinations for load factor design are contained in Table 2-3 of Part 2, Chapter 8, Concrete Structures and Foundations of the AREMA Manual. From the table it is determined that load factor Group I governs.

Slab loading:

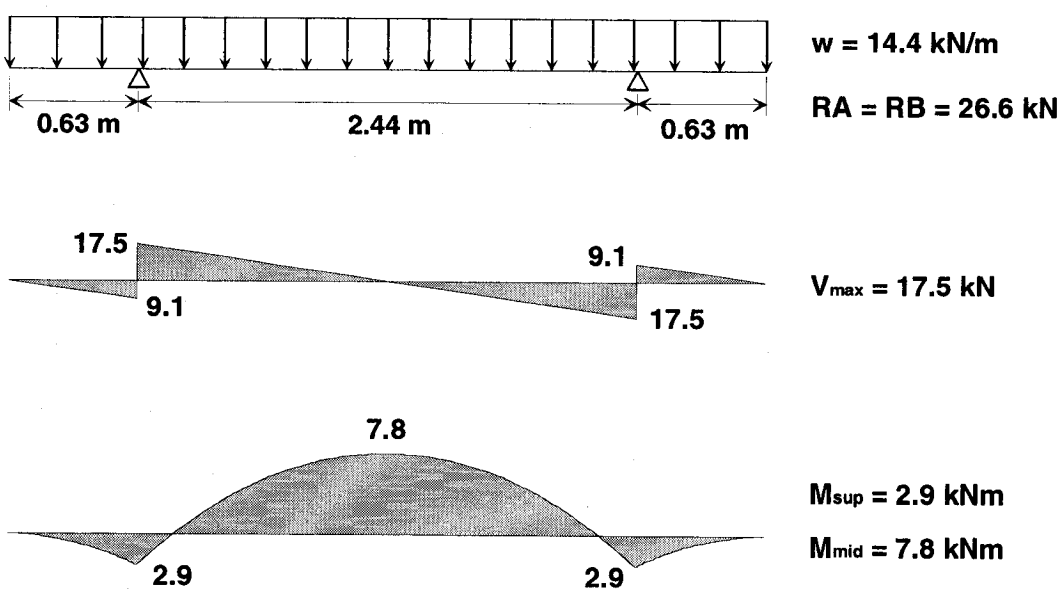

Figure 2.3 Load, shear force and bending moment diagrams due to slab dead load

Track loading consisting of slab, rail, ties and ballast:

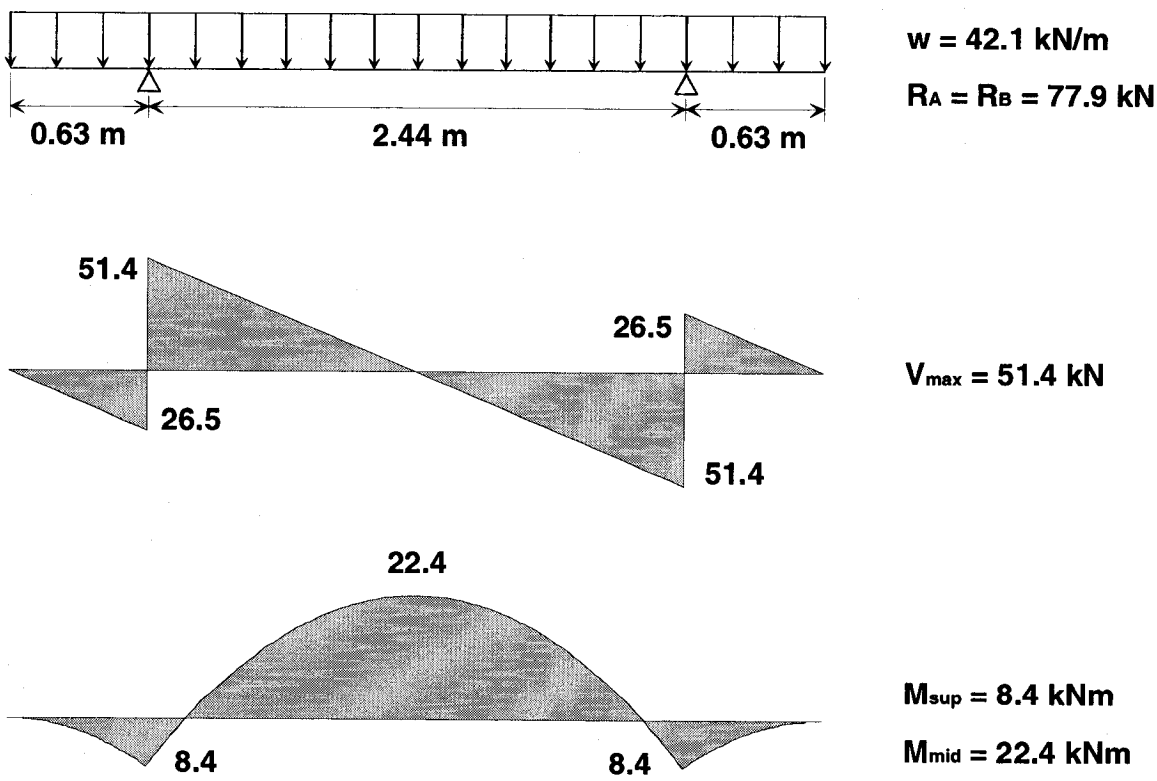

Figure 2.4 Load, shear force and bending moment diagrams due to track dead load

Live Load and Impact

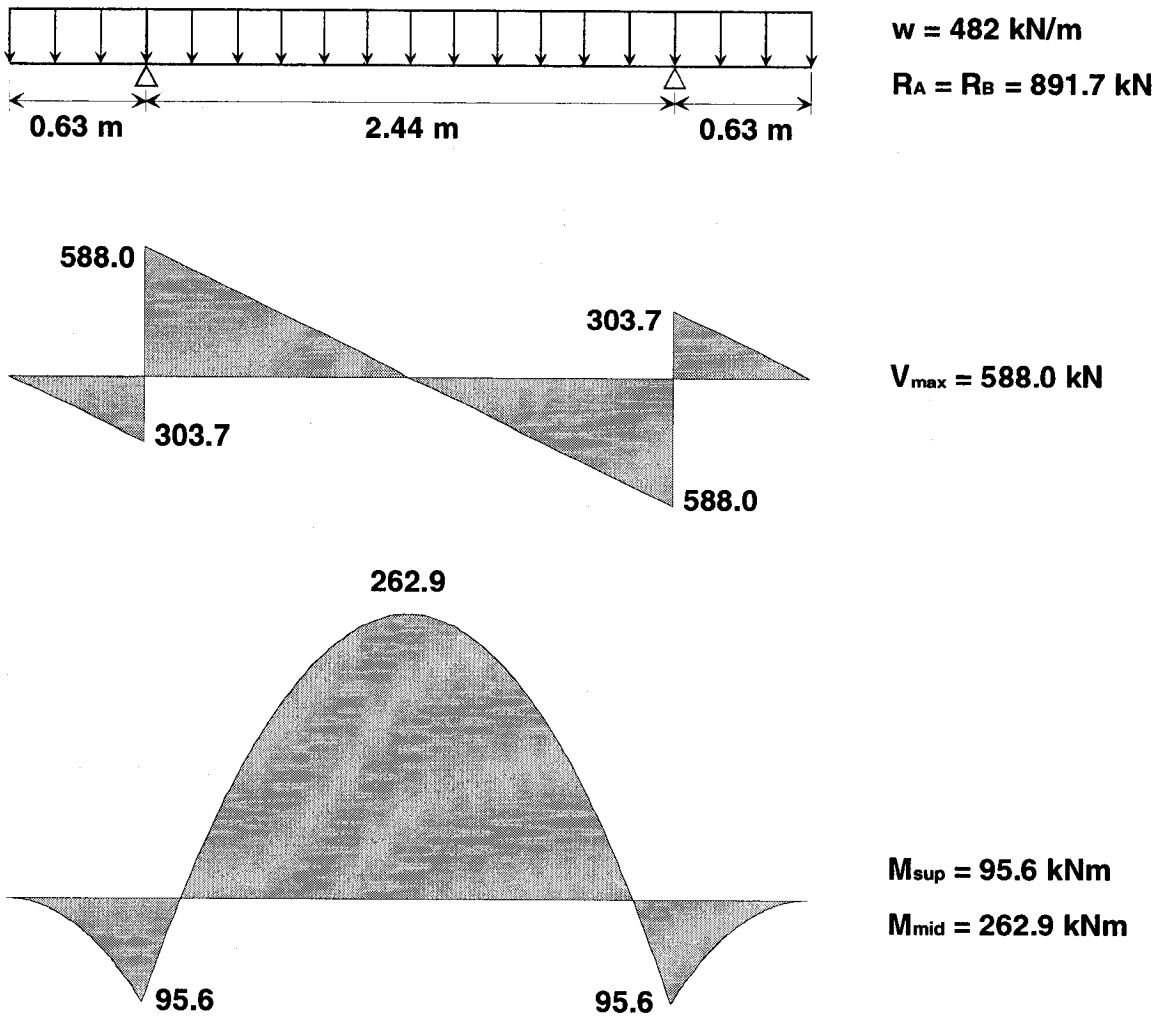

Figure 2.5 Load, shear and bending moment diagrams due to live load plus impact

In service loading (slab, ballast, track, live loading plus impact)

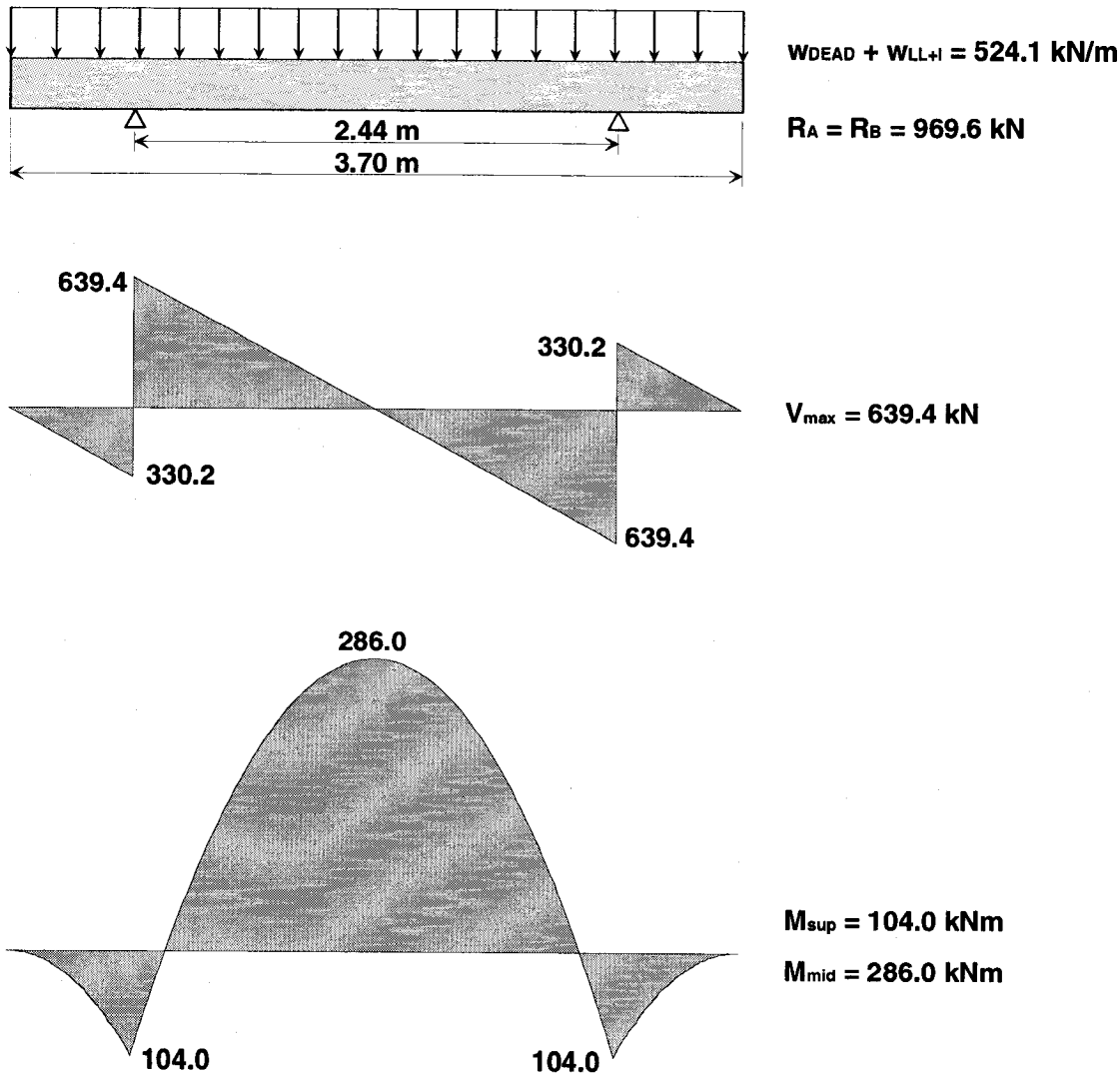

Figure 2.6 Load, shear and bending moment diagrams due to dead loading, live loading and impact.

2.4 Design for Negative Moment

The current AREMA Manual does not have a derailment loading requirement for slabs. The Swiss Railway code does. For the purpose of this research the Swiss Railway Code Type I derailment load has been adopted. A derailment loading consisting of 2 wheels

loads of 178 kN (40,000 lb.) each has been selected. This load will be applied at 180 mm (7 in.) beyond each support (at the curb edge) to obtain the negative moment capacity for the slab.

2.4.1 Negative Moment at the Support

The assumed wheel spacing (from Cooper's E loading) is 1.524 m (5 ft.).

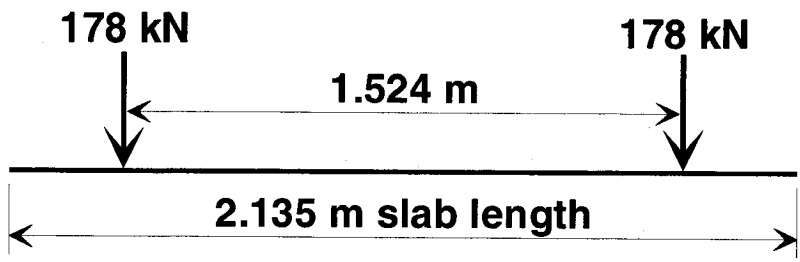

Figure 2.7 Wheel spacing on length of slab for derailment loading

On a 2.135 m slab there would be: $2 + \frac{2.135 - 1.524}{1.524} = 2.4$ wheels.

The derailment loading is therefore 2.4 x 178 = 427.2 kN (96.1 kips).

M_{derail} = - 427.2 x 0.18 = - 76.9 kN-m (56.8 kip-ft.)

The existing negative moment caused by the slab, ballast and track must be added to the derailment moment to obtain the total negative moment at the support.

M_{sup} = - (76.9 + 8.4) = - 85.3 kN-m (-63.0 kip-ft.)

This is less than the moment caused by the live load at the support.

85.3 kN-m < 104.0 kN-m

Therefore -104.0 kN-m (-76.8 kip-ft.) will be taken as the negative moment at the support.

2.5 Stresses in Concrete:

15 mm (0.59 in.) diameter low relaxation seven wire strand will be used

Grade f_{pu} = 1860 MPa (270 ksi)

A_{ps} = 140 mm (0.217 in.^{2})

2.5.1 Initial Prestressing Force

The initial prestressing force in each strand is given by Clause 17.6.5.4 9 (d) of the AREMA Manual.

Try $f_i = 0.70\ f_{pu}$ 2.4

= 0.70 x 1860 MPa = 1,302 MPa (188.8 ksi)

P_i = 1302 x 10^{-3} x 140 = 182.3 kN (41.0 kips)

Use P_i = 185 kN/strand (41.6 kips)

therefore f_i = 185,000/140 = 1,321 MPa (191.5 ksi)

1,321 MPa (191.5 ksi) = 0.71f_{pu}

2.5.2 Prestress Losses

The prestress losses are given in Clause 17.6.6.e and Table 17.3 of the AREMA Manual.

For fc' greater than 34.5 MPa (5,000 psi) and for low relaxation strand use:

losses = 241 MPa (35,000 psi)

Final prestress after losses = 1,321 - 241 = 1,080 MPa (156.6 ksi)

Final prestress force = $P_f = \frac{1{,}080 \times 140}{1{,}000}$ =151 kN/strand (34 kips/strand)

2.5.3 Allowable Stressses

The allowable stresses within the concrete at various stages, is given by clause 17.6.4 of the AREMA Manual.

At prestress transfer:

- f_{ci} = 35 MPa (5,100 psi)
- allowable compression

  = 0.60 f_{ci} = 0.6 x 35 = 21 MPa (3,000 psi)
- allowable tension

  $=0.25\sqrt{f_{ci}} =0.25 \times \sqrt{35} =1.48$ MPa (214 psi)

At service loading:

- f_c' = 70 MPa (10,150 psi)
- allowable compression

  = 0.40 f_c' = 0.40 x 70 = 28 MPa (4,100 psi)
- allowable tension = 0

2.6 Design Procedure:

The force-in-tendon approach will be used to design the slab. This approach uses the self-equilibrating stresses due to prestressing and then adding the externally applied stresses due to other applied loading.

This approach uses the following formula to determine the allowable concrete stresses:

At the top of the slab:

$$\sigma_{top} = \frac{P}{A} - \frac{Pe}{S_t} + \frac{M}{S_t} \qquad 2.5$$

and at the bottom of the slab:

$$\sigma_{bot} = \frac{P}{A} + \frac{Pe}{S_b} - \frac{M}{S_b} \qquad 2.6$$

where:

- P = final prestressing force
- A = gross cross sectional area of concrete at section under consideration
- e = eccentricity
- M = applied moment
- S_t = section modulus of top of slab
- S_b= section modulus of bottom slab
- σ_{top} = stress in concrete at outer most top fiber of the slab
- σ_{bot} = stress in concrete at outer most bottom fiber of the slab

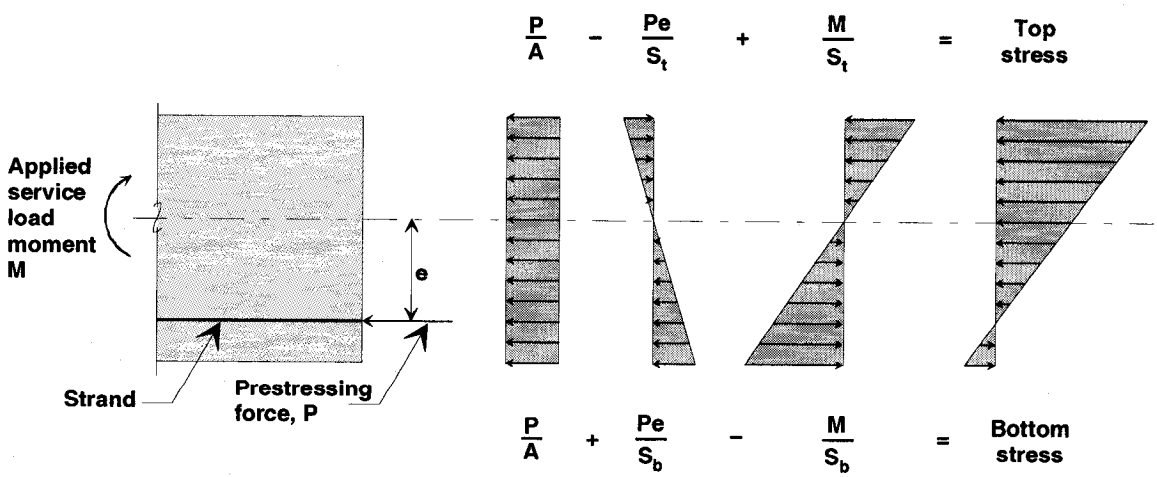

Figure 2.8 Concrete stresses due specified loads (adopted from the CPCI Metric Design Manual)

In the above calculations the transformed area of concrete was not used used. Calculations using the transformed area (a transformed area of 548,506 mm^2 versus a concrete area 533,750 mm^2) results in a 1.3 percent difference in the stress calculations. Because of the small discrepancy, most designers find it sufficiently accurate to use the gross area of concrete.

A spreadsheet in Excel was developed to evaluate simultaneously the effect increasing prestress force and eccentricity had on the strength of the slab. The use of this spreadsheet helped in the selection of the optimum eccentricity and prestressing force required. From the prestressing force, the area of prestresing steel can easily be determined. This spreadsheet is appended in Appendix B. See Table 2.1 and Figure 2.9 for final slab dimensions and geometry details.

Based on the results of this analysis, the following have been selected and used in the final design of the test slabs:

- Area of prestressing steel = 4,760 mm^2 (7.38 $in.^2$)
- Number of 15 mm diameter prestressing strands 34
- Eccentricity at midspan = 35 mm (1.38 in.)
- Eccentricity at the supports = 24 mm (0.94 in.)
- Initial prestressing force = 6,290 kN (1,415 kips)
- Final prestressing force = 5,100 kN (1,148 kips)

2.7 Distribution of Prestressing Strands

The distribution of the prestressing strand within the slab is determined by taking moments of the strand area about the top of the slab and knowing that:

$$A_{PS} = A_{PS1} + A_{PS2} \qquad 2.7$$

where:

A_{ps1} = prestress area at depth d_1 below the top of slab

A_{ps2} = prestress area at depth d_2 below the top of slab

A_{ps} = total area of prestress reinforcement = 4,760 mm^2 (7.38 in.^{2})

Therefore:

$A_{ps2} = 4{,}760 - A_{ps1}$

The bottom strand will be placed at a depth d_1 = 180 mm (7.09 in.) at midspan in order to allow room for temperature and creep reinforcement, which will be placed so as to give 50 mm (2 in.) concrete cover. The top layer of strand will be placed at a depth of d_2 = 95 mm (3.74 in.) at midspan. This allows room for temperature and creep steel that will be placed so as to give a minimum concrete cover at the ends of 50 mm (2 in.). At midspan, the centroid of the prestressing steel is located 35 mm (1.38 in.) below the neutral axis of the slab, or 160 mm (6.30 in.) below the top of slab.

$$\sum M \text{ @ } top\ of\ slab = 0$$

$$A_{PS1} \times d_1 + A_{PS2} \times d_2 = 160 \times A_{PS}$$

Substituting yields:

$$180 \times A_{PS1} + 95 \times (4{,}760 - A_{PS1}) = 160 \times 4{,}760$$

$A_{PS1} = 3640\ mm^2\ (5.64\ in.^2)$

$A_{PS1} = 26\ strands$

$A_{PS2} = 8\ strands$

2.8 Negative Moment Capacity Over Supports

The critical section for the cantilevered portion of the slab is at the supports. A check at this location is required to determine if cracking will occur under the live load moment of 104.0 kN-m (76.8 kip-ft.).

The support is located 630 mm (25 in.) from the end of the slab.

- The transfer length is taken as 50 strand diameters = 50 x 15 = 750 mm (29.5 in.)
- The stress in the prestressed reinforcement at factored resistance f_{ps} at 750 mm (29.5 in.) = 1,079 MPa (156 ksi)

The stress in the prestressed reinforcement at the support is:

$$f_{ps(\text{sup})} = \frac{630}{750} \times 1{,}079 = 906 \text{ MPa (131 ksi)}$$

The code provision is to use 50% of this value = 906/2 = 453 MPa (65 ksi). Therefore, the force per strand is:

$$= \frac{453 \times 140}{1{,}000} = 63.4 \text{ kN (14.3 kips)}$$

$$P = 34 \times 63.4 = 2{,}156 \text{ kN (486.2 kips)}$$

Flexural cracking will occur when the tensile stress in the top fibre of the slab over the

support reaches an approximate value of $0.5\sqrt{f'_c} = 0.5\sqrt{70} = 4.2$ MPa (610 ksi)

The compressive stress at the top fibre is:

$$\sigma_{top} = \frac{P}{A} - \frac{Pe}{S_t} \qquad 2.8$$

where:

e at the supports = 24 mm (0.94 in.)

P = 2,156 kN (486.2 kips)

$S_t = 18.5 \times 10^6$ mm^3 (1,098 in.^{3})

A_c = 480,375 mm^2 (745 in.^{2})

Substituting yields:

σ_{top} = 1.62 MPa (235 psi)

The moment to cause cracking is therefore:

$$M_{cr} = (1.6 + 4.2)18.5 \times 10^6$$

M_{cr} = 107.3 kN-m (79.2 kip-ft.)

Factor of safety against cracking is therefore:

$$F.S. = \frac{107.3}{104.0} = 1.03$$

This indicates that considerably more negative moment reinforcement over the supports is required. CN has been accommodating this by adding addition prestress reinforcement to the top layer.

2.9 Shrinkage and Temperature Steel

To provide resistance against shrinkage and temperature stresses, steel reinforcement at the top and bottom faces of the slab should be provided. The AREMA Manual does not

specify shrinkage and temperature steel for prestressed concrete but does specify shrinkage and temperature steel for reinforced concrete. For reinforced concrete, a steel area of 529 mm^2 per m of slab (0.25 $in.^2$/ft.) on each surface as measured perpendicular to the direction of the steel is required.

10M bars will be used.

Area = 78.5 mm^2 (0.12 $in.^2$) and f_y = 400 MPa (58 ksi)

In 3.7 m direction:

Minimum area = 3.7 x 529 = 1,958 mm^2 (3.0 $in.^2$)

Provide 15 bars = 15 x 78.5 = 1,178 mm^2 (1.83 $in.^2$) spaced at 250 mm (9.8 in.) c/c.

In the 2.135 m direction:

Minimum area = 2.135 x 529 = 1,129 mm^2 (1.75 $in.^2$)

Provide 9 bars = 707 mm^2 (1.1 $in.^2$) spaced at 250 mm (9.8 in.) c/c.

As the slabs were to be used for test purposes and not place into service, it was decided to limit the shrinkage and temperature steel to 60 percent of that required so as to save on the cost of the full scale specimens. Alternatively, shrinkage and temperature steel could be eliminated in the prestressed direction and the full amount used in the non prestressed direction.

2.10 Deflection

From the slab design program and the final design selected, the deflections of the slab at various stages can be calculated.

The initial upward deflection (camber) of the slab is given by the following equation:

$$\Delta = \frac{P_i e l^2}{8 E_C I_g} \qquad 2.9$$

where:

P_i = initial prestress force before losses

e = eccentricity

l = slab width

$E_C = 5500\sqrt{f_C'} = 5500\sqrt{70} = 46{,}016$ MPa (6,672 ksi)

$$I_g = \frac{bh^3}{12} = \frac{2135 \times 237.5^3}{12} = 2.38\times10^9 \text{ mm}^4 \text{ (5718 in.}^4\text{)}$$

If the section remains uncracked, then the gross moment of inertia may be used. As the top surface of the slab is sloped to shed water, the gross moment of inertia will be based on the average slab thickness. Therefore:

$$\Delta = \frac{6{,}290{,}000 \times 34 \times 3700^2}{8 \times 46{,}016 \times 2.38\times10^9}$$

$\Delta = 3.44$ mm (0.14 in.) upwards

However, the initial camber is not important. The final camber after losses is the required value. Therefore, the long term upward deflection (camber) after losses is given by the following equation:

$$\Delta = \frac{P_f e l^2}{8 E_C I_g} \qquad 2.10$$

where:

P_f = final prestress force after losses

$$\Delta = \frac{5{,}100{,}000 \times 34 \times 3700^2}{8 \times 46{,}016 \times 2.38 \times 10^9}$$

Δ = 2.71 mm (0.11 in.) upwards

From the above value, the self weight of the slab must be deducted to obtain the net upward deflection (camber).

$$\Delta_{Slab} = \frac{5 w_{slab} l^4}{384 E_C I_g} \qquad 2.11$$

where:

w_{slab} = 14.4 kN/m = 14.7 N/mm

Δ = 0.06 mm (0.002 in.) downwards

The net camber at release is:

3.44 - 0.06 = 3.38 mm (0.13 in.) upwards.

The net camber after long term losses are taken into account is:

2.71 – 0.06 = 2.65 mm (0.10 in.) upwards. However, this is the camber for a 3700 mm (12ft.-2 in.) span. The net camber for a 2440 mm (8 ft.) span is 2.40 mm (0.09 in.).

The deflection due to the superimposed dead load (ballast and track) is:

$$\Delta_{DL} = \frac{5 w_{DL} l^4}{384 E_C I_g} \qquad 2.12$$

where:

w_{DL} = 27.7 kN/m = 27.7 N/mm

Δ_{DL} =0.12 mm (0.005 in.) downwards

The deflection due to live load and impact is:

$$\Delta_{LL+I} = \frac{5 w_{LL+I} l^4}{384 E_C I_g} \qquad 2.13$$

where:

w_{LL+I} = 482 kN/m = 482 N/mm

Δ_{LL+I} = 2.03 mm (0.08 in.) downwards

Total deflection due to dead load and live load plus impact is:

$\Delta_{Total} = \Delta_{DL} + \Delta_{LL+I}$ = 0.12 + 2.03 =2.15 mm (0.09 in.) downwards

The final deflection of the slab taking into account camber is:

2.34 – 2.15 = 0.19 mm (0.007 in.) upwards

It should be noted that the deflection due to live load plus impact of 2.03 mm (0.08 in.) is equivalent to a limit of:

$$\Delta = L/1200 \qquad 2.14$$

Note that in the above calculations for deflection, the transformed moment of inertia I_t of 2.42 x 10^9 mm^4 (5,814 $in.^2$) could have been used. However, the difference between the gross concrete moment of inertia and the transformed moment of inertia is only 1.6 percent. Therefore, the current calculation for deflection has overstated the deflection by 1.6 percent.

2.11 Fatigue Capacity

A theoretical fatigue analysis has been performed on the slab design in order to obtain an order of magnitude approximation of the fatigue life of the slabs.

The fatigue strength of prestressed concrete is generally related to that of the reinforcement and the stress range ($f_{\max}$ *to* $f_{\min}$) to which the reinforcement is being subject.

A study at Lehigh University by Tide and Van Horn [1966] indicated that the fatigue life of prestressing strand can be approximated using the following relationship:

$$\log N = 10 - 3.6 \log\left(\frac{100 \times \Delta f_p}{f_{pu}}\right) \qquad 2.15$$

where: $\Delta f_p = f_{\max} - f_{\min}$ = stress range 2.16

and $f_{pu} = 1860 MPa$

Further testing at Lehigh by Hanson et al [1970] indicate that the fatigue life of tendons in beams was much less than comparable tendons tested in air. Recommendations coming from the research suggest reducing the above cycles by 0.90 to account for this phenomenon.

In the case of the bridge deck slab, the design stress range to which the strand is subjected is determined by calculating the stress in the strand due to full live loading and impact minus the stress in the strand due to ballast and track loading. This value is the fluctuating stress.

The prestress reinforcement will then be working in the following range:

At minimum loading:

$$\varepsilon_{ps} = \frac{1{,}070}{1860} = 0.575 f_{pu}$$

At maximum loading:

$$\varepsilon_{ps} = \frac{1{,}116}{1{,}860} = 0.60 f_{pu}$$

Therefore the strand will approximately be working between 58 to 60 percent of ultimate capacity or:

$$\Delta f_p = f_{\max} - f_{\min}$$

= 1,116 – 1,070 = 46 MPa (6.68 ksi)

Substituting into the above equation yields:

N = 384 x 10^6 cycles

Therefore, the number of cycles to fatigue failure is:

N = 0.10 x 384 x 10^6 cycles

N = 38.4 x 10^6 cycles

To put this number into perspective, an average 50 million gross ton line (MGT) would see approximately 16 trains per day with an average trailing tonnage of 8,600 tons. The number of wheels causing impacts of 45,500 kg (100 kips) or greater at the rail level is 10 per train. Based on 160 possible cycles per day or roughly 60,000 cycles per year, the slabs would have a fatigue life of:

$$\frac{38.4 \times 10^6}{60{,}000} = 640 \text{ years}$$

Clearly from the above, fatigue of the strands is not an issue.

2.12 Summary of Final Design

The following table is a summary of the final design details of this slab:

Description	Value
Width	3,700 mm (12 ft. 2 in.)
Length	2,135 mm (7 ft.)
Height at center	250 mm (9.84 in.)
Height at curb	225 mm (8.85 in.)
Area of concrete at midspan	533,375 mm^2 (827 $in.^2$)
Area of concrete at slab end	480,375 mm^2 (7445 $in.^2$)
Moment of inertia at midspan	2.78 x 10^9 mm^4 (6.67 x 10^3 $in.^4$)
Moment of inertia at slab end	2.03 x10^9 mm^4 (4.89 x 10^3 $in.^4$)
No. of 15 mm (0.60 in.) dia. 7 wire strands	34
No. strands in top layer	8
No. strands in bottom layer	26
Depth of top layer strand at midspan	95 mm (3.74 in.)
Depth of bottom layer strand at midspan	180 mm (7.09 in.)
Area of presssing steel	4,760 mm^2 (7.38 $in.^2$)
Initial prestressing force	185 kN/strand (41.6 kips/strand)
Final prestresing force	151 kN/strand (34 kips/strand)
Total initial prestressing force	6,290 kN (1,415 kips)
Total final prestressing force	5,134 kN (1,155 kips)
Eccentricity at midspan	35 mm (1.38 in.)
Eccentricity over supports	24 mm (0.94 in.)
28 Day compressive strength of concrete	70 MPa (10,150 psi)
Compressive strength at release	35 MPa (5,075 psi)
Ultimate strength of prestressing strand	1860 MPa (270,000 psi)
Water/cement ratio	Maximum 0.30
Air entrainment	5 to 6 %

Table 2.1 Summary of Slab Design Details

Figure 2.9 shows a drawing of the slab as detailed in the above summary. This drawing was used for construction purposes and supplied to the slab fabricator.

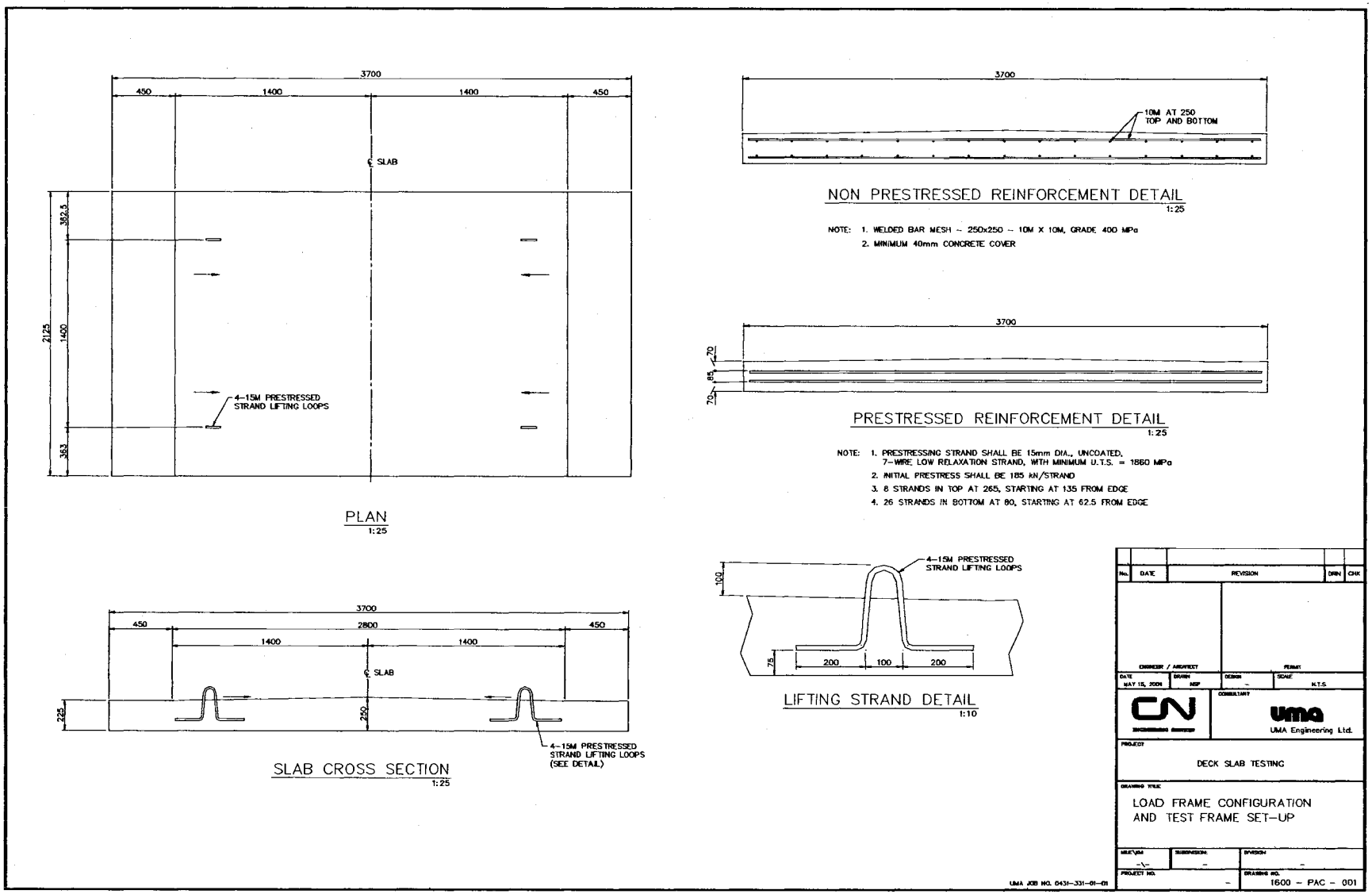

Figure 2.9 Deck slab detail drawing used for manufacture

2.13 Mix Design

The mix design for the slabs, which was supplied by Con-Force Concrete is shown in Table 2.1 below.

CONCRETE MIX ANALYSIS			
Material	**Mass**	**Units**	**Density kg/m^3**
Cement Type I/II	546	kg/m^3	3150
Silica Fume	34	kg/m^3	3100
Sand	557	kg/m^3	2650
Stone 14mm	1050	kg/m^3	2620
Water (Total)	175	L/m^3	1000
Rheobuild 1000	4.00	L/m^3	
Pozzolith 122R	1.00	g/m^3	
Conv. Air %	5.0	%	
Properties			
Yield (m3)	1.0242	m^3	
Slump	175 +/- 25	mm	
Air Content	6 +/- 1	%	
Density	2362	kg/m^3	
Comp. Strength @ 28-days	70.0	MPa	
Comp. Strength @ Release	35.0	MPa	
Volumes			
Total CA	1050	kg/m^3	
CM volume	184	L/m^3	
Sand volume	210	L/m^3	
CA volume	401	L/m^3	
Paste volume	359	L/m^3	
Mortar volume	569	L/m^3	
Ratios			
CA/solids volume	0.50		
Sand/Mortar volume	0.37		
Sand/Aggregate volume	0.34		
Sand/paste volume	0.59		
W/CM by volume	0.95		
CA/concrete volume	0.40		
SF/Cementitious	6	%	
W/Cementitious	0.30		
W/Cement	0.32		

Table 2.2 Mix Design for Test Slabs

2.14 Reduced Slab Dead Load

There are two methods by which the existing CN slab design can be reduced in mass. The first is by reducing the thickness of the slab, as is proposed in design detailed above. The second is by decreasing the volume of concrete used in the curbs. This can best be accomplished by inserting a cardboard tube (similar to that used for piles or columns) lengthwise along the slab. Figure 2.10 indicates the curb with a 175 mm (7 in.) diameter tube inserted. Alternatively a rectangular or trapezoidal block of Styrofoam could also be used.

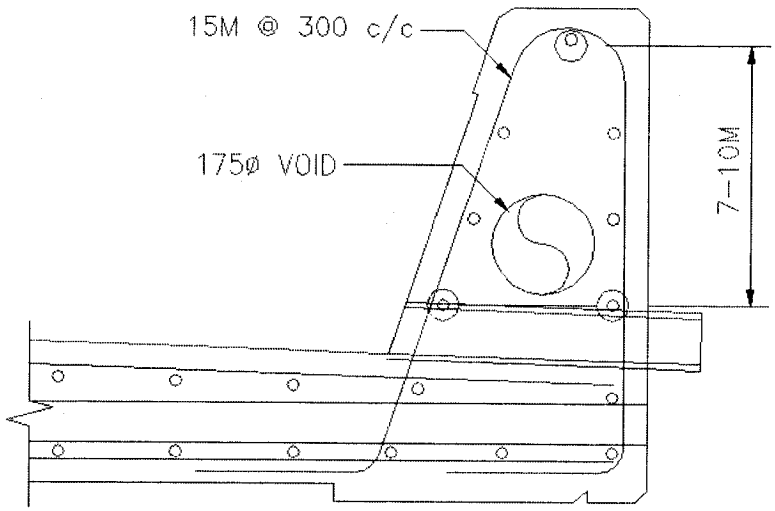

Figure 2.10 Cross section of slab curb with proposed 175 mm diameter void

Table 2.3 below details the volume and mass reduction that can be achieved by the above methods for a 2.44 m (8 ft.) long slab and a 3.05 m (10 ft.) long slab. These in turn are compared to the existing thicker 2.4 m (8 ft.) long slab.

Slab Thickness and Length*	Location of Reduction	Volume of Concrete Removed (m^3)	Mass of Concrete Removed (kg)	Gross Slab Mass (kg)	Mass per unit Length (kg/m)
Existing CN standard slab T = 275 mm L = 2.44 m				**8,000**	**3,278**
Experimental slab T= 250 mm L = 2.135 m	Deck	0.197	475		
	Curbs**	0.103	247		
	Total	**0.300**	**722**	**6,278**	**2,940**
New slab T = 250 mm L = 2.44 m	Deck	0.226	542		
	Curbs	0.117	282		
	Total	**0.343**	**824**	**7,175**	**2,940**
New slab T = 250 mm L = 3.05 m	Deck	0.282	678		
	Curbs	0.147	352		
	Total	**0.429**	**1,030**	**8,969**	**2,940**

* based on 3.7 m slab width

* * experimental slab with curbs added

Table 2.3 Comparison of Reduced Volumes and Mass for Various Length Slabs

The new 3.05 m length slab design would therefore afford an increase in slab length of 25% over the existing CN standard 2.44 m length slab, but only a 12 % increase in weight. CN have indicated that the above mass for a 3.05 m (10 ft.) long slab represents the safe limit of their crane capacity considering boom angle and wind factors. The economics behind this slab length increase are discussed in Chapter 5, under economic analysis.

CHAPTER 3

Description of the Experimental Program

3.1 General Description

Six prestressed concrete deck slabs were fabricated at the Con-Force facility in Winnipeg, Manitoba in February and March, 2002. The slabs were cast in pairs and removed from the forms after approximately 16 hours of curing. They were then stored indoors for a period of one week, before being moved outside for storage.

Three concrete batches were used to manufacture the six slabs. During casting several 152 mm x 305 mm (6 in. x 12 in.) cylinders were made from each concrete batch, and moist cured for later testing.

After all the slabs were fabricated, the slabs were loaded on semi-trailers and transported to the Concordia University Structures Laboratory in Montreal for subsequent testing. Upon arrival, the slabs were off-loaded, placed on timber supports and stacked in the structures laboratory until testing began in June 2002.

The deck slabs were full scale specimens, 3700 mm (12 ft.-2 in.) wide by 2135 mm (7 ft.) long and each weighing 4650 kg (10, 230 lb.). Initially, it had been hoped to test slabs 3050 mm (10 ft.) long. Unfortunately, the load frame columns were designed for 2440 mm (8 ft.) between faces, which precluded a longer slab being tested. Consequently it was decided to proceed with a deck slab length of 2135 mm (7 ft.) in order to allow for

manoeuvring the deck slab into position and also for viewing and marking the sides for cracking during testing.

Also, due to the maximum capacity of the overhead crane, which has a load limit of 5 tonnes (11,000 lb.), it was decided to eliminate the curb detail, as retaining them would have exceeded the capacity of the overhead crane. Figure 3.1 below shows a typical slab specimen being readied for testing.

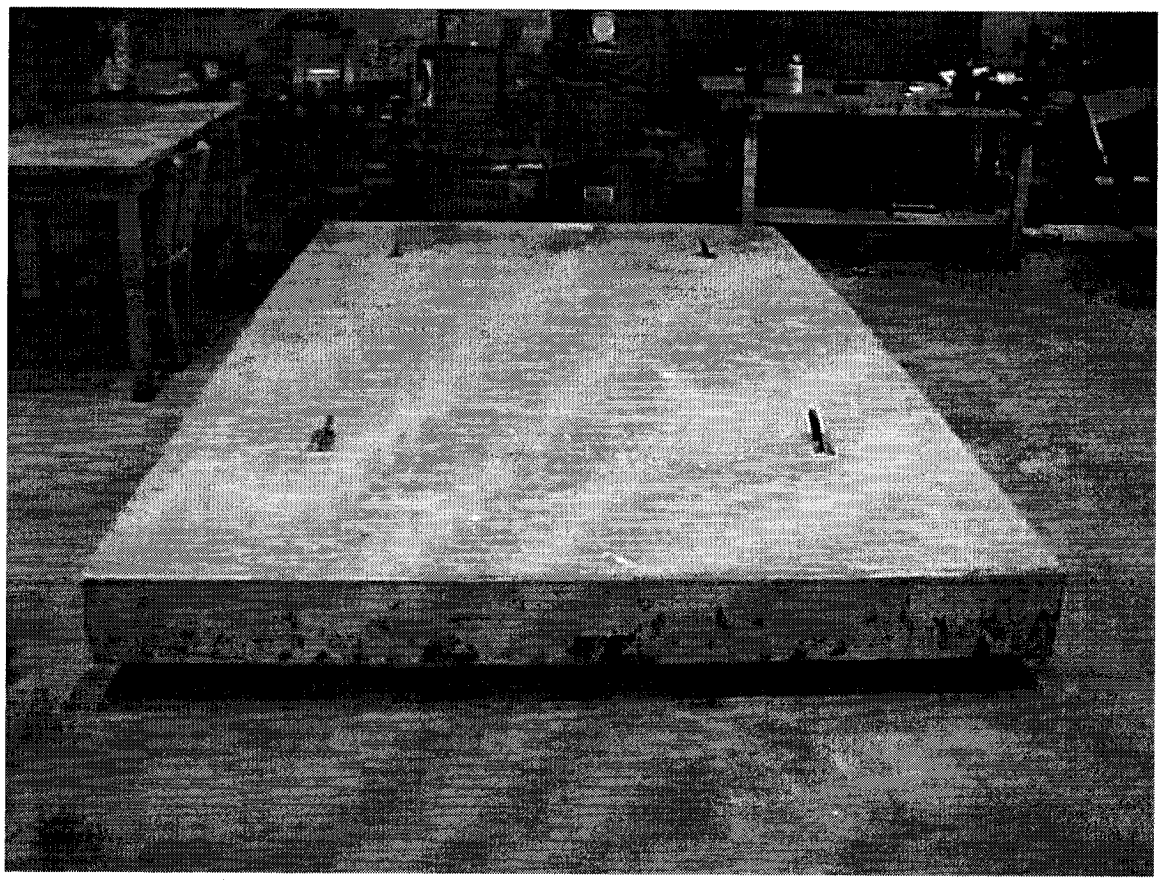

Figure 3.1 Photo of full scale slab specimen

The full scale deck slabs have been given designations in order to aid in their identification during the experimental program and also in the presentation of the results. The slabs have been designated 1 through 6. Table 3.1 below indicates the test configuration for these slabs. Figure 3.2 indicates diagrammatically the applied loading scheme for this series of tests.

Test Number	Deck Slab Number	Date Tested	Shear Span a (m)	Shear Span b (m)	Remarks
1	1	June 14/02	1.22	1.22	Loading at midspan
2	2	July 12/02	1.22	1.22	Loading at midspan
3	6	Aug. 29/02	1.22	1.22	Slab inverted
4	5	Sept. 26/02	0.92	1.52	Loading at 3/8 span
5 a	4	Oct. 28/02	0.61	1.83	Loading at ¼ span
5 b	4	Oct. 30/02	0.61	1.83	Loading at ¼ span
6	3	Nov. 1/02	0.92	1.52	Loading at 3/8 span

* Test terminated prior to failure and slab reused in test 5b.

Table 3.1 Summary of Experimental Test Program

3.2 Test Set Up

The slabs were individually placed in the load frame and static load tested to first cracking and then to ultimate capacity. Figure 3.3 indicates the load frame configuration for this series of tests. It should be noted that once the load frame was set up and configured, only the placement of the slabs and its supports varied from test to test. Calculations were performed to determine the capacity and safety of the load frame at large loads. It was decided to limit the applied loading to 227,000 kg (500,000 lb.).

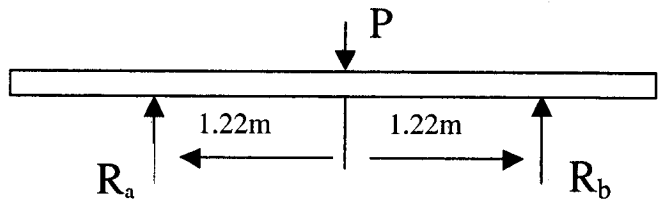

Test No. 1 and 2

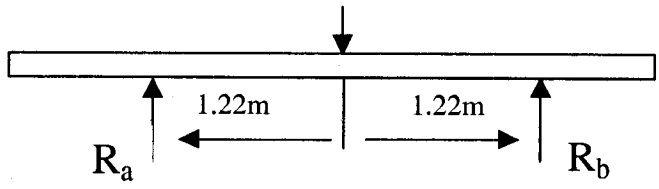

Test No. 3 (Slab Invented)

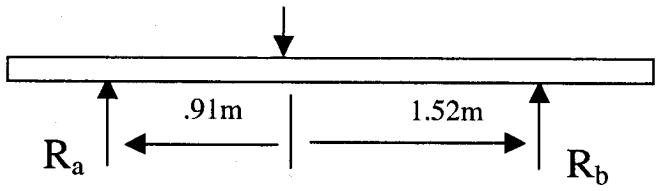

Test No. 4

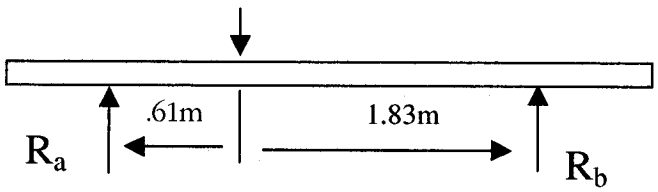

Test No. 5(a)

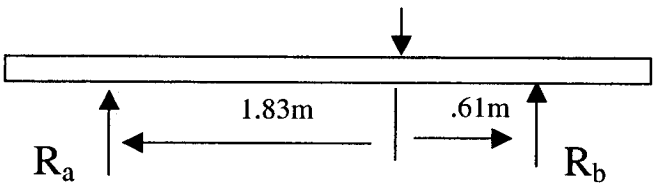

Test No. 5(b)

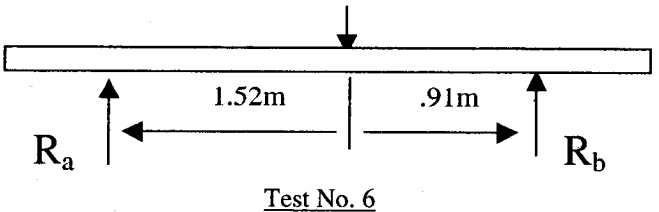

Test No. 6

Figure 3.2 Diagram of applied loading schemes

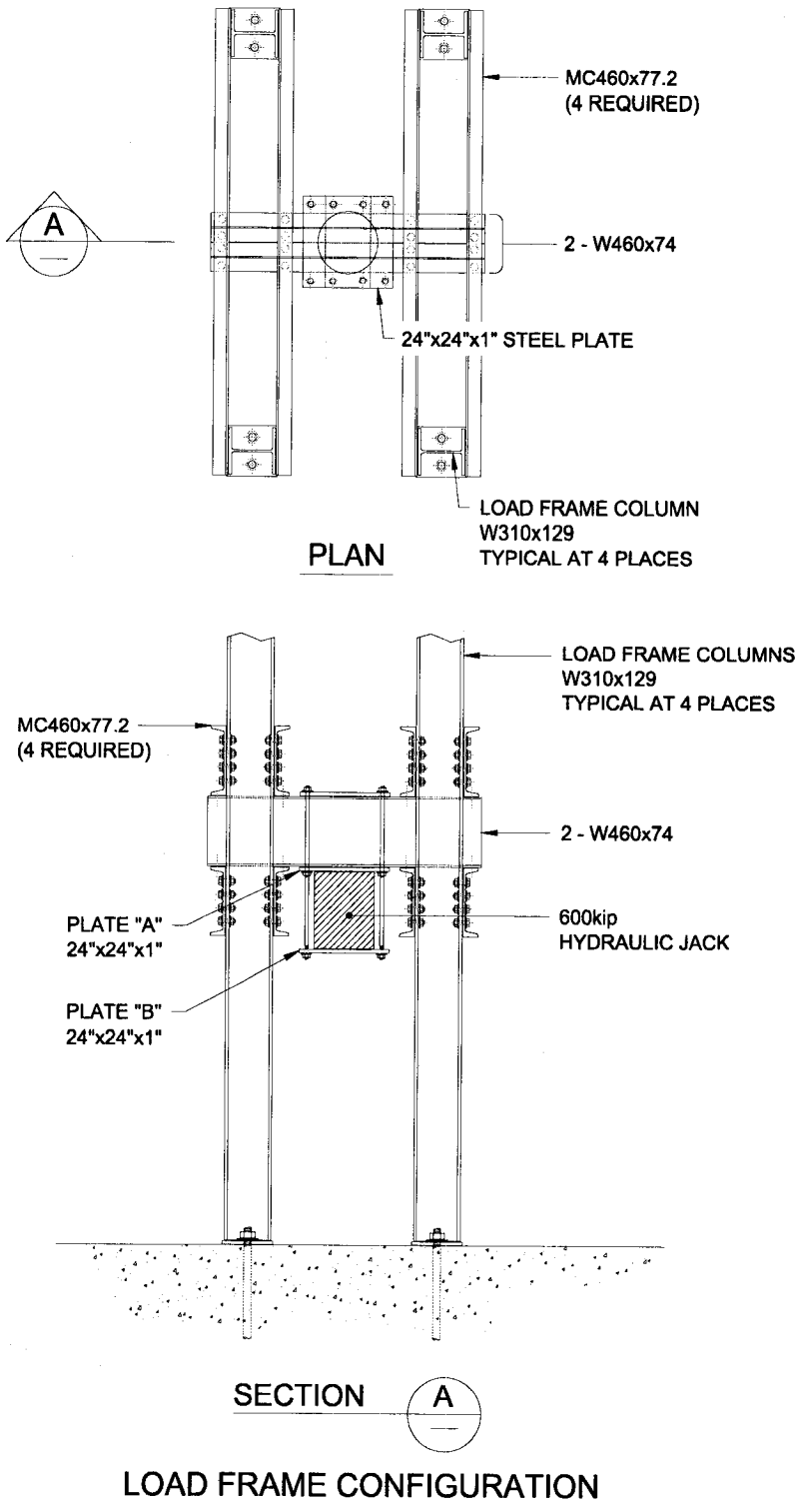

Figure 3.3 Schematic of load frame (N.T.S.)

Figure 3.4 Photo showing load frame configuration.
Note stored slabs for testing in upper right hand corner.

Each slab was simply supported on a 2.44 m (8 ft.- 0 in.) span by two WWF 700 x 175 beams. In addition, the loading was applied to the slabs through a single 273,000 kg (600 kip) hydraulic jack and then through a single WWF 700 x 175 spreader beam. Neoprene strips 13 mm (½ in.) thick were placed between the slabs and support beams and the slabs and spreader beams See Figure 3.6 for details. The neoprene between the slab and spreader beam was 30 mm (12 in.) wide, while the neoprene between the underside of the slab and the support beams was 10 mm (4 in.) wide.

3.3 Set Up for Test Number 1 and 2

Test set up number 1 is shown in Figure 3.5. In this set up, deck slabs 1 and 2 were loaded in such a way that a concentrated strip loading was applied at mid span of the two slabs. Both slabs were tested in the upright position.

Loading was applied in increments of approximately 2,000 kg (4,400 lb.) until first cracking was reached. Crack propagation as well as load level to that point was marked on the slabs. Loading continued after first cracking, in increments of 10,000 kg (22,000 lb.) until ultimate capacity was reached. See Figure 3.6 for typical test set up details.

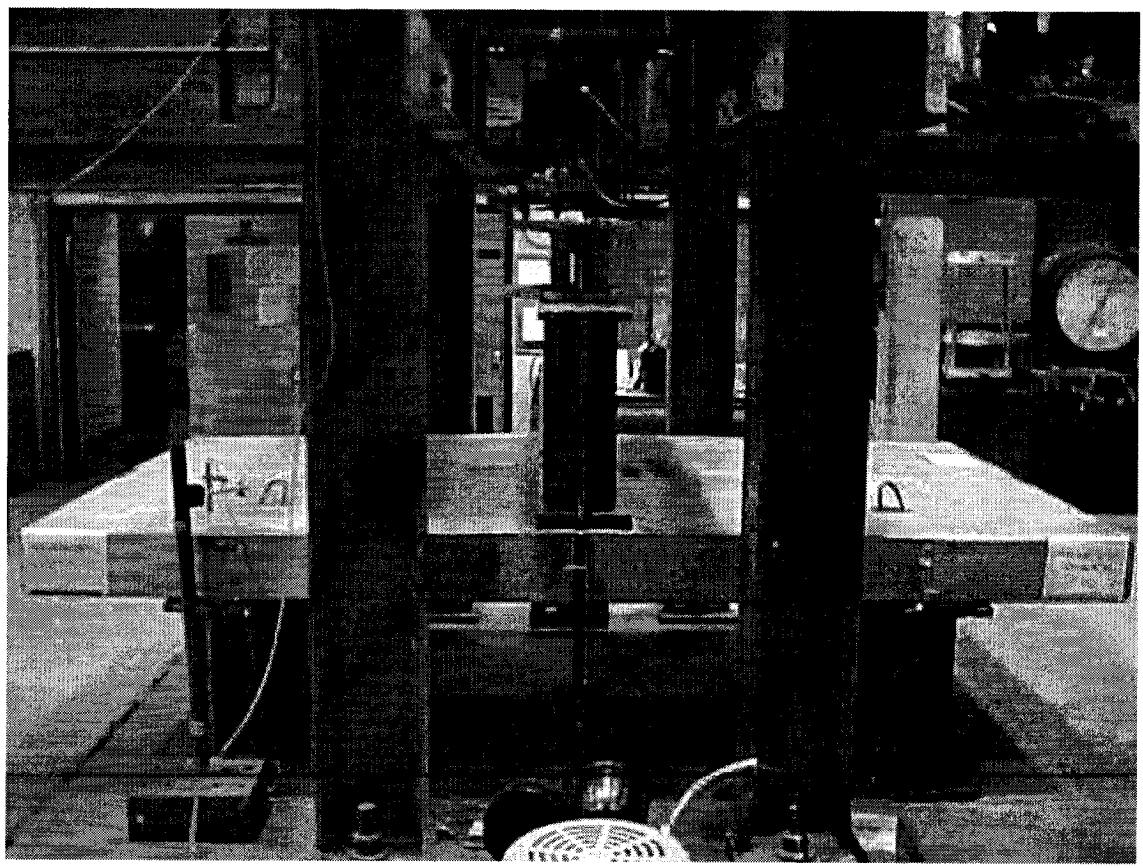

Figure 3.5 Photo showing set up for tests number 1 and 2.

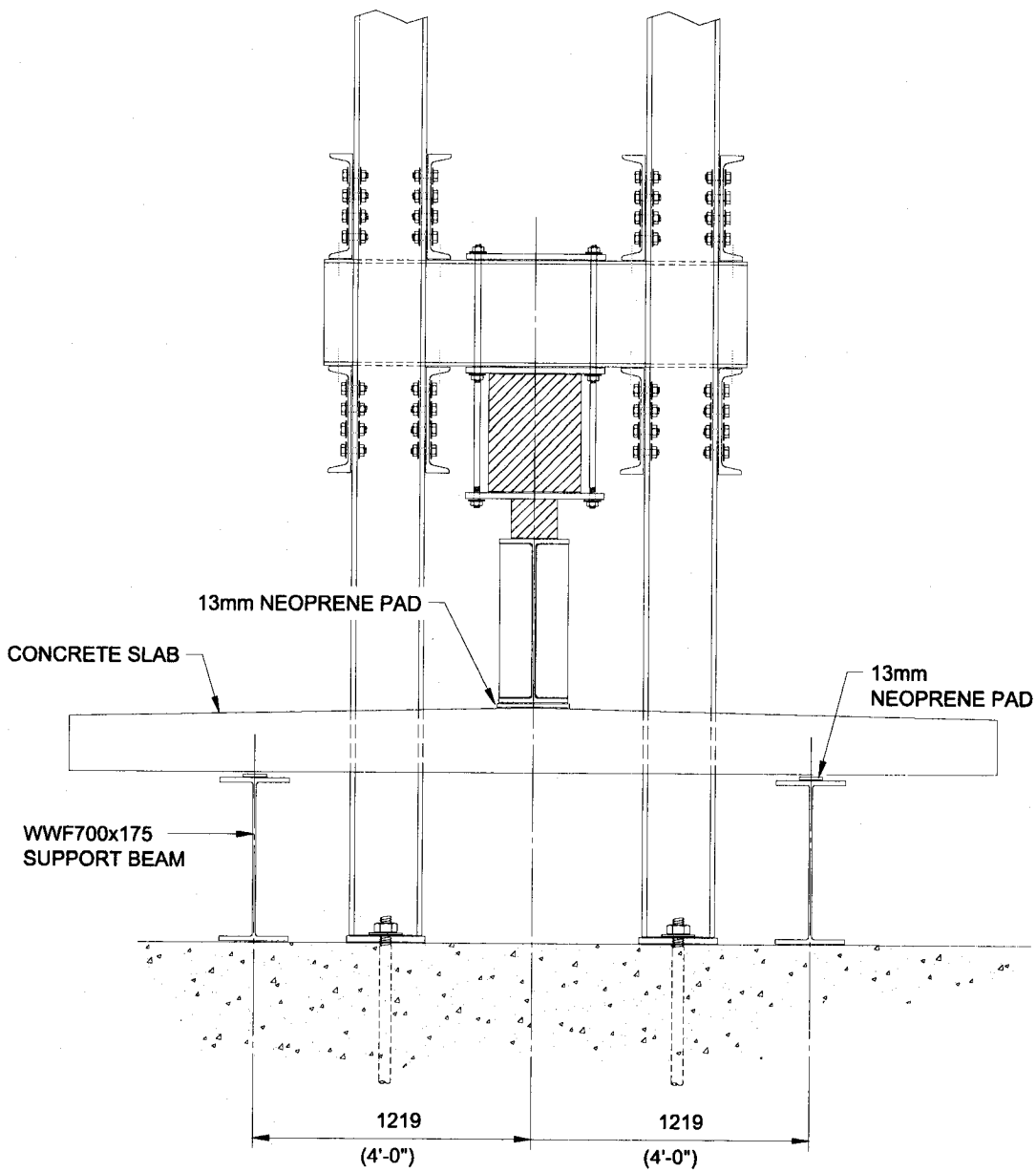

Figure 3.6 Schematic of test configuration for tests 1 and 2 (N.T.S.)

3.4 Set Up for Test Number 3

An inverted slab, deck slab number 6, was loaded at midspan, in increments of 2,000 kg (4,400 lb.) until first cracking was reached. Loading continued thereafter in 10,000 kg (22,000 lb.) increments until the slabs ultimate capacity was reached. See Figure 3.8 for this test set up. Throughout the loading procedure crack propagation and load level were recorded on the slab. See Figure 3.7 for typical test details.

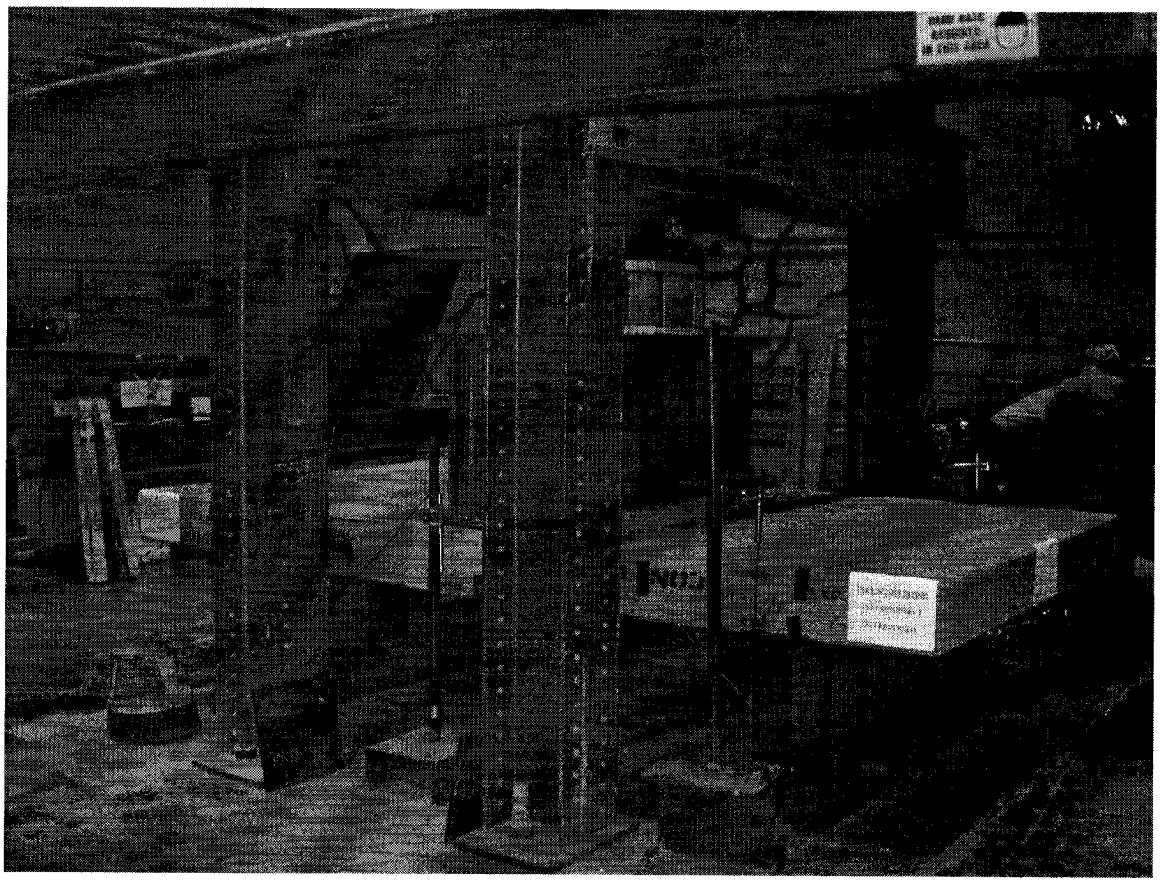

Figure 3.7 Photo of set up for test number 3 on inverted slab

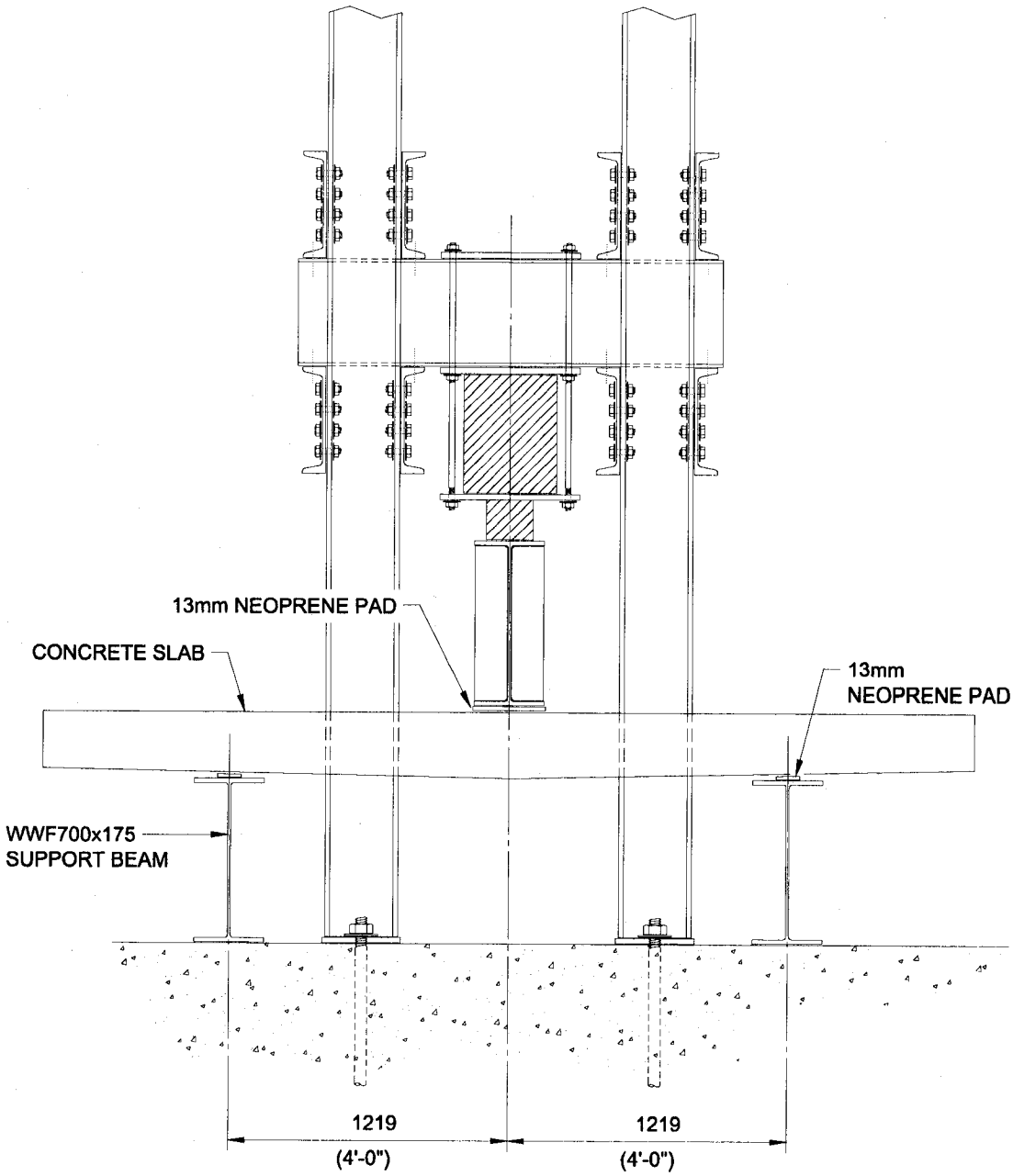

Figure 3.8 Schematic of test configuration for test number 3. (N.T.S.)

3.5 Set Up for Test Number 4 and 6

Two deck slabs, number 3 and number-5, were loaded at shear span a = 910 mm (3 ft.). See Figure 3.10 for layout configuration. Loading was in increments of 2,000 kg (4,400 lb.) until first cracking was reached. Loading continued thereafter in 10,000 kg (22,000 lb.) increments until ultimate capacity was reached. Throughout the loading procedure, both crack propagation and load level were recorded on the slabs. See Figures 3.9 for typical test set up details.

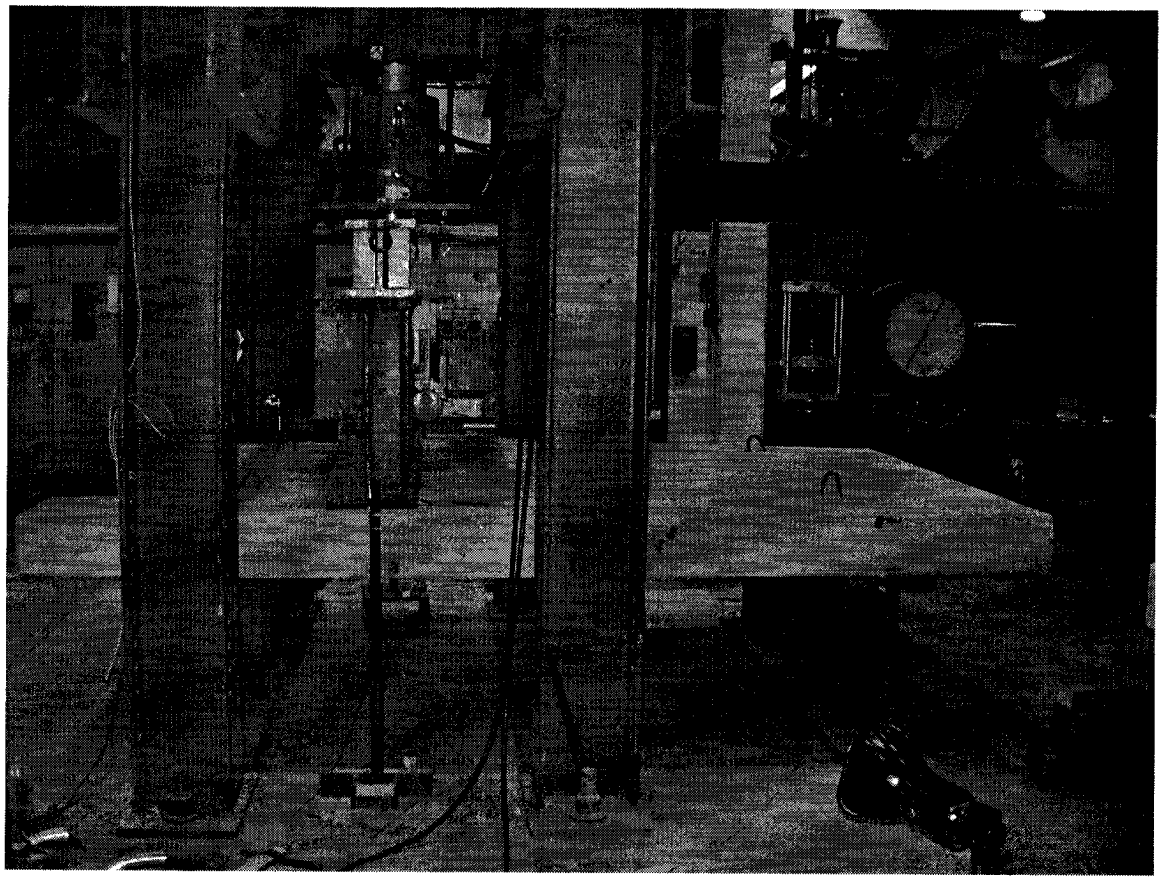

Figure 3.9 Photo showing set up for test number 4 and 6

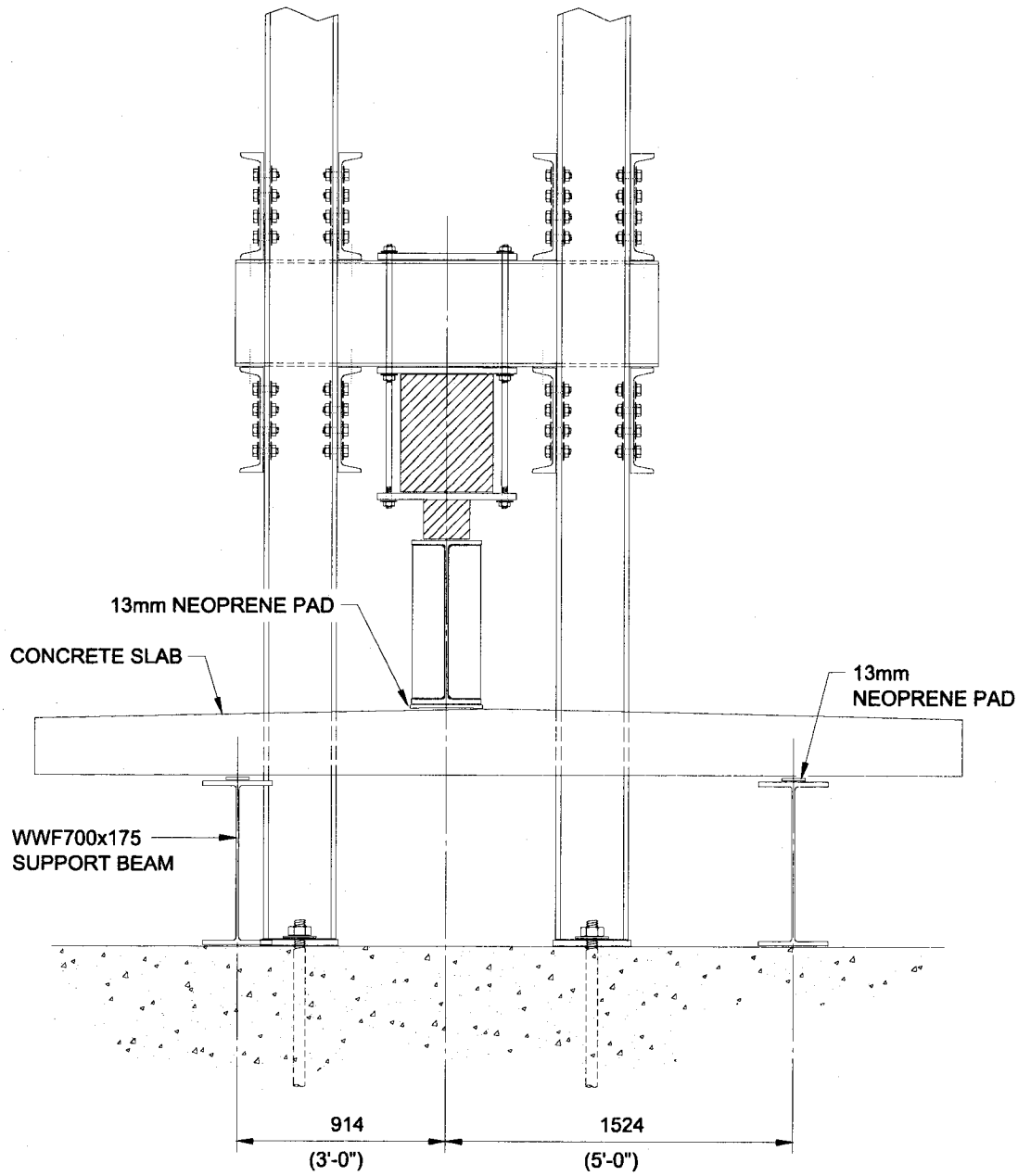

Figure 3.10 Schematic of test configuration for tests 4 and 6 (N.T.S.)

3.6 Set Up for Test Number 5a

Deck slab number 4 was loaded at shear span a = 610 mm (2 ft.), equivalent to ¼ span, in increments of 2,000 kg (4,400 lb.) until first cracking was reached. Loading continued in 10,000 kg (22,000 lb.) increments until a load of 195,000 kg (429,000 lb.) was reached at which time the test was terminated. Throughout the loading procedure, crack propagation and load level were recorded on the slab. See Figure 3.11 for typical test set up details and Figures 3.12 for the test configuration.

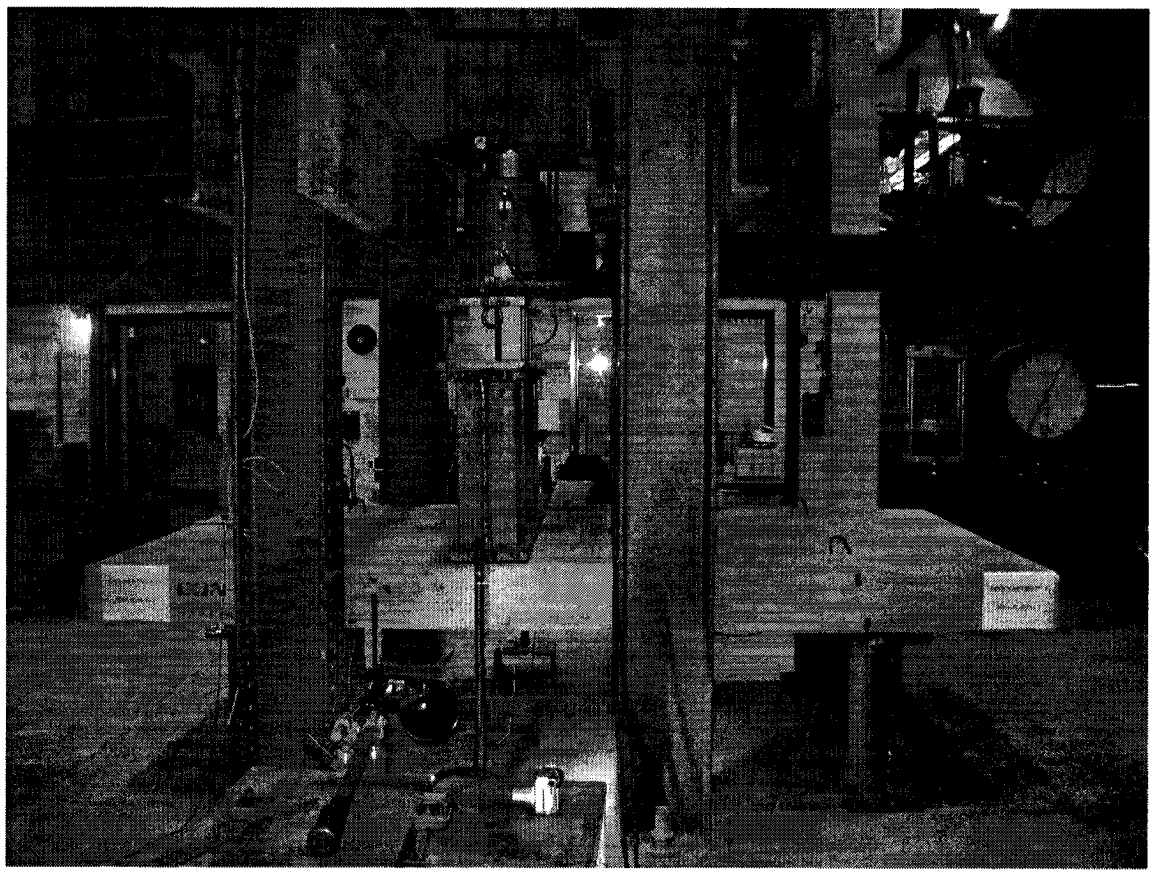

Figure 3.11 Photo showing set up for test number 5a.
Note hydraulic jack and load cell at top center and hand pump in foreground.

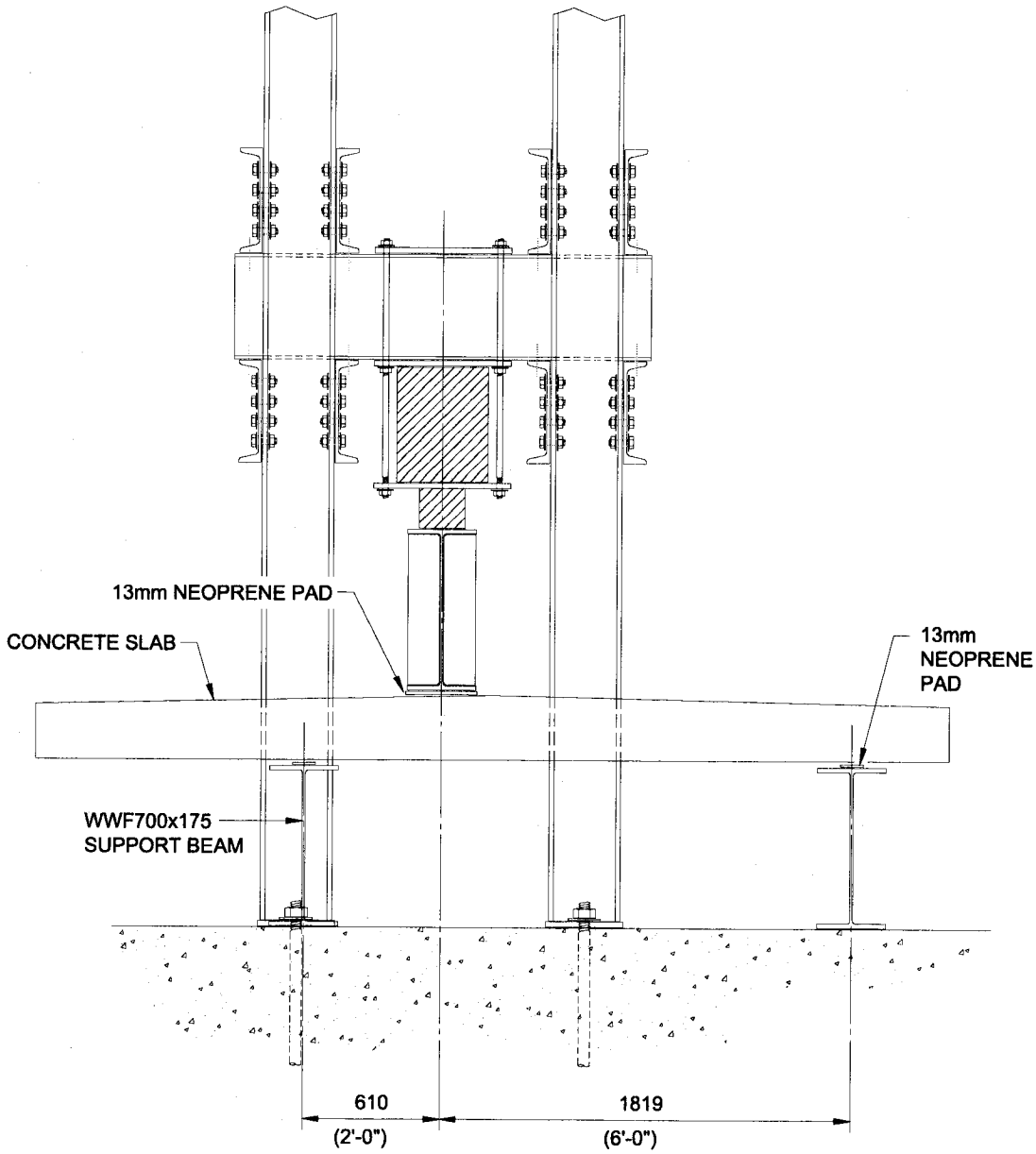

Figure 3.12 Schematic of test configuration for test 5a (N.T.S.)

3.7 Set Up for Test Number 5b

Deck slab number 4 used in test 5a, was loaded at shear span a = 610 mm (2 ft.), equivalent to ¼ span, but instead of the shear span being located on the right hand side, it was now located on the left hand side. Load was applied in increments of 2,000 kg (4,400 lb.) until first cracking was reached. Loading thereafter continued in 10,000 kg (22,000 lb.) increments until ultimate capacity was reached. Throughout the loading procedure, crack propagation and load levels were recorded on the slab. See Figure 3.13 for the test set up details and Figure 3.14 for test configuration details.

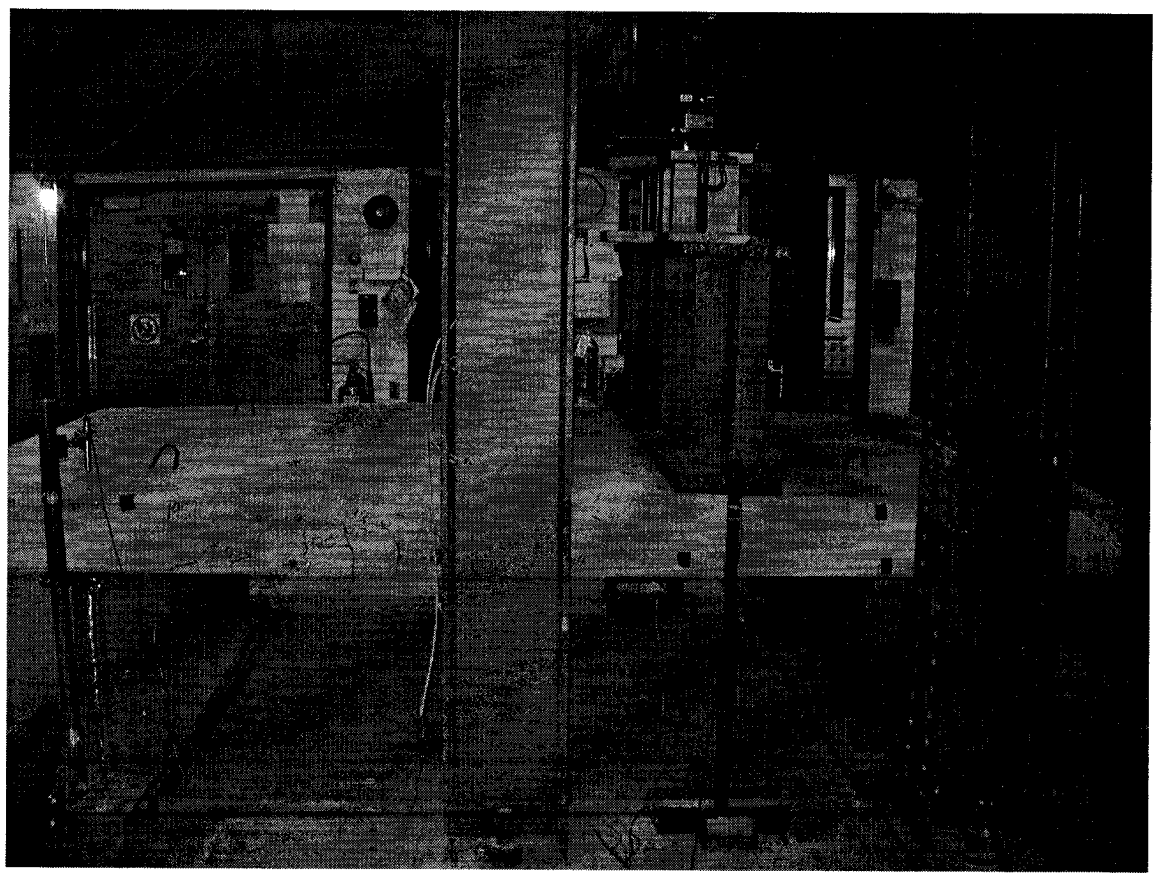

Figure 3.13 Photo showing set up for test number 5b.
Note cracking pattern marked on slab from test number 5a

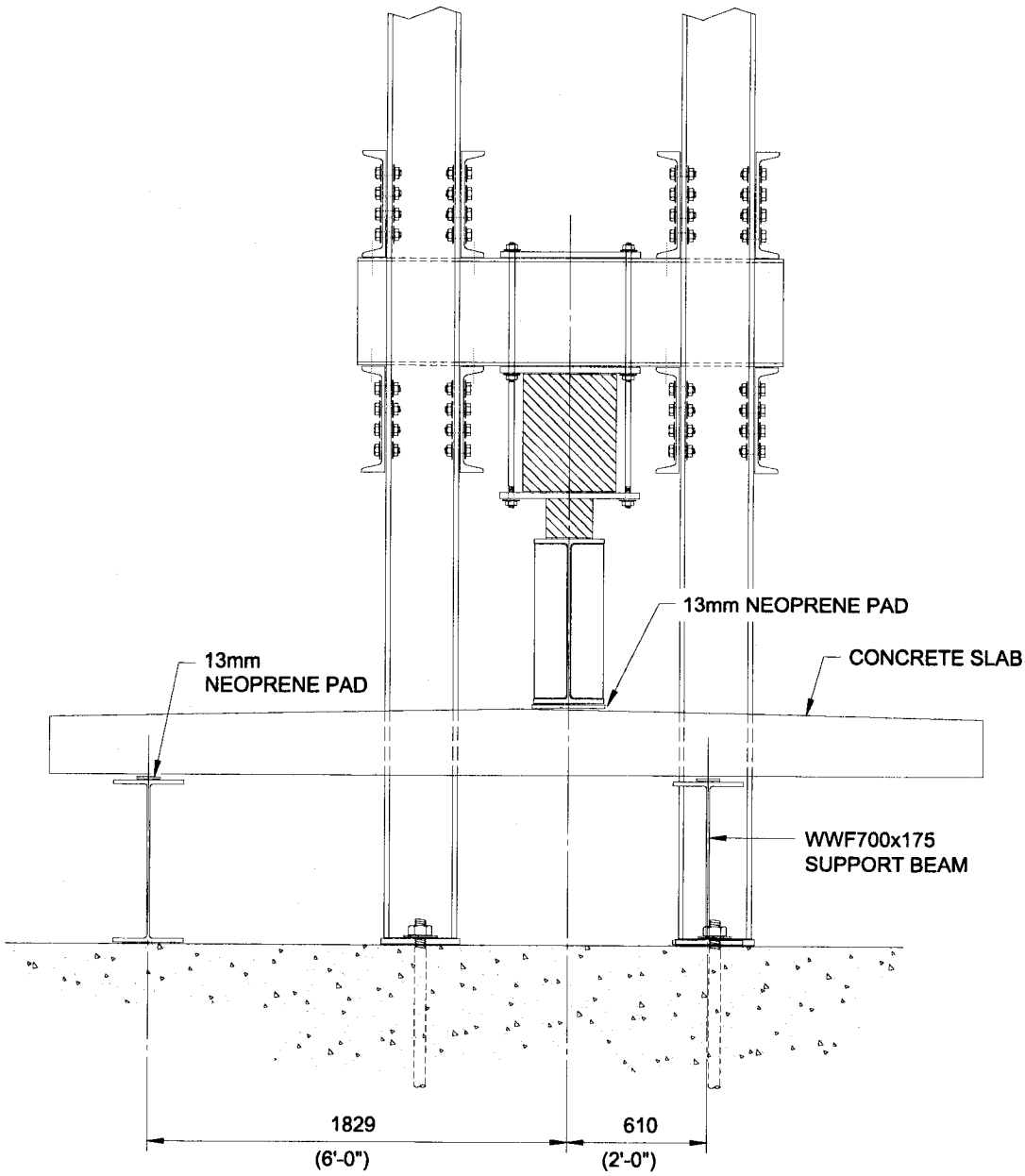

Figure3.14 Schematic of test configuration for test 5b (N.T.S.)

3.8 Instrumentation

All deck slabs were loaded using a Tempelton Kenly Pine Model RJ-300-6-5713000 hydraulic jack, with a capacity of 273,000 kg (600 kips) at a 45.3 MPa (6,575 psi) operating pressure and a 150 mm (6 in.) stroke and 225 mm (9 in.) diameter cylinder. The hydraulic jack was powered by a Tempelton Kenley Pine Force-Pak® hydraulic auxiliary hand pump, model PRE 88, with a 68.9 MPa (10,000 psi) maximum operating pressure rating and a reservoir capacity of 14.9 x10^6 mm^3 (910 $in.^3$). It was equipped with two speed outputs.

Directly above the hydraulic cylinder was a K Toyo Model 296 W - 300000 compression load cell with a rated capacity of 300,000 kg (660 kips) and a safety factor of 1.5. The rated output was 2 millivolts, with an excitation of 10 volts and an input/output resistance of 700 ohms.

The short term surface strains were obtained by application of 120 ohm electrical resistance strain gauges from Intertechnology, model CAE-XX-500UW-120. These gauges had a gauge length of 50 mm (2 in.) and a gauge factor of 2.1. The strain gauge material consisted of a sensing alloy of copper-nickel on a polymide backing. The strain gauges were applied as shown in Figure 3.15. Strain gauge rosettes were also applied to some of the slabs as detailed in Table 3.2 below. Note that in table 3.2, LHS and RHS are abbreviations for left hand side and right hand side respectively.

Test Number	Front Shear Span (a)	Front Shear Span (b)	Rear Shear Span (a)	Rear Shear Span (b)
4	RHS			LHS
5a		RHS	LHS	
5b		LHS	RHS	
6	LHS			RHS

Table 3.2 Location of Strain Gauge Rosettes (as seen facing the front of the slab)

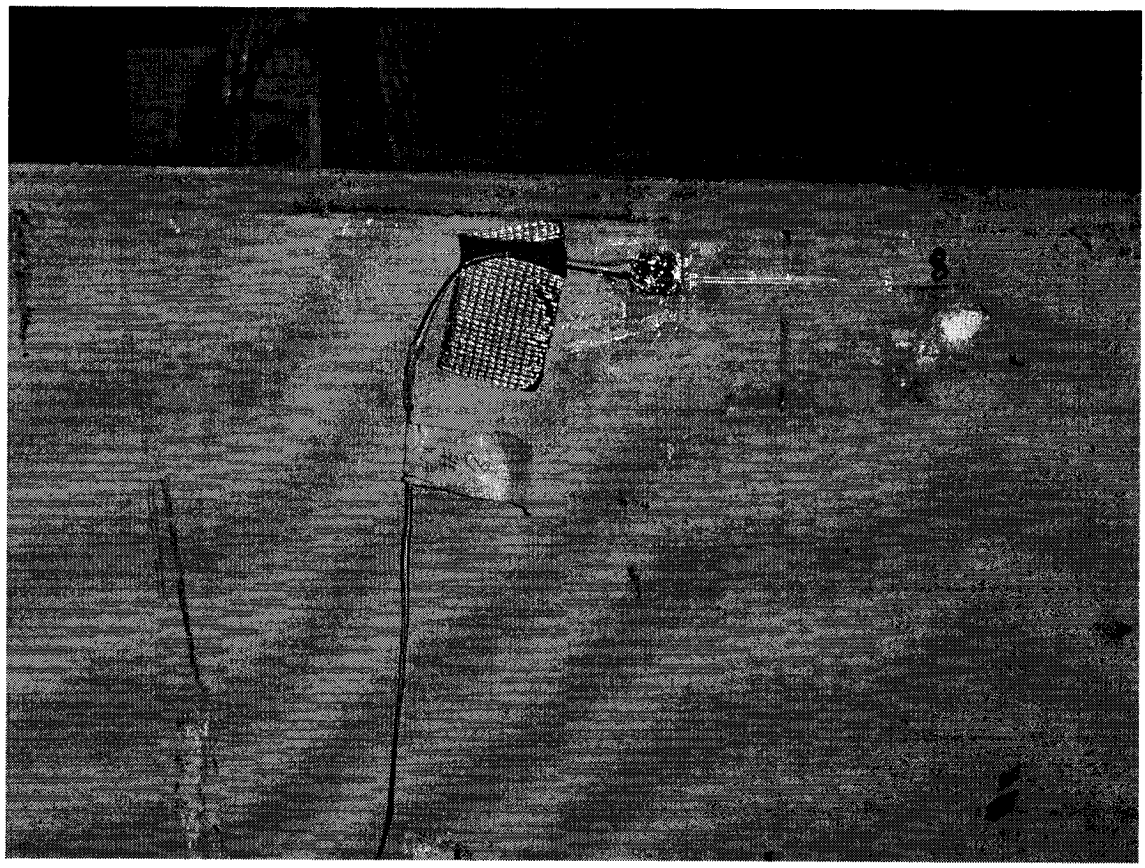

Figure 3.15 Typical strain gauge placement on side of concrete slab.

Slab displacements were measured by the use of linear velocity displacement transducers (LVDT's). Two Sangamo Schlumberger LVDT's, model DCR 150, were placed at either end of the spreader beam, directly under the load application points. These LVDT's had a

travel of ± 150 mm (± 6 in.). Two Sangamo Schlumbereger LVDT's, model DCR50, were also applied over the supports on one side of the slab. These LVDT's had a travel of ± 50 mm (± 2 in.).

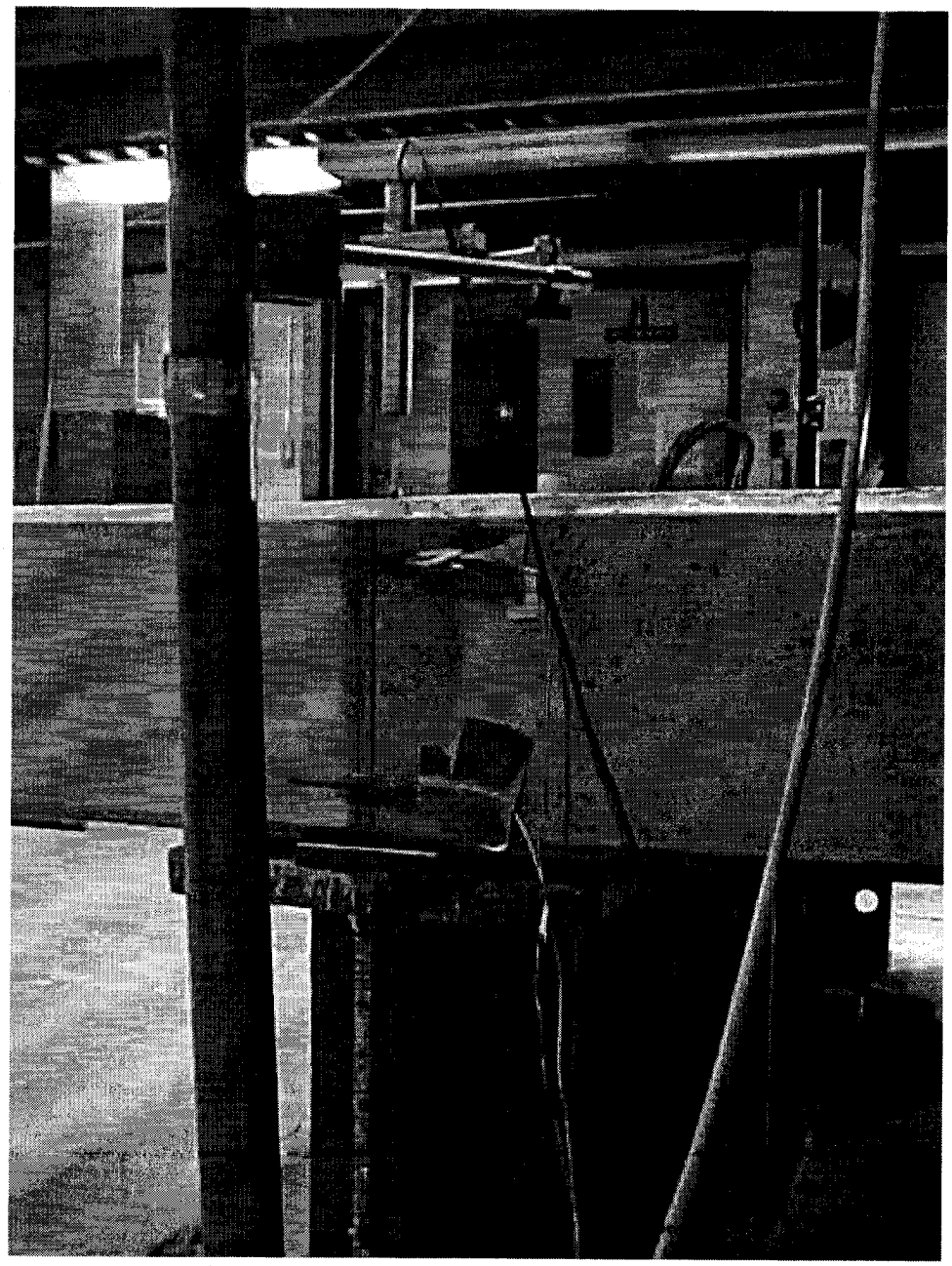

Figure 3.16 Photo showing LVDT placement at slab support location

The LVDT's were attached to pedestals which sat on the structural floor and were not attached to any part of the load frame. This was done to isolate them from any movement which might occur in the load frame during testing. See figures 3.16 and 3.17 for typical attachment details of the LVDT's at the supports.

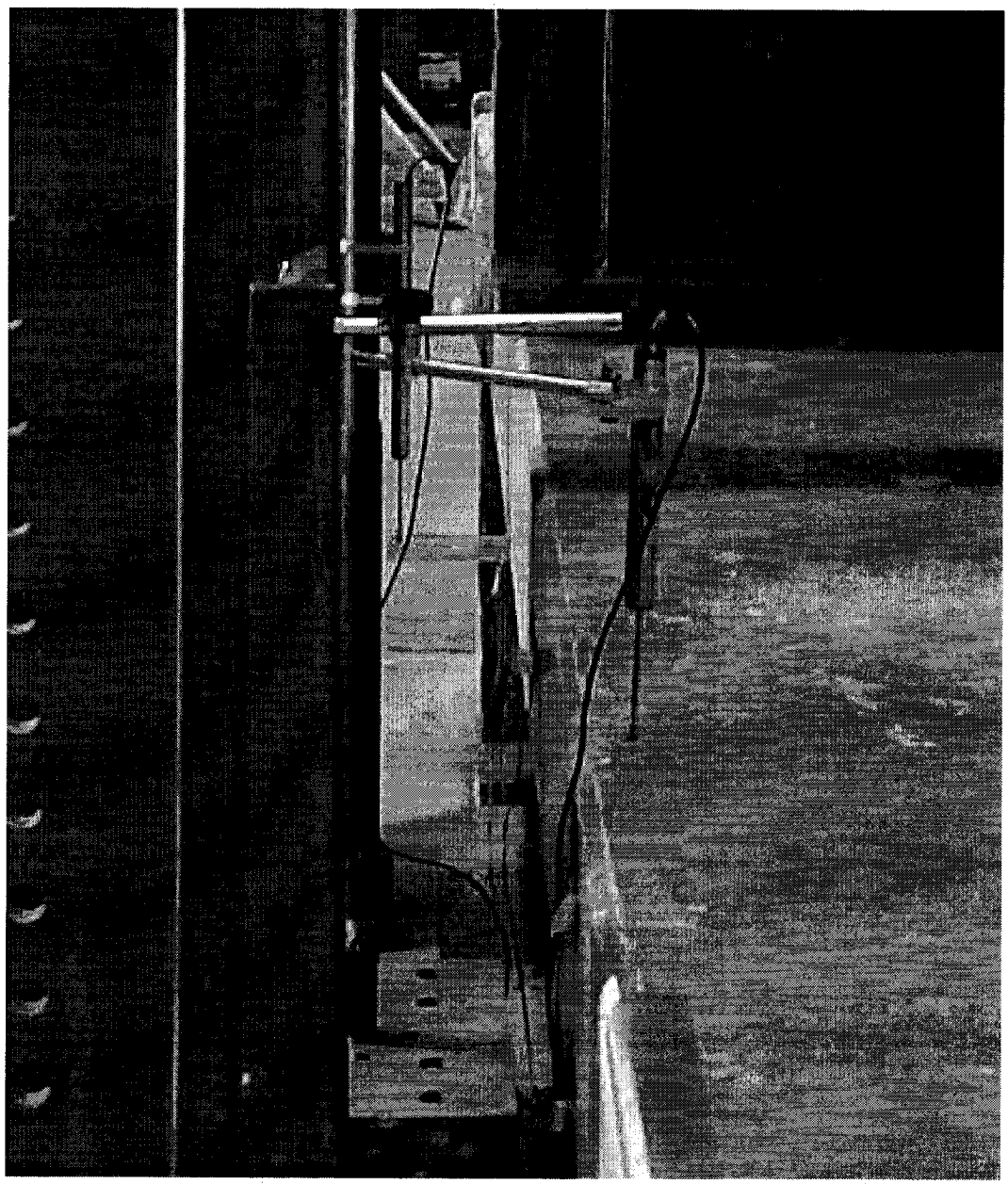

Figure 3.17 Photo showing placement of LVDT over support. Note placement of the center LVDT in the background.

The LVDT's used to measure displacement at the load application point, used a 50 mm by 150 mm (2 in. by 6 in.) strip of plexiglass glued to the underside of the slab at each end, from which the LVDT's could reference. See Figure 3.18 for details of LVDT placement under point of loading. The LVDT's above the support were in direct contact with the top of the slab at the centerline location of the deck slab supports.

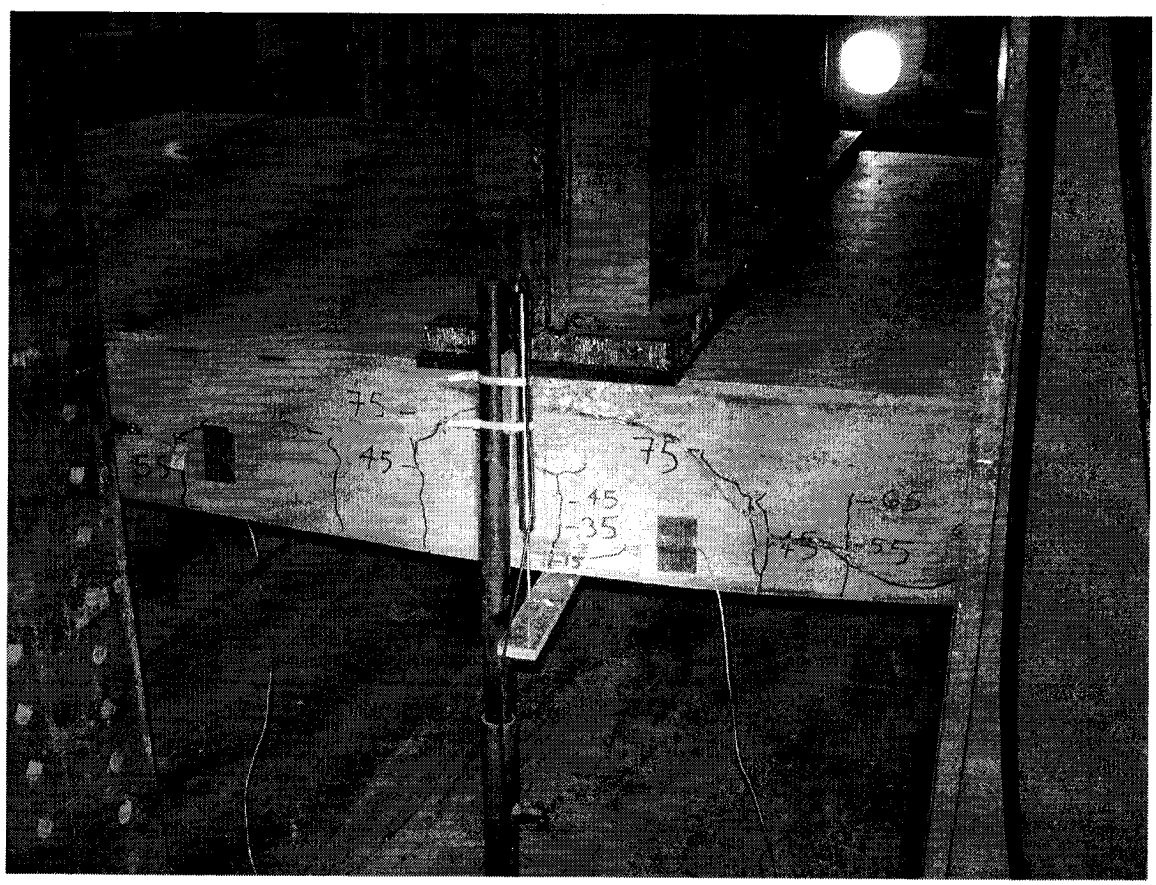

Figure 3.18 Photo showing placement of LVDT at load application point. Note Plexiglas glued to underside of slab

The load cell, strain gauges and LVDT's were all connected to a 20 channel, Vishay Measurements Group, System 5000 data acquisition scanner unit (DAU). The system 5000 hardware used the StrainSmart® Software to measure strain, displacement and force. See Figure 3.19 for details.

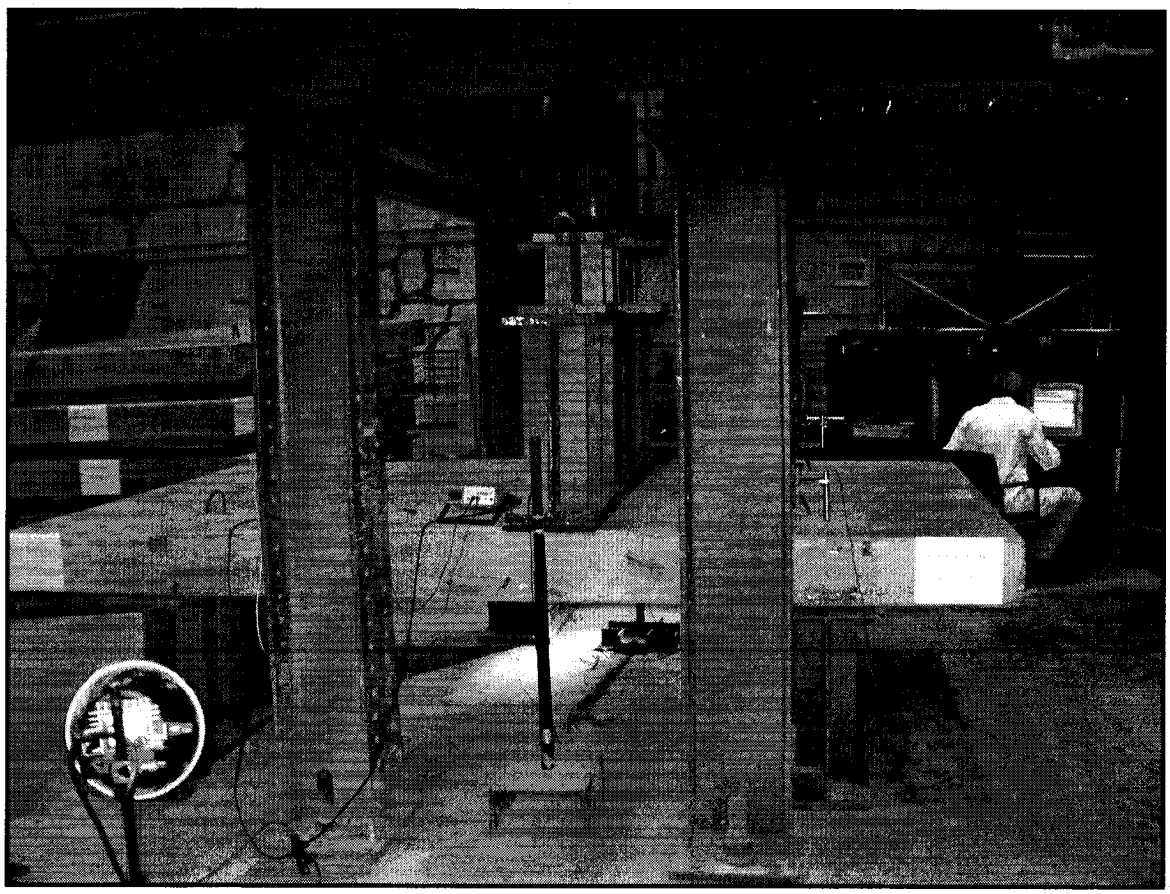

**Figure 3.19 View of load frame from back with slab positioned.
Note LVDT located above slab support on right hand side.
Also note data acquisition unit and PC monitor in background.**

A total of 15 channels were available for the load cell and strain gauge connections and 5 channels available for LVDT connections. The System 5000 data acquisition unit was connected to a PC for real time data display, retrieval and storage. The software is designed to function with a variety of measurement sensors, but also takes into account

such parameters as temperature, leadwire resistance, inherent nonlinearalities in the Wheatstone bridge circuit and other such sources of potential errors which could affect the test results.

The average test time was between 2½ to 3 hours. This resulted in load application rates of 590 kg/min. to 1,300 kg/min. (1,300 lb./min to 2,860 lb./min).

3.9 Precision

The StrainSmart® software can be set to the desired level of precision required depending on the quantity being measured. For the purpose of this experimental program, measurement were taken in the SI units and preset to the following levels:

- loading in kg. was measured to the nearest kg.
- strain was measured to nearest microstrain (με) and
- deflection was measured to the nearest 0.1mm.

Immediately prior to each test the strain gauges and LVDT's were "zeroed".

CHAPTER 4

Analysis of Results

4.1 Test Schedule

Testing was carried out over a period of approximately 6 months. Table 4.1 indicates the test schedule as well as the test configuration. By the time testing commenced, all slabs were at least 100 days old.

Test Number	Deck Slab Number	Date Tested	Shear Span a (m)	Shear Span b (m)
1	1	June 14/02	1.22	1.22
2	2	July 12/02	1.22	1.22
3	6**	Aug. 29/02	1.22	1.22
4	5	Sep. 26/02	0.91	1.53
5 a	4*	Oct. 28/02	0.61	1.83
5 b	4	Oct. 30/02	0.61	1.83
6	3	Nov. 1/02	0.91	1.53

* Test terminated prior to failure
** Slab inverted

Table 4.1 Summary of Experimental Tests

4.2 Compressive Strength:

The only know variable between any of the slab specimens was the compressive strength of the concrete fc′ which varied from 80 to nearly 100 MPa (11,600 to 14,000 psi). This was primarily because the slabs were cast in pairs. All slabs exhibited compressive strengths that exceeded the specified minimum compressive strength of 70 MPa (10,200 psi). The minimum compressive strength at release was specified as 35 MPa (5,100 psi).

Table 4.2 below indicates the compressive strength of the slabs versus age at specified times after poring including the day of slab testing. It should be noted that all cylinder tests were performed at the Con-Force facility in Winnipeg and the results provided to CN for this project.

Deck Slab Number	Specified fc' (MPa)	At Release (16 hours) (MPa)	At 7 Days MPa)	At 28 Days (MPa)	At 56 Days (MPa)	At Time of Test MPa)
1 and 2	70	36.4	49.9	71.3	76.8	79.9
3 and 4	70	47.5	55.8	78.6	82.9	89.6
5 and 6	70	47.1	63.5	88.8	92.1	98.6
Average	70	43.7	56.4	79.6	83.9	89.4

Table 4.2 Summary of Concrete Compressive Strengths (MPa)

The development of the compressive strength over time is shown in Figure 4.3. Clearly it can be seen that all six slabs exhibited similar strength gains, but not identical strengths. This is evidenced by the parallel nature of the lines in the graph. Also interesting to note is that on average there was roughly a 5% increase in the compressive strength of the concrete past the 56 day strength. Although purely coincidental, to the nearest MPa, the concrete compressive strengths of the slabs tested were 80, 90 and 100 MPa (11,600, 13,100 and 14,500 psi).

Age in days was plotted against the ratio of $\frac{cylinder\ strength}{cylinder\ strength\ at\ 28 days}$ and is shown in Figure 4.4. From this graph it can be seen that up to the 28 day strength the slabs experienced similar percentage increases in strength, however after the 28 day mark the slabs experienced dissimilar increase in strength rates.

The concrete displayed good workmanship. All the concrete failure planes were seen to be through the aggregate, as is normal for high strength concretes and is discussed in Appendix A. Figure 4.1 indicates a typical fracture surface. The sample shown was from one of the tests and is approximately 100 mm by 450 mm (4 in. by 18 in.).

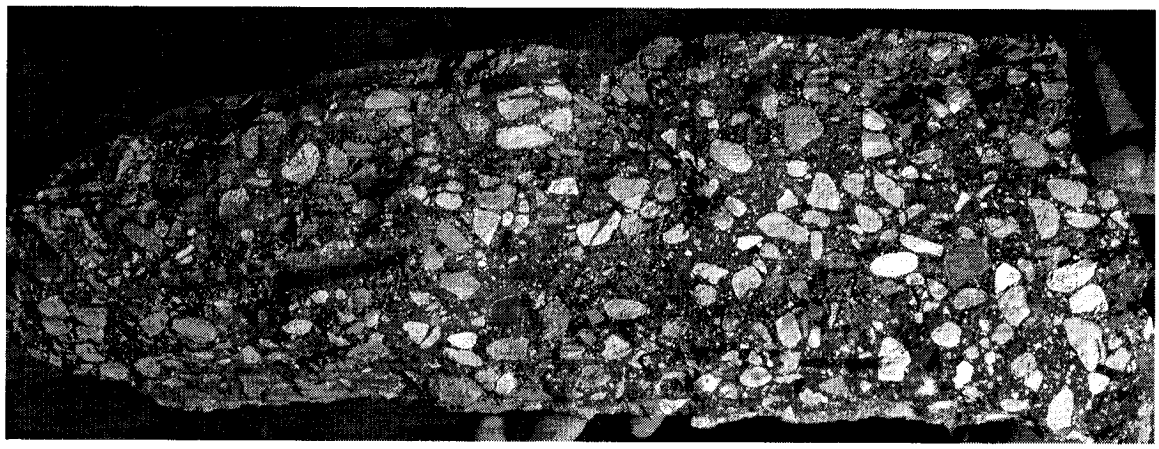

Figure 4.1 Fracture surface of high strength–high performance concrete

According to Collins and Mitchell [1987] if only the cylinder strengths of the concrete are known, those values can be used to determine the initial tangent modulus of elasticity. The initial tangent modulus can be determined reasonably accurately by use of the following equation:

$$E_{ct} = 5500\sqrt{f_c'} \quad \text{in MPa} \qquad 4.1$$

Where E_{ct} is the initial slope of the parabolic stress-strain curve as shown in Figure 4.2. The stress corresponding to f'_C is given by the following:

$$\varepsilon'_C = \frac{2 \times f'_C}{E_{ct}} \qquad 4.2$$

and an approximation of the cracking strength of concrete can be obtained by:

$$f_r = 0.60\lambda\sqrt{f'c} \text{ in MPa} \qquad 4.3$$

Where: f_r = modulus of rupture in MPa

λ = 1.0 for normal density concrete

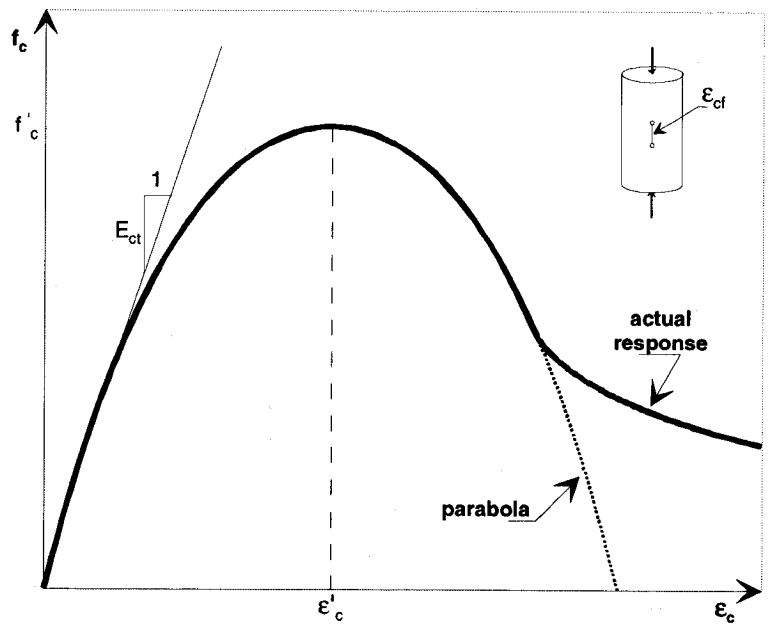

Figure 4.2 Stress-strain relationship for concrete in compression (adopted from Collins and Mitchell)

From the compressive strength of concrete taken at the time of each slab test, various properties for each slab were determined. These properties are listed in Table 4.3 below. From the compressive strength the following were determined based on equations 4.1, 4.2 and 4.3.

Deck Slab Number	f_c' at time of test (MPa)	$\sqrt{f_c'}$ (MPa)	f_r (MPa)	E_c (MPa)	$\mu\varepsilon'_c$ (microstrain)	$n = \frac{E_S}{E_c}$
1 and 2	79.9	8.9	5.3	48,950	326	4.1
3 and 4	89.6	9.5	5.7	52,250	343	3.8
5 and 6	98.6	9.9	5.9	54,450	362	3.7
Ave. All Slabs	89.4	9.4	5.7	51,883	344	3.9

Table 4.3 Summary of properties related to compressive strength

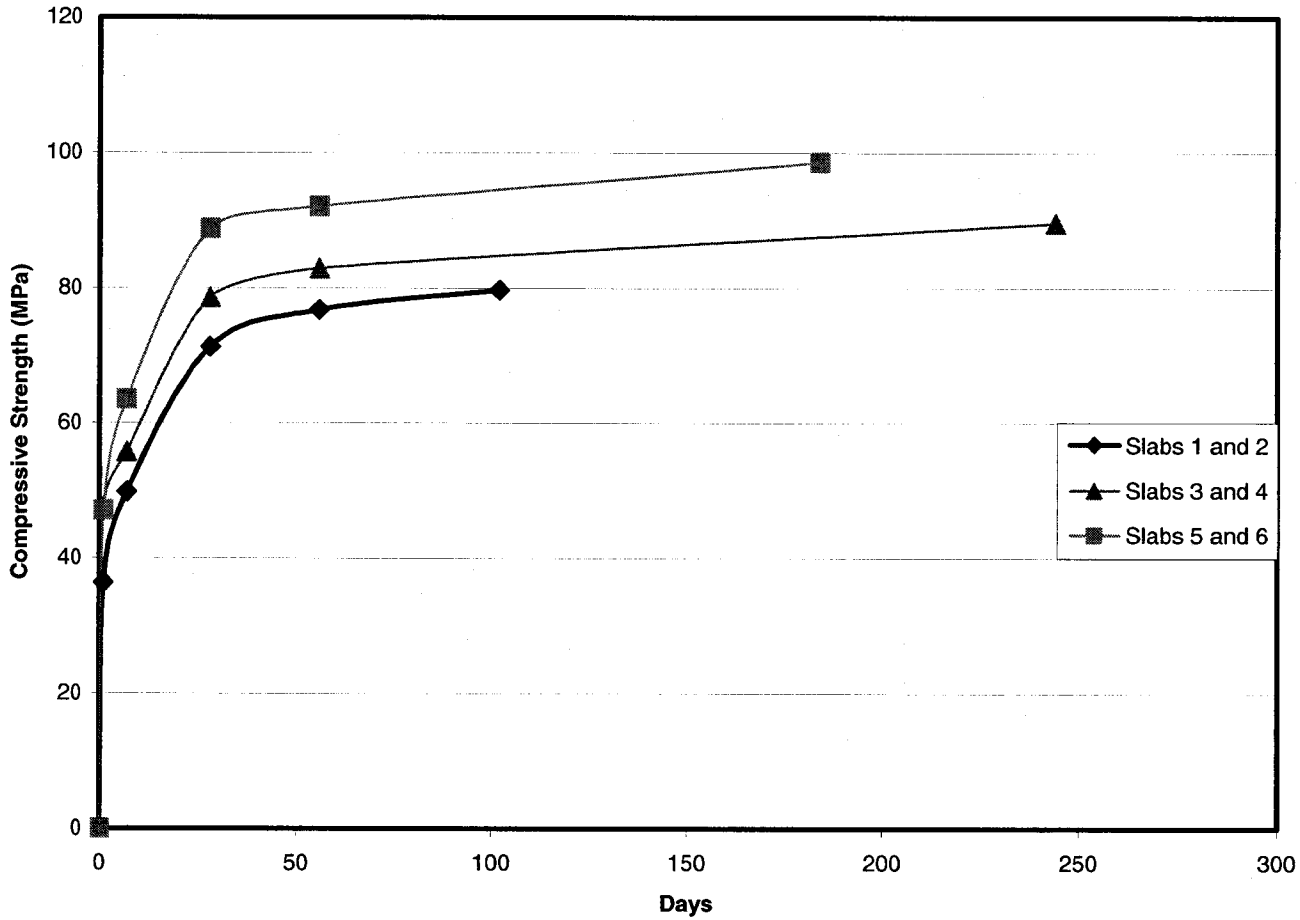

Figure 4.3 Graph of average concrete compressive strengths

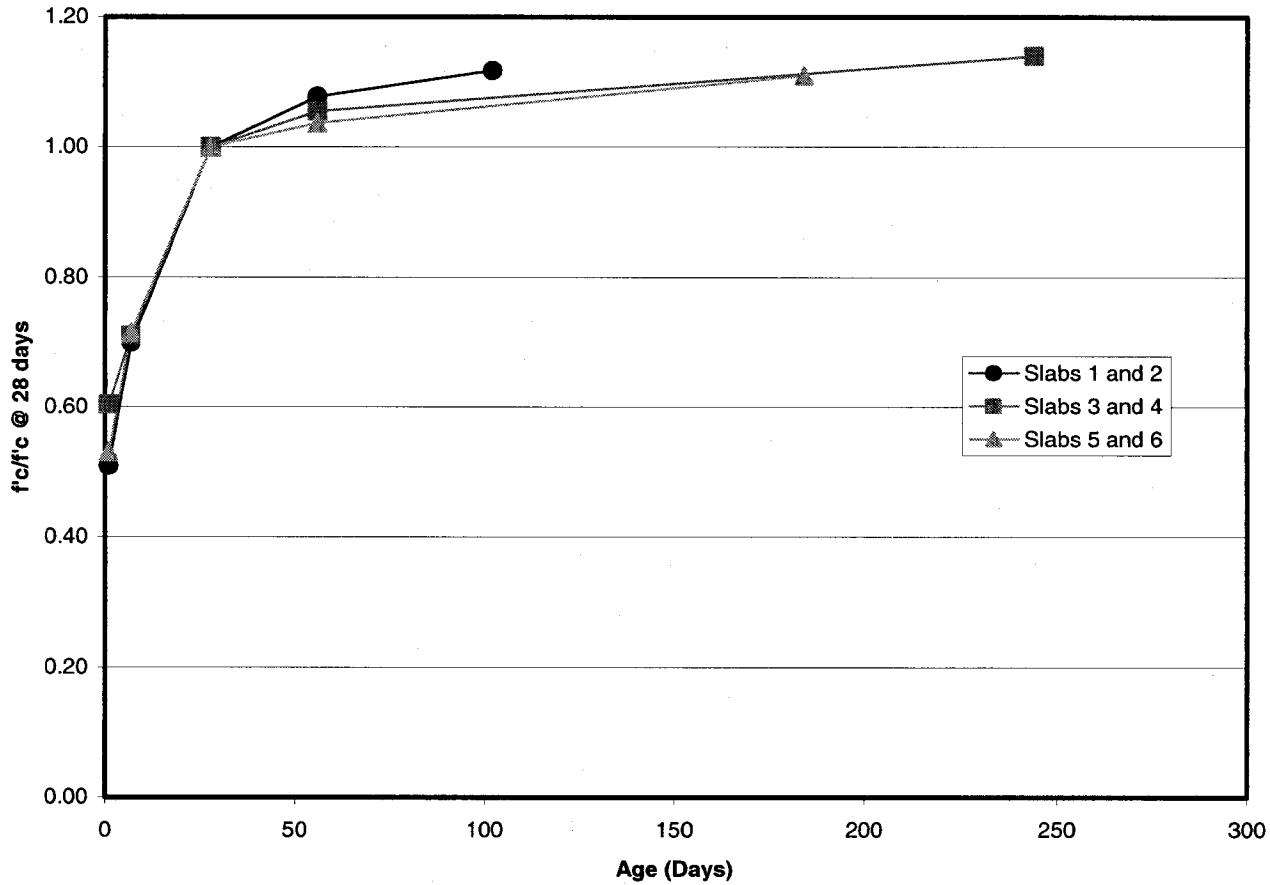

Figure 4.4 Graph of compressive strength gain with time, all slabs.

4.3 Modes of Failure of Slabs

4.3.1 Failure Mode of Slab 1 in Test Number 1

The load was applied to slab number 1 in increments of 20 kN (4,500 lb.) until first flexural cracking was visually detected on the rear face of the slab at a load of 712kN (160,200 lb.). Thereafter, the load was increased and applied in increments of approximately 50 kN (11,250 lb.) until ultimate failure of the slab was reached at 1,678 kN (377,550 lb.). Cracks were monitored and their progression marked from the point of visually detected first cracking up to a load of 1,520 kN (342,000 lb.).

The flexural cracks continued to propagate upwards until about 1,340 kN (301,500 lb.) at which time the cracks closest to the applied load turned inwards towards the centerline of the slab and formed flexural shear cracks.

The first visually detected flexural shear crack was observed in the rear face of the slab at an approximate load of 1,341 kN (301,500 lb.). Flexural shear cracks were visually detected on the front face shortly thereafter at approximately 1,410 kN (317,250 lb.) These cracks were located in the center of the web roughly 480 mm (19 in.) from the center of the applied load. From there the cracks grew quickly at a 45 degree angle and at an applied load of about 1,500 kN (337,000 lb.) these cracks formed into diagonal splitting cracks.

This diagonal splitting progressed across the face of the slab at roughly 25 degrees intersecting some of the flexural shear cracks and culminating in crushing of the concrete

directly under the load application point. Failure was accompanied by a loud explosive noise indicating a sudden release of energy. At the moment of failure the slab underwent an average deflection of 34.5 mm (1.36 in.).

Figure 4.5 below indicates the front face of slab number 1 immediately after failure. A crack at the top of the slab ran from the front face to the rear face just below the left hand side bottom flange of the loading beam. Pieces of broken concrete from this crack can be seen in the picture on the top of the slab. A similar crack ran the length of the underside of the slab at the other end of the 23 degree diagonal splitting crack. Concrete from that crack can be seen on the laboratory floor.

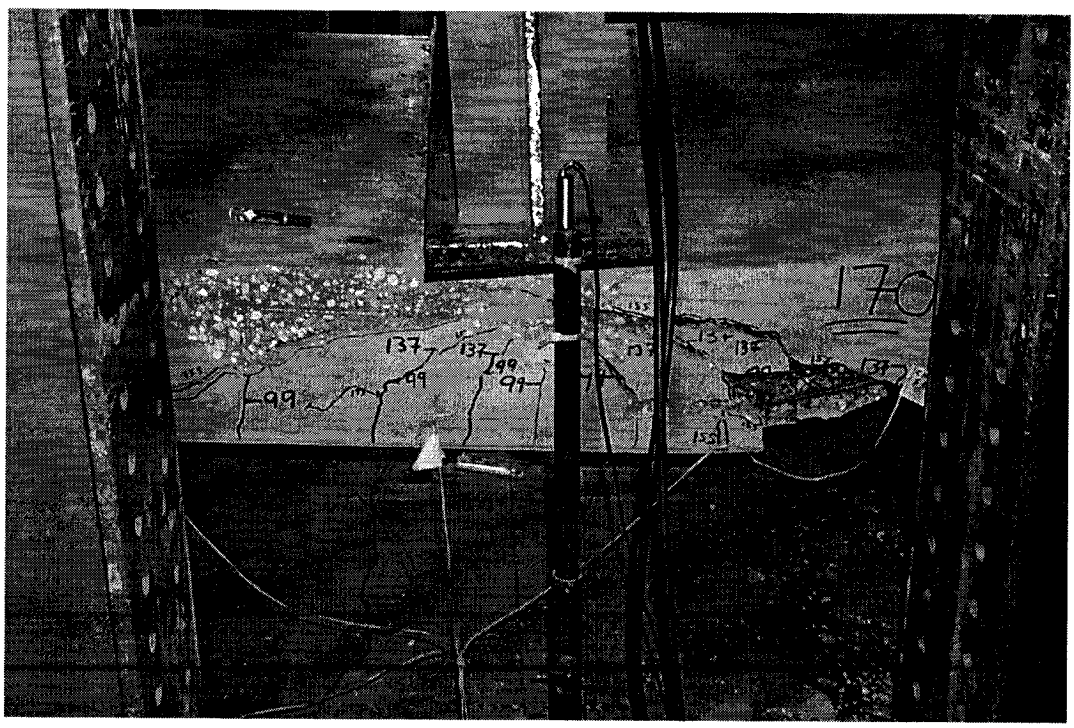

Figure 4.5 Front face of slab number 1, test number 1, immediately after failure.

Figure 4.6 indicates a close up of the prestressing strand. Note also the location of non prestressed reinforcement. Also note loss of concrete bond between the concrete and the strand at this location.

Figure 4.6 Close up of view of prestressing strand after failure of slab 1, test no. 1

4.3.2 Failure Mode of Slab No. 2, Test No. 2

Slab number 2 was tested in the identical fashion as slab number 1. Load was applied in increments of 20 kN (4,500 lb.) until first flexural cracking was visually detected on the rear face of the slab at a load of 589 kN (132,525 lb.). Thereafter, the load was increased and applied in increments of approximately 50 kN (11,250 lb.) until ultimate failure of

the slab was reached at 1,697 kN (381,825 lb.). Cracks were monitored and their progression marked from the point of visually detected first cracking up to a load of 1,570 kN (353,250 lb.).

The flexural cracks continued to propagate upwards until about a load of 834 kN (187,490 lb.) at which time these cracks turned inwards towards the centerline of the slab and formed 45 degree flexural shear cracks. These first flexural shear crack was visually detected on the rear face of the slab at an approximate load of 834 kN (187,490 lb.). Flexural shear cracks were visually detected on the front face at an approximate load of 1,030 kN (231,760 lb.). These cracks were located in the center of the web, roughly 150 mm (6 in.) from the center of the applied load. At about 1,500 kN (337,500 lb.) diagonal splitting cracks had formed at an angle of approximately 14 degrees.

Diagonal splitting progressed across the face of the slab at roughly 14 degrees from just inside the support location to a point under the applied loading. This resulted in crushing of the concrete directly under the load application point resulting in a loud explosive noise indicating a sudden release of energy. Up to the point of failure the slab underwent an average deflection of 34.5 mm (1.36 in.), which was identical to that of slab 1.

Figure 4.7 below indicates the rear face of slab number 2 immediately after failure, but with the load removed.

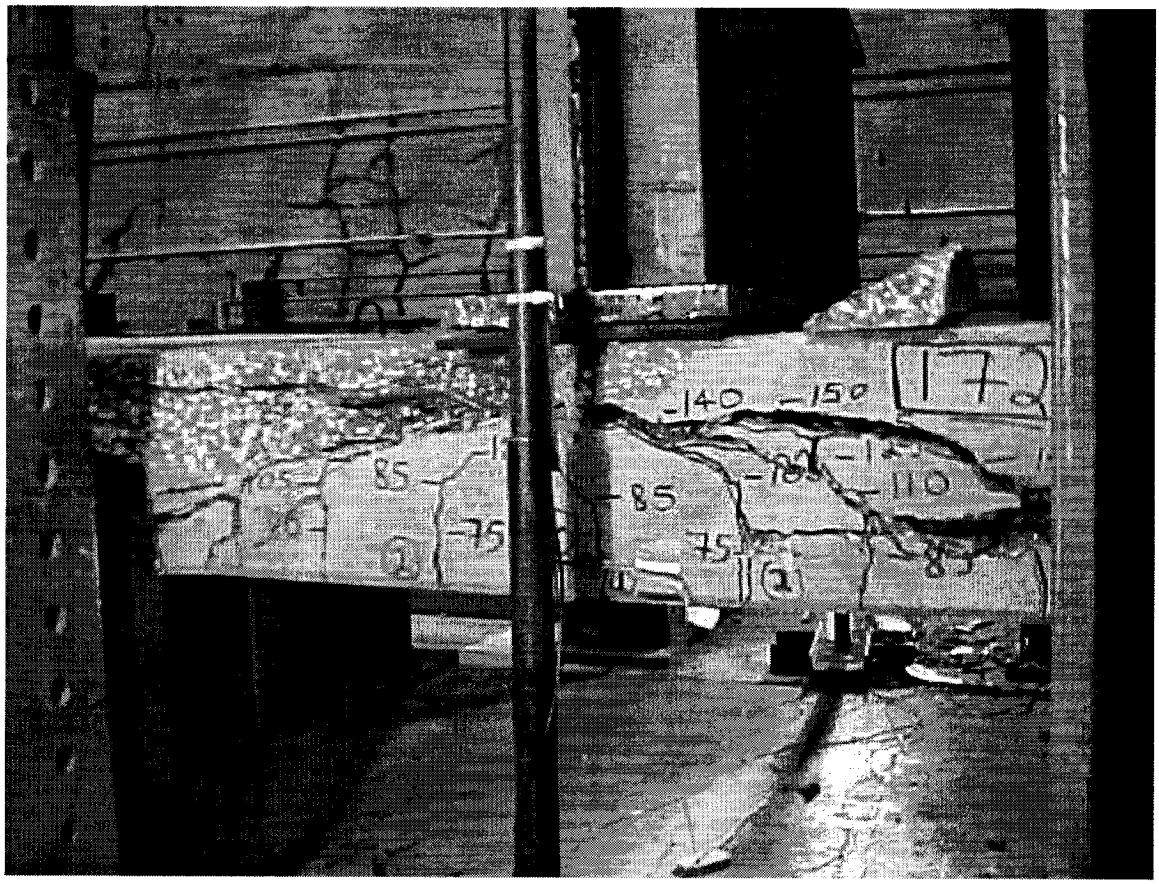

Figure 4.7 Rear face of slab after failure, slab No. 2, test number 2.

4.3.3 Failure Mode of Slab No. 6, Test Number 3

Slab number 6 was tested in a similar manner as in tests number 1 and 2 with loading applied at mid span of the slab however, the slab was inverted to test for negative moment capacity.

Again load was applied in increments of 20 kN (4,500 lb.) until first flexural cracking was visually detected on the front face of the slab at a load of 147 kN (33,075 lb.). Thereafter, the load was increased and applied in increments of approximately 50 kN (11,250 lb.) until ultimate failure of the slab was reached at 873 kN (196,500 lb.). Cracks

were monitored and their progression marked from the point of visually detected first cracking up to a load of 785 kN (177,000 lb.).

Failure of this slab was characterized by fewer flexural cracks that were much more widely spaced than in tests 1 and 2. Flexural shear cracking started at an approximate load of 441 kN (99,225 lb.) on the rear face of the slab.

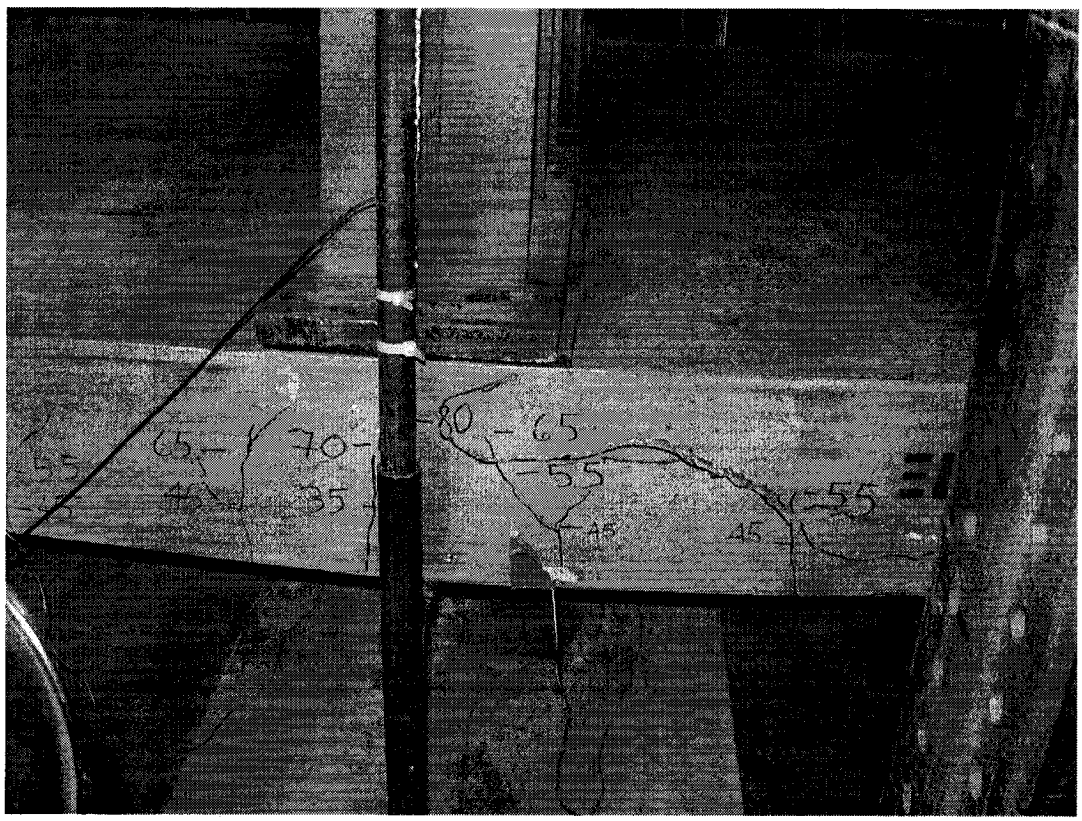

Figure 4.8 View of rear face of slab before failure, test number 3

Failure was from a diagonal splitting that developed at an applied load of 540 kN (121,500 lb,). This diagonal splitting ran at approximately 18 degrees from the load application strip to the bottom layer of prestressing strand at which time it then changed

direction and ran horizontally along the height of the bottom strand layer to the support. Although not measured, it is suspected that loss of bond occurred in this area.

When failure of this slab did occur, it displayed very little noise characteristic of the other slabs. This is related to the lower failure load and the lower potential energy stored within the slab. The average deflection of the slab at the load application point was 30 mm (1.18 in.). Figure 4.8 indicates the amount of cracking and crack spacing prior to failure.

4.3.4 Failure Mode of Slab Number 5, Test Number 4

The load was applied to slab number 5 in increments of 20 kN (4,500 lb.) until first flexural cracking was visually detected on the rear face of the slab at a load of 957 kN (215,325 lb.). Thereafter, the load was increased and applied in increments of approximately 50 kN (11,250 lb.) until ultimate failure of the slab was reached at 1,942 kN (437,000 lb.). Cracks were monitored and their progression marked from the point of visually detected first cracking up to a load of 1,668 kN (375,300 lb). The recorded average slab deflection at failure was 28.5 mm (1.12 in.).

The flexural cracks continued to propagate upwards until about 1,079 kN (242,800 lb.) at which time the cracks closest to the applied load turned inwards towards the load application strip and formed flexural shear cracks on shear span a on the rear face of the slab. On the front face of the slab flexural cracks did not propagate into flexural shear cracks until a load of 1,275 kN (287,000.lb.) was reached.

Diagonal splitting occurred on shear span a at an applied load of 1,472 kN (331,000 lb.). This crack progressed upwards until it intersected the area under the applied load, at which time the slab failed abruptly from crushing of the concrete directly under the load application strip. This diagonal splitting crack on shear span a, ran from the support to the point of load application. A similar crack on shear span b, ran from the load application strip at a similar angle, to the bottom layer of prestress reinforcement, at which time it ran horizontally to the other support.

Failure was characterized by a loud explosive noise indicating a sudden release of energy and a large amount of concrete expelled from the underside of the slab. Figure 4.10 indicates the amount of concrete expelled from the slab.

Figure 4.9 View of rear face of slab number 5, test number 4 after failure.

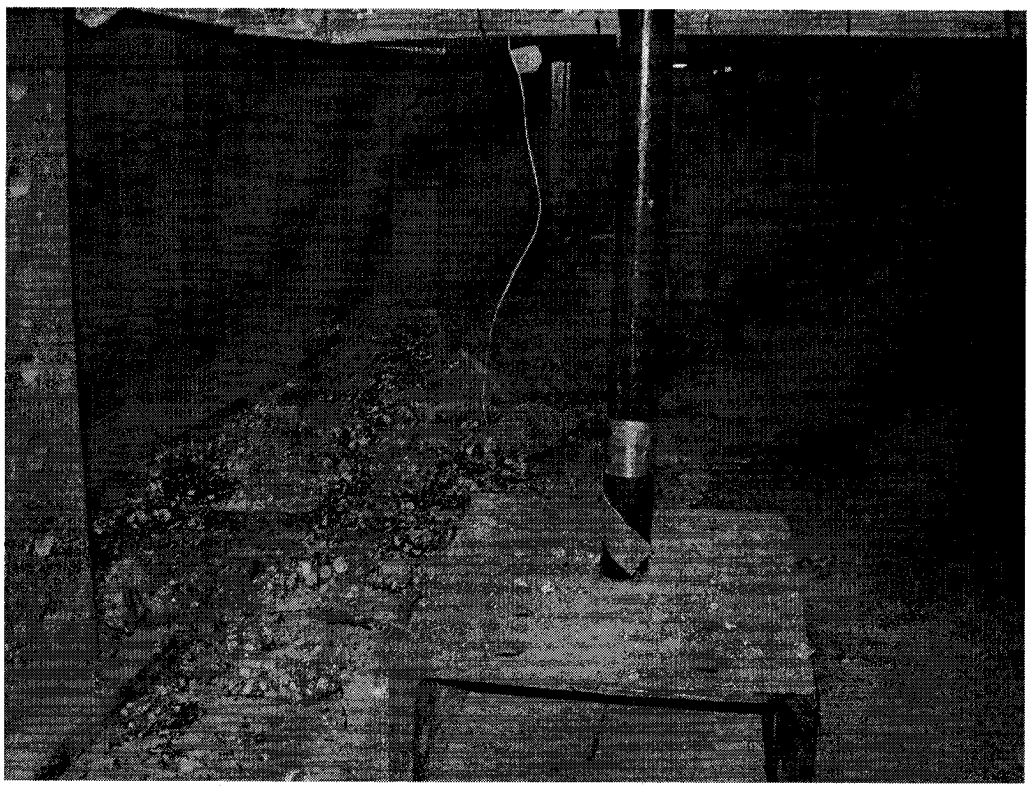

Figure 4.10 View of concrete expelled from slab at failure.

4.3.5 Cracking Mode of Slab Number 4, Test Number 5a

Loading was applied to slab number 4 in increments of 20 kN (4,500 lb.) until first flexural cracking was visually detected on the rear face of the slab at a load of 883 kN (198,675 lb.) Thereafter, the load was increased and applied in increments of approximately 50 kN (11,250 lb.) until a load of 1,922 kN (432,450 lb.) was reached at which time the test was terminated so that the slab could be reused for test 5b.

Cracks were monitored and their progression marked from the point of visually detected first cracking up to a load of 1,864 kN (419,500 lb.). The recorded average slab deflection at the time the test was terminated was 17 mm (0.67 in.).

The flexural cracks continued to propagate upwards until about 1,275 kN (286,875 lb.) at which time the cracks closest to the applied load turned inwards towards the load application strip and formed diagonal flexural shear cracks. At an approximate loading of 1,472 kN (331,000 lb.) a diagonal slitting crack developed. This crack continued to grow until the test was terminated. Figure 4.11 below indicates the formation of the diagonal splitting crack on the shear span a of the slab.

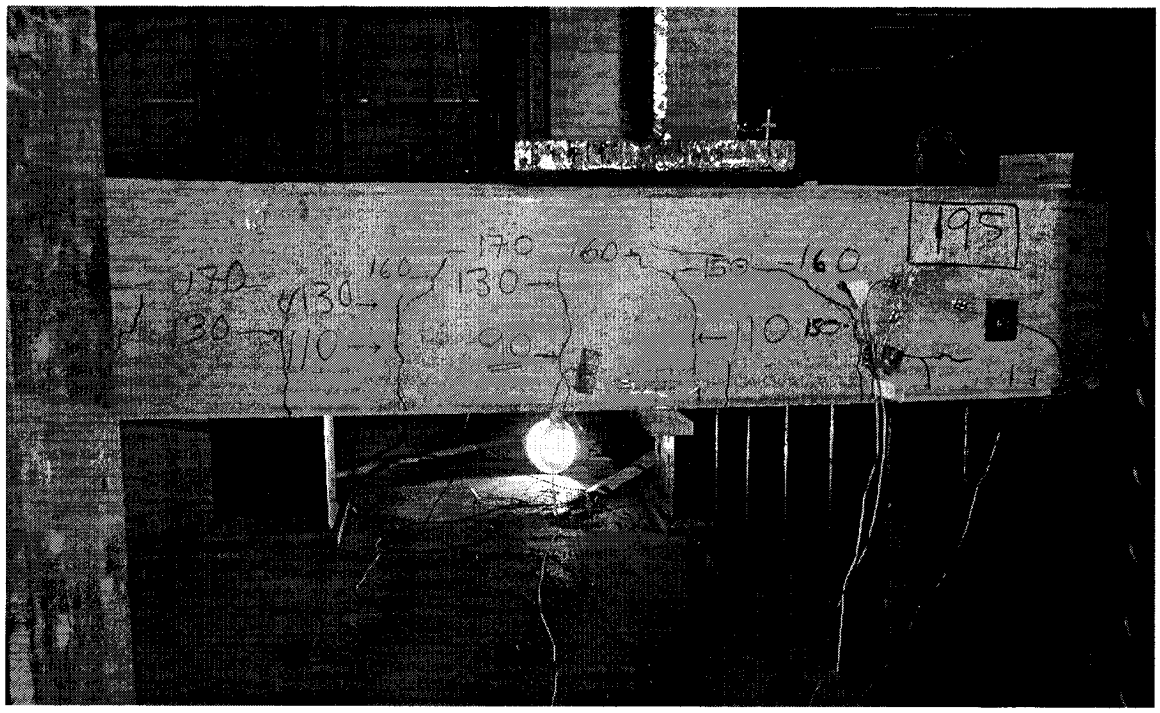

Figure 4.11 View of rear face of slab number 4, test 5a, shortly after termination.

4.3.6 Failure Mode of Slab Number 4, Test Number 5b

Slab number 4 was repositioned and retested with a similar shear span as in test 5a. Loading was applied in increments of 20 kN (4,500 lb.) until first flexural cracking was visually detected on the rear face of the slab at a load of 883 kN (198,675 lb.). Thereafter,

the load was increased and applied in increments of approximately 50 kN (11,250 lb.) until ultimate failure of the slab was reached at 2,138 kN (480050 lb.). Cracks were monitored and their progression marked from the point of visually detected first cracking up to a load of 1,962 kN (441,450 lb.). At failure the slab displayed an average deflection of 25 mm (1 in.).

The flexural cracks continued to propagate upwards until about a load of 1,300 kN (292,500 lb.) at which time these cracks turned inwards towards the centerline of the slab and formed flexural shear cracks.

At a loading of approximately 1,273 kN (309,000 lb.) a diagonal splitting crack developed in shear span a, at an angle of approximately 18 degrees. This crack continued to grow under increased loading until it intersected the area directly beneath the load application strip. This caused crushing of the concrete directly under the load application strip and the failure of the slab.

A similar crack occurred on shear span b, running from the point of load application at a similar angle and then running horizontally along the level of prestress reinforcement. This crack stopped approximately 350 mm (14 in.) short of the opposite support.

Figure 4.12 indicates the cracking pattern at failure and the diagonal splitting crack. Again failure of the slab was characterized by a loud explosive noise indicating a sudden release of energy.

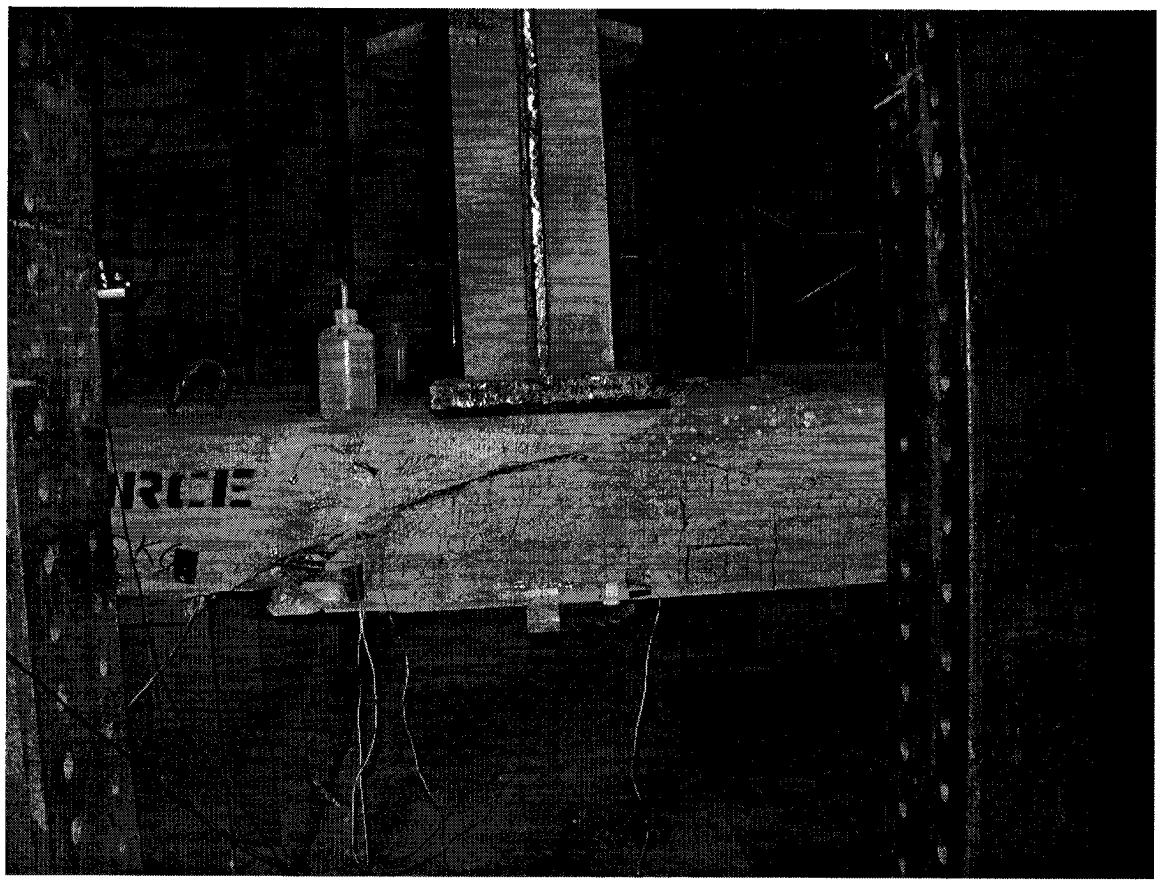

Figure 4.12 View of rear of slab number 4, test 5b

4.3.7 Failure Mode of Slab Number 3, Test Number 6

Slab number 3 was loaded in increments of 20 kN (4,500 lb.) until first flexural cracking was visually detected on the front face of the slab at a load of 756 kN (170,100 lb.). Thereafter, the load was increased and applied in increments of approximately 50 kN (11,250 lb.) until ultimate failure of the slab was reached at 1,884 kN (423,900 lb.). Cracks were monitored and their progression marked from the point of visually detected first cracking up to a load of 1,815 kN (408,375 lb.). At failure the slab displayed an average deflection of 31 mm (1.22 in.).

The flexural cracks continued to propagate upwards until an approximate load of 1,375 kN (309,375 lb.) was reached at which time these cracks turned inwards towards the applied loading strip and formed flexural shear cracks.

At an approximate loading of 1,570 kN (353,200 lb.) a diagonal splitting crack developed at an angle of 19 degrees on the front face of shear span a. This crack continued to grow until it intersected the area directly under the load application strip at which time the slab failed by crushing of the concrete in that area. This crack ran from just inside the support on shear span a to the load application strip.

A similar, but somewhat flatter angled crack ran from the load application area at the top of the slab to the height of the prestressing strand at which time it ran horizontally back to the support at shear span b and to the diagonal splitting crack in shear span a. This indicated a loss of bond with the strand at failure. Figures 4.13 and 4.14 indicate this cracking pattern at failure and the diagonal splitting cracks. Again failure of the slab was characterized by a loud explosive noise indicating a sudden release of energy.

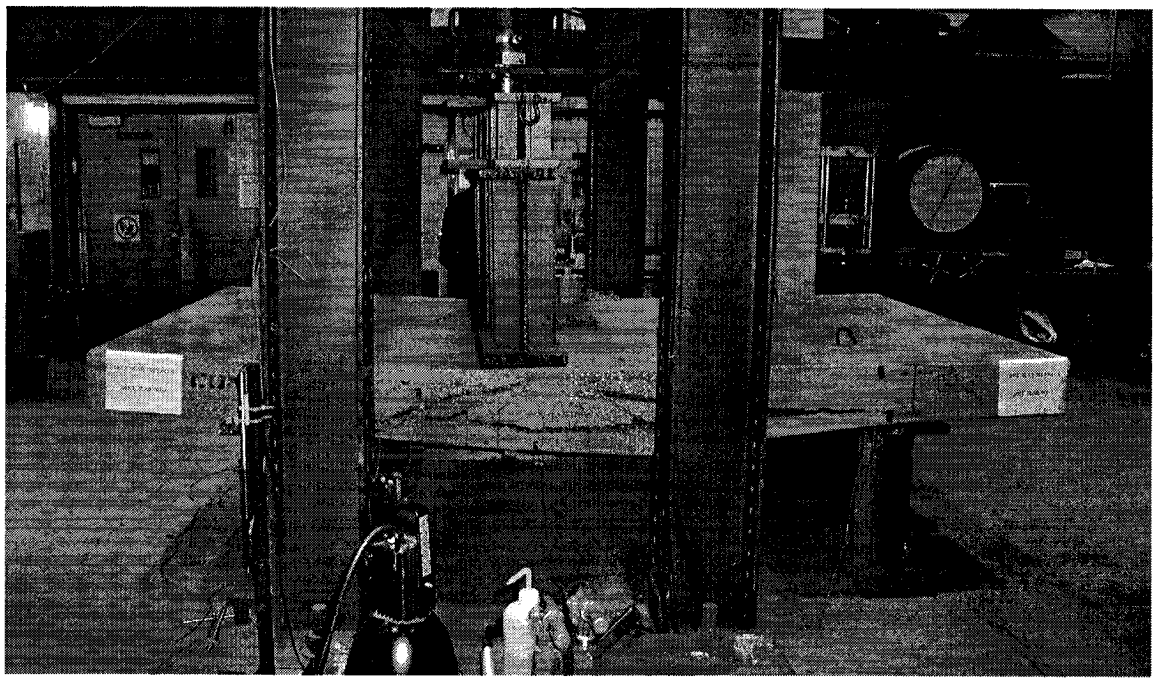

Figure 4.13 Front view of slab number 3, test number 6, and associated cracking

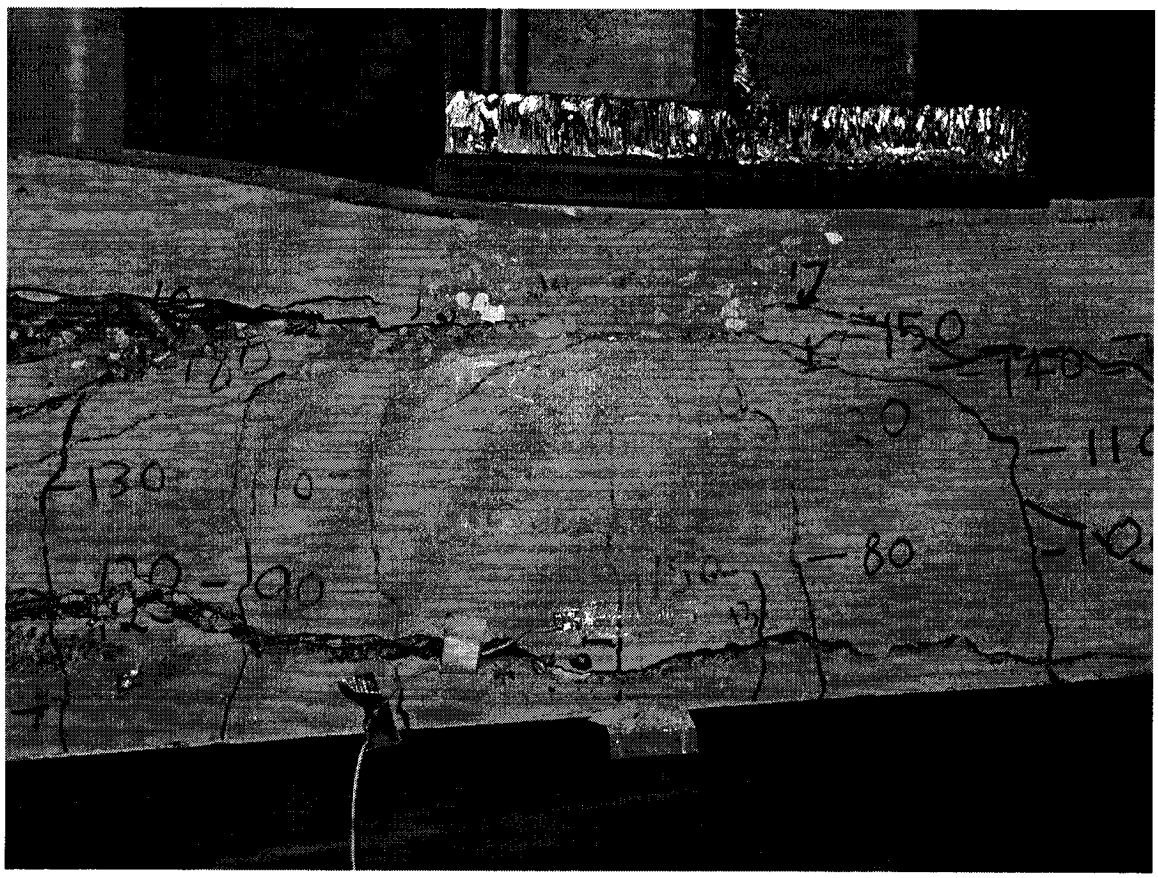

Figure 4.14 View of rear of slab no. 3, test no. 6, indicating cracking pattern

4.4 Cracking Moment

The theoretical cracking moment and cracking load for each slab was calculated by means of the following equation:

$$M_{cr} = \left(\frac{P}{A} + \frac{Pe}{S_b} + 0.5\sqrt{f_c'} \right) S_b \qquad 4.4$$

These calculations are contained in Appendix D. Table 4.4 indicates the comparison between the theoretical cracking moment based on (a) the specified minimum compressive strength of concrete, (b) the actual compressive strength of concrete and (c) the experimental cracking moment.

Test Number	Deck Slab Number	M_{cr} Based on Specified Strength kN-m	M_{cr} Predicted on Actual Strength kN-m	M_{cr} Based on Experimental Results kN-m	Ratio of Experimental M_{cr} / predicted M_{cr}
Slabs Tested in Normal Position					
1	1	484.0	490.4	433.8	0.88
2	2	484.0	490.4	359.0	0.73
4	5	459.2	475.8	548.2	1.15
6	3	459.2	470.9	427.4	0.91
5a	4	434.5	445.6	403.9	0.91
5b	4	434.5	445.6	403.9	0.91
Average					**0.92**
Slabs Tested in the Inverted Position					
3	6	127.0	144.6	89.8	0.62

Table 4.4 Summary of Cracking Moments

It is clear from Table 4.4 that all the slabs except one cracked prior to the theoretical cracking moment. The average experimental positive cracking moment was 92% of the theoretical positive cracking moment. The reason for the discrepancy between the predicted and the experimental values is that the formula for determining cracking moment is approximate at best. The cracking moment is dependant upon such factors as

the pre-compression state within the slab, the strength and size of aggregate and the water cement ratio.

From the results of this experimental program, there does not appear to be a correlation between cracking moment and compressive strength of concrete. Indeed, it would appear that increasing the compressive strength of concrete has little or no effect on the cracking moment.

It would appear from the results that formula 4.4 overstates the cracking moment. Based on the experimental results obtained in this research, a more accurate formula for the cracking moment for prestressed members constructed from HPC is:

$$M_{cr} = \left(\frac{P}{A} + \frac{Pe}{S_b} + 0.3\sqrt{f_c'} \right) S_b \qquad 4.5$$

4.5 Cracking Loads

First cracking was detected by the use of alcohol sprayed on the surface of the slab. The alcohol quickly evaporates leaving any cracks visible as a damp line. The load at which first cracking was detected was marked on the slab along with the corresponding crack outline in felt tipped marker. Figure 4.15 indicates first cracking in slab test number 1 at an applied load of 712 kN (72,580 kg)

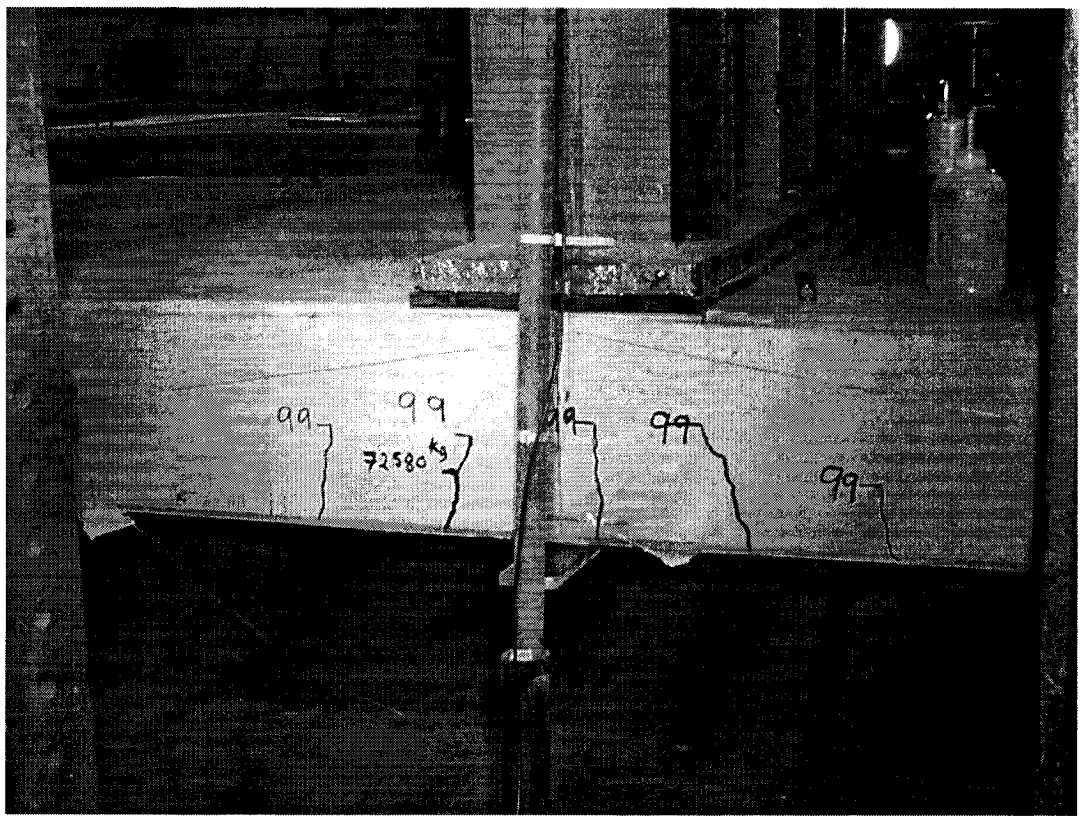

Figure 4.15 First cracking at 72,580 kg marked on the slab.

In actuality the first cracking on a micro crack bases had occurred much sooner. The crack only became visible to the naked eye at a load of 72,580 kg (159,680 lb.). There is much discussion on what constitutes first cracking. Suffice to say that what was being

detected were macro (hairline) cracks which had grown from a micro crack. This will be discussed in greater detail under the load-strain curves.

A few observations regarding first cracking from the test program are:

1) all first cracks were located under the point of load application.

2) first cracking did not occur simultaneously on both sides of the slab

3) when the cracks did become visible to the naked eye, they had a substantial length to them, generally in the 50 to 100 mm (2 to 4 in.) range.

Table 4.5 compares first cracking loads. The same comments apply to cracking loads as cracking moments.

Test Number	Deck Slab Number	P_{cr} Based on Specified Strength (kN)	P_{cr} Predicted On Actual Strength (kN)	P_{cr} Based on Experimental Strength (kN)	Ratio of Experimental P_{cr} / Predicted P_{cr}
Slabs Tested in Normal Position					
1	1	793.5	803.9	711.0	0.88
2	2	793.5	803.9	588.5	0.73
4	5	803.0	832.0	958.6	1.15
5a	4	949.8	974.0	882.8	0.91
5b	4	949.8	974.0	882.8	0.91
6	3	803.0	823.4	747.4	0.91
Average					**0.92**
Slabs Tested in the Inverted Position					
3	6	208.3	236.8	147.2	0.62

Table 4.5 Summary of First Cracking Loads

4.6 Experiment Cracking Moments Compared to in Service Moments

4.6.1 Negative Moment

From the first cracking results of section 4.4 (Table 4.4), the visually detected positive first cracking moment occurred at an average of 92% of the predicted. From section 2.8, the predicted negative cracking moment over the supports was 107.3 kN-m (79.2 kip-ft.). Therefore, based on the test results, the actual cracking moment would be:

0.92 x 107.3 = 98.7 kN-m (72.9 kip–ft.)

This value will be used to determine if cracking would occur over the support under live loading conditions. The moment value for the slab due to live loading was taken as 95.6 kN-m (70.6 kip-ft.). The load applied to the cantilevered slab required to cause cracking at the girder support is:

$$M_{cr} = \frac{wa^2}{2} \qquad 4.6$$

The slab, ballast and track cause an existing negative moment over the support of 8.4 kN-m (6.2 kip-ft.), which must be subtracted from the 98.7 kN-m (72.9 kip-ft.) to obtain the additional applied moment to cause cracking. Therefore:

98.7 - 8.4 = 90.3 kN-m (66.6 kip-ft.)

The design factor of safety (F.S.) against negative cracking over the supports is therefore:

$$F.S. = \frac{90.3}{95.6} = 0.94$$

This indicates that substantially more reinforcement will be required in the top of the slab.

4.6.2 Positive Cracking Moment

The average positive experimental cracking moment obtained from 6 of the 7 experiments (Table 4.4) was 429.4 kN-m (316,900 kip-ft.). The live and impact loading to cause cracking is simply the distributed cracking load minus the distributed design track loading of 42.1 kN/m (2,888 lb/ft.).

The loading to cause cracking is simply:

$$M_{cr} = \frac{wa^2}{2}$$

$$429.4 = \frac{w(0.63)^2}{2}$$

$$w = 2{,}163.8 \text{ kN/m}$$

$$w_{LL+I} = 2{,}163.8 - 42.1 = 2{,}121.7 \text{ kN/m}$$

The design live loading including 100% impact was 482 kN/m (33,064 lb/ft.) as detailed previously in Chapter 2. Therefore, the factor of safety against cracking is:

$$F.S. = \frac{2{,}121.7}{482} = 4.40$$

4.7 Ultimate Moment Capacity

The ultimate moment capacity for each slab was calculated by means of the stress–strain compatibility method. These calculations are contained in Appendix C. The exact analysis of the ultimate moment capacity of a prestressed concrete slab is a complicated theoretical problem. This is because both the steel and the concrete are stressed beyond their elastic range and are now working in the elasto-plastic range.

The stress-strain compatibility method can according to Lin [1967] still predict with sufficient accuracy the ultimate load and corresponding moment, but with some limitations. These are as follows:

a) the failure must be one of flexure with no shear bond or anchorage failure that would decrease the strength of the slab.
b) the slab must be bonded.
c) the slab must be statically determinate.
d) the calculated failure load is the ultimate load obtained as a direct result of an applied short duration static load.

The results from the experiments as well as from the calculations are presented in Table 4.6. From Table 4.6, it can be seen that there was excellent agreement between the calculated ultimate loads and the experimental calculated loads. The value of P_U experimental divided by P_U calculated, indicates that the experimental results were within 3% of the calculated values, with the exception of test 5b. It is concluded that test 5b failed earlier than expected due to the significant pre-cracking that existed within the slab as a result of test 5a.

The mode of failure of the slabs was one of an under-reinforced section. This type of failure results in the characteristic elongation and yielding of the pre-stressing prior to crushing of concrete. The slabs had a steel percentage of:

$$\rho = A_{ps}/A_c \qquad 4.7$$

$$= \frac{34 \times 140}{250 \times 2135} \times 100 = 0.90\% .$$

Test Number	Deck Slab Number	P_U Based on Specified Strength (kN)	P_U Predicted On Actual Strength (kN)	P_U Based on Experimental Strength (kN)	Experimental P_U / Predicted P_U
Slabs Tested in Normal Position					
1	1	1,683	1,737	1,678	0.97
2	2	1,683	1,737	1,697	0.98
4	5	1,791	1,938	1,962	1.05
5a	4	2,244	2,393	1,922*	N.A.
5b	4	2,244	2,393	2,139	0.90
6	3	1,791	1,910	1,884	0.99
Average					**0.98**
Slabs Tested in the Inverted Position					
3	6	787	899	873	0.97

* Test terminated prior to failure at applied load of 1,922 kN

Table 4.6 Ultimate Load Capacity Comparison

From the calculated and experimental ultimate loads, the ultimate moment capacity of each slab has been calculated and is shown in Table 4.7. Again the calculated results compare favourably with test results.

Test Number	Deck Slab Number	M_u Based on Specified Strength kN-m	M_u Predicted On Actual Strength kN-m	M_u Based on Experimental Results kN-m	Experimental M_u / Predicted M_u
Slabs Tested in Normal Position					
1	1	1,025	1,051	1,024	0.97
2	2	1,025	1,051	1,035	0.98
4	5	1,025	1,076	1,125	1.05
5a	4	1,025	1,086	879*	N.A
5b	4	1,025	1,086	978	0.90
6	3	1,025	1,076	1,080	1.0
Average					**0.98**
Slabs Tested in the Inverted Position					
3	6	480	548	533	0.97

* Test terminated prior to failure.

Table 4.7 Ultimate Moment Capacity Comparison

4.8 Post Cracking Capacity and Post Yielding Ductility

4.8.1 Post Cracking Capacity

The post cracking capacity is simply the ratio of the ultimate moment to the cracking moment. It is an indicator of the reserve strength within the slab after first cracking has occurred. A slab will be considered to have sufficient ductile response if it has a sufficient post cracking capacity to ensure yielding of the steel.

Table 4.8 indicates both the calculated and experimental post cracking capacities. Note that in all cases the experimental post cracking capacity exceeded the predicted post cracking capacity. This is because the experimental cracking moment was 93% of the predicted cracking moment, thus increasing the experimental post cracking capacity slightly. Note also that test 5a is omitted as it was not tested to failure.

Test Number	Predicted Cracking Moment M_{cr} kN.m)	Predicted Ultimate Moment M_u (kN.m)	Predicted Post Cracking Capacity	Experimental Cracking Moment M_{cr} (kN.m)	Experimental Ultimate Moment M_u (kN.m)	Experimental Post Cracking Capacity
Slabs Tested in Normal Position						
1	481.1	1,051	2.2	433.8	1,024	2.4
2	481.1	1,051	2.2	359.0	1,035	2.9
4	467.5	1,076	2.3	548.2	1,125	2.1
5b	439.7	1,086	2.2	403.9	978	2.4
6	462.6	1,076	2.3	427.4	1,080	2.5
Average						**2.5**
Slabs Tested in the Inverted Position						
3	135.1	548	4.0	89.8	533	5.9

Table 4.8 Summary of Post Cracking Capacity

As a comparison it should be noted that similar tests conducted by Peters [1992] at Concordia University on 16 prestressed concrete bridge ties with an identical span and

using conventional strength concrete, yielded $\frac{M_u}{M_{cr}}$ ratios in the 1.7 to 2.0 range. The ratios from the current tests are in the 2.4 range and are indicative of higher post cracking ductility.

The moment at ultimate capacity divided by the moment at first cracking has been plotted against the compressive strength of concrete to see if there might be a relationship between the two and is indicated in Figure 4.16. Even though the data base is limited, the results do indicate that as the compressive strength of concrete increases, post cracking ductility as denoted by the $\frac{M_u}{M_{cr}}$ ratio decreases slightly.

4.8.2 Post Yielding Ductility

On the basis of experimental work undertaken by Taplin et al [2000] on the ductility of prestressed concrete beams, it is suggested that the ratio of the curvature at ultimate capacity divided by the curvature at yielding $\frac{\phi_u}{\phi_y}$ is a more accurate reflection of the ductility of a beam or slab rather than deflection itself. Since the curvatures at yielding and ultimate are related to the moment, a simpler way to view this is on the basis of the ratio of the ultimate moment to the yield moment. This gives a sense of the ductility after yielding.

The calculated yield moment as well as the predicted and experimental moment ratios, $\frac{M_u}{M_y}$, for all tests have been calculated and are included in Table 4.9 below. It can be seen that all slabs displayed similar $\frac{M_u}{M_y}$ ratios, which would indicate similar ductile behaviour in the slabs after yielding, regardless of strength of concrete.

Test Number	Slab Number.	Moment at Yielding kN-m	Moment at Predicted Ultimate Capacity kN-m	Moment at Experimental Ultimate Capacity kN-m	Predicted M_U/M_Y	Experimental M_U/M_Y
Slabs Tested in Normal Position						
1	1	951	1051.0	1024	1.11	1.08
2	2	951	1051.0	1035	1.11	1.09
4	5	976	1076.0	1125	1.10	1.15
5a	4	966	1086.0	N/A	1.12	N/A
5b	4	966	1086.0	978	1.12	1.01
6	3	966	1076.0	1090	1.10	1.13

Table 4.9 Comparison of Predicted and Experimental Post Yielding Capacity

4.9 Deflection:

The deflection on either edge of the slab at the point of strip loading, has been averaged and the maximum deflections at failure of the slab are shown in Table 4.10. Of particular note is the amount of deflection that occurred prior to failure. The least amount of deflection was 25 mm (1 in.), while the maximum was 34.5 mm (1.36 in.).

Load deflection graphs for each pair of similar tests, with the exception of test number 3 which was a single test on an inverted slab, have been plotted and are included as Figures 8.17 to 8.21 inclusive.

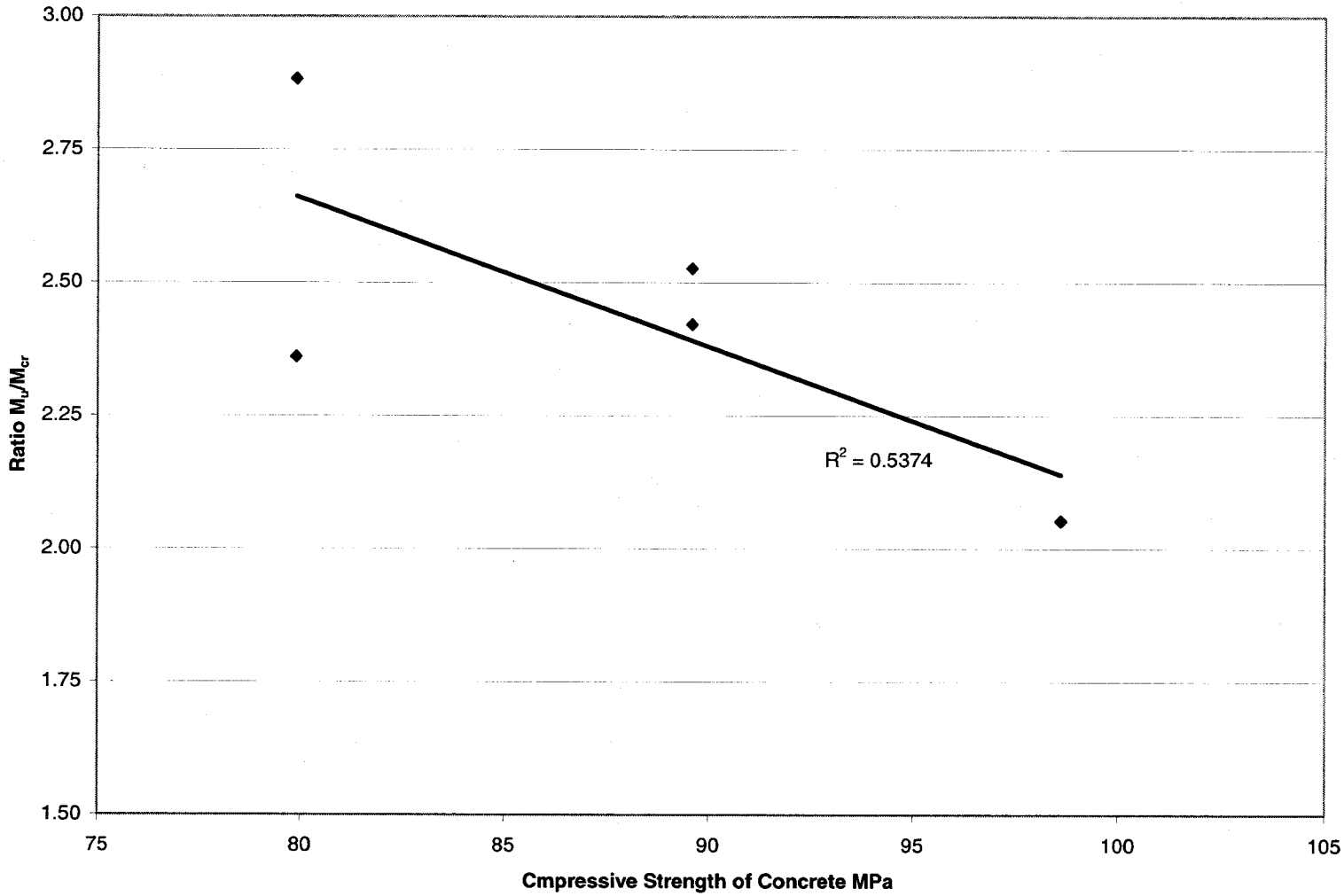

Figure 4.16 Post cracking capacity versus compressive strength of concrete

Review of the load deflection curves indicates that in the early stages of loading all curves displayed nearly linear inclination. This indicates that in the early stages of loading all slabs had similar stiffness. As the load increased the load deflection curves for all slabs flattened towards the x (deflection) axis. This indicates a "softening" behaviour, due to progressive crack propagation.

Also of note is that all curves displayed a cubic parabola relationship, whose coefficients of determination (R^2) are extremely high.

In the case of the slabs that were tested in the upright position, it is noted that regardless of where along the slab the load was applied, the slab cracked when an average deflection of 6 mm (1/4 in.) was reached. This is contrasted by the deflection at ultimate which increased as the load approached the center of the slab. The deflection values contained in Table 4.10 below have been plotted against the corresponding distance from the support and are shown in Figure 4.22. As would be expected the deflections at ultimate increase as the applied load distance from the support increases. The deflections at first cracking though do not follow this trend and remain relatively flat (constant) at approximately 6 mm (1/4 in.).

Test Number	Deck Slab Number	Shear Span a (m)	Shear Span b (m)	Ultimate Load (kN)	Maximum Average Deflection Under Point of Load Application	
					at first cracking mm	at ultimate mm
Slabs Tested in Normal Position						
1	1	1.22	1.22	1,678	7	34.5
2	2	1.22	1.22	1,687	5	34.5
4	5	0.92	1.52	1,942	5.5	28.5
6	3	0.92	1.52	1,884	5	31
5a	4	0.61	1.83	1,922*	5.5	17
5b	4	0.61	1.83	2,139	7	25
Average					5.8	30.7
Slabs Tested in the Inverted Position						
3	6	1.22	1.22	873	2	30

Table 4.10 Summary of Maximum Deflections Under Strip Loading

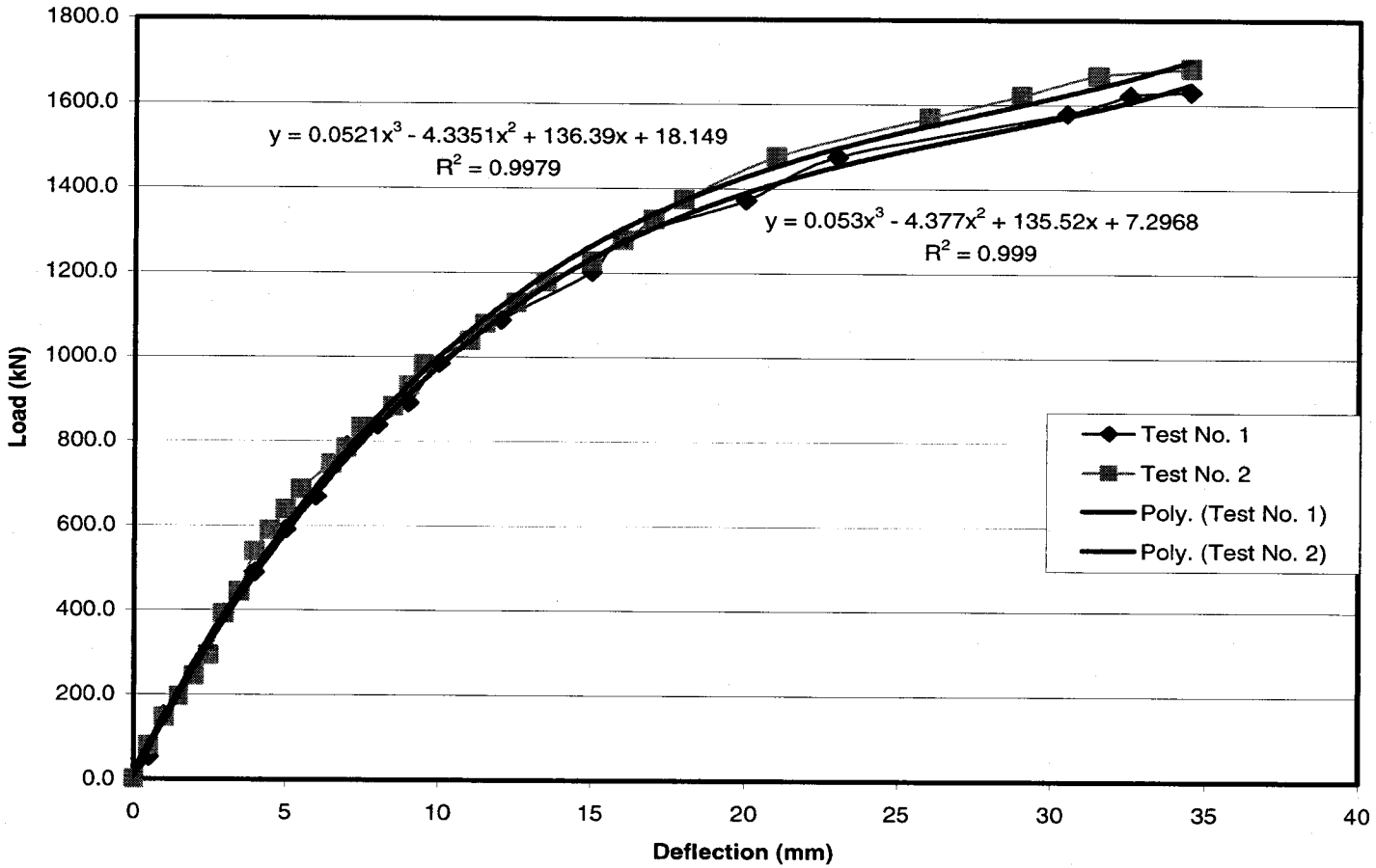

Figure 4.17 Load-Deflection Curves for Test Number 1 and 2

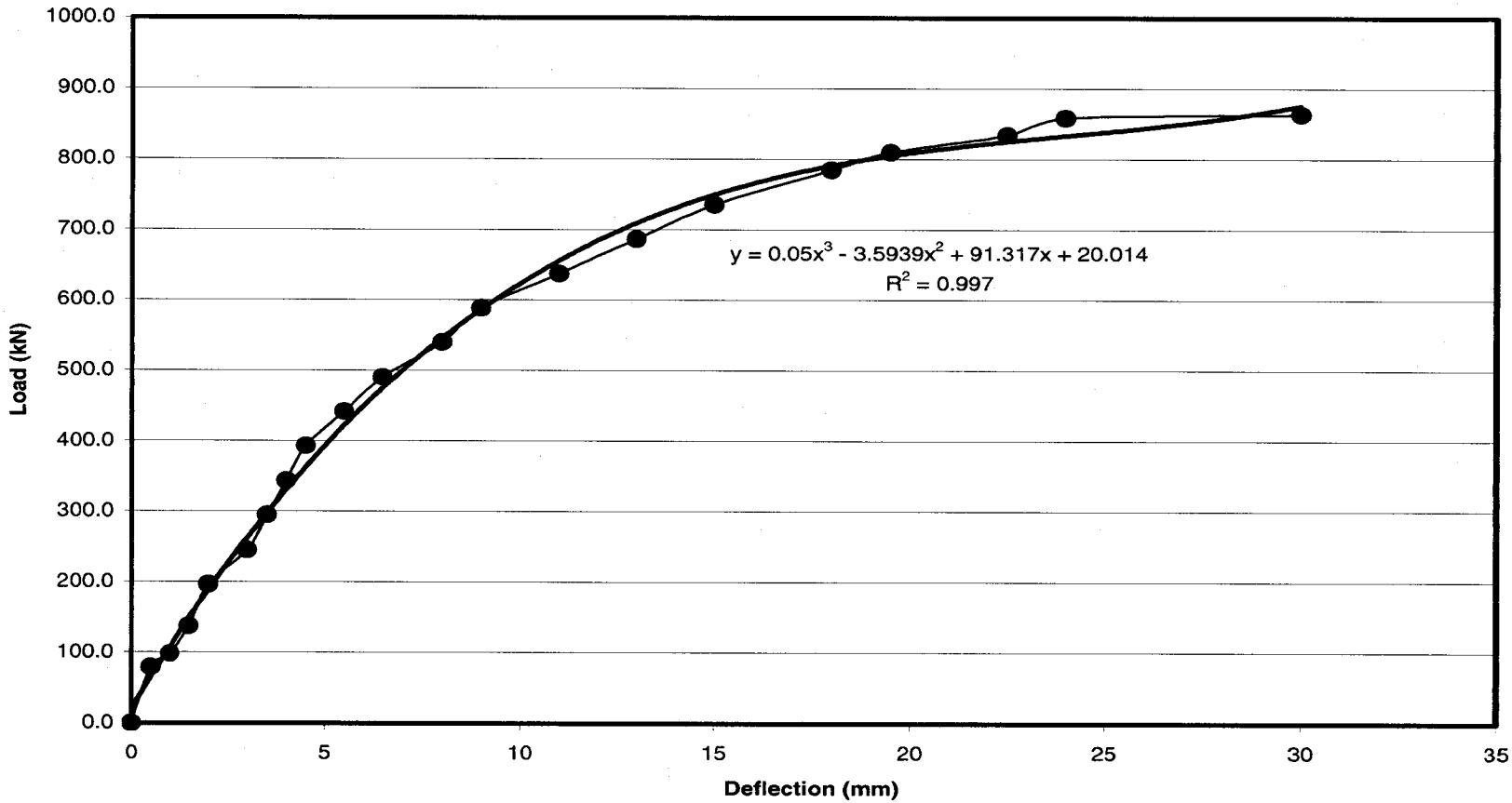

Figure 4.18 Load–Deflection Curve for Test Number 3

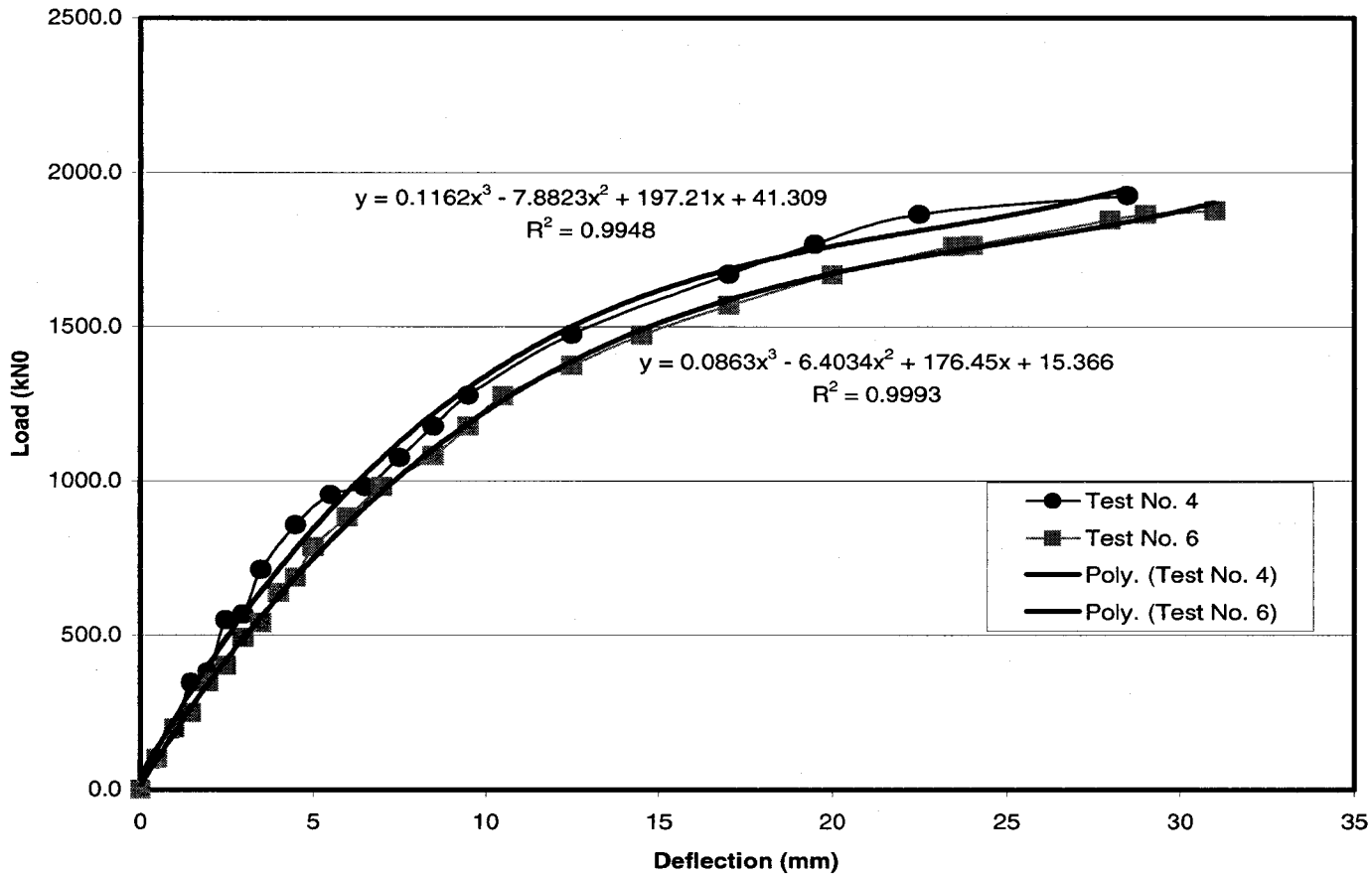

Figure 4.19 Load–Deflection Curves for Test Number 4 and 6

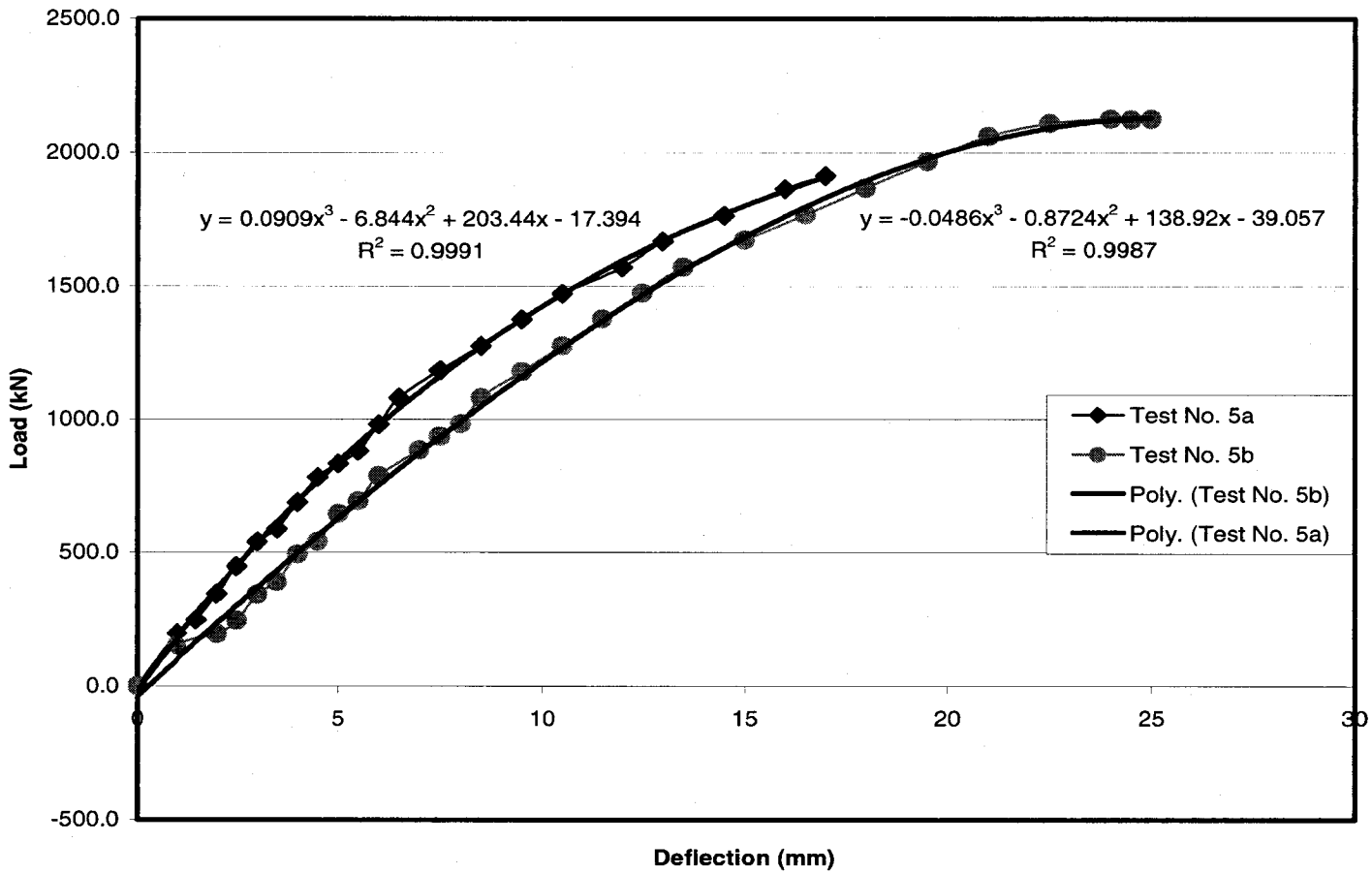

Figure 4.20 Load–Deflection Curves for Number Test 5a and 5b.

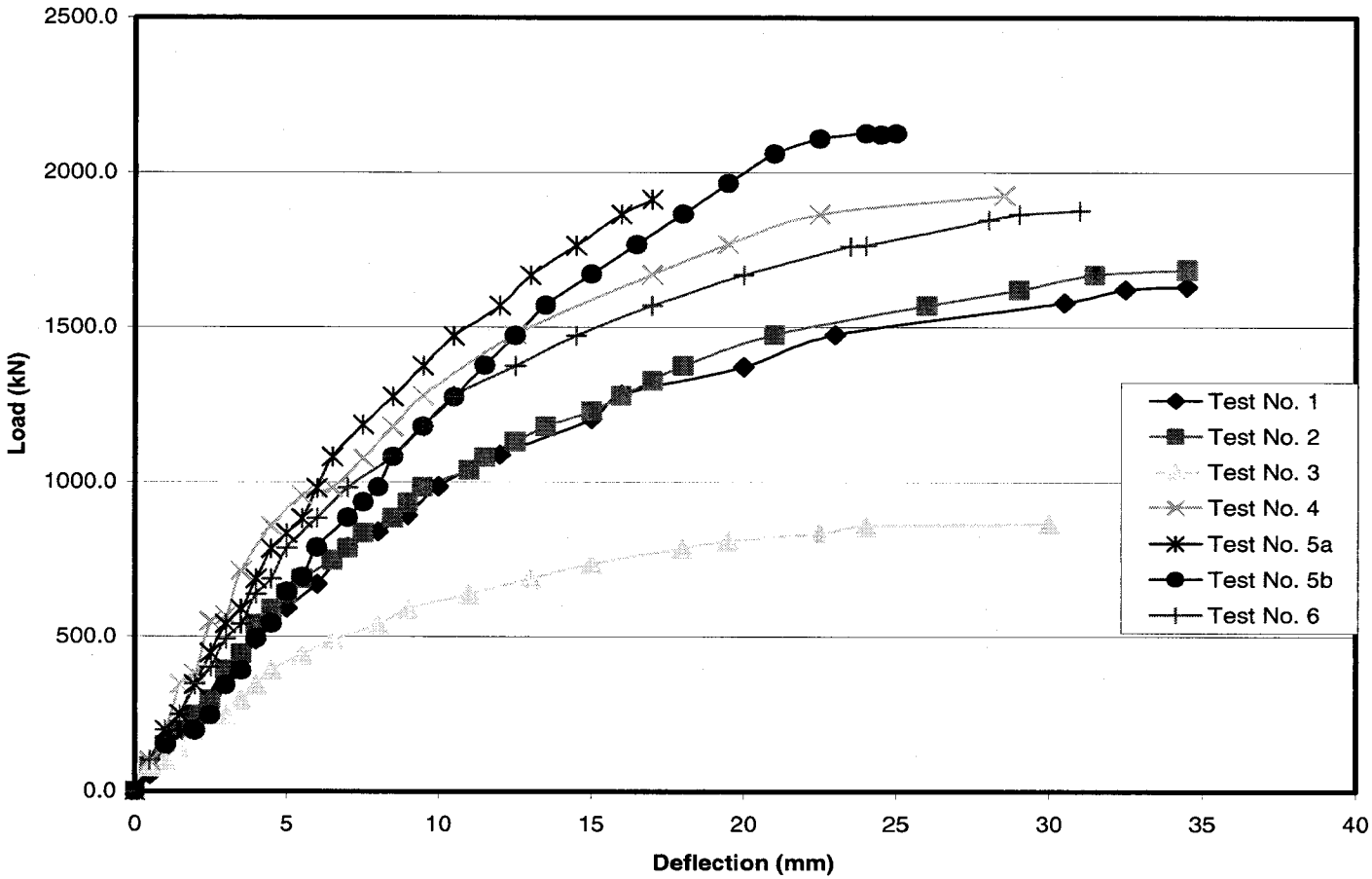

Figure 4.21 Load–Deflection Curves for all Tests

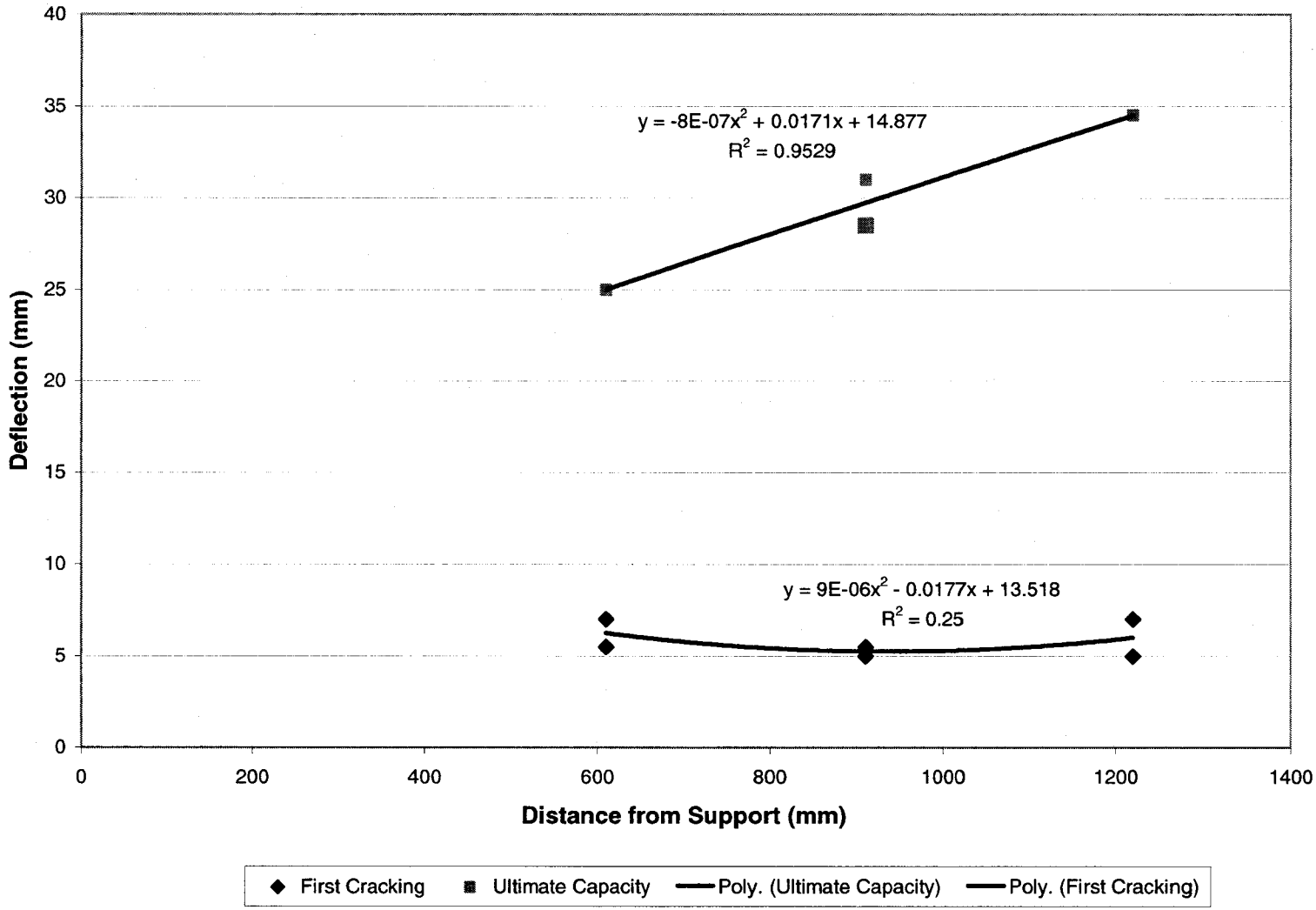

Figure 4.22 Comparison of Deflection Versus Distance from Support

4.10 Strain Gauge Readings

The load–strain data from each of the test has been graphed in Figure 4.23 to 4.27 inclusive. From the figures it can been seen that the concrete strain readings generally are linear up to the point of first cracking and thereafter drop off dramatically until reaching zero. The reason for the decline in strain, even though load is increasing is due to the start of bond failure and thus a decrease in the tensile force in the concrete.

The applied loading at which first cracking was detected visually is different from that detected by the strain gauges. Table 4.11 compares the load at first cracking as detected by the strain gauge readings to the load at visually detected first cracking. Where "off-scale" is shown in the Table, it means that particular strain gauge stopped reading properly most likely due to cracks running through it.

Slab No.	Test No.	Strain at first cracking as detected by strain gauges (microstrain)	Load at first cracking detected by strain gauges (kN)	Strain at visually detected first cracking (microstrain)	Load at visually detected first cracking (kN)	Ratio of load detected by strain gauges/ load at visual detection
1	1	427	415	Off-scale	711	N/A
2	2	412	491	326	589	0.55
6	3	95	N/A	Off-scale	147	N/A
5	4	365	690	300	957	0.72
4	5a	409	783	306	883	0.89
4	5b	401	740	303	883	0.84
3	6	319	638	Off scale	746	N/A

Table 4.11 Strain Gauge Versus Visually Detected First Cracking

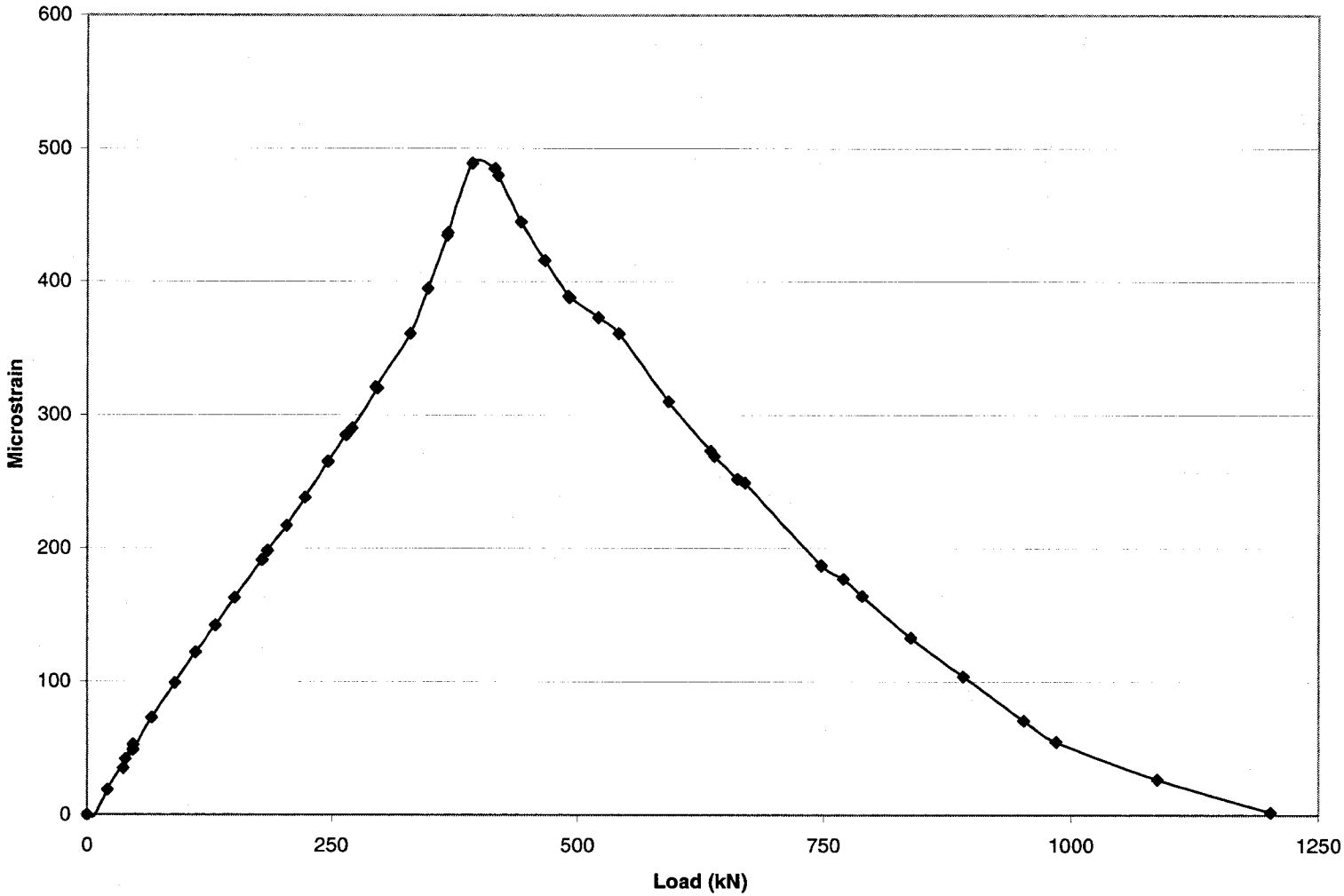

Figure 4.23 Load Versus Strain for Test Number 1

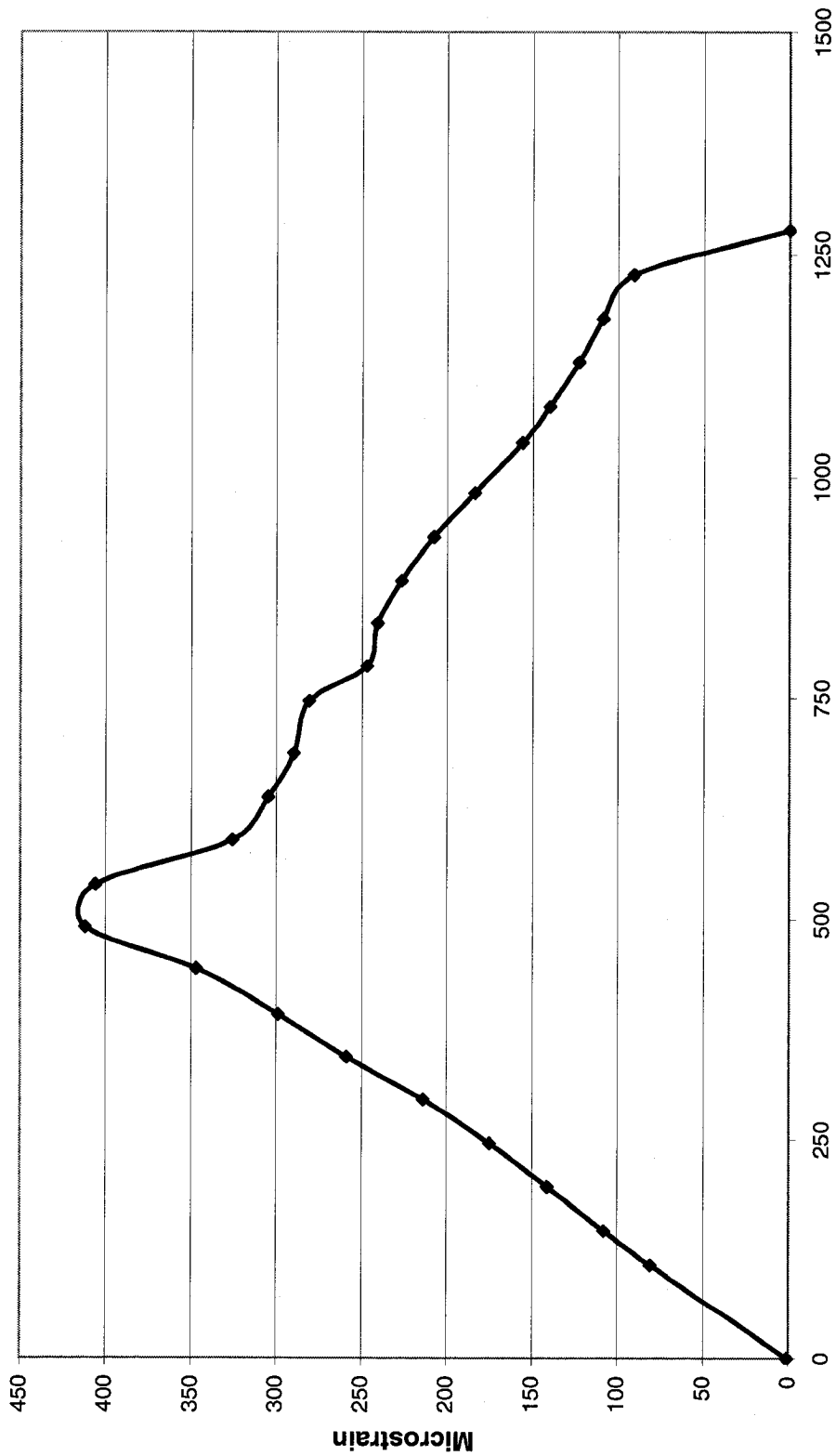

Figure 4.24 Load Versus Strain for Test Number 2

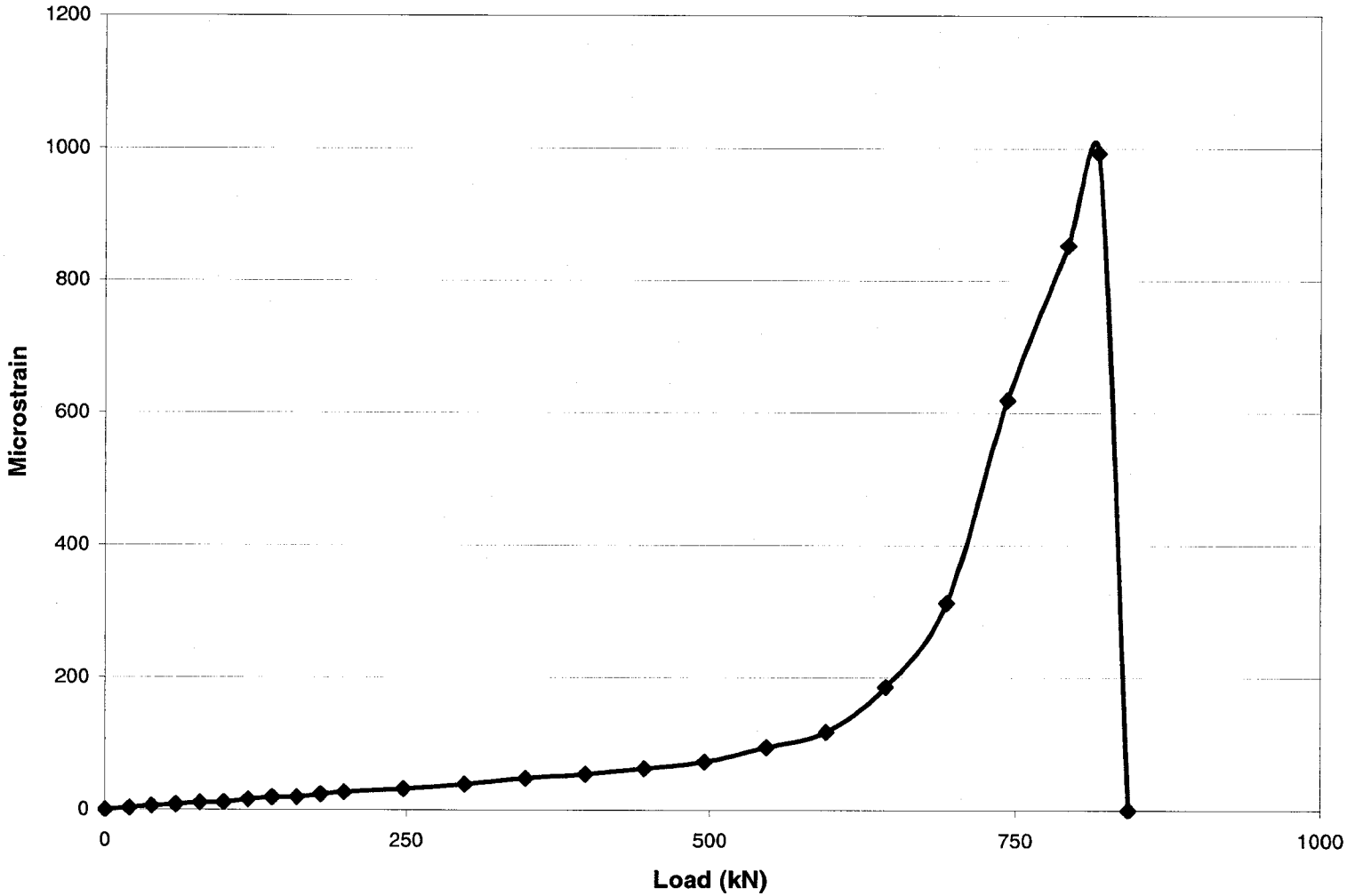

Figure 4.25 Load Versus Strain for Test Number 3

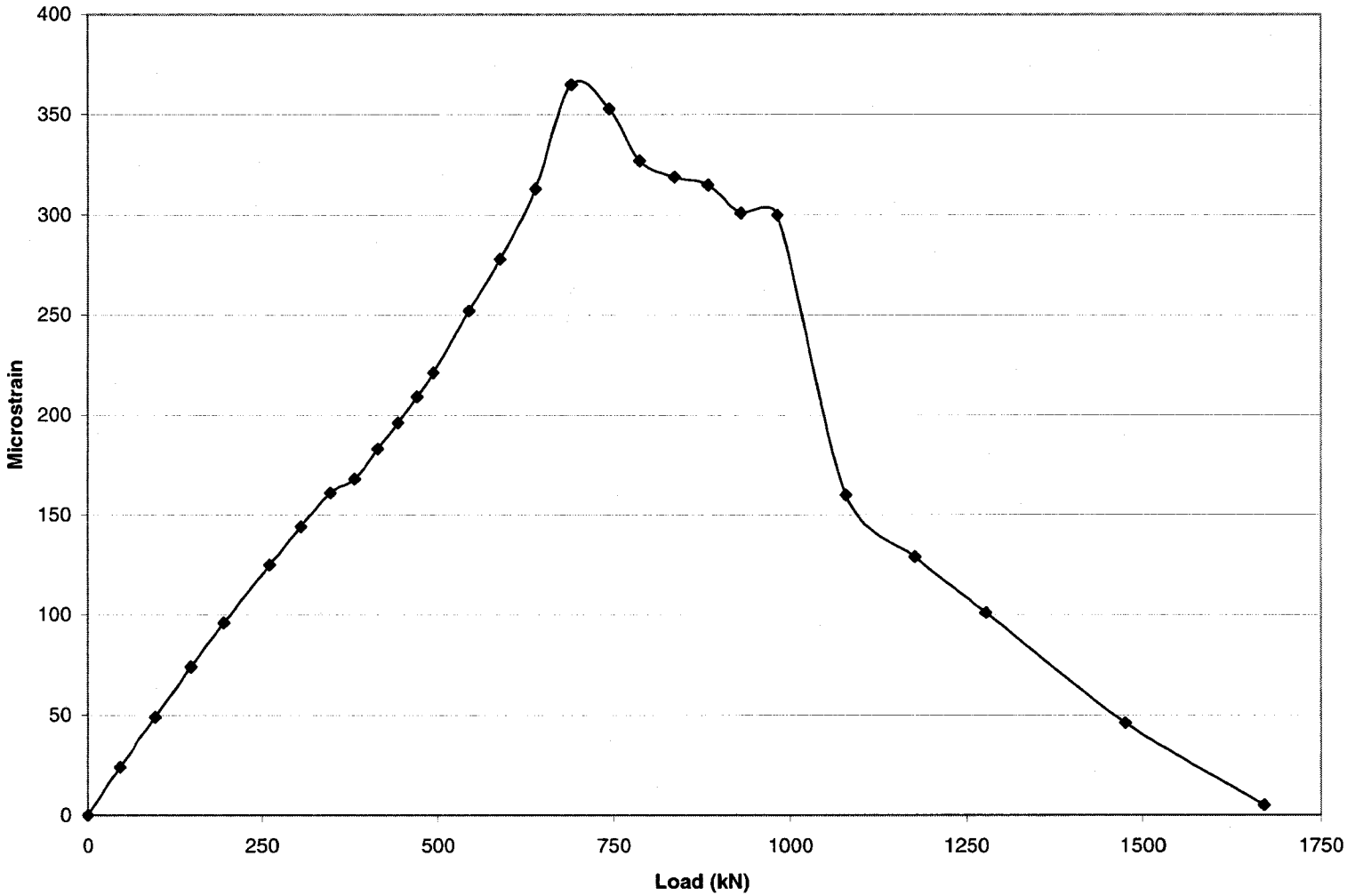

Figure 4.26 Load Versus Strain for Test Number 4

Figure 4.27 Load Versus Strain for Test Number 5a

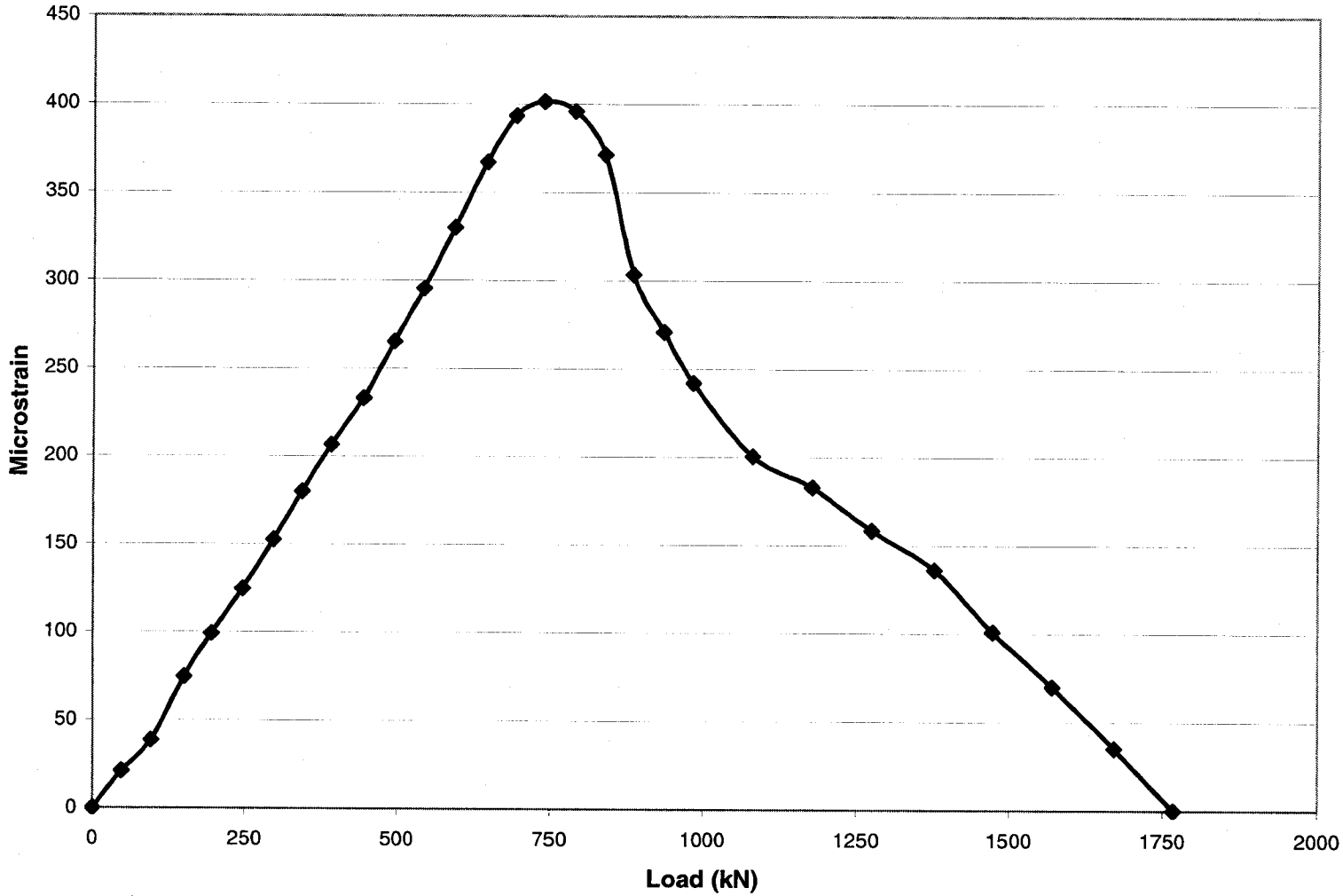

Figure 4.28 Load Versus Strain for Test Number 5b

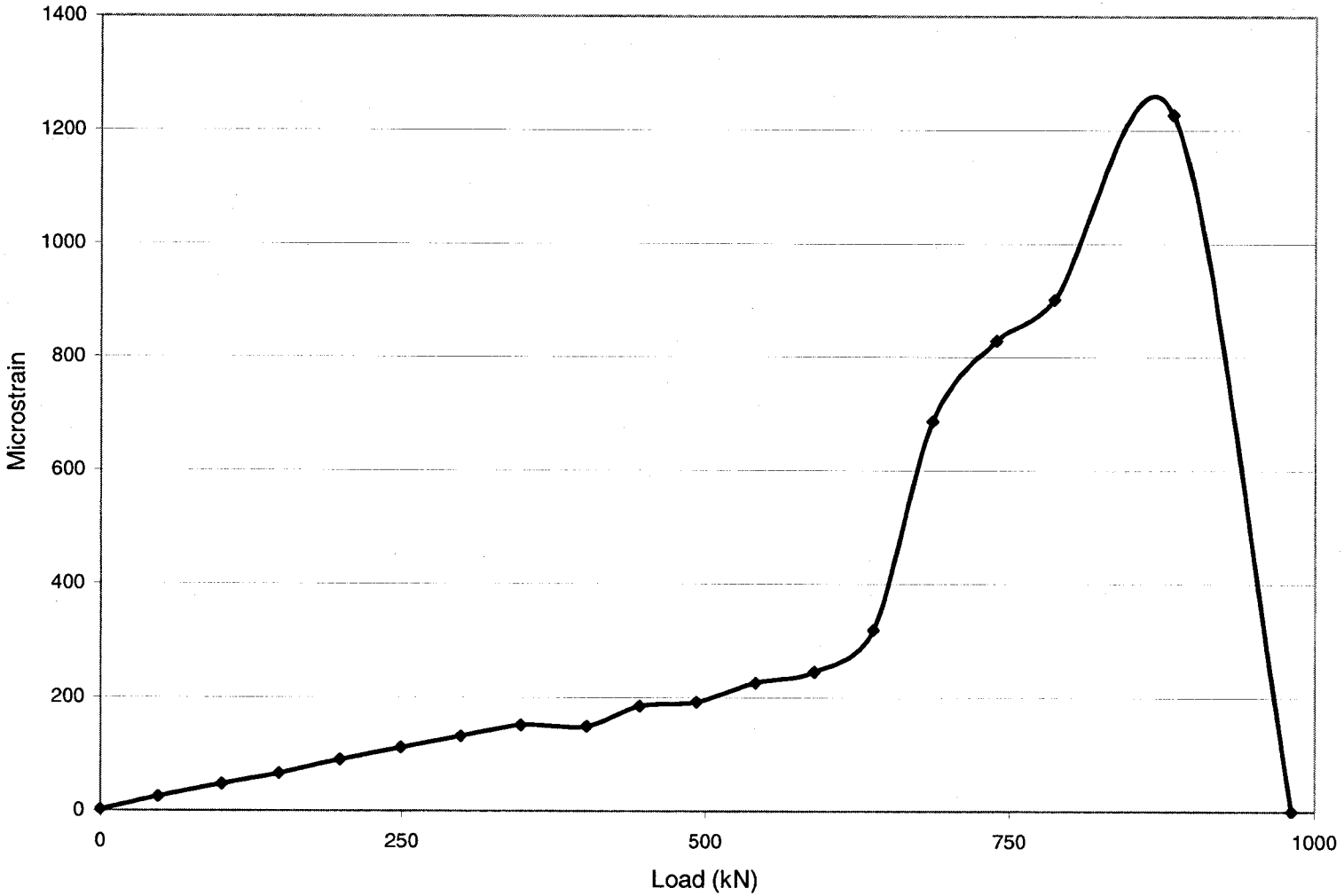

Figure 4.29 Load Versus Strain for Test Number 6

4.11 Behavior of Strain Gauges

Based on a calculated modulus of elasticity for concrete, the concrete strain due to prestress transfer was calculated. The bottom fibre strains based on the compressive strength of the concrete at time of transfer are shown in Table 4.12 below. Note that compressive strains have been indicated as positive, while tensile strains are indicated as negative.

Slab No.	Test No.	Stress at transfer (MPa)	fc_i (MPa)	E (MPa)	Strain at transfer X 10^{-6}
Slabs Tested in Normal Position					
1	1	20.66	36.4	33,180	622
2	2	20.66	36.4	33,180	622
3	6	20.66	47.5	37,900	545
4	5a	20.66	47.5	37,900	545
4	5b	20.66	47.5	37,900	545
5	4	20.66	47.1	37,750	547
Slabs Tested in the Inverted Position					
6	3	3.02*	47.1	37,750	80

Table 4.12 Bottom Fibre Stresses and Strains due to Prestress Transfer

At the time of testing, the strain in the slabs would have decreased due to prestress losses. The calculated strains within the concrete at the time of testing, but before the application of load are shown in Table 4.13.

Slab No.	Test No.	Stress at time of test (MPa)	fc' (MPa)	E (MPa)	Strain at time of test X 10^{-6}
Slabs Tested in Normal Position					
1	1	16.54	79.7	49,100	336
2	2	16.54	79.7	49,100	336
3	6	16.54	89.6	52,060	318
4	5a	16.54	89.6	52,060	318
4	5b	16.54	89.6	52,060	318
5	4	16.54	98.6	54,610	303
Slabs Tested in the Inverted Position					
6	3	1.54*	98.6	54,610	28

Table 4.13 Bottom Fibre Stresses and Strains Just Prior to Testing

The bottom strain gauges were affixed to each slab 38 mm (1.5 in.) above the bottom of the slab. Table 4.14 below indicates the strains at first cracking, as detected by the strain gauges and the corresponding strain at the bottom of the slab. These are the apparent strains. The true strain is the addition of the pre-existing compressive strain in the slab at the bottom fibre plus the addition of the tensile strain from applied loading up to the point of first cracking.

The data from the strain gauges at the bottom of slab number 3, test number 6, were not reliable. It can be seen from Table 4.14 that the true strain at the time of first cracking is significantly different from that of the other tests. Therefore, if the data from test number 6 and 3 (slab inverted) is ignored, the average true cracking strain is -0.000152 in tension. Using an average modulus of 51,946 MPa (7,532,000 psi) for all slabs tested, indicates that the slabs cracked when the concrete reached an average tensile stress of 7.9 MPa (1,150 psi).

Slab Number.	Test Number.	Bottom fibre strain, due to prestress, at time of test x 10^{-6}	Strain at first cracking as detected by strain gauge x 10^{-6}	Strain at first cracking at bottom of slab x 10^{-6}	True strain in bottom of slab at first cracking x 10^{-6}
Slabs Tested in Normal Position					
1	1	336	-428	-503	-167
2	2	336	-412	-485	-148
3	6	318	-319	-375	-57
4	5a	318	-409	-481	-163
4	5b	318	-402	-472	-154
5	4	303	-365	-429	-126
Slabs Tested in the Inverted Position					
6	3	28	-95	-118	-90*

Table 4.14 True Strain in Bottom of Slab at Time of First Cracking

Based on the average compressive strength of concrete of 89.4 MPa (12,963 psi), slab cracking occurred when the tensile stress within the concrete reached a value of 7.9/ 89.4 = 0.088 fc', and is somewhat below previously published data of 0.1 fc' by Zielinski [1969].

In Tests 1, 2, 4, 5a and 5b, cracks opened on either side of strain gauges but did not run through them. In Tests 3 and 6, Figures 4.25 and 4.29 cracks ran across the gauges and unnaturally stretched them before they ruptured. Therefore, none of the readings beyond the linear stage can be used in calculations because cracking near and or across the gauge has affected the results. Figure 4.30 is a representation of what occurs as crack tips initiate and progress up and beyond the gauge position.

When cracks are just on the verge of starting with tips ready to appear at location 1, the apparent strain at gauge position is approximately 400uε. When the crack tips reach

location 2, the tensile strain at the crack drops to zero, and the average strain across the 50 mm (2 in.) gauge length is reduced to about 350uε. When the cracks reach location 3, the stretching of the concrete has been further relieved, and the average strain may now be only 250uε along the gauge length.

At crack tip location 4, the crack has opened sufficiently wide at gauge position that the concrete there receives little tensile pull, and the gauge reading may be reduced to as little as 100uε.

At crack tip location 5, there remains essentially a piece of concrete clinging to the strand and surrounding concrete has almost no influence on its behaviour. The strand by this point has been significantly stretched and reduced in diameter. This was not measured however it is very likely that by this time loss of bond and slippage might have occurred. Again this was not measured.

Tests 1, 2, 4 & 5b seem to fit the above described pattern, but Test 5a shows increasing tension after a significant reduction. It can only be surmised that a new crack ran across the gauge and stretched it unnaturally

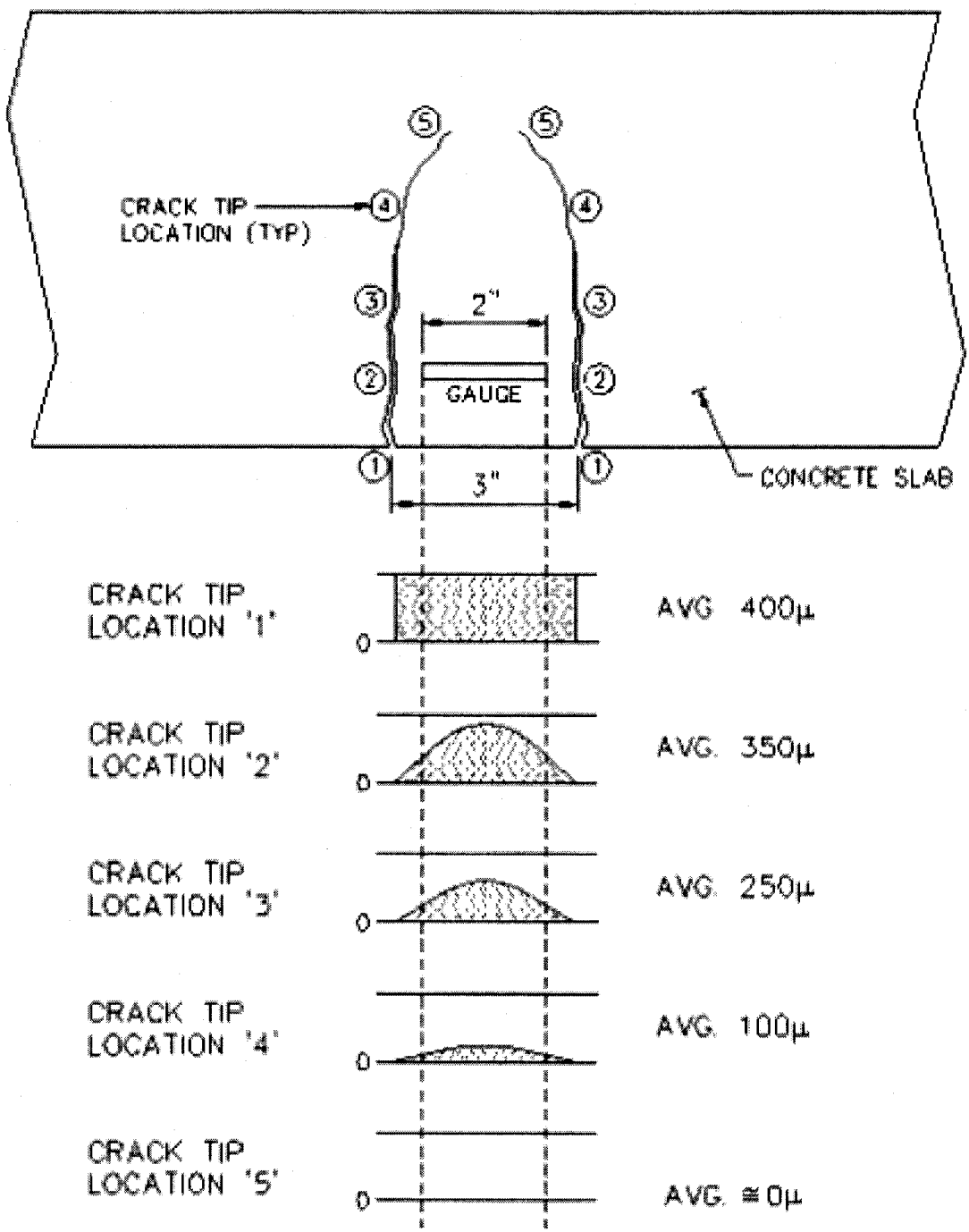

Figure 4.30 Representation of strain behaviour after first cracking

The true stress-strain graph for each test is shown in Figures 4.31 to 4.37 inclusive. Note that this is the stress-strain in the concrete obtained from the gauge location 37.5 mm (1.5 in.) above the bottom of the slabs. These graphs were obtained by adding to the measured tensile strain and the calculated compressive strain from prestress. Concrete will crack when the tensile strain within the concrete reaches a value of 140 to 200 microstrain. It can be seen that at first cracking, the tensile strains are lower than the above values and is indicative of slightly earlier cracking behaviour.

These graphs indicate the initial compression within the slab at the strain gauge level and the effect of increasing loading, which induces tension. When a large enough loading is applied to cause the principal tensile stress to equal the cracking strength of concrete, flexural cracking occurs.

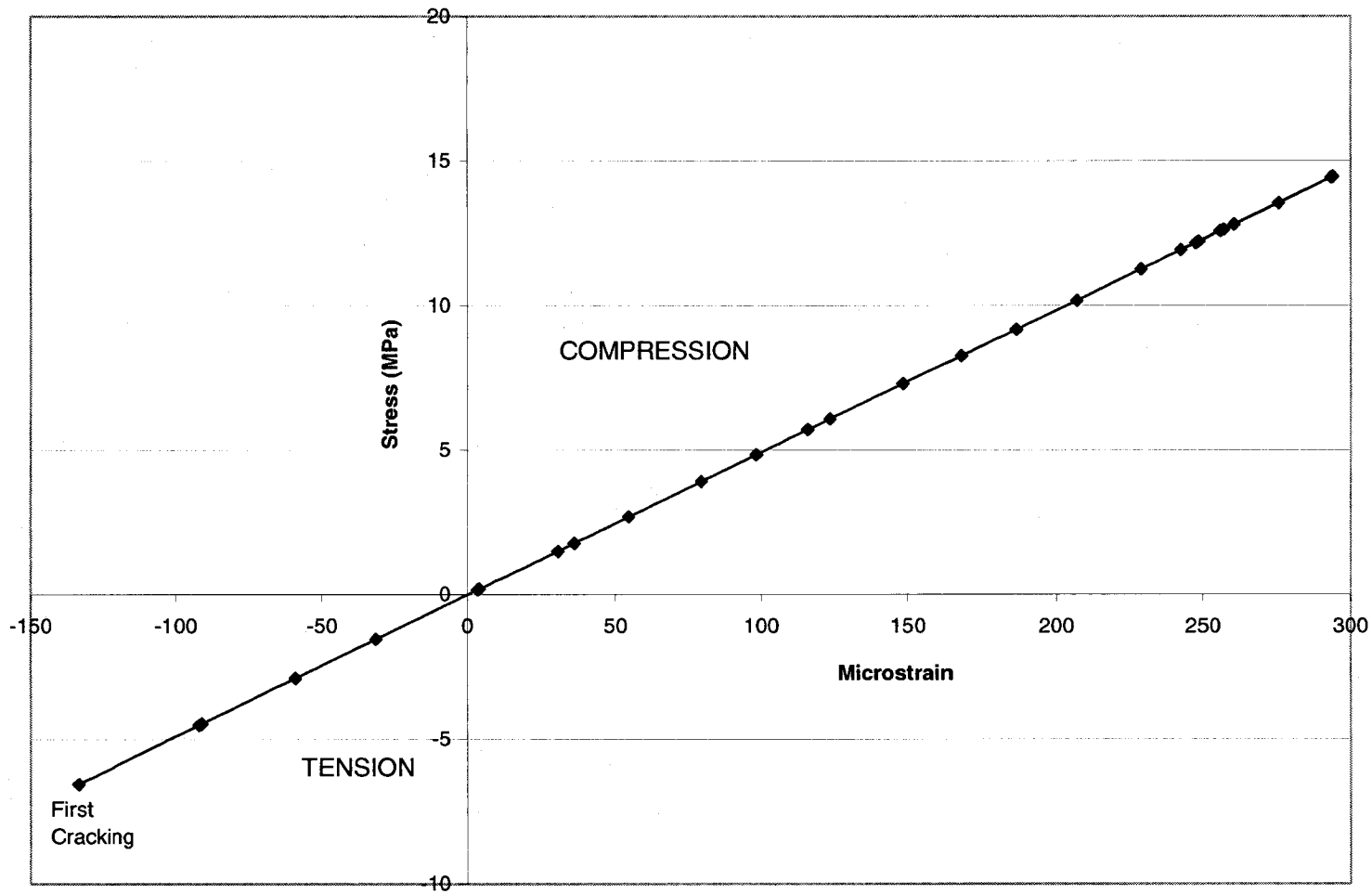

Figure 4.31 Computed true stress- strain curve up to first cracking for test number 1

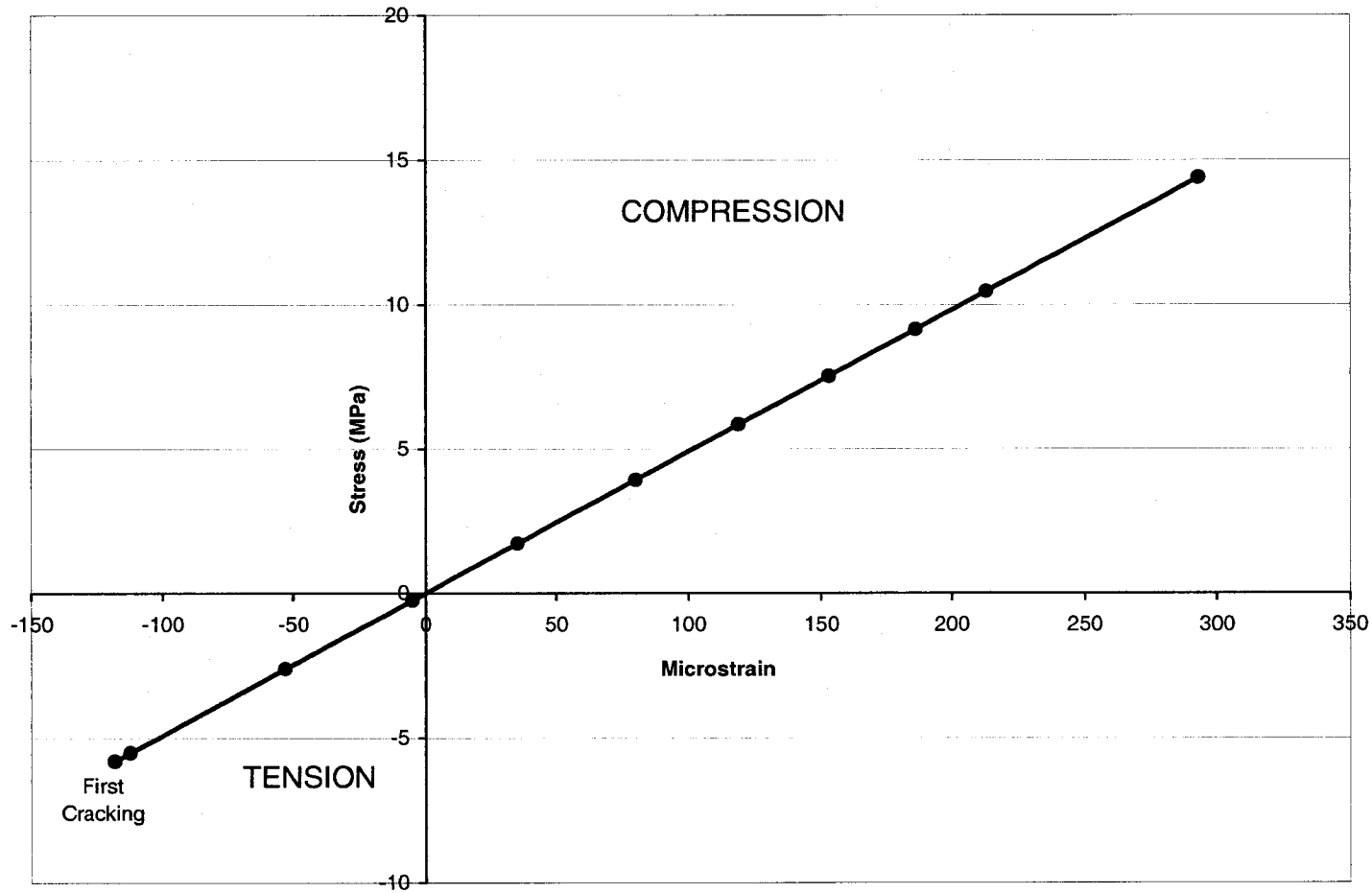

Figure 4.32 Computed true stress-strain curve up to first cracking for test number 2

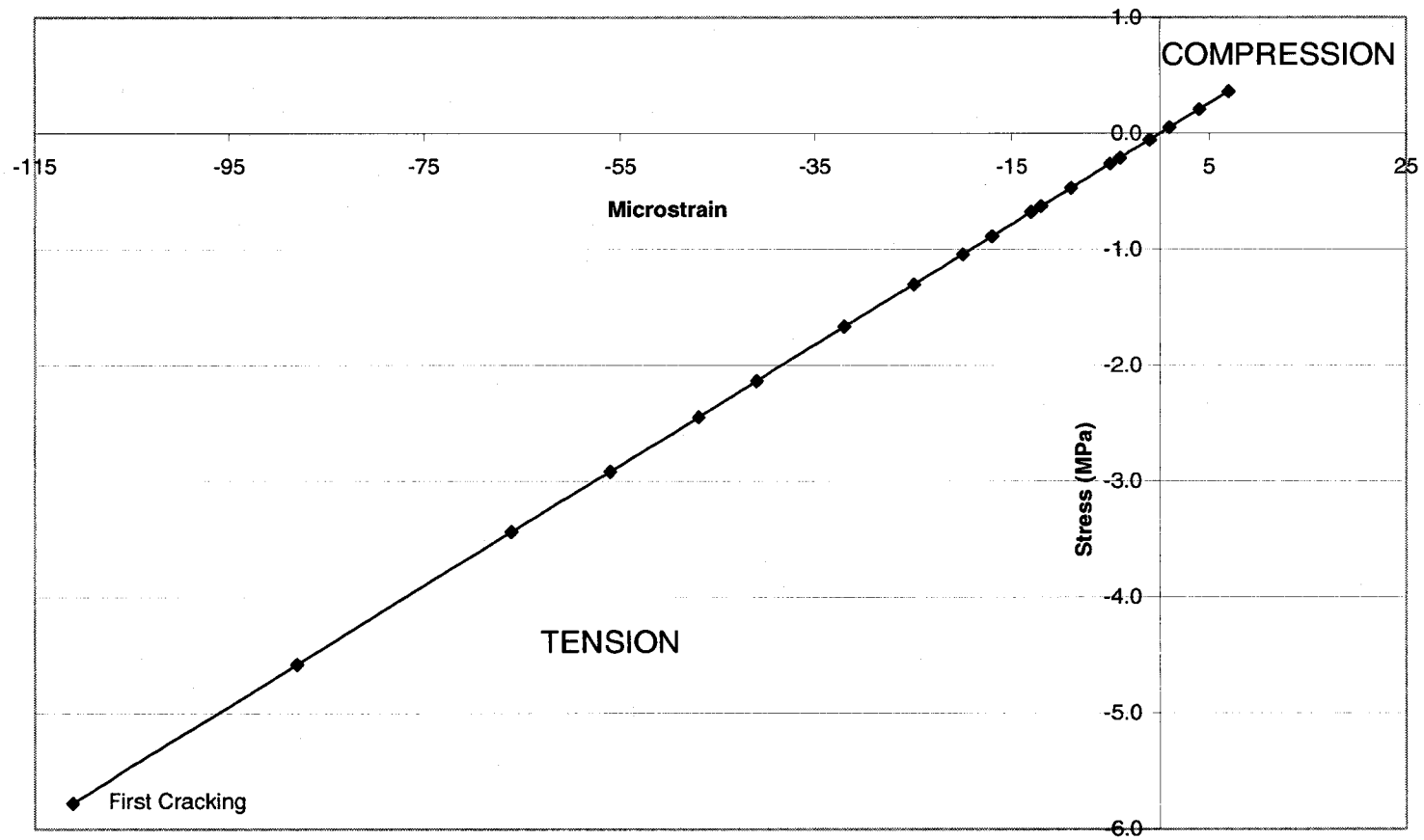

Figure 4.33 Computed true stress-strain curve up to first cracking for test number 3

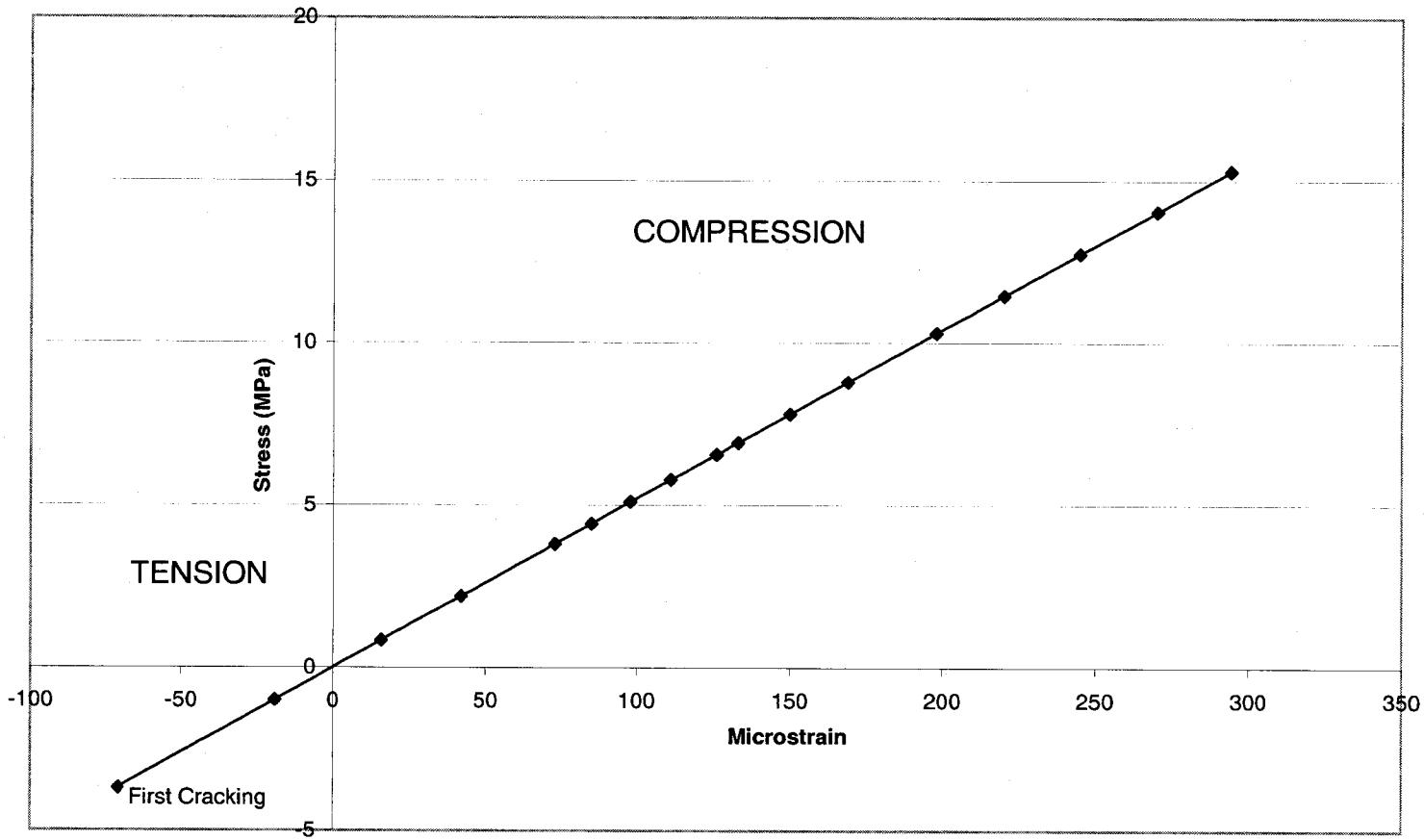

Figure 4.34 Computed true stress-strain curve up to first cracking for test number 4

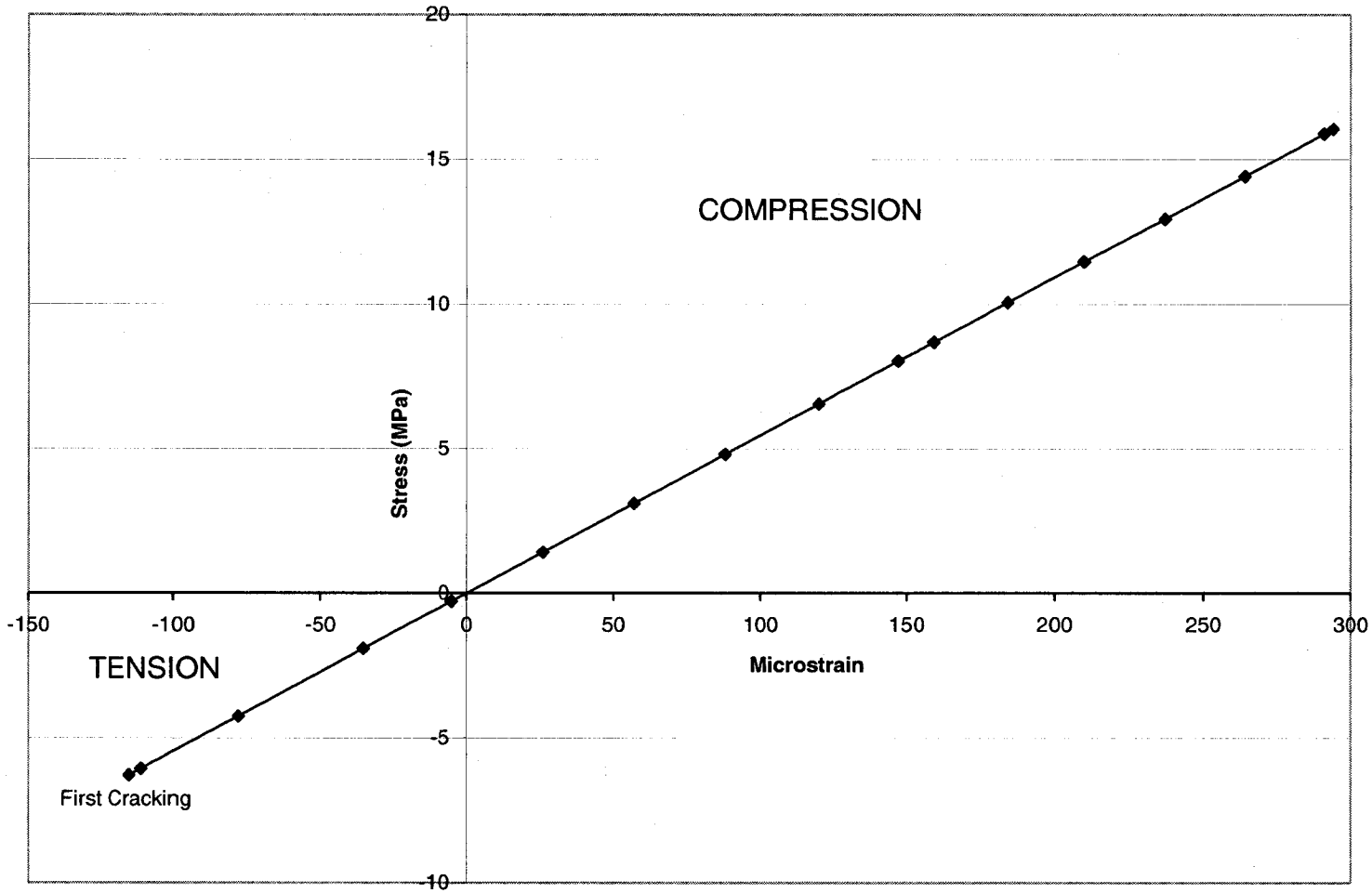

Figure 4.35 Computed true stress-strain curve up to first cracking for test number 5a

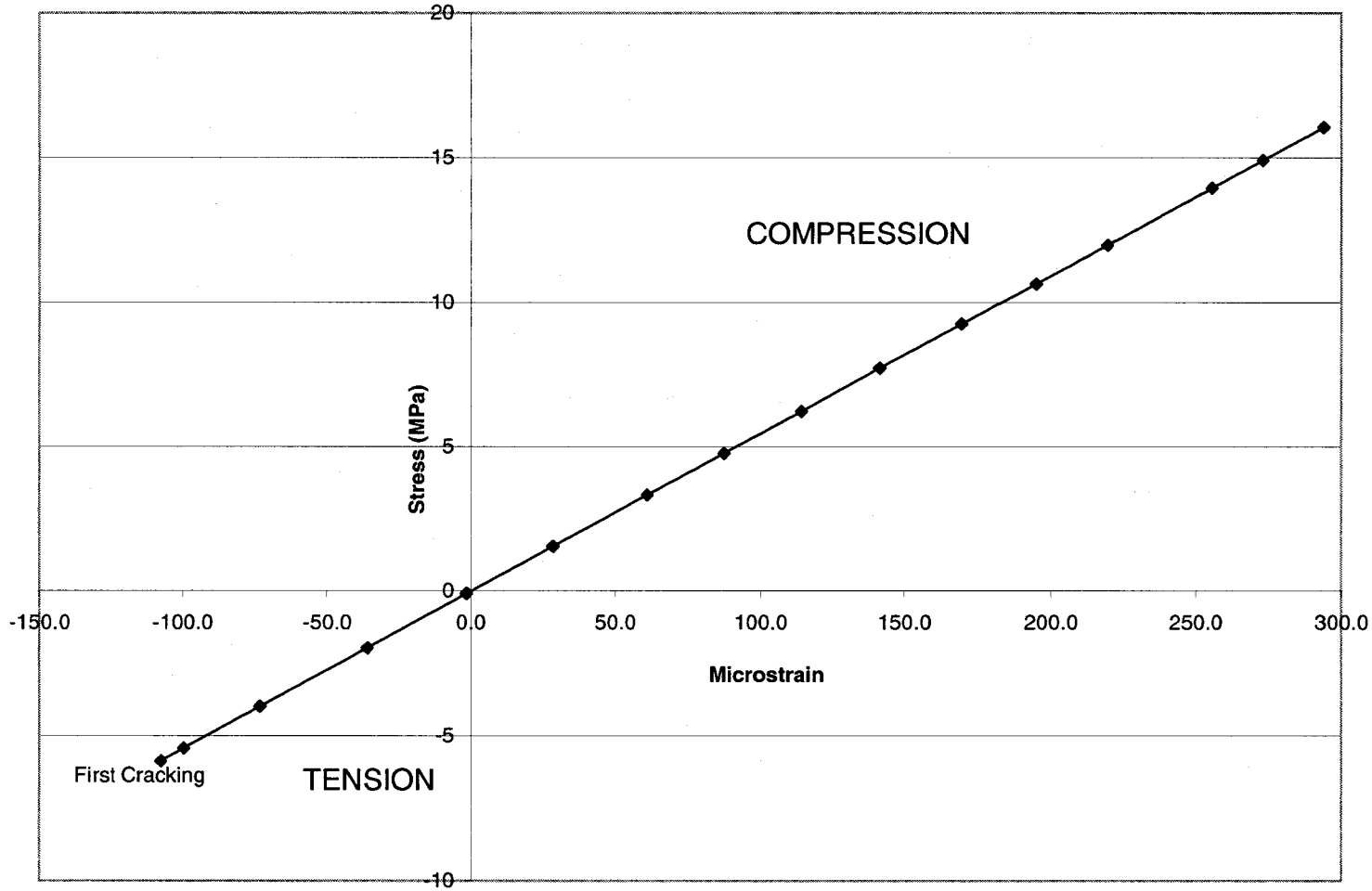

Figure 4.36 Computed true stress-strain curve up to first cracking for test number 5b

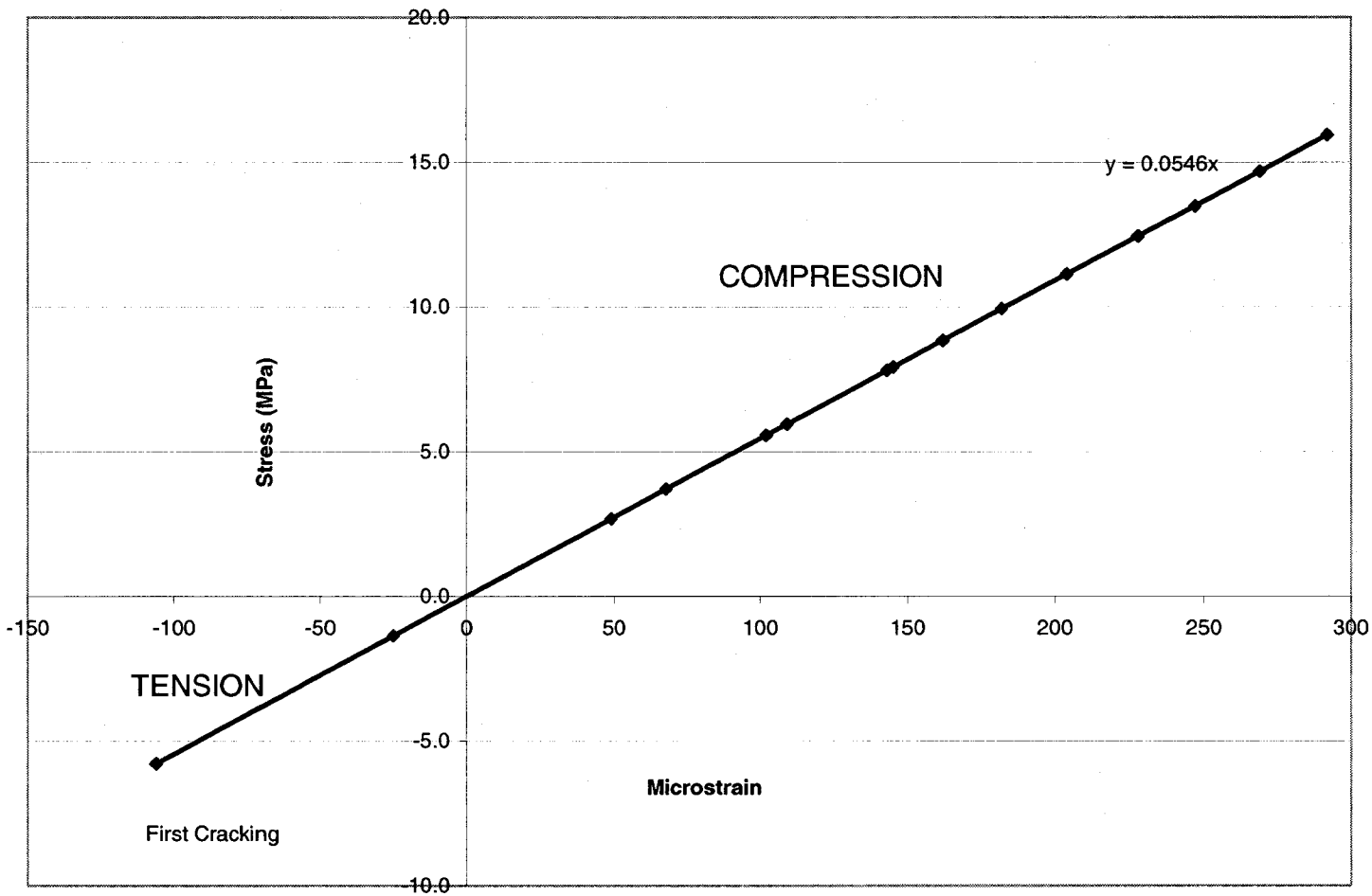

Figure 4.37 Computed true stress-strain curve up to first cracking for test number 6

4.12 Shear Capacity

4.12.1 Vertical Shear Force

Table 4.15 below indicates the theoretical vertical shear force in each shear span at the ultimate capacity of each slab.

Test Number	Deck Slab Number	Shear Span a (m)	Shear Span b (m)	Load at Ultimate (kN)	Shear in Span a (kN)	Shear in Span b (kN)
1	1	1.22	1.22	1,678	839	839
2	2	1.22	1.22	1,697	839	839
3	6	1.22	1.22	873	437	437
4	5	0.91	1.53	1,962	1,230	732
5 a	4*	0.61	1.83	1,922*	1,442	550
5 b	4	0.61	1.83	2,139	1,604	535
6	3	0.91	1.53	1,884	1,181	703

Table 4.15 Shear Force Values Based on Experimental Load at Ultimate

4.12.2 Flexural Shear Cracking

Flexural shear cracking is defined as the extension of flexural cracks by inclined cracking at approximately 45 degrees to the axis of the slab. This is due to the presence of tensile stresses normal to crack and equal in magnitude compressive stresses parallel to the crack

According to the ACI code, the flexural shear value, V_{ci}, in prestressed concrete members is obtained from the addition of $0.05\sqrt{f'c}\,b_w d$ to the shear that existed when flexural cracking first formed. The resulting equation for flexural cracking then becomes:

$$V_{ci} = 0.05\sqrt{f_c'}\,b_w d + \frac{V}{M} M_{cr} \qquad 4.8$$

Where: $\frac{V}{M}$ = the shear to moment ratio at the section being considered

M_{cr} = the moment to cause flexural cracking at the section being considered

f_c' = the compressive strength of concrete

b_w = the width of the web of the prestressed concrete member

d = is the greater of the distance from the extreme compression fibre to the centroid of the prestresses reinforcement or 0.8 times the overall depth of slab (0.8h)

$$M_{cr} = \left(\frac{P}{A} + \frac{Pe}{S_b} + 0.5\sqrt{f_c'} \right) S_b \qquad 4.9$$

The calculated flexural shear cracking and the experimental shear cracking load for each slab is shown in Table 4.17. The flexural shear has been calculated for increments of 0.1a, where a is the length of shear span. These are compared against the experimental flexural shear cracking values. It can be seen that the experimental flexural shear values exceeded the calculated values for all slabs tested.

4.12.3 Web Shear Cracking

Web shear cracking, V_{cw}, is defined as the diagonal cracking that forms at mid height of the member, near the centroid, in concrete that had not previously developed cracks. The AREMA formula for web shear cracking is as follows:

$$V_{cw} = \left(0.29\sqrt{f_c'} + 0.3 f_{pc}\right) b_w d \qquad 4.10$$

Where :

f_c' = the compressive strength of concrete

$$f_{pc} = \frac{P}{A} \qquad 4.11$$

b_w = the width of the web of the prestressed concrete member

d = the distance from the extreme compression fibre to the centroid of the (tension) prestressing reinforcement, but in no case less than 0.8h

Table 4.16 below indicates the theoretical web shear cracking values for each slab, based on the actual compressive strength of concrete.

Test No.	Slab No.	V_{cw} (kN)
1	1	2339
2	2	2339
3	6	2462
4	5	2432
5a	4	2346
5b	4	2346
6	3	2376

Table 4.16 Web Shear Cracking Values

Test No.	Predicted		Experimental	
	Distance from Support (m)	V_{ci} (kN)	Distance from Support (m)	V_{ci} (kN)
Test No. 1 Slab No. 1	0.1	4,128		
	0.2	2,194		
	0.3	1,550		
	0.4	1,229		
	0.5	1,038		
	0.6	910		
	0.7.	820		
	0.8	752		
	0.9	700	0.902	1,344
	1.0	658		
	1.1	625	1.07	971
	1.22	594		
Test No 2 Slab No. 2	0.1	4,128		
	0.2	2,194		
	0.3	1,550		
	0.4	1,229		
	0.5	1,038		
	0.6	910		
	0.7.	820		
	0.8	752		
	0.9	700	0.90	1,079
	1.0	658		
	1.1	625	1.1	834
	1.22	594		
Test No. 4 & 6 Slab No. 5 & 3	0.1	4,387		
	0.2	2,331		
	0.3	1,570		
	0.4	1,261		
	0.5	1,073		
	0.6	946	0.60	1,766
	0.7	840		
	0.8	774	0.75	1,472
	0.9	724		
Test No. 5a & 5b Slab No. 4	0.1	4,187		
	0.2	2,229		
	0.3	1,578	0.30	1,668
	0.4	1,253		
	0.5	1,059	0.45	1,275
	0.6	930		

Table 4.17 Comparison of Flexural Shear Cracking Values

4.13 Arching Action

According to Zielinski [1969] shear theory is only applicable for bonded members in the early stages of elastic behaviour up to the onset of 45 degree inclined cracking. Beyond that, it ceases to apply and the internal arching action of concrete replaces it.

In addition, Bakht and Jaeger [1985] and Mufti, Bakht and Jaeger [1986] have shown that deck slabs instead of working in pure flexure also develop an internal arching system. In prestressed deck slabs, the tie to the transverse arch is provided by the prestress reinforcement near the bottom of the slab. Under increasing loading cracks develop at or near the point of applied loading. This results in a net compressive force at the bottom of the slab at the support locations. At the point of applied loading the compressive force moves towards the top of the slab. See Figure 4.38 for an illustration of the internal arching action within slabs.

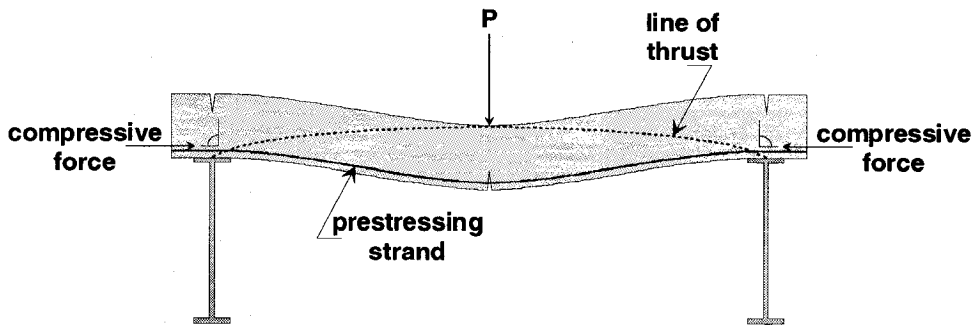

Figure 4.38 Idealization of the arching scheme within a slab

The transition of the compressive force from the bottom of the slab at the supports to the top of the slab at the applied load corresponds to an internal arch. According to Bakht and

Jaeger, the internal aching action within the slab is difficult to predict with any degree of accuracy even with refined analytical methods.

Test No.	Slab No.	Shear Span a mm	Effective Depth mm	a/d Ratio	$\frac{Experimental\ M_U}{Predicted\ M_U}$
Slabs Tested in Normal Position					
1	1	1,220	160	7.6	0.97
2	2	1,220	160	7.6	0.98
4	5	910	152	6.0	1.05
5a	4	610	144	4.2	N.A
5b	4	610	144	4.2	0.90
6	3	910	152	6.0	1.00
Slabs Tested in the Inverted Position					
3	6	1.220	90	13.6	0.97

Table 4.18 Span to Depth and Cracking Moment to Ultimate Moment Ratios for all Slabs

Figure 4.39 indicates the relationship of a/d ratio on the shear strength of members without stirrups, adopted from MacGregor and Bartlett [2000]. The vertical axis represents the ratio of the moment at the load point to cause failure (M) to the flexural moment capacity of the member (M_n). Superimposed on this graph are the values for each slab test.

Members with a/d ratios < 1.0 are considered very short and generally fail by anchorage failure at the supports after developing inclined cracks from the support to the load point. After inclined cracking begins, the behaviour of the member changes from one of beam action to that of arch action. Members with a/d ratios of 1.0 to 2.5 are considered short members and generally fail by loss of bond, splitting failure or failure of the compression strut. These members carry additional load in part by arch action.

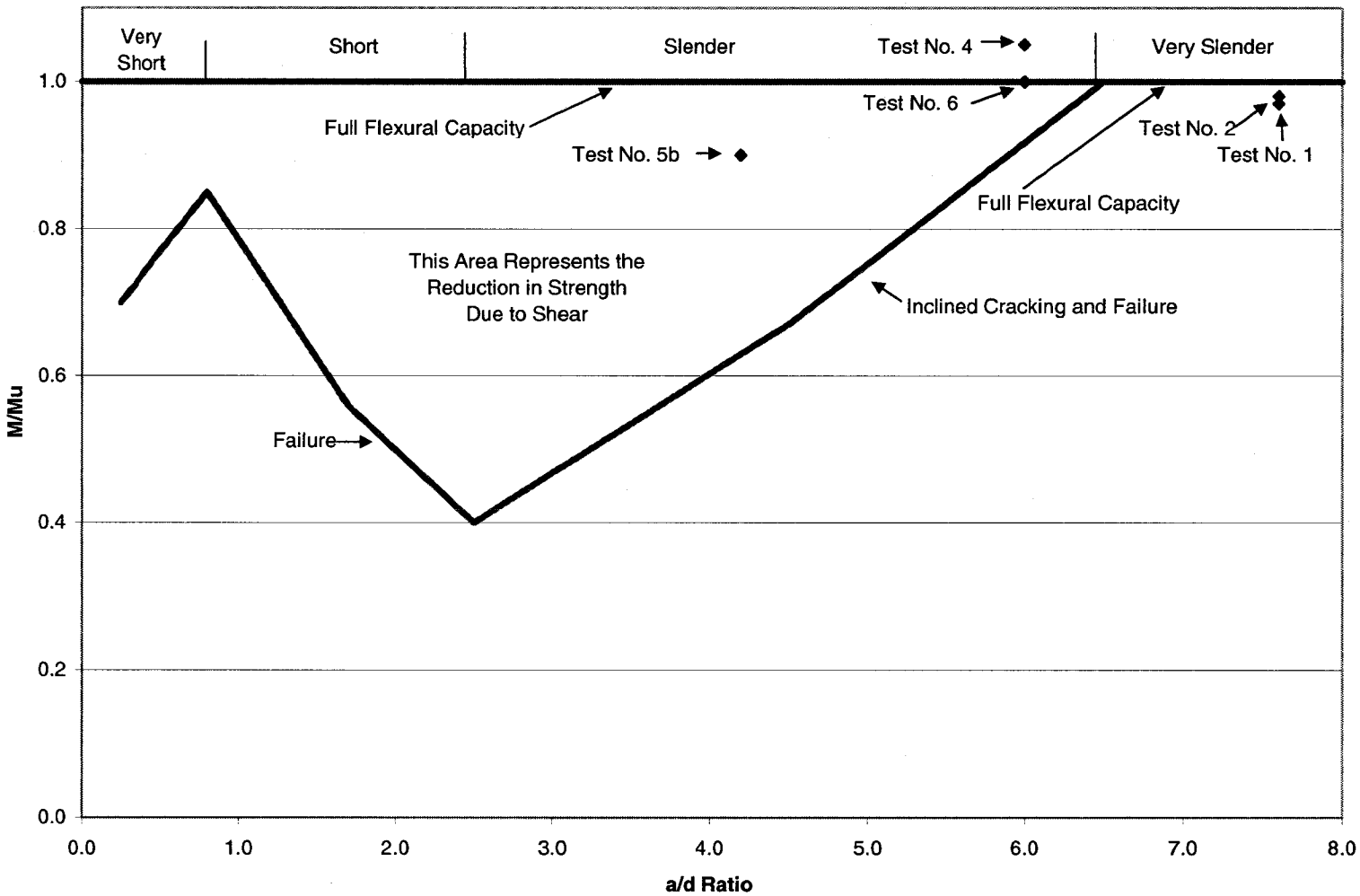

Figure 4.39 Relationship of a/d ratio on shear strength of slabs without stirrups (adopted from MacGregor and Bartlett)

Members with a/d ratios of 2.5 to 6.5 are considered as slender and generally fail by inclined cracking. Members with a/d ratios > 6.5 are considered very slender and fail by flexure as the shear to form inclined cracking exceeds the shear corresponding to flexural failure. Flexural failure occurs before inclined cracking begins.

From the a/d ratios in Table 4.18 it can be seen that the slabs are categorized as either slender or very slender members. Slabs in tests 1, 2 and 3 should be expected to reach their full flexural capacity. However, slabs in test 4, 5b and 6 should have failed in shear. It is possible that a tied arch action within the slabs helped achieve their full flexural capacity.

Reaching full flexural capacity also implies that both the bond development length must have been sufficient to develop the yield force in the strand. Table 4.19 indicates the minimum transfer lengths required by various codes. Figure 4.40 indicates the theoretical development of stress in the strand.

Code Name	Transfer Length Expression	Transfer Length Mm
ASHTO 1996	$L_t = 50D$	762
ASHTO 1998	$L_t = 60D$	914
CSA	$L_t = 50D$	762
ACI 318-99	$L_t = \frac{f_{se} D}{20.7}$	789

Table 4.19 Comparison of Prestress Transfer Lengths

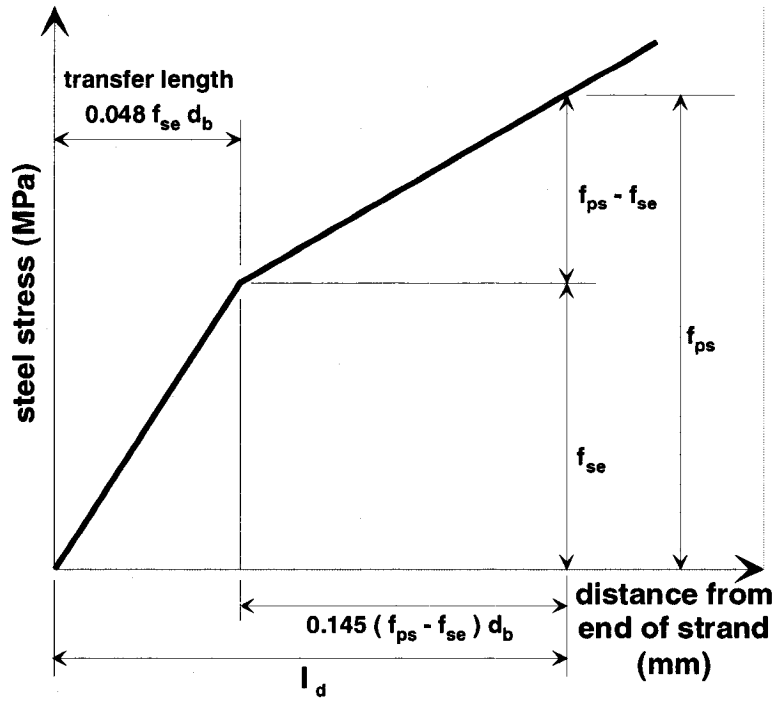

Figure 4.40 Development of stress in strand (adopted from Collins and Mitchell)

Table 4.20 below indicates the various prestress development lengths by various codes. The prestress development length is defined as the sum of both the transfer length and flexural bond length. Note that the imperial expressions have been converted to metric with the appropriate conversion factor.

Code Name	Development Length Expression	Slab 1 and 2 mm	Slab 3 and 4 mm	Slab 5 and 6 mm
CSA	$0.048f_{se}d_b + 0.145(f_{ps}-f_{se})d_b$	2882	2145	2180
AREMA	$0.145(f_{ps}-.66\ f_{se})d_b$	2120	2166	2201
ASHTO 1996	$0.145(f_{ps}-.66\ f_{se})d_b$	2120	2166	2201
ACI 1999	$0.145(f_{ps}-.66\ f_{se})d_b$	2120	2166	2201

Table 4.20 Comparison of Prestress Development Lengths

An interesting observation is that only test 5b, deck slab number 4, failed by more than 5 percent from the calculated ultimate capacity. It failed at 90 percent of the predicted ultimate capacity. Test 5a performed on the same slab was terminated prior to failure, so

that the slab could be reused for test 5b. It is noted that in both tests 5a and 5b the slab was loaded at a distance of 610 mm from the support. At that point the development length would only have been 1240 mm.

Tests 4 and 6 loaded the slab at a distance of 910 mm from the support. In those tests, the maximum development length was 1540 mm. Those slabs reached 105 and 100 percent of their calculated ultimate capacity respectively. This suggests that the bond development length for those slabs was adequate and that the code requirements are conservative.

In their research work on transfer and bond development length on 15 mm strand, Kahn, Dill and Reutlinger [2002] found that 15 mm strand showed good bond and development characteristics. In fact they noted that the required transfer length was 41 to 51 percent less than that calculated by ASHTO 1996 specification. In addition the required development length was found to be 20 percent less than calculated by the current ASHTO 1996 code requirements.

The current research, based on the results of tests 4 and 6 suggests that the code requirements for bond development length for high performance concrete may be closer to 30 percent too conservative. These results are in keeping with the results obtained by Rosenburg [1986] who found increased bond strength in HPC of 40 percent and DeLarrar et al [1988] who also found increased bond strength in HPC slabs. This is generally attributed to the use of silica fume.

CHAPTER 5

Economic Analysis

5.1 Economic Analysis

The economic analysis of the slab will be divided into two sections. The first section will deal with the economics associated with the slab itself in terms of the amount of concrete and steel used in the manufacture. The second section will deal with the economic impact on work blocks and train delays associated with a longer deck slab.

5.2 Economic Impact on Manufacture

The manufacturer of the slab has indicated to CN that for every m^3 of concrete either added or removed from the existing slab would result in a cost adjustment of $250.00 Can. (in 2004 dollars). Similarly, for every m^3 of steel strand that is added or removed from the existing slab would result in a cost adjustment of $7,857.14 Can. (in 2004 dollars).

An analysis was undertaken to determine the relationship of thickness of slab at centre to the amount of prestressing steel required. Imposed stress requirements at prestress transfer and at service loading prevent the slab from being less than 200 mm (8 in.) thick. Figure 5.1 indicates the linear relationship between the amount of concrete required for a 4 m by 2.44 m slab (13 ft. by 8 ft.) with the curbs excluded and the slab thickness. Logically, as the slab thickness decreases so does the amount of concrete required for the slab.

Figure 5.2 indicates the relationship between slab thickness and the amount of prestressing steel required to maintain the same stress levels under service loading as the design used in this experimental program. It can be seen that as the slab thickness decreases the amount of prestressing steel increases almost linearly.

Table 5.1 below, indicates the amount of prestressing steel and concrete required for the varying thickness of slab between 200 and 300 mm (8 in. to 12 in.) in 25 mm (1 in.) increments as well as the associated cost impacts. The existing 275 mm (11 in.) thick slab has been taken as the baseline for the purpose of this analysis. Note that savings are indicated as positive while costs as negative.

Slab Thickness (mm)	Total Volume of Concrete (m^3)	Volume Difference from Baseline (m^3)	Concrete Savings from Baseline $	Total Volume of Steel (m^3)	Volume Difference from Baseline (m^3)	Steel Savings from Baseline $	Total Savings from Baseline $
200	1.66	-0.64	160.13	0.0230	0.0050	-39.60	120.53
225	1.87	-0.43	106.75	0.0213	0.0034	-26.40	80.34
250	2.09	-0.21	53.38	0.0196	0.0017	-13.20	40.18
275 (Baseline)	2.30	0	0	0.0179	0	0	0
300	2.51	0.21	-53.37	0.0168	-0.0011	-8.80	-44.57

Table 5.1 Varying Slab Thickness on Volume of Concrete and Prestressing Steel and Associated Cost Impacts

It can be clearly seen from Table 5.1 that reducing the slab thickness has the greatest benefit on manufacture costs. Figure 5.3 indicates graphically the cost savings associated with varying thickness of the slab.

It should also be noted that there is an additional cost saving that can be obtained from the removal of material from the curbs as detailed in Chapter 2, Section 2.14. That

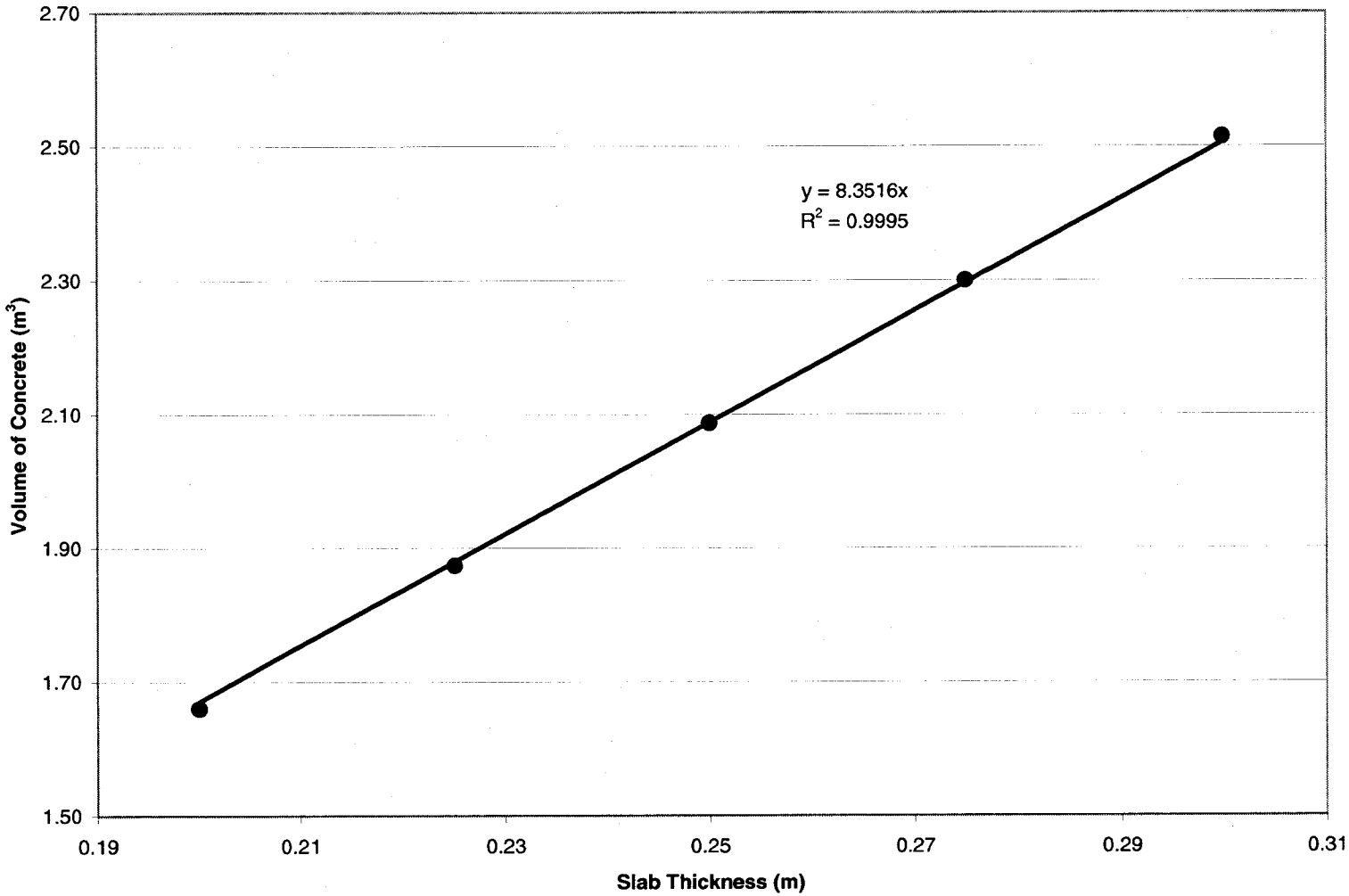

Figure 5.1 Relationship of slab thickness versus volume of concrete

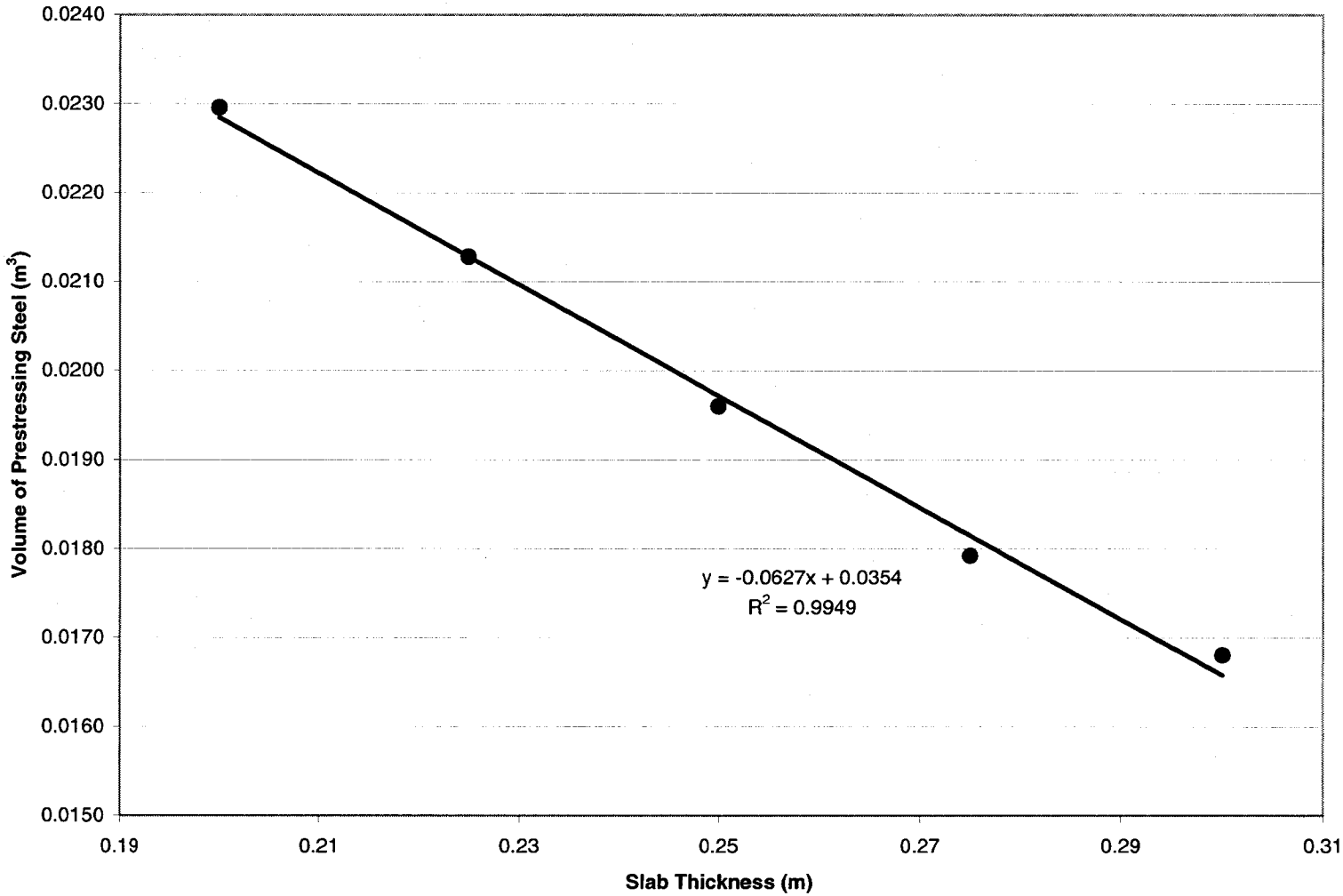

Figure 5.2 Relationship of slab thickness versus volume of prestresing steel

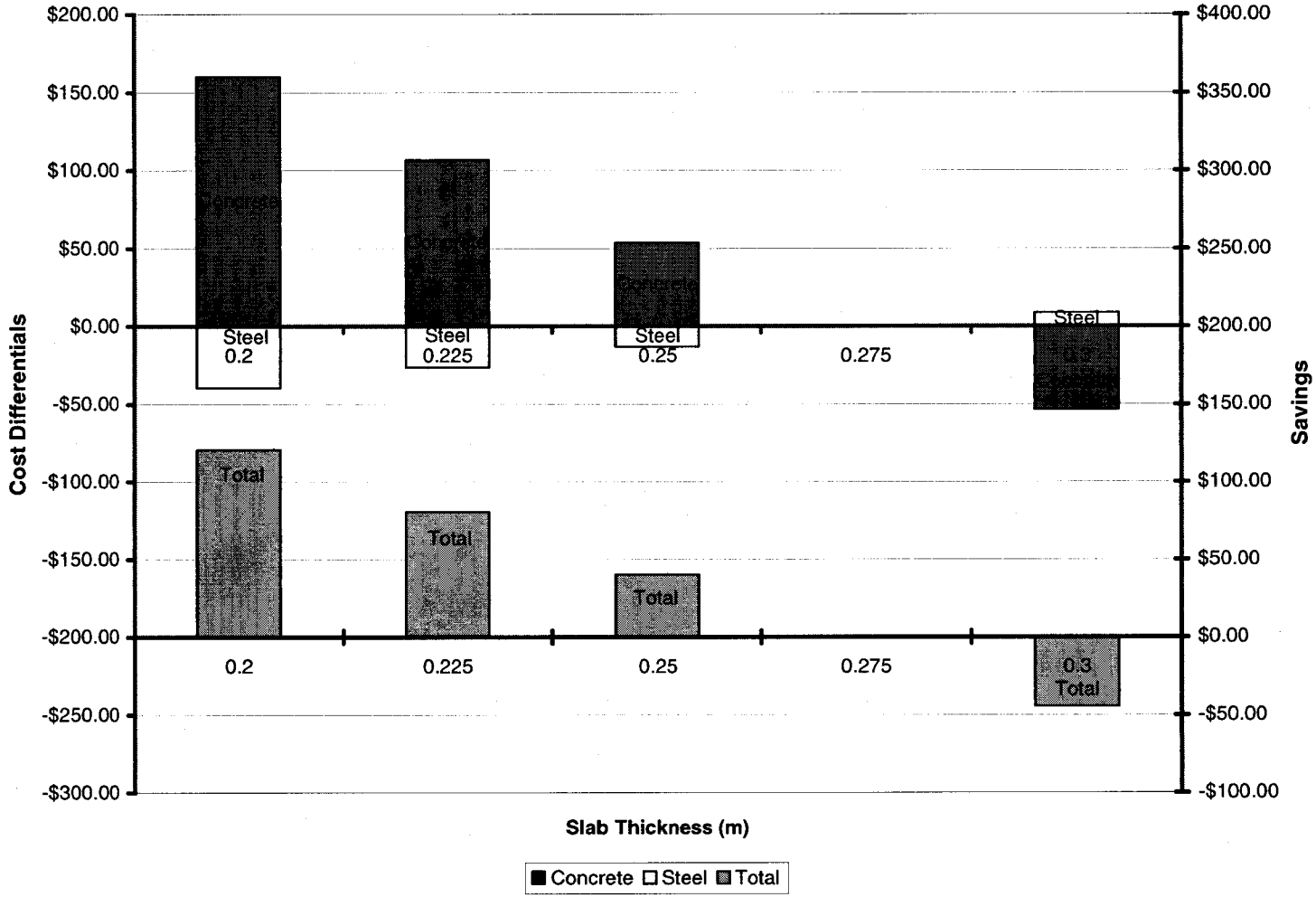

Figure 5.3 Cost savings associated with varying slab thickness

volume was calculated to be 0.117 m^3 (4.13 $ft.^3$). Table 5.2 below indicates the total savings that can be achieved through thinning the slab and removing weight from the curbs.

Slab Thickness (mm)	Savings from Thinning Slab	Savings from Removing Curb Material	Total Savings
200	$120.53	$29.25	$149.78
225	$80.35	$29.25	$109.60
250	$40.18	$29.25	$64.43
275 (baseline)	0	$29.25	$29.25
300	-$44.57	$29.25	-$15.32

Table 5.2 Total Achievable Manufacture Savings Per Slab

Clearly the savings to be achieved by thinning the slab and reducing the concrete in the curbs is not significant. Other savings may be realized as a reduced slab thickness requires less of a ballast raise on the bridge approaches to meet the new top of rail elevation.

5.3 Economic Impact to Work Blocks and Train Delay

Data received from CN on bridge deck conversion indicates that the average time required to pick up a slab, move it into position, place it then return for the next slab is 15 minutes. It has been assumed for the purpose of this analysis that the placement time would be the same if a 2.44 m (8 ft.) or 3.05 m (10 ft.) long slab was used.

The average gang size for such work is 13 men. This represents a direct labour cost of approximately $400/hr. Can. (in 2004 dollars). For the purpose of this analysis, the current approximate CN overhead charges of 185 percent on labour will be factored into this cost. Therefore, the cost for labour would be $1,140.

As detailed in Chapter 1, CN estimates that for each hour of work block the negative impact on trains etc. is $20,000 Canadian. With overheads applied this amount is $57,000. Clearly then there may be economic benefit to placing longer and fewer slabs. Table 5.3 below highlights the time and monetary savings in placing 2.44 m (8 ft.) versus 3.05 m (10 ft.) slabs. Note that Table 5.3 only tabulates values for bridges up to 305 m (1000 ft.) in length.

Bridge Length (m)	No. of 2.44 m Slabs	No. of 3.05 m Slabs	Reduction in Slabs Placed	Time Savings (hrs)	Labour Savings	Train Delay Savings	Total Savings
12.2	5	4	1	0.25	$285	$14,250	$14,535
24.4	10	8	2	0.5	$570	$28,500	$29,070
36.6	15	12	3	0.75	$855	$42,750	$43,605
48.8	20	16	4	1	$1,140	$57,000	$58,140
61	25	20	5	1.25	$1,425	$71,250	$72,675
73.2	30	24	6	1.5	$1,710	$85,500	$87,210
85.4	35	28	7	1.75	$1,995	$99,750	$101,745
97.6	40	32	8	2	$2,280	$114,000	$116,280
109.8	45	36	9	2.25	$2,565	$128,250	$130,815
122	50	40	10	2.5	$2,850	$142,500	$145,350
134.2	55	44	11	2.75	$3,135	$156,750	$159,885
146.4	60	48	12	3	$3,420	$171,000	$174,420
158.6	65	52	13	3.25	$3,705	$185,250	$188,955
170.8	70	56	14	3.5	$3,990	$199,500	$203,490
183	75	60	15	3.75	$4,275	$213,750	$218,025
195.2	80	64	16	4	$4,560	$228,000	$232,560
207.4	85	68	17	4.25	$4,845	$242,250	$247,095
219.6	90	72	18	4.5	$5,130	$256,500	$261,630
231.8	95	76	19	4.75	$5,415	$270,750	$276,165
244	100	80	20	5	$5,700	$285,000	$290,700
256.2	105	84	21	5.25	$5,985	$299,250	$305,235
268.4	110	88	22	5.5	$6,270	$313,500	$319,770
280.6	115	92	23	5.75	$6,555	$327,750	$334,305
292.8	120	96	24	6	$6,840	$342,000	$348,840
305	125	100	25	6.25	$7,125	$356,250	$363,375

Table 5.3 Impact of Slab Length on Labour and Train Delay Savings

Figure 5.4 indicates graphically the relationship between slab length and the number of slabs required for bridges up to 305 m (1,000 ft.). This indicates that the greatest benefit will be derived from the longer bridges.

Figure 5.5 indicates graphically the labour and train delay savings that can be achieved by adopting a longer slab. Adopting a longer slab should result in the placement of fewer slabs and a corresponding decrease in work block time required.

The economic analysis clearly indicates that the greater benefit to CN is not in the thinning of the deck slab itself and the resultant savings in manufacture, but rather in the reduction of weight per unit length allowing for a longer slab of similar weight to be placed. The result is large savings in train and operation delays to CN. Monetarily, these far eclipse either savings in manufacture or savings in gang labour.

During the past 4 years, CN has on average converted 610 m (2,000 ft.) of bridge deck from open deck to ballast deck. From Table 5.3 above, it can be seen that savings of $728,000 Canadian annually in labour and train delay can be realized by adopting the use of HPC. If the savings in manufacture cost on 200 – 3.05 m slabs of $24,000 are added a total annual saving of $752,000 could be realized.

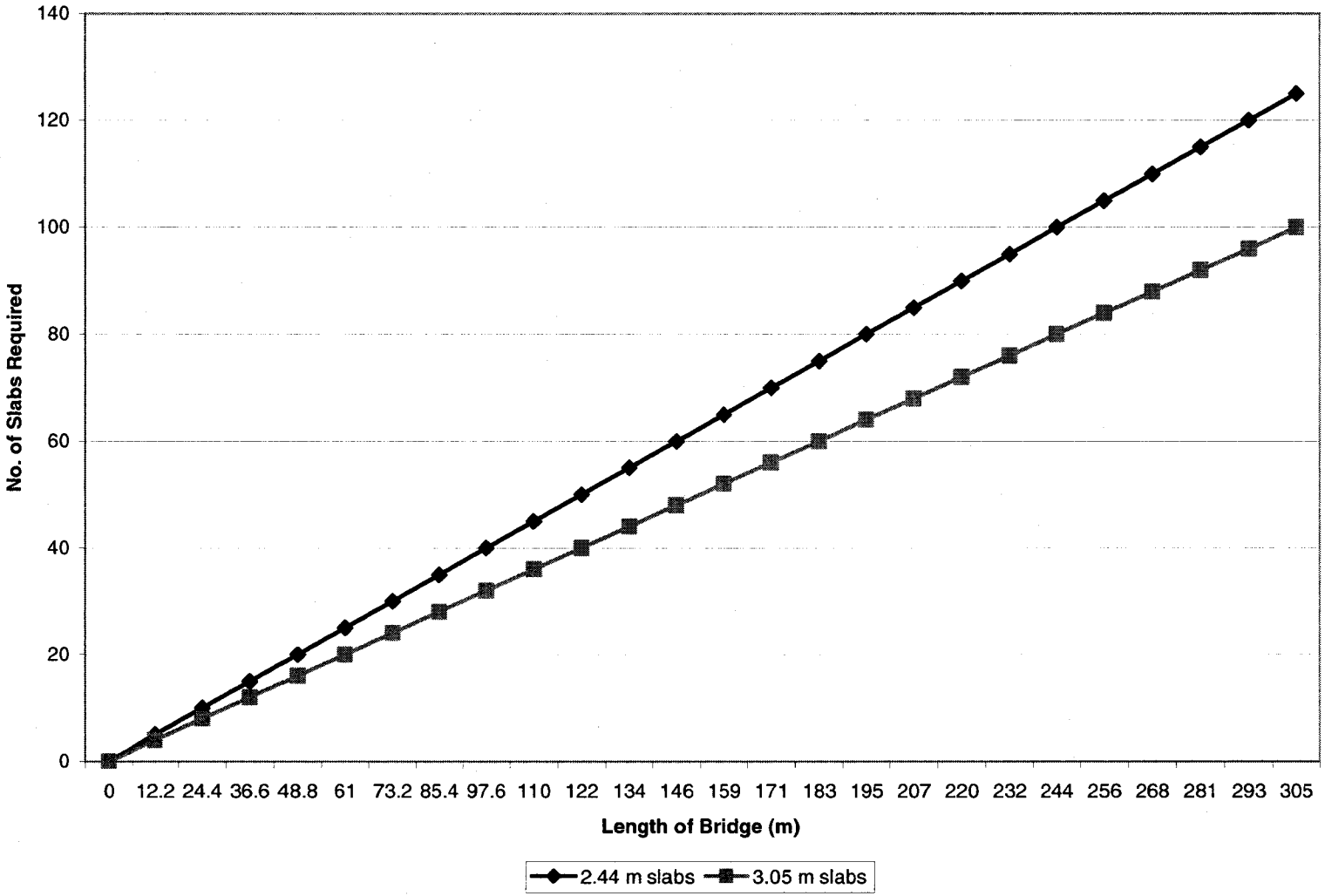

Figure 5.4 Relationship between slab length and No. of slabs required for bridges up to 305 m long.

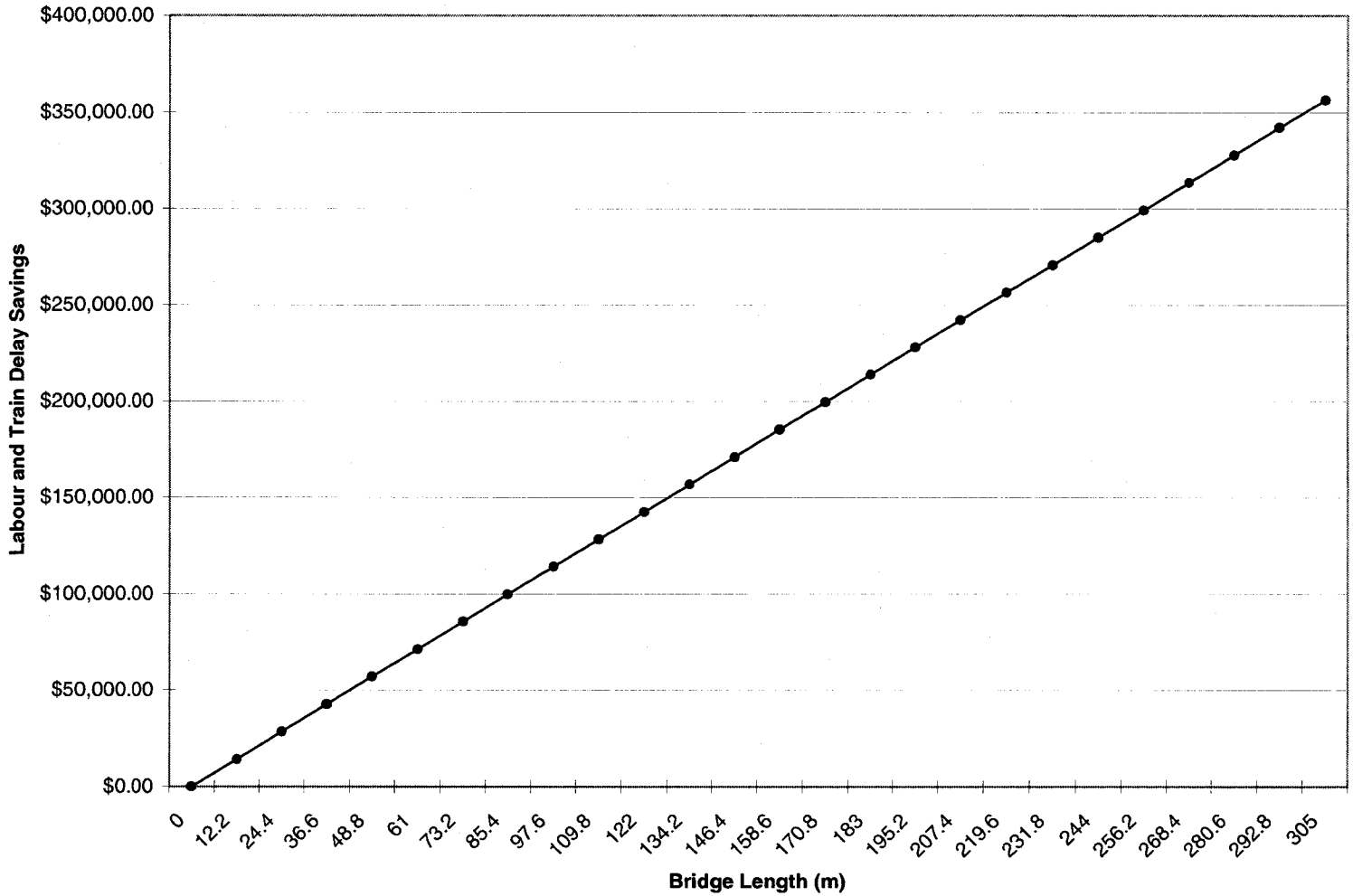

Figure 5.5 Relationship between bridge length and labour and train delay savings

CHAPTER 6

Conclusions and Recommendations

6.1 General Overview

With the use of HPC gaining widespread use on highway bridges across North America, CN wanted to assess the applicability of this concrete to railway bridges, specifically in precast, prestressed bridge slabs and as an alternative to its existing deck slab design. Therefore, the major effort of this research study was to investigate the behaviour of HPC deck slabs from both a material and economic perspective.

A thinner, but stronger prototype slab was designed and manufactured from concrete with compressive strengths of 80, 90 and 99 MPa. A laboratory program was developed to statically test six full scale slabs specimens, to evaluate cracking, ultimate moment, shear, ductility and bond strength. An economic impact of a thinner but longer deck slab on railway operations was also undertaken.

6.2 Specific Conclusions

Based on both the theoretical analysis and experimental research work undertaken during the course of this study, the following major conclusions can be drawn from work:

Evaluation of Ultimate Moment Capacity of the Slabs

1) The average experimental ultimate moment capacity of the slabs was 98 percent of that predicted by the stress-strain compatibility method. This indicates that

the stress-strain compatibility method can be used to accurately predict the ultimate moment capacity of members constructed from HPC.

2) All slabs reached their full predicted flexural capacity due in part to the internal tied arch effect after inclined cracking commenced.

Evaluation of Failure Mode of the Slabs

3) In all cases the failure mode of the slabs was from crushing of concrete after inclined cracks intersected the top of the concrete directly under the strip loading point. This was after considerable deflection and cracking had occurred.

Evaluation of Shear Capacity of the Slabs

4) The flexural shear capacity of the slabs exceeded that predicted on the basis of conventional shear theory. In addition, the reaching of full flexural capacity indicates that the Railway's practice of adding no shear reinforcement to the slabs is justified.

Evaluation of First Cracking

5) The average positive first cracking moment of the slabs occurred at 92 percent of the predicted value. The cause of this is most probably that the many factors that govern first cracking are highly variable and not well captured in cracking formulas. For example, first flexural cracking did not occur until about 41 percent of ultimate capacity. This compares well with previous testing on

prestressed concrete deck slabs fabricated from conventional concrete which displayed similar results.

8) The proposed cracking formula $M_{cr}=\left(\frac{P}{A}+\frac{Pe}{S_b}+0.3\sqrt{f_c'}\right)S_b$ gave cracking strengths that had better agreement with the experimental values than did the conventional formula. The average predicted cracking strength to experimental cracking strength ratio strength rose from 92 percent to 98 percent using the proposed formula.

9) The slab design requires additional negative moment reinforcement to prevent cracking over the supports. The experimental design has a factor of safety against cracking of only 1.03. The slab design has adequate resistance to cracking in positive bending.

Evaluation of Ductility of the Slabs

10) The test results indicate that the slabs displayed adequate post cracking capacity as indicated by the ultimate to cracking moment ratio which averaged approximately 2.5 in positive bending. As the compressive strength of concrete increased, there was a slight decrease in the post cracking capacity.

11) The substantial deflection in the slabs at ultimate capacity indicates that the slabs provide adequate warning of pending failure. In addition, the slabs

displayed significant cracking over the entire span area. Both these indicate adequate ductility and provide warning of incipient failure.

Evaluation of Bond Strength

12) The high strength-high performance concrete displayed good bond development length, indicating reserve bond strength even at ultimate. This research confirms previous research that indicates the required bond lengths specified in the various codes can be decreases by approximately 30 percent.

Economic Impact of using High Strength-High Performance Concrete

13) An economic analysis indicates that the greatest savings in using high strength-high performance concrete is on train delay. For every 4 - 3.05 m (10 ft.) long slabs placed, a train delay and labour savings of $14,535 could be achieved over placing the standard 2.44 m (8 ft.) long slab. These savings are greatest on longer span bridges, where the largest work block times are required. On an annual basis it is estimated that CN could realize savings of $752,000 Canadian by adopting the use of HPC.

6.3 Recommendations

From the theoretical analysis and experimental research work undertaken during the course of this study, the following recommendations on future slab design are presented:

1) Based on the performance of the experimental slabs, the Railway should adopt a similar slab design to that used in the experimental program (but with additional reinforcement for negative moment over the supports).

2) The Railway should stay with the specified concrete compressive strength of 70 MPa. (10,150 psi).

3) When using high strength-high performance concrete, the initial jacking stress limit contained in AREMA, should be increased from $0.7f_{pu}$ to 0.8. This is a direct result of the higher bond strength afforded by this type of concrete. In the case of the experimental slabs, this would have resulted in a 12 percent decrease in the areas of prestressing steel required.

4) The bond development length as contained in several codes should be adjusted for the higher bond resistance afforded by HPC. Future slab designs should take this into account, especially when calculating negative cracking moments over supports at cantilevered sections. Bond development length reductions in the 30 percent range should be considered.

5) In order to further reduce the mass of the deck slabs, the curbs design should be reviewed with the aim of decreasing the mass within these sections. Alternatively, round cardboard tubes (used for cast in place piles) could be inserted within the curbs in order to reduce both the volume of concrete used and also the mass of the slabs. Figure 2.10 indicates such a scheme. This concept will remove 116 kg/meter length of slab and when combined with the savings in mass associated with a thinner slab, can be added back to achieve a longer slab.

6) The proposed formula for determining cracking appears to be accurate and better reflects the experimental cracking moments. Its applicability should be further investigated.

7) The use of 15 mm diameter, 7 wire prestressing strand should be adopted as standard because of adequate bond characteristics displayed in this and other experimental programs. In addition, from a practical perspective, the number of strands to be placed and jacked is much reduced.

8) Even though current state of the art testing indicates HPC has greater durability than conventional concrete due to decreased permeability, a 3 percent air entrainment of the concrete should be retained as a requirement to prevent the possible affects from freeze thaw cycles.

9) As further research work in this area, the railway should proceed with conducting field tests by converting an open deck bridge to a ballast deck bridge using a similar design slab as used in this experimental program. These slabs should be strain-gauged and their behaviour under live load conditions monitored and studied. To this end, a 26.8 m (88 ft.) open deck bridge over the Rouge River at Mile 34.6 of CN's Kingston Subdivision has been selected for this field test.

10) Based on the results of this experimental program the Railway should proceed with the implementation of the use of HPC.

11) The railway should apply the results of this experimental program to the expanded use of HPC in other areas of bridge construction, such as girders, segmental box girders and precast piles, etc.

12) The Railway should use the results of this experimental program, to help develop and revise the AREMA Manual Specifications on HPC, so that the entire North American Railway industry can benefit from this knowledge.

References

ACI, "Building Code Requirements for Reinforced Concrete" (ACI 318 – 99), American Concrete Institute, Detroit, 1999.

AREMA, "Manual of Recommended Practice", American Railway Engineering and Maintenance of Way Association, Baltimore, 2000.

Bakht, B. and Jaeger, L. G., "Bridge Analysis Simplified", McGraw Hill Book Company, New York, 1985

Canadian Standards Association, "CSA A23.3-94 Design of Concrete Structures", Rexdale, Ontario, 1994, pp. 199.

Collins, M., P. and Mitchell, D., "Prestressed Concrete Basics", Canadian Prestressed Concrete Institute, Ottawa, First Edition, 1987.

CPCI, "Metric Design Manual: Precast and Prestressed Concrete", Canadian Prestressed Concrete Institute, Ottawa, Second Edition, 1987.

Hanson, J., Hulsbos, M., Cornie, L., and Van horn, D. A., "Fatigue Tests of Prestressed Concrete I beams", Journal of the Structural Division, American Society of Civil Engineers, Volume 96, Number ST11, November 1970.

Issa, M. A., Yousif, A. A., and Issa, M. A., "Experimental Behaviour of Full-Depth Precast Concrete Panels for Bridge Rehabilitation", ACI Structural Journal, Volume 9, May–June 200, pp. 397 to 407.

Khan, L. R., Dill, J. C. and Reutlinger, C. G., " Transfer and Development Length of 15 mm Strand in High Performance Concrete Girders", Journal of Structural Engineering, Vol. 128, Number 7, July 1, 2002, pp. 913 to 921.

References

Lin, T. Y., "Design of Prestressed Concrete Structures", John Wiley and Sons Inc., New York, Second Edition, Fourth Printing, 1967.

MacGregor, J. G., and Bartlett, M. F., " Reinforced Concrete – Mechanics and Design", Prentice Hall Canada Ltd., Scarborough, Ontario, First Canadian Edition, 2000.

Mufti, A. A., Bakht, B. and Jaeger, L., "Bridge Superstructures – New Developments", National Book Foundation, Islamabad, 1966

Murphy, R. C. F. and Eisenbeis, K. R., "Conversion of a Deck Plate Girder to a Deck Truss", paper presented to the American Railway Engineering and Maintenance of Way Association Annual Technical Conference, Chicago, March 1998, American Railway Engineering and Maintenance of Way Association, 1998, 11 pp.

Peters, N. W., "Optimization of Prestressed Concrete Bridge Ties for Open Deck Railway Bridges" M.A.Sc. Thesis, Concordia University, Montreal, March 1992.

Tadros, M. K. and Mantu, C. B., "Rapid Replacement of Bridge Decks" NCHRP Report 407, Transportation Research Board, National Research Board, Washington, D.C., National Academy Press, 1998, 51 pp.

Taplin, G., Al-Mahaidi, R., Boully, G., and Kwei, S., "Strength Assessment of Prestresses Concrete Rectangular Beams", Monash University, 2000, obtained from Monash University web site: www:civil.eng.monash.edu.au/people/staff/teaching_staff/taplinfolder/gtpapers2000_Austroads_3pdf., on December 17, 2003.

Tide, R. H. R., and Van Horn, D. A., "A Statistical Study of the Static and Fatigue Properties of High Strength Prestressing Strand", Fritz Engineering Laboratory Report Number 309.2, Lehigh University, June 1966.

References

Zielinski, Z. A., "A New approach to Ultimate Strength of Reinforced Concrete Beams in Inclined Cracking and Reduction of Web Shear in Bridge Girders", Paper No. SP 26-17 contained in Second International Symposium on *Concrete Bridge Design*, ACI Publication SP-267, American Concrete Institute, Detroit, 1969, pp. 411 to 455.

APPENDIX A

DEFINITION, DEVELOPMENT AND PROPERTIES OF HIGH PERFORMANCE CONCRETE

APPENDIX A

DEFINITION, DEVELOPMENT AND PROPERTIES OF HIGH PERFORMANCE CONCRETE

A.1 Definition of High Performance Concrete

A.1.1 High Strength Concrete Versus High Performance Concrete

In a review of the current literature, there appears to be much confusion over the terms and definitions of high strength concrete (HSC) and high performance concrete (HPC) by many authors. Since the term "high performance concrete" was first introduced, the concrete industry has attempted numerous times to develop a clear definition. The ACI, according to Russell [1999], define HPC as "*Concrete meeting special combinations of performance and uniformity requirements that cannot always be achieved using conventional constituents and normal mixing, placing and curing practices.*"

The Federal Highway Administration [1998] defines HPC in the following manner: "*HPC is concrete that has been designed to be more durable and, if necessary, stronger than conventional concrete. HPC mixes are composed of essentially the same materials as conventional concrete mixes. But the proportions are designed, or engineered, to provide the strength and durability needed for the structural and environmental requirements of the project.*"

The Strategic Highway Research Program (SHRP - FHWA) and Goodspeed et al [1996] have defined HPC as concrete meeting the following three requirements:

1) It has a maximum water cementitious material ratio [w / (c+m)] of 0.35.

2) It has a minimum durability factor of 80 percent, as determined by ASTM C 666 Method.

3) It has a minimum compressive strength of either of the following:

- 21 MPa (3,000 psi) within 4 hours after placement
- 34 MPa (5,000 psi) within 24 hours after placement
- 69 MPa (10,000 psi) within 28 days after placement

Under SHRP four categories of HPC have been developed. These are illustrated in table A.1 below.

HPC Type	Minimum Strength Criteria	Water Cementitious Ratio	Minimum Durability Factor
Very Early Strength (VES)	14 MPa in 6 hours 2,000 psi in 6 hours	≤ 0.4	80%
High Early Strength (HES)	34 MPa in 24 hours 5,000 psi in 24 hours	≤ 0.35	80%
Very High Strength (VHS)	69 MPa in 28 days 10,000 psi in 28 days	≤ 0.35	80%
Fiber Reinforced	HES + (steel or poly)	≤ 0.35	80%

Table A.1. High Performance Concrete as Developed By SHRP

To add more confusion to the situation, Rangan [1998] has used the ACI definition of HPC, but has in turn referred to the concrete as high strength-high performance concrete (HSHPC). While this may be a better description of the concrete, few authors have followed suite and used this term.

There is obviously more confusion amongst researchers as to what is a clear definition of HPC. For instance, some authors such as Breitenbucher [1997] and Konin, Francois and Arliguie [1998] have used the term HPC in the titles of their papers and then referred to the concrete as HSC throughout their paper. Another example is from the Proceedings of the International Conference on High Performance Concrete, held in Malaysia in 1997, and edited by Malhotra [1997] wherein a total of 52 papers from around the world were presented. Of these 52 papers, 11 (20%) referred to the concrete as "high strength concrete" (HSC). It is obvious, therefore, that there are many definitions of HPC around the world and that the influence of each Countries concrete code has a significant influence.

It is interesting to note that the Portland Cement Association does not yet have a definition for HPC. CSA also does not have a definition for HPC in CSA A23.1-1998, however, is expected to develop one in the next issuance of A23.1.

As a matter of interest the American Concrete Institute (ACI) Committee 363 [1997] has defined high strength concrete as concrete having a specified strength for design of 41 MPa (6,000 psi) or greater. Concrete containing "exotic" materials or techniques is omitted from the definition on purpose. The Committee did not want to concern itself with such concrete as polymer-impregnated concrete, epoxy concrete, artificial normal and heavy weight aggregates, and the like.

To overcome the difficulty in defining HPC, the trend in many countries is to move towards a performance specification to define the expectations of the finished product, Bickley [1998] and Pitt et al [1992].

A.1.2 Development of High Performance Concrete

High performance concrete (HPC) is often considered as a relatively new material. However, its development has been gradual over the last 50 years or so. Coupled with this development has been the evolving definition of high strength concrete. For instance, in the 1950's, concrete with a compressive strength of 34 MPa (5,000 psi) was considered as high strength. In the 1960's concrete with compressive strengths in the range of 41 to 52 MPa (6,000 to 7,500 psi) was used in the construction of many buildings. In the early 1970's 62 MPa (9,000 psi) concrete was being produced and used commercially. In the 1980's to mid 1990's concrete with compressive strength in the range of 69 MPa (10,000 psi) to 103 MPa (15,000 psi) was common. Today, compressive strengths approaching 138 MPa (20,000 psi) are being used in cast in place buildings, Cook [1989].

In prior years, only concrete with a compressive strength of 41 MPa (6,000 psi) was available commercially. Recently, however the demand for and the application of HPC has increased dramatically, so that HPC is now widely available. This demand has spurred the technological developments in material technology. Table A.2 and A.3 below indicate the development of concrete used in buildings and bridges respectively.

Currently, the largest application of HPC has been in high rise structures, where its use in columns has been used to great advantage. It has also been used in highway bridges, but to a lesser extent (see table A.3). The application of high strength concrete in bridges has been primarily in precast prestressed bridge girders. It has been found by Carpenter [1980] that span length for integral deck tees, for closely spaced girders, increased with increasing concrete strength. For wider spaced girders span length increased when the concrete strength was increased to about 55 MPa (8,000 psi) Above that, it was found that span length was not increased because insufficient prestress force could not be obtained.

Building	Location	Year Constructed	Number of Stories	Design Strength MPa (psi)
Lake point Tower	Chicago	1965	70	52 (7500)
Midcontinental Plaza	Chicago	1972	50	62 (9000)
Royal Bank Plaza	Toronto	1975	43	61 (8800)
Water Tower Place	Chicago	1975	79	62 (9000)
River Plaza	Chicago	1976	56	62 (9000)
Helmsley Plaza Hotel	New York	1978	53	55 (8000)
Richmond–Adelaide Center.	Toronto	1978	33	61 (8800)
Larimer Place Condo.	Denver	1980	31	55 (8000)
Texas Commerce Tower	Houston	1981	75	52 (7500)
City Center Project	Minneapolis	1981	52	55 (8000)
S.E Financial Center	Miami	1982	53	48 (7000)
Petrocanada Building	Calgary	1982	34	50 (7250)
Chicago Mercantile Bank	Chicago	1982	40	62 (9000)
Columbia Center	Seattle	1983	76	66 (9500)
Interfirst Plaza	Dallas	1983	72	67 (10000)
900 N. Michigan Annex	Chicago	1986	15	97 (14000)
Eugene Terrace	Chicago	1987	44	76 (11000)
Two Union Square	Seattle	1987	62	97 (14000)
Scotia Plaza	Toronto	1988	68	67 (10000)
311 South Wacker Dr.	Chicago	1988	70	83 (12000)
225 West Wacker Dr.	Chicago	1988	30	97 (14000)

Table A.2 Buildings Constructed of High Performance Concrete

In post tensioned box girder highway bridges, Carpenter found that high strength concrete also increased span length. Again though, maximum allowable prestress force limited maximum spans. For segmental box girder bridges, Carpenter reports that, HPC is only feasible in those regions where member thickness is controlled by stress alone. Where thickness is controlled by other factors (stiffness, etc) HPC may not be beneficial.

One of the most significant applications of HPC in North America is the Huntington, West Virginia to Proctorville, Ohio, highway bridge which used 55 MPa (8,000 psi) concrete. This bridge consisted of asymmetrical cable stayed girder superstructure with a main span of 275 m (900 ft.). This length span would not be feasible without the use of HPC.

In Japan, Engineering News Record [1982] has reported the construction of railway bridges (see table A.3) using concrete with compressive strength of 76 MPa (11,000 psi) and 79 MPa (11,400 psi) respectively. These strengths were obtained with cast in place concrete (CIP).

Searbrook et al [1997] have reported that in Canada alone nearly 100 highway bridges have been constructed using high strength concrete. These structures have utilized precast and cast in place (CIP) elements, with conventional reinforcement and with prestressed. Such construction is expanding rapidly due to the economic advantages offered by HPC concrete. These are reduced member size, projected increase in service life, lower transportation costs and accelerated construction, Moreno [1998].

Of the approximately 100 highway bridges using HPC in Canada, the majority of them are in New Brunswick. Much of the pioneering work on high strength concrete was done in Quebec by the Quebec ministry of Transportation and researchers from the Center of Excellence on High Performance Concrete.

Bridge Name	Location	Year Constructed	Max. span m (ft.)	Design Strength MPa (psi)
Willows Bridge	Toronto	1967	48 (158)	41 (6000)
Nitta Highway Bridge	Japan	1968	30 (98)	59 (8500)
San Diego to Coronado Bridge	California	1969	43 (140)	41 (6000)
Kaminoshima Highway Bridge	Japan	1970	86 (282)	59 (8500)
Ootanabe Railway Bridge	Japan	1973	24 (79)	79 (11400)
Fukamitsu Highway Bridge	Japan	1974	26 (85)	69 (10000)
Akkagawa Railway Bridge	Japan	1976	46 (150)	79 (11400)
Pasco-Kennewick Intercity Bridge	Washington	1978	299 (981)	41 (6000)
Linn Cove Viaduct	North Carolina	1979	55 (180)	41 (6000)
Houston Ship Canal	Texas	1981	229 (750)	41 (6000)
Huntington to Proctorville	W. Va. to Ohio	1984	274 (900)	55 (8000)
Anncis Island Bridge	Vancouver	1986	465 (1526)	55 (8000)
Tower Road Bridge	Washington	1987	49 (161)	62 (9000)
Confederation Bridge	N. B. to P.E.I.	1997	250 (820)	60 (8700)

Table A.3 Bridges Constructed of High Performance Concrete

A.1.3 Successful Use of HPC in Highway Bridge Construction

Several US states have successfully used HPC in the construction and rehabilitation of highway bridges. Heald [1999] and Ralls [1999] wrote of the benefits and success of HPC on bridge projects in Texas. Waszczuk [1999] wrote of the successful application of HPC in New Hampshire, in achieving "a highly impermeable, crack free, freeze thaw resistant concrete deck". Waszczuk and Juliano [1999] report that on HPC bridge decks in New Hampshire, "the final product exceeded expectations. No visible cracks were found in several post construction reviews...". Miller [1999] reported on the successful use of HPC box girders in Ohio to increase span lengths and eliminate piers.

Wiegel [2000] has similarly reported on the use of HPC in "supper girders", in Washington State highway bridges. Wiegel states that these I girders improve construction economy, while at the same time allowing for longer spans to keep piers out of waterways and satisfy environmental concerns. Alampalli and Owens [2000] investigated the use of HPC in highway deck slabs in New York State. They report that bridge deck performance has improved since the introduction of HPC and that HPC results in "increased crack resistance without compromise in workability, construction practices, or cost".

Binseel [2000] has reported on the successful use of HPC on bridges in Maryland. He does state, though, that lack of familiarity within the design and construction industry, is a potential barrier to the use of HPC. Beacham [1999] has also reported favorably on the use of HPC in Nebraska and the state's strategic plan to further implement HPC.

Rochelle [2000] has reported on North Carolina's introduction of a durability design procedure for HPC exposed to a chloride environment.

Ozyildirim [1999] has reported on Virginia's testing of HPC for their resistance to chloride penetration. Ozyildirim states that VDOT have complied a specification for HPC, which encompasses limits on air content, slump and temperature. These he states will address the durability issue and result in "long lasting and cost effective bridge decks". Ozyildirim [1993] and [1999], reports that both field and laboratory studies by

VDOT indicate that HPC bridge decks with a water-binder ratio of less than 0.45 containing pozzolan or slag will result in durable bridge decks.

Rodriguez [2000] has also reported on Alabama's (ALDOT) experience with HPC. Their experience seems to mirror those of other states. Moore [1999] discusses the use of HPC by various states in highway bridge projects. He concludes that even with the varying climate, locally available materials and construction methods, use of HPC is a success.

Russell [1997] discusses various benefits in using HPC in both buildings and bridges. The reported benefits of HPC are longer spans; increased girder spacing, shallower members, increased durability and enhanced mechanical properties.

It would therefore appear that based on the success of the use of HPC in highway bridge applications, there is no technical or economic reason for not implementing the use of HPC in railway bridge decks.

A.2 The Mechanical Properties of High Performance Concrete

A.2.1 Compressive Strength

It is often thought that the mechanical properties of high performance concrete are simply those related to strength. This is not necessarily so, although compressive strength plays a major part.

The compressive strength of high performance concrete, like normal strength concrete, increases as the water/binder ratio decreases. In normal strength concrete, the hydrated

cement paste determines the strength of the mix. However, with high performance concrete the water binder mix determines the strength of the concrete, until the crushing strength of the course aggregate is reached. At this point, the only way to increase the strength of the concrete is by using higher strength course aggregate. Decreasing the water binder ratio will not increase the strength significantly.

If a strong course aggregate is selected Aitcin [1998] suggests the following guide on the compressive strength of high performance concrete as a function the water/ binder ratio:

Water/Binder Ratio	Max. Compressive Strength	Max. Compressive Strength
0.40 to 0.35	50 to 75 MPa	7 to 11 ksi
0.35 to 0.30	75 to 100 MPa	11 to 15 ksi
0.30 to 0.25	100 to 125 MPa	15 to 18 ksi
0.25 to 0.20	125 MPa and greater	18 ksi and greater

Table A.4 Compressive Strength of High Performance Concrete

The above table assumes the course aggregates are stronger than the concrete.

There are essentially three things to consider when analyzing the compressive strength of high performance concrete. These are:

- the early compressive strength of high performance concrete
- the influence of the maximum temperature reached during curing
- the long term development of the compressive strength

A.2.2 Early Age Compressive Strength

An ideal concrete should remain plastic for a long as possible to aid in placement. It should then harden quickly without excessive heat generation, shrinkage or creep. High performance concrete offers none of these.

The setting and hardening of high performance concrete, like normal strength concrete, is strongly influenced by the temperature at time of delivery, the ambient temperature and the amount of superplasticizer in the mix. A low ambient temperature will significantly delay the start of concrete hardening. In addition, superplasticizer, used to decrease the water/binder ratio to achieve the required compressive strength, retards the onset of hydration. However, when it does start, it develops very rapidly. For this reason, Aitcin suggests that for pre-cast members it is more advisable to formulate a high performance concrete with a high amount of binder rather than designing it with the lowest amount of water possible.

A decrease in the water binder ratio can be achieved in two ways:

- by decreasing the water content through the use of superplasticizer, or
- by increasing the binder content.

It is possible to achieve high early strengths of high performance concrete in the 20 to 30 MPa (3000 to 4400 psi) range, without heating and within 24 hours, with a water/binder ratio of 0.30 to 0.35, at an ambient temperature of about 20°C. However, obtaining high early strengths prior to 12 hours is extremely difficult with high performance concrete. An additional 2 to 4 hours of curing time at 20°C is required. When HPC mixes have been properly designed, it is possible to achieve compressive strengths of 25 MPa (3,600 psi) in 12 hours, 40 MPa (5,700 psi) in 16 hours and 45 MPa (6,400 psi) in 24 hours.

The material from which the forms are constructed also plays a critical part in the strength development of the concrete. Khan, Cook and Mitchel [1996] found that ambient conditions influence concrete hardening depending on thermal conductivity of the forms and the thickness of the element. Metallic forms can cause high thermal gradients, whereas plywood forms protect the concrete longer from the early effect of ambient temperature.

A.2.3 Effect of Early Temperature Rise in Curing of HPC on the Compressive Strength

The temperature of HPC rises significantly within the first 24 to 48 hours after placement of the concrete. Cook et al [1992] have reported temperatures of 65° C to 70° C in some massive HPC members.

The temperature rise is attributable to the actual amount of cement in the mix that is hydrating and not to the total amount of cement present in the mix, as is commonly thought.

In HPC, the low water/binder ratio (w/b) and the scarcity of water, limits the amount of cement that is hydrating, in spite of the high amount of cement in the mix. The water content limits the maximum temperature.

In normal strength concrete, early external applied heat results in an increase in early strength, but a decrease in the 28 day strength. This is not the case with HPC, cores

extracted from field structures constructed of HPC, indicate 28 day compressive strengths similar to that of standard cured specimens.

A.2.4 Influence of Air Entrainment on Concrete Strength

HPC no matter what strength will contain anywhere from 0.5 to 2.5% entrapped air. In addition, HPC can also contain air purposely entrained to aid in the resistance to frost action and thereby increase durability. Air entrainment of 4 to 6% weakens the compressive strength of HPC. According to Lessard, Baalbaki and Aitcin [1995] for every 1% difference in air entrainment in two identical HPC mixes, a 4 to 5% decrease in the compressive strength results. This finding does not differ from the behavior of normal strength concrete.

A.2.5 Long Term Compressive Strength

Aitcin [1998] has found that the 91 day or one year compressive strength of water cured HPC specimens has no direct correlation to that of concrete in field structures. This can lead to overly optimistic estimates of the in-situ compressive strength of the member. The cause of this is related to a lack of water or too low a relative humidity within the pore system of the field member.

A.2.6 Tensile Strength

There is significant increase in the tensile strength of HPC as compared to normal strength concrete, but less so than the increase in the compressive strength of HPC. The ratio f_c/f_t decreases to about 1/20 for some of the highest strength HPC. However,

splitting strength values of 6 MPa (870 psi) or greater have be attained in many HPC mixes. This becomes especially beneficial in the construction of precast, prestressed members.

Tensile strength values are attained in a shorter period than compressive strength values. This is due to the densification of the paste aggregate interface. Splitting tests have shown that the fracture surface is transgranular, indicating that the concrete material is quite homogeneous. Tensile strength gain ceases at about 14 days of age. However, the compressive strength of HPC will increase anywhere from 10 to 30% after that date.

Rangan [1998] suggests the following be used to obtain lower bound estimates:

Principle Tensile Strength $= 0.4\sqrt{f'_c}$ in MPa.

Flexural Tensile Strength $= 0.6\sqrt{f'_c}$ in MPa.

Rangan also recommends that for large surface areas such as slabs and walls, the flexural tensile strength be taken as $0.3\sqrt{f'_c}$ to allow for the effects of restrained shrinkage and temperature. This is similar to that contained in the Canadian Concrete Code.

Aitcin [1998] has investigated the various International codes and found the following: relationships for tensile splitting strength:

1) The Comite' Euro-International du beton CEB-FIP [1978] suggests the use of the following relationship:
   - $f_{sp} = 0.273\ f'^{2/3}_c$ in MPa.

2) Carrasquillo et al suggest the use of the following relationship for HPC with compressive strengths ranging from 21 to 83 MPa:

- $f_{sp} = 0.54\ f'^{1/2}_c$ in MPa.

3) Raphael suggests the use of the following relationship for HPC with compressive strengths less than 57 MPa:

- $f_{sp} = 0.313\ f'^{1/2}_c$ in MPa.

4) ACI Committee 363, on HSC [1984] suggest the use of the following relationship for HPC with compressive strengths in the range of 21 to 83 MPa (3,000 to 12,000 psi):

- $f_{sp} = 0.59\ f'^{0.55}_c$ in MPa.

5) Ahmad and Shah suggest the use of the following relationship for HPC with compressive strengths lees than 84 MPa (12,000 psi):

- $f_{sp} = 0.462\ f'^{0.55}_c$ in MPa

6) Burg and Ost suggest the use of the following for moist cured concrete with compressive strengths in the range of 85 to 130 MPa (12,300 to 19,000 psi)

- $f_{sp} = 0.61\ f'^{1/2}_c$ in MPa.

7) De Larrard and Mailer [1992] indicate that the following equation contained in the French Code gives very good agreement with experimental results:

- $f_{sp} = 0.6 + 0.06\ f'_c$ in MPa

A closer examination of these relationships indicates that, with the exception of the French equation, which does not use a root function, they are all reasonably close to each other and would therefore yield similar values.

A.2.7 Modulus of Rupture

Modulus of Rupture (MOR) tests are usually performed according to ASTM C78. The relationship between MOR and tensile splitting strength for normal strength concrete is not difficult to determine because the splitting strength values are low and vary very little. This is not the case in HPC because the water/binder (w/b) ratio and compressive strength vary over a much wider range.

Aitcin [1998] presents various relationships for the modulus of rupture ($f_{r)}$, as suggested by the following authors:

1) Carrasquillo et al suggest the use of the following relationship:

- $f_r = 0.94 f'^{1/2}_c$ in MPa

  Note: This also happens to be the equation adopted and recommended by ACI Committee 363.

2) Burg and Ost suggest the use of the following relationship:

- $f_r = 1.03 f'^{1/2}_c$ in MPa

3) Khayat et al suggest the use of the following equation:

- $f_r = 0.23 + 0.12 f'_c - 2.18 \times 10^{-4} f'^2_c$ in MPa

4) Iravani's [1996] experimental test results suggested the use of the following relationship:

- $f_r = 0.97 f'^{1/2}_c$ in MPa

  Iravani found that the experimental results varied by plus/minus 10% and therefore, recommended the use of the ACI Committee 363 formula for the determination of the MOR

A.2.8 Modulus of Elasticity

The modulus of elasticity is one of the most important mechanical properties of HPC concrete. It is closely related to the properties of the cement paste, the strength of the aggregate and the particular method used to determine the modulus. The precise determination of the Modulus of Elasticity is important when calculating the deformation of a structure.

There are normally two ways to determine the modulus of elasticity. The first known as the dynamic modulus, uses the tangent to the origin of the stress strain curve. The second is known as the static modulus and is determined from the secant line to a point on the stress strain curve. International codes generally determine a relationship between either of the static or dynamic modulus and the strength of the concrete.

The influence of aggregates on the modulus of elasticity can be substantial. For example, aggregate by volume in HPC can be in the 70 to 75% range. Therefore, the strength of the aggregate has a significant influence on the modulus that in turn, causes wide modulus variations.

Gutierrez and Canovas [1995] based on experimentation, have proposed the following formula to calculate the modulus of elasticity. This formula takes into account the strength of the aggregate by introducing an α_β factor and is applicable to HPC in the range of 25 to 120 MPa (3,600 to 17,400 psi).

$E_c = \alpha_\beta \, 8480 \, \sqrt[3]{f'c}$ (in MPa)

Where: α_β is obtained from the table below.

Aggregate	Minimum	Maximum	Average
Quartzite	1.15	1.50	1.33
Sandstone	0.50	1.0	0.75
Limestone	0.75	1.50	1.13
Basalt	0.75	1.50	1.13
Ophite	1.15	1.20	1.17
Andesite	1.15	1.20	1.17
Dacite	0.75	0.90	0.83
Rhyolite	0.75	0.90	0.83
Granite	0.95	1.10	1.03
Syenite	0.95	1.10	1.03
Diorite	0.95	1.10	1.03
Diabase	1.25	1.50	1.38

Table A.5 Values of α_β for Different Aggregates

De Larrard and Malier [1992] suggest Hashin's formula provides good correlation in predicting the modulus of elasticity of HPC. It is based on three key parameters of the mix, these are:

V_a – the volume of aggregate

E_p – the modulus of paste

E_a – the modulus of the aggregate

$$E = \frac{E_P\left[(1-V_a)E_P + (1+V_a)E_a\right]}{E_P(1+V_a) + (1-V_a)E_a}$$

The modulus of the paste is mainly controlled by the packing density of the mix.

Aitcin [1998] cites the following moduli from various national codes:

1) The CEB-FIP ([990] suggests the use of the following relationship:

- $E_{28} = 10{,}000\ (f'_c + 8)^{1/3}$ in MPa.

2) The Norwegian Code [1992] suggests the use of the following relationship:

- $E = 9{,}500\ (f'_c)^{0.3}\ (\rho/2400)^{1.5}$ in MPa with ρ in kg/m^3

3) Carrasquillo et al [1981] and ACI Committee 363 suggests the use of the following relationship:

- $E_c = 3{,}320\ \sqrt{f'_c} + 6{,}900$ in MPa or
- $E_c = [3{,}320(f'_c)^{0.5} + 6{,}900)\ (\rho\ /2346)]$ in MPa with ρ in kg/m^3

4) The European Code for Buildings CEB [1990] suggests the use the following relationship:

- $E_c = 10{,}000(f'_c + 8)^{1/8}$ in MPa

5) The Canadian Code, CAN A23.3-M90 Design of Concrete Structures for Buildings, suggests the use of the following equation:

- $E_c = 5{,}000(f'_c)^{0.5}$ in MPa.

6) Rangan [1998] indicates that the New Zealand code equation for modulus of elasticity of HPC shows good correlation with measured values. The equation is:

- $E_c = [(3{,}320\sqrt{f'_c} + 6{,}900)(\rho\ /2300)^{1.5}]$ in MPa with ρ in kg/m^3

7) De Larrard and Mailier [1992] suggest the use of the following relationship:

- $E_c = 1{,}100\ (f'_c)^{1/3}$ in MPa

The increase or growth in the modulus of elasticity of HPC with time is roughly the same as that of tensile strength, but without the leveling off after 14 days.

A.2.9 Poisson's Ratio

A review of available literature indicates that there is very little experimental data on values of Poisson's ratio. Iravani [1996] found Poisson's ratios, for HPC ranging from 55 to 125 MPa, in the order of 0.15 to 0.24. Iravani suggests the use of an average value of 0.20. Aitcin [1998] also confirms the limited data on the Poisson's ratio for concrete and the fact that there is even less data for HPC. However, reported values range from 0.18 to 0.32. Based on the literature the use of a 0.20 value for Poisson's ratio seems the most practical.

A.2.10 Shrinkage

When considering shrinkage drying shrinkage is of primary interest. As mentioned previously, final endogenous shrinkage is roughly doubled that of normal strength concrete, however, the drying shrinkage is greatly reduced as the mix contains very little free water after hydration. In summary, the total shrinkage of HPC is about half that of normal strength concrete.

A.2.11 Creep

Total creep is the sum of the "basic creep" and of the additional strain called desiccation creep. Creep of HPC is characterized by the following:

- rapid kinetics (at 7 days loading, 67% of the strain of one year is attained as opposed to 41% for normal strength concrete)

- a very low amplitude ($K_c \leq 0.6$ as compared to 2.0 for normal strength concrete)
- independent of the effects of moisture and geometry of the structure.

A.2.12 Bond Strength

Rosenberg [1986] found that in HPC the mean adherence increases by nearly 40%, coupled with an increase in compressive strength of 50%, over that of normal strength concrete

Others, Wecharatana et al [1987] and Hegger et al [1997] have noted a more brittle behaviour to HPC, coupled with a reduction in ductility. Experiments undertaken by Burge [1987] indicated that adherence increased more on a pure paste than on a mortar, which in turn adhered better than concrete.

The immediate benefit of improved adherence is the corresponding reduction in anchorage length and bond development length. This benefit will be most notable in the design of reinforced concrete beams, where cracking is judged harmful.

De Larrard et al [1988] have shown that for HPC slabs, bent in one direction, with the reinforcing working to their mechanical maximum, will still have crack widths smaller than similar slabs made from normal strength concrete. This is a result of the increased bond strength between the reinforcing steel and the cement paste.

A.3 Other Properties of High Performance Concrete

A.3.1 Effect of Aggregate Strength on HPC

In normal strength concrete (NSC) the strength of the course aggregate plays a lesser role than in HPC. The compressive strength of NSC is controlled by the strength of the cement paste. This means that the strength of the aggregate in NSC is not the limiting factor in its compressive strength. The strength of the cement paste in NSC is in turn controlled by the water cement ratio.

The opposite of the above is true in HPC. For instance, the bond between the aggregate and the cement paste is so much stronger that it results in a large transfer of stress across the cement paste interface, known as the transition zone. The strength of the cement paste as explained is very great, frequently greater than the strength of the aggregate, Aitcin [1993]. Research has found, that in fracture surfaces of concrete cylinders made from HPC, pass directly through the course aggregate rather than the cement paste. This has lead to the belief by Ezeldin and Aitcin [1991] and Taerwe [1993] that the strength of the course aggregate limits the compressive strength of HPC. Therefore, proper and careful selection of course aggregate in a HPC mix is essential.

A.3.2 Durability of HPC

The durability of concrete is primarily related to two factors. These are resistance to freeze thaw cycles and resistance to chemical attack

A.3.2.1 Mechanisms of Freezing

When water freezes, its volumetric expansion is close to 9%. If the water is contained in a closed containment vessel which is more than 92 % full, stresses will be generated that could cause failure of the vessel. Concrete, however is not a closed vessel, bur rather a material containing air filled cavities of various sizes. There are essentially two types of cavities, capillaries cavities caused by entrapped air and air bubbles purposely added as entrained air, usually in the 4 to 6% range.

Powers [1975] a pioneer in the field of concrete durability, suggests that when water freezes, there are enough air filled voids in the concrete to accommodate the increase in water volume. As displaced water, due to expansion at freezing, flows from areas of freezing, the viscous resistance of the concrete structure develops destructive stresses within the concrete. If the water content within the concrete is above the critical saturation point, such destructive flow will take place. The resistance to flow is proportional to the length of flow path. Therefore, there is a critical length of flow path, above which the hydraulic pressure exceeds the strength of the concrete.

However, the theory by Powers only partly explains the deterioration of concrete in freezing conditions. It has been further suggested by Powers that in some cases the damage caused by freezing in cement pastes was caused by the movement of unfrozen water to sites that are freezing. This movement is similar to osmosis and the osmotic pressures generated are sufficiently large to account for the disintegration of cement pastes.

The main function of entrained air within the cement paste is to prevent the development of osmotic pressure. Moisture within an air bubble will freeze as soon as freezing in capillary cavities occurs. Any unfrozen capillary water will diffuse (flow) to either, the ice and solution in the air bubble or to the capillary cavity. If it moves towards a capillary already full of ice, osmotic pressure will develop. However, if it moves to an air bubble, no osmotic pressure develops because the bubble will be far from being full. This causes a withdrawal of water from the cement paste and a freeze drying effect.

According to Gagne et al [1992] the most resistant cement paste to freeze–thaw cycles uses the lowest possible water to binder ratio. This is because the lower amount of mixing water used results in the cement particles being closely packed, which in turn results in a more dense paste with low porosity. HPC offers such characteristics. However, Gagne et al and Aitcin [1998] both suggest the use of air entrainment in HPC, especially those HPC's with water binder ratio's greater than 0.30.

There is a close relationship between durability of concrete and the permeability of the concrete according to Ithuuralde [1992]. The degree to which concrete can resist being saturated is directly related to its porosity. A dense concrete with very fine, non open pores will ensure a low permeability factor. This is generally the case with HPC, which has a low water to binder ratio.

Kumaat and Lorrain [1996] found that HPC slabs are more resistant to macrocracking than NPC, due to the increase in strength of the mechanical properties of the constituent

materials. Such resistance to cracking will also lead to increased resistance to freeze thaw effects, as cracks through which water might penetrate are greatly diminished.

A.3.3 Long Term Durability

Seki [1975] investigated coastal concrete structures exposed to see breezes. These structures ranged in age from 14 to 40 years. Seki found that the main factors influencing the long term durability of concrete were the construction practice and workmanship. These practices related to concrete production, placing, casting and curing.

Gerwick [1975] and Seki [1975] have both linked poor concrete durability to the high water-cement ratio used in the mix. A ratio of greater than 0.5 was considered as leading to serious deterioration and to a highly permeable cement paste. Structures built in the 1950's and 1960s used ordinary Portland cement and water-cement ratios of 0.60 to 0.70 to obtain workability.

Today, with the use of HPC, a water/binder ratio of between 0.2 to 0.3 is common place. Such low water/binder ratio's, lead to a dense, less permeable concrete microstructure, with few or no capillary pores, and ultimately a more durable concrete. Breitenbucher [1998] recommends a maximum water binder ratio of 0.33, and the addition of silica fume to obtain good durability of HPC.

Since HPC is relatively new, there is not a lot of experience with the durability of this material. Early use of HPC was in columns of buildings protected from harsh

environments. Unfortunately, those structures do not tell much about the long term durability of HPC.

Martschuk and Stark [1998] found that adding fine cementitious (silica fume, granulated blast furnace slag, fly ash) material to HPC significantly improves the freeze thaw and de-icing salt attack resistance. Tests indicated that scaling was reduced 85% compared to that of NPC.

The Railway bridge decks could be exposed to salt air as well as freeze thaw cycles. However, unlike highway structures, they are not likely to be exposed to chloride attack from de-icing salts. Therefore, durability in that regard is not of paramount concern and will not be discussed here.

A.3.4 Use of Silica Fume in HPC

The properties of HPC rely on several factors. The main factor is the low water to cementitious ratio of the mix. A water to cementitious ratio below 0.4 is generally not achievable in HPC without the addition of water reducers or superplasticizers to the mix. The other factors include superplasticizer and cement compatibility, quality of course aggregate and selection and dosage of pozzolanic material, such as silica fume, Baalbaki et al [1992].

Silica fume is often termed as a "supplementary cementatious material" and is obtained as a by-product of the reduction of high purity quartz and coal (or coal tar) in an electric

arc furnace, during the production of silicon metal or ferrosilicon alloys. The silica fume is collected as it condenses from the furnace gas as a very fine dust in the gas filters, Hamad and Itani [1999]. Silica fume contains anywhere from 85 to 98 percent silicon dioxide (SiO_2). The fume consists of extremely fine spherical glass like particles, whose average size is 0.1 μm, which is about two orders of magnitude finer than the average cement particle. The use of silica fume containing less than 0.75% ferrocsilicon is not recommended, ACI Committee 234 [1996].

Research has shown, Aitcin and Neville [1993] and ACI Committee 234 [1996], that silica fume is added to concrete as a properties enhancing agent. It primarily increases the strength of the concrete and the concrete durability, especially against freeze–thaw action. Silica fume increases the strength of the cement paste by acting as a filler in the spaces between the cement particles. In normal strength concrete, these spaces would remain as air voids. At the same time silica fume also increases the density of the cement paste and therefore, decreases permeability.

The increase in both strength and density of HPC by use of silica fume is linked by many researchers such as Aitcin and Neville [1993], Hamad and Itani [1999], ACI [1996], de Larrard [1992] and Gjorv et al [1990] to packing density. The analogy is that silica fume particles increase the packing density of the cement paste by filling the spaces between the cement grains. The cement fills the spaces between the fine aggregate and the fine aggregate fills the spaces between the course aggregate. The result being that HPC

behaves very much like an ideal composite material, with the stress being shared between the aggregate and the cement paste.

A.3.5 The Use of Blast Furnace Slag in HPC

Ground granulated blast furnace slag (GGBFS) is a by-product of steel making. Slag, which is formed on top of pig iron, in a blast furnace, is tapped off at periodic intervals at temperatures exceeding 1500 °C. The composition of GGBF depends largely on the ores used, but is generally comprised of silicon, calcium, aluminum and manganese. These constituents account for at least 95 % of the content of GGBF slag.

In order for the slag to be useful as a cementitious material, the molten slag must be rapidly cooled. This is achieved by spraying with high-pressure water jets. If the slag is allowed to cool slowly, it will contain a predominately crystalline structure that does not necessarily posses the required cementitious properties. The slag will typically be converted into about 4 to 5 mm aggregate sized particles. These are later ground to a fineness exceeding that of portland cement.

GGBF slag is usually substituted for portland cement in the concrete mix on a one to one ratio by mass. The optimum blend of GGBF slag with portland cement, that produces the greatest 28 day strength is found to be about 50 %, depending on the grade of GGBF slag used. Concrete with GGBF slag has greater placeability, workability and ease of compaction. This results in greater amounts of course aggregates being used to reduce the water demand and hence the water cementitious ratio. An increase in course aggregate is

often desirable as it increases the overall strength of the concrete. Generally, the use of GGBF slag results in a 3 to 5 % lower water requirement than without the use of GGBF slag. The use of GGBF slag also results in the reduction of high range water reducing admixtures, generally in the vicinity of 25%, ACI [1995].

GGBF slag, due to its slower reactive nature as compared to portland cement, will display a lower 3 day and sometimes even 7 day strength than portland cement alone. However, at 28 days, GGBF slag concrete will exhibit a greater compressive strength than made from portland cement.

A.3.6 The Use of Fly Ash in HPC

Fly ash is a by-product of burning coal in electrical power generation plants. The airborne ash is collected by filtering the furnace exhaust gases, generally electrostatic or mechanical precipitators. The resulting ash particles are glassy and spherical in shape. They range in size from 1 μm to (0.00004 in) to 80 μm (0.0032 in.).

The spherical shape of the fly ash particles permits the water cement binder ratio to be reduced for a given workability. In addition, the use of fly ash increases pumpability of the mix. This is because fly ash increases cohesion of the mix and prevents segregation. The use of fly ash in air-entrained concrete requires a larger amount (dosage) of air entraining admixture. This is because the carbon in the ash acts in a similar fashion to porous activated carbon which acts as a filter. In the concrete these porous particles absorb air-entrainmemt admixtures.

Typically, concretes with fly ash show a decrease in the seven day strength, but an increase in the 28, 56 and 91 day strength, over concretes without fly ash. Tests have shown that strengths of concrete at one year with fly ash have a 50 % increase in strength over their 28 day strength, as opposed to a 30 % increase for concrete without fly ash.

The strength increase in concrete is dependent on the bond increase with both the steel and aggregate. Fly ash increases the paste volume (similar to silica fume), thereby increasing the surface volume adhering to the aggregate and reinforcing steel. The fly ash typically occupies the voids where bleed water would normally collect, at the aggregate-cement paste interface and the reinforcing steel-cement paste interface, which reduces the amount of bleed water and increases bond.

The use of fly ash also increases the resistance to freeze thaw by decreasing the permeability of the cement paste. This decrease in permeability of fly ash concrete reduces the rate of ingress of water, corrosive chemicals and oxygen. In addition, the use of fly ash increases the resistance of concrete to attack by sulfates. This increase is linked to the chemical reaction between fly ash and the hydroxides in the concrete.

A.3.7 Use of Superplasticizers

High range water reducing admixtures (HRWRA), better known as superplasticizers, are often added to concrete mixes in order to modify the properties of concrete. For instance an admixture may be the only feasible method of obtaining high strength, resistance to

freezing and thawing, retarding or accelerating setting time and increasing the workability of the mix.

In the early usage years of superplasticizers, these were modified lignosulphonates, sulphonated naphthalene formaldehyde condensates and sulphonated melamine formaldehyde condensates, Hanna et al [1989]. The first superplasticizer was invented in Japan in 1964 by Kenichi Hattori. These were primarily used to produce high slump flowing concrete of 0.4 to 0.5 water cement ratios. The more recent practice is to use superplasticizers in the production of high strength concrete from 69 to 150 MPa, so as to reduce the water/binder ratio to below 0.35 and to increase workability of the fresh mix.

Superplasticizers are especially effective in dispersing the cementitious particles in water. This action is enabled by the superplasticizers ability to reduce the surface tension of the water by creating a lubricating film at the particles surface, Jerath and Yamane [1987]. Sufficient cohesion is still maintained so that segregation does not occur, resulting in increased densification of the concrete.

There are four basic categories of superplasticizers. These are:

- Type A, based upon sulfonated melamine-formaldehyde condensates
- Type B, based upon sulfonated napthalene-formaldehyde condensates
- Type C, based upon modified ligninsulfonates, and
- Type D, based upon sulfonic esters or carbohydrate esters

According to Jerath and Yamane [1987] types A and B are the most commonly used:

Bickley [1998], Seabrook [1997], ACI Committee 212 [1991], Aitcin [1998], Hanna et al [1989] and others have all warned about the incompatibility of some superplasticizers and cementitious materials. A check with both the concrete supplier and the admixture supplier should be made. In addition, it is advisable to undertake trial mixtures.

A.3.8 Air-Entrainment

Air-entrainment agents are added to concrete to provide entrained air to be entrapped in the concrete during mixing. These are usually added to increase workability and frost resistance. This entrained air takes the form of minute air bubbles dispersed throughout the cement paste. In a cubic meter of concrete there are billions of such bubbles, ACI 211 [1991]. The void size must be very small to provide protection against freeze–thaw. In addition the spacing factor must be 0.20 mm (0.008 in.) and the surface of air voids be 24 mm^2/mm^3 (600 in^2/in^3), according to Powers [1949].

There are several different types of air-entraining agents. These may be liquid or water soluble powders. These agents are composed of the following:

- Salts of wood resins
- Synthetic detergents
- Salts of sulfonated lignin
- Salts of petroleum acids
- Salts of proteinaceous materials
- Fatty and resinous acids and their salts

- Organic salts of sulfonated hydrocarbons

The majority of air-entraining agents are in liquid form, with a few in powder form.

Losses of entrained air can occur after mixing, transportation and consolidation. Over mixing, improper transportation and over vibrating the placed concrete can all lead to air loss, ACI 212 [1991], Bickley [1998] and Seabrook [1997]. In addition, certain superplasticizers and air-entrainmement agents may not be compatible and may result in the air-entrainment agent be less effective than if used in NPC.

Air-entrainment results in a strength loss of between 4 to 5% for each percent of air entrained. Research has shown, ACI [1991] that for good resistance against freeze thaw action in HPC, 3 to 5% entrained air is required.

References for Appendix A

ACI, "Chemical Admixtures of Concrete", ACI Committee 212 Report, American Concrete Institute, 1991, pp. 212.3R-1 to 212.3R- 31.

ACI, "Use of Fly Ash in Concrete", ACI Committee 232 Report, American Concrete Institute , 1996, pp. 232.2R-1 to 232.2R-34.

ACI, "Ground Granulated Blast Furnace Slag as a Cementitious Constituent in Concrete", ACI Committee 233 Report, American Concrete Institute, 1995, pp. 233R-1 to 233R-18.

ACI, "Guide for the Use of Silica Fume in Concrete", ACI Committee 234 Report, American Concrete Institute, 1996, pp. 234R-1 to 234R-51.

ACI, "State of the Art Report on High Strength Concrete", ACI Committee 363 Report, American Concrete Institute, 1997, pp. 363R-1 to 363R-55.

Aitcin, P.-C., "High Performance Concrete", First Edition, E & FN Spon, London, England, 1998.

Aitcin, P.-C. and Neville, A., "High Performance Concrete Demystified" , Concrete International, Volume 15, Number 1, January 1993, pp. 21 to 26.

Alampalli, S. and Owens, F. T., "Improved Performance of New York State Bridge Decks", HPC Bridge News, US Department of Transportation, Federal Highway Administration, Washington, D.C., Issue Number 7, January/February 2000.

Baalbaki, M., Sarker, S. L., Aitcin, P.-C. and Isabelle, H., "Properties and Microstructure of high Performance Concretes Containing Silica Fume, Slag, and Fly Ash", SP-132, *Fly Ash, Silica Fume, Slag and Natural Pozzolans in Concrete,* American Concrete Institute, Detroit, 1992, pp. 121 to 142.

References for Appendix A

Beacham, M. W., "Implementing HPC Bridges in Nebraska", HPC Bridge News, U.S. Department of Transportation, Federal Highway Administration, Washington, D.C., Issue Number 3, May/June 1999.

Beacham, M. W., "HPC Deck in Nebraska", Concrete International, Volume 21, Number 2, February 1999, pp. 66 to 68.

Bickley J. A., "High Performance Concrete Specification: A Canadian Perspective", 1997, 11 pp., forwarded to the author in private correspondence with Portland Cement Association of Canada.

Binseel, E., "High Performance Concrete Bridges: Not Just for States Anymore", HPC Bridge News, U.S. Department of Transportation, Federal Highway Administration, Washington, D.C., Number 9, May/June 2000.

Breitenbucher, R., "Developments and Applications of High Performance Concrete", Materials and Structures, Volume 31, No, 207, April 1998, pp. 209 to 215.

Burge, T. A., "Densified Matrix Improves Bond with Reinforced Steel", paper presented to the MRS Symposium, Boston, 1987.

Canadian Standards Association, "CSA A23.3-94 Design of Concrete Structures", Rexdale, Ontario, 1994, pp. 199.

Carpenter, J. E., "Applications of High Strength Concrete for Highway Bridges', Public Roads, Volume 44, Number 2, September 1980, pp. 76 to 83.

Cook, W. D., Miao, B., Aitcin, P.-C. and Mitchell, D., "Thermal Stresses in Large High Strength Concrete Columns", ACI Materials Journal, Volume 89, Number 1, January/February 1992, pp. 61 to 68.

References for Appendix A

Cook, J. E., "10,000 psi Concrete", Concrete International, Volume 10, Number 10, October 1989, pp. 67 to 75.

De Larrard, F. and Mailer, Y., " Engineering Properties of Very High Performance Concretes", contained in *High Performance Concrete: From Material to Structure*, First English Edition, E & FN Spon, London, England, 1992, pp. 85 to 114.

De Larrard, F., "A Method for Proportioning High Strength Concrete Mixtures", ASTM, Cement, Concrete and Aggregates, Volume 12, Number 2, Summer 1990, pp. 47 to 52.

Ezeldin, A. S. and Aitcin, P.-C., "Effect of Course Aggregate on the Behavior of Normal and High Strength Concretes", ASTM Cement, Concrete and Aggregates, Volume 13, Number 2, Winter 1991, pp.121 to 124.

FHWA, "What is High Performance Concrete?", U.S. Department of Transportation, Federal Highway Administration, Washington, D.C., obtained from FHWA web site: http://hpc.fhwa.dot.gov/about.htm, on August 23, 2000, 2 pp.

FHWA, "Implementation Program on High Performance Concrete", Report FHWSA-SA-96-075, U.S. Department of Transportation, Federal Highway Administration, Washington, D.C., August 1996.

Gagne, R., Aitcin, P.-C., Pigeon, M. and Pleau, R., "Frost Durability of High Performance Concretes", contained in *High Performance Concrete: From Material to Structure*, First English Edition, E & FN Spon, London, England, 1992, pp. 239 to 251.

References for Appendix A

Gerwick, B. C., "Practical Methods of Ensuring Durability of Prestressed Concrete Ocean Structures", paper SP 47-14 contained in *Durability of Concrete*, ACI Publication SP-47, American Concrete Institute, Detroit, 1975, pp. 317 to 324.

Gjorv, O. E., Monteiro, J. M. and Mehta, P.K., "Effect of Condensed Silica Fume on the Steel Concrete Bond", ACI Materials Journal, Volume 87, Number 6, November/December 1990, pp. 573 to 580.

Goodspeed, C, Vanikar, S. and Cook, R., "High Performance Concrete Defined for Highway Structures", Concrete International, Volume 18, Number 2, February 1996, pp. 62 to 67.

Guitierrez, P. A. and Canovas, M. F., "The Modulus of Elasticity of High Performance Concrete", Materials and Structures, Volume 28, Number 184, December 1995, pp. 559 to 568.

Hamad, B. S. and Itani, M. S., "Bond Strength of Reinforcement in High Performance Concrete: The Role of Silica Fume, Casting Position, and Superplasticizer Dosage", ACI Materials Journal, American Concrete Institute, Volume 95, Number 5, September/October 1998, pp. 499 to 511.

Hanna, E., Luke, K., Perraton, D. and Aitcin, P.-C., "Rheological Behavior of Portland Cement in the Presence of a Superplasticizer", SP-119, *Superplasticizers and Other Chemical Admixtures in Concrete*, American Concrete Institute, Detroit, 1989, pp. 171 to 188.

Heald, W., "Expectations for HPC Bridges", HPC Bridge News, U.S. Department of Transportation, Federal Highway Administration, Washington, D.C., Issue Number 4,

References for Appendix A

Hegger, J., Nitsch, A. and Burkhardt, J., "High Performance Concrete in Precast Construction", Concrete Precasting Plant and Technology, Volume 63, Number 2, 1997, pp. 81 to 90.

Iravani, "Mechanical Properties of High Performance Concrete", ACI Materials Journal, American Concrete Institute, Volume 93, Number 5, September/October, 1996, pp. 416 to 426.

Jerath, S. and Yamane, L. C., "Mechanical Properties and Workability of Superplasticized Concrete", ASTM Cement Concrete and Aggregates, Volume 9, Number 1, Summer 1987, pp. 12 to 19.

Khan, A. K., Cook, W. and Mitchell, D., "Tensile Strength of Low, Medium and High Strength Concretes at Early Ages", ACI Materials Journal, Volume 93, Number 5, September/October 1993, pp. 487 to 493.

Konin, A., Francois, R. and Arliguie, G., "Analysis of Progressive Damage to Reinforced Ordinary and High Performance Concrete in Relation to Loading" Materials and Structures, Volume 31, Number 205, January/February 1998, pp. 27 to 35.

Kumaat, E. and Lorrain, M., "Cracking of Plain Reinforced High Performance Concrete Slabs", International Journal of Structures, Volume 16, Number 1, June 1996, pp.1 to 22.

Lessard, M., Baalbaki, M. and Aitcin, P.-C., "Mix Design of Air Entrained High Performance Concrete", contained in *Concrete under Severe Conditions, Environment and Loading*, Volume. 2, E and FN Spon, London, England, 1986, pp. 1025 to 1031, as reported in Aitcin, P.-C., *High Performance Concrete*, First Edition, E & FN Spon, London, England, 1998.

References for Appendix A

LoPresti, J. A. and Otter, D. E., "Longitudinal Forces in a Two Span Open Deck Steel Bridge at Fast", Technology Digest Number 98-020, Transportation Technology Center, Inc., The Association of American Railroads, Washington, D.C., August 1998, 4 pp.

Lorrain, M., "Bond Properties of High Performance Concrete" contained in., *High Performance Concrete: From Material to Structure*, Edited by Malier, Y., First English Edition, E & FN Spon, London, England, 1992.

Malhotra, V. M., "High Performance Concrete: Design and Materials and Recent Advances in Concrete Technology", Proceedings of the ACI International Conference on Concrete, Malaysia, 1997, Publication SP-172, American Concrete Institute, Michigan, 1997.

Martschuk, V. and Stark, J., "High Performance Concrete with High Durability", Concrete Precasting Plant and Technology, Volume 64, Number 4, 1998, pp. 73 to 83.

Mehtra, P. K. and Aitcin, P.-C., "Principles Underlying Production of High Performance Concrete", ASTM, Cement, Concrete and Aggregates, Volume 12, Number 2, Winter 1990, pp. 70 to 78.

Miller, R. A., "From Three Spans to One with HPC', HPC Bridge News, U.S. Department of Transportation, Federal Highway Administration, Washington, D.C., Issue Number 4, July/ August 1999.

Moore, J. A., "High Performance Concrete for Bridge Decks", Concrete International, Volume 21, Number 2, February 1999, pp.58.

References for Appendix A

Moreno, J., "High Performance Concrete: Economic Considerations", Concrete International, Volume 20, Number 3, March 1998, pp. 68 to 71.

Ozyildirim, H. C., "Specifying Durable Bridge Decks", HPC Bridge News, U.S. Department of Transportation, Federal Highway Administration, Washington, D.C., Issue Number 3, May/June 1999.

Ozylidirim, H. C., "High Performance Concrete for Transportation Structures", Concrete International, January 1993, pp. 33 to 38.

Ozyilidirim, C., "HPC Bridge Decks in Virginia", Concrete International, Volume 21, Number 2, February 1999, pp. 59 to 60.

Ozyilidirim, C., "Experimental Installation of a Concrete Bridge Deck Overlay Containing Silica Fume", Transportation Research Record 1204, Transportation Research Board, Washington, D.C., pp. 36 to 41.

Pitt, J. M., Seshardi, M. and Covey, D. L., "Reliability-Based Design for Freeze Thaw Resistant Concrete", from the Proceedings of the Materials Engineering Congress entitled *Material: Performance and Prevention of Deficiencies and Failures,* Atlanta, Georgia, August, 1992, Edited by T. D. White, American Society of Civil Engineers, 1992.

Powers, T. C., "Freezing Effects in Concrete" ACI Paper SP 47-1, from the proceedings of the Symposium on *Concrete Durability*, Atlantic City, 1973, American Concrete Institute, Detroit, 1975, pp. 1 to 12.

Ralls, M. L., "Texas HPC Bridge Decks", Concrete International, Volume 21, Number 2, February 1999, pp. 63 to 65.

References Appendix A

Rangan, V. B., "High Performance High Strength Concrete: Design Recommendations", Concrete International, Volume 20, Number 11, November 1998, pp. 63 to 68.

Rochelle, R. D., " Corrosion Modeling for HPC Specifications in North Carolina" HPC Bridge News, U.S. Department of Transportation, Federal Highway Administration, Washington, D.C., Issue Number 9, May/June 2000.

Rodriguez, S., " Concrete Specification Requirements for Alabama's HPC Bridges", HPC Bridge News, U.S. Department of Transportation, Federal Highway Administration, Washington, D.C., Issue Number 9, May/June 2000.

Rosenburg, A. M. and Gaidis, J. M., "A New Admixture of High Strength Concrete: Proposed Mechanism for Strength Enhancement", supplementary paper presented to the Second International Conference on the *Use of Fly Ash, Silica Fume, Slag and Natural Pozzolans in Concrete*, Madrid, 1986.

Russell, H. G., "ACI Defines High Performance Concrete", Concrete International, Volume 21, Number 2, February 1999, pp. 56 to 57.

Russell, H. G., "High Performance Concrete – from Buildings to Bridges", Concrete International, Volume 19, Number 8, August 1997, pp. 62 to 63.

Seabrook, P. T., "The Use of HPC in Bridge Deck Construction", paper presented at the *Developments in Concrete Bridge Design and Construction* Seminar, Canadian Portland Cement Association Vancouver, B.C., May 1997, 29 pp.

Seki,, H., "Deterioration of Concrete of Coastal Structures in Japan", paper SP 47-13 contained in *Durability of Concrete*, ACI Publication SP-47, American Concrete Institute, Detroit, 1975, pp. 293 to 316.

References for Appendix A

"Stronger Concrete", Engineering News Record, Japan, Volume 189, June 1982, pp 12.

Taerwe, L. R., "Bond Fracture and Crack Propagation in High Strength Concrete", Proceedings of the Third International Symposium on the *Utilization of High*

Waszczuk, C. M. and Juliano, M. L., "Application of HPC in a New Hampshire Bridge", Concrete International, Volume 21, Number 2, February 1999, pp.61 to 62.

Waszczuk, C. H., "Crack Free HPC Bridge Deck – New Hampshire's Experience", HPC Bridge News, U.S. Department of Transportation, Federal Highway Administration, Washington, D.C., Issue Number 4, July/August 1999.

Wecharatana, M. and Chimamphant, S., "Bond Strength of Deformed Bars and Steel Fibers in High Strength Concrete", paper presented to the *MRS Symposium*, Boston, 1987.

Weigel, J., "HPC in Washington State", HPC Bridge News, U.S. Department of Transportation, Federal Highway Administration, Washington, D.C., Issue Number 7, January/February 2000.

APPENDIX B

SLAB DESIGN MODEL

EXCEL PROGRAM FOR CALCULATING SLAB STRESSES

Input Values for Calculations

At Midspan

Description	Value	Units
Length	2.1350	m
Height	0.2500	m
Section Modulus	0.0221	m**3
Area of Concrete	0.5313	m**2
Transfer Moment	25.0000	kN-m
Service Moment	293.9000	kN-m

At Support

Description	Value	Units
Length	2.1350	m
Height	0.2250	m
Section Modulus	0.0179	m**3
Area of Concrete	0.4781	m**2
Transfer Moment	10.7000	kN-m
Support Moment	106.9000	KkN-m

Allowable Stress Levels

At Transfer	35 MPa at release		
Compression	bottom	0.6 f'c	21 MPa
Tension	top	3 $(f'c)^{1/2}$	1.5 MPa
In Service	70 MPa in service		
At Midspan			
Compression	top	0.4 f'c	28 MPa
Tension	bottom	0	0 MPa
At Support			
Tension	top	0	0 Mpa
Compression	bottom	0.4f'c	28 MPa

AT TRANSFER AT MIDSPAN

Eccentricity M	# of strands N	Prestress Force kN	P/A MPa	Pe/S MPa	M/S MPa	Stress Top MPa	Stress Bottom MPa
0.025	30	5,550	10.45	6.27	1.13	5.31	15.59
0.025	31	5,735	10.80	6.48	1.13	5.45	16.14
0.025	32	5,920	11.14	6.69	1.13	5.59	16.70
0.025	33	6,105	11.49	6.90	1.13	5.73	17.26
0.025	34	6,290	11.84	7.10	1.13	5.87	17.81
0.025	35	6,475	12.19	7.31	1.13	6.00	18.37
0.025	36	6,660	12.54	7.52	1.13	6.14	18.93
0.025	37	6,845	12.88	7.73	1.13	6.28	19.49
0.025	38	7,030	13.23	7.94	1.13	6.42	20.04
0.025	39	7,215	13.58	8.15	1.13	6.56	20.60
0.025	40	7,400	13.93	8.36	1.13	6.70	21.16
0.03	30	5,550	10.45	7.52	1.13	4.05	16.84
0.03	31	5,735	10.80	7.77	1.13	4.15	17.44
0.03	32	5,920	11.14	8.02	1.13	4.25	18.04
0.03	33	6,105	11.49	8.27	1.13	4.35	18.64
0.03	34	6,290	11.84	8.52	1.13	4.44	19.24
0.03	35	6,475	12.19	8.78	1.13	4.54	19.83
0.03	36	6,660	12.54	9.03	1.13	4.64	20.43
0.03	37	6,845	12.88	9.28	1.13	4.74	21.03
0.03	38	7,030	13.23	9.53	1.13	4.83	21.63
0.03	39	7,215	13.58	9.78	1.13	4.93	22.23
0.03	40	7,400	13.93	10.03	1.13	5.03	22.83

AT TRANSFER AT MIDSPAN

Eccentricity M	# of strands N	Prestress Force kN	P/A MPa	Pe/S MPa	M/S MPa	Stress Top MPa	Stress Bottom MPa
0.035	30	5,550	10.45	8.78	1.13	2.80	18.09
0.035	31	5,735	10.80	9.07	1.13	2.86	18.73
0.035	32	5,920	11.14	9.36	1.13	2.91	19.37
0.035	33	6,105	11.49	9.65	1.13	2.97	20.02
0.035	34	6,290	11.84	9.95	1.13	3.02	20.66
0.035	35	6,475	12.19	10.24	1.13	3.08	21.30
0.035	36	6,660	12.54	10.53	1.13	3.14	21.94
0.035	37	6,845	12.88	10.82	1.13	3.19	22.58
0.035	38	7,030	13.23	11.12	1.13	3.25	23.22
0.035	39	7,215	13.58	11.41	1.13	3.30	23.86
0.035	40	7,400	13.93	11.70	1.13	3.36	24.50
0.04	30	5,550	10.45	10.03	1.13	1.55	19.35
0.04	31	5,735	10.80	10.36	1.13	1.56	20.03
0.04	32	5,920	11.14	10.70	1.13	1.58	20.71
0.04	33	6,105	11.49	11.03	1.13	1.59	21.39
0.04	34	6,290	11.84	11.37	1.13	1.60	22.08
0.04	35	6,475	12.19	11.70	1.13	1.62	22.76
0.04	36	6,660	12.54	12.04	1.13	1.63	23.44
0.04	37	6,845	12.88	12.37	1.13	1.64	24.12
0.04	38	7,030	13.23	12.70	1.13	1.66	24.81
0.04	39	7,215	13.58	13.04	1.13	1.67	25.49
0.04	40	7,400	13.93	13.37	1.13	1.69	26.17

AT SERVICE LOADING (WITH 100% IMPACT LOADING) AT MIDSPAN

Eccentricity M	# of strands N	Prestress Force kN	P/A MPa	Pe/S MPa	M/S MPa	Stress Top MPa	Stress Bottom MPa
0.025	30	4,500	8.47	5.08	13.28	16.67	0.28
0.025	31	4,650	8.75	5.25	13.28	16.78	0.73
0.025	32	4,800	9.04	5.42	13.28	16.89	1.18
0.025	33	4,950	9.32	5.59	13.28	17.00	1.63
0.025	34	5,100	9.60	5.76	13.28	17.12	2.08
0.025	35	5,250	9.88	5.93	13.28	17.23	2.53
0.025	36	5,400	10.16	6.10	13.28	17.34	2.99
0.025	37	5,550	10.45	6.27	13.28	17.46	3.44
0.025	38	5,700	10.73	6.44	13.28	17.57	3.89
0.025	39	5,850	11.01	6.61	13.28	17.68	4.34
0.025	40	6,000	11.29	6.78	13.28	17.80	4.79
0.03	30	4,500	8.47	6.10	13.28	15.65	1.29
0.03	31	4,650	8.75	6.30	13.28	15.73	1.78
0.03	32	4,800	9.04	6.51	13.28	15.81	2.26
0.03	33	4,950	9.32	6.71	13.28	15.89	2.75
0.03	34	5,100	9.60	6.91	13.28	15.97	3.23
0.03	35	5,250	9.88	7.12	13.28	16.04	3.72
0.03	36	5,400	10.16	7.32	13.28	16.12	4.21
0.03	37	5,550	10.45	7.52	13.28	16.20	4.69
0.03	38	5,700	10.73	7.73	13.28	16.28	5.18
0.03	39	5,850	11.01	7.93	13.28	16.36	5.66
0.03	40	6,000	11.29	8.13	13.28	16.44	6.15

AT SERVICE LOADING (WITH 100% IMPACT LOADING) AT MIDSPAN

Eccentricity M	# of strands N	Prestress Force kN	P/A MPa	Pe/S MPa	M/S MPa	Stress Top MPa	Stress Bottom MPa
0.035	30	4,500	8.47	7.12	13.28	14.63	2.31
0.035	31	4,650	8.75	7.35	13.28	14.68	2.83
0.035	32	4,800	9.04	7.59	13.28	14.72	3.35
0.035	33	4,950	9.32	7.83	13.28	14.77	3.87
0.035	34	5,100	9.60	8.06	13.28	14.81	4.39
0.035	35	5,250	9.88	8.30	13.28	14.86	4.91
0.035	36	5,400	10.16	8.54	13.28	14.90	5.43
0.035	37	5,550	10.45	8.78	13.28	14.95	5.95
0.035	38	5,700	10.73	9.01	13.28	14.99	6.46
0.035	39	5,850	11.01	9.25	13.28	15.04	6.98
0.035	40	6,000	11.29	9.49	13.28	15.08	7.50
0.04	30	5,550	10.45	10.03	13.28	13.70	7.20
0.04	31	5,735	10.80	10.36	13.28	13.71	7.88
0.04	32	5,920	11.14	10.70	13.28	13.72	8.56
0.04	33	6,105	11.49	11.03	13.28	13.74	9.25
0.04	34	6,290	11.84	11.37	13.28	13.75	9.93
0.04	35	6,475	12.19	11.70	13.28	13.76	10.61
0.04	36	6,660	12.54	12.04	13.28	13.78	11.29
0.04	37	6,845	12.88	12.37	13.28	13.79	11.98
0.04	38	7,030	13.23	12.70	13.28	13.81	12.66
0.04	39	7,215	13.58	13.04	13.28	13.82	13.34
0.04	40	7,400	13.93	13.37	13.28	13.83	14.02

AT SUPPORT AT SERVICE LOADING

Eccentricity M	# of strands N	Prestress Force kN	P/A MPa	Pe/S MPa	M/S MPa	Stress Top MPa	Stress Bottom MPa
0.014	30	4,500	9.41	3.51	5.96	-0.06	18.89
0.014	31	4,650	9.73	3.63	5.96	0.13	19.32
0.014	32	4,800	10.04	3.75	5.96	0.33	19.75
0.014	33	4,950	10.35	3.87	5.96	0.53	20.18
0.014	34	5,100	10.67	3.98	5.96	0.72	20.61
0.014	35	5,250	10.98	4.10	5.96	0.92	21.04
0.014	36	5,400	11.29	4.22	5.96	1.12	21.47
0.014	37	5,550	11.61	4.33	5.96	1.31	21.90
0.014	38	5,700	11.92	4.45	5.96	1.51	22.33
0.014	39	5,850	12.24	4.57	5.96	1.71	22.77
0.014	40	6,000	12.55	4.68	5.96	1.90	23.20
0.019	30	4,500	9.41	4.77	5.96	-1.32	20.14
0.019	31	4,650	9.73	4.93	5.96	-1.16	20.62
0.019	32	4,800	10.04	5.09	5.96	-1.01	21.09
0.019	33	4,950	10.35	5.25	5.96	-0.85	21.56
0.019	34	5,100	10.67	5.40	5.96	-0.70	22.03
0.019	35	5,250	10.98	5.56	5.96	-0.55	22.51
0.019	36	5,400	11.29	5.72	5.96	-0.39	22.98
0.019	37	5,550	11.61	5.88	5.96	-0.24	23.45
0.019	38	5,700	11.92	6.04	5.96	-0.08	23.92
0.019	39	5,850	12.24	6.20	5.96	0.07	24.40
0.019	40	6,000	12.55	6.36	5.96	0.23	24.87

AT SUPPORT AT SERVICE LOADING

Eccentricity M	# of strands N	Prestress Force kN	P/A MPa	Pe/S MPa	M/S MPa	Stress Top MPa	Stress Bottom MPa
0.024	30	4,500	9.41	6.02	5.96	-2.57	21.40
0.024	31	4,650	9.73	6.22	5.96	-2.46	21.91
0.024	32	4,800	10.04	6.43	5.96	-2.35	22.43
0.024	33	4,950	10.35	6.63	5.96	-2.24	22.94
0.024	34	5,100	10.67	6.83	5.96	-2.12	23.46
0.024	35	5,250	10.98	7.03	5.96	-2.01	23.97
0.024	36	5,400	11.29	7.23	5.96	-1.90	24.48
0.024	37	5,550	11.61	7.43	5.96	-1.78	25.00
0.024	38	5,700	11.92	7.63	5.96	-1.67	25.51
0.024	39	5,850	12.24	7.83	5.96	-1.56	26.03
0.024	40	6,000	12.55	8.03	5.96	-1.44	26.54
0.029	30	4,500	9.41	7.28	5.96	-3.83	22.65
0.029	31	4,650	9.73	7.52	5.96	-3.76	23.21
0.029	32	4,800	10.04	7.76	5.96	-3.69	23.77
0.029	33	4,950	10.35	8.01	5.96	-3.62	24.32
0.029	34	5,100	10.67	8.25	5.96	-3.54	24.88
0.029	35	5,250	10.98	8.49	5.96	-3.47	25.43
0.029	36	5,400	11.29	8.73	5.96	-3.40	25.99
0.029	37	5,550	11.61	8.98	5.96	-3.33	26.55
0.029	38	5,700	11.92	9.22	5.96	-3.26	27.10
0.029	39	5,850	12.24	9.46	5.96	-3.19	27.66
0.029	40	6,000	12.55	9.70	5.96	-3.12	28.22

AT SUPPORT (with derailment loading)

Eccentricity M	# of strands N	Prestress Force kN	P/A MPa	Pe/S MPa	M/S MPa	Stress Top MPa	Stress Bottom MPa
0.014	30	4,500	9,412	3,514	3,569	2,329	16,495
0.014	31	4,650	9,725	3,631	3,569	2,525	16,926
0.014	32	4,800	10,039	3,748	3,569	2,722	17,357
0.014	33	4,950	10,353	3,865	3,569	2,918	17,788
0.014	34	5,100	10,667	3,982	3,569	3,115	18,218
0.014	35	5,250	10,980	4,099	3,569	3,312	18,649
0.014	36	5,400	11,294	4,216	3,569	3,508	19,080
0.014	37	5,550	11,608	4,334	3,569	3,705	19,511
0.014	38	5,700	11,922	4,451	3,569	3,901	19,942
0.014	39	5,850	12,235	4,568	3,569	4,098	20,373
0.014	40	6,000	12,549	4,685	3,569	4,295	20,803
0.019	30	4,500	9,412	4,769	3,569	1,074	17,750
0.019	31	4,650	9,725	4,928	3,569	1,228	18,223
0.019	32	4,800	10,039	5,087	3,569	1,383	18,695
0.019	33	4,950	10,353	5,245	3,569	1,538	19,168
0.019	34	5,100	10,667	5,404	3,569	1,693	19,641
0.019	35	5,250	10,980	5,563	3,569	1,847	20,113
0.019	36	5,400	11,294	5,722	3,569	2,002	20,586
0.019	37	5,550	11,608	5,881	3,569	2,157	21,059
0.019	38	5,700	11,922	6,040	3,569	2,312	21,531
0.019	39	5,850	12,235	6,199	3,569	2,467	22,004
0.019	40	6,000	12,549	6,358	3,569	2,621	22,477

AT SUPPORT (with derailment loading)

Eccentricity M	# of strands N	Prestress Force kN	P/A MPa	Pe/S MPa	M/S MPa	Stress Top MPa	Stress Bottom MPa
0.024	30	4,500	9,412	6,024	3,569	-181	19,005
0.024	31	4,650	9,725	6,224	3,569	-68	19,519
0.024	32	4,800	10,039	6,425	3,569	45	20,034
0.024	33	4,950	10,353	6,626	3,569	158	20,548
0.024	34	5,100	10,667	6,827	3,569	271	21,063
0.024	35	5,250	10,980	7,027	3,569	383	21,577
0.024	36	5,400	11,294	7,228	3,569	496	22,092
0.024	37	5,550	11,608	7,429	3,569	609	22,606
0.024	38	5,700	11,922	7,630	3,569	722	23,121
0.024	39	5,850	12,235	7,831	3,569	835	23,635
0.024	40	6,000	12,549	8,031	3,569	948	24,150
0.029	30	4,500	9,412	7,278	3,569	-1,436	20,260
0.029	31	4,650	9,725	7,521	3,569	-1,365	20,816
0.029	32	4,800	10,039	7,764	3,569	-1,294	21,372
0.029	33	4,950	10,353	8,006	3,569	-1,223	21,929
0.029	34	5,100	10,667	8,249	3,569	-1,152	22,485
0.029	35	5,250	10,980	8,492	3,569	-1,081	23,041
0.029	36	5,400	11,294	8,734	3,569	-1,009	23,598
0.029	37	5,550	11,608	8,977	3,569	-938	24,154
0.029	38	5,700	11,922	9,219	3,569	-867	24,710
0.029	39	5,850	12,235	9,462	3,569	-796	25,267
0.029	40	6,000	12,549	9,705	3,569	-725	25,823

APPENDIX C

ULTIMATE MOMENT CAPACITY CALCULATIONS

Sample Calculations of Ultimate Moment and Ultimate Load

Using the Stress Strain Compatibility Method

The following sample calculations are based on the specified compressive strength of concrete (f'c) of 70 MPa (10,150 psi). For high strength concrete the stress block factors must be adjusted as per the following formulas to better account for the wider range of concrete strength.

$$\alpha_1 = 0.85 - 0.0015 f_C' \geq 0.67$$

$$\beta_1 = 0.97 - 0.0025 f_C' \geq 0.67$$

Therefore, for 70 MPa concrete: $\alpha_1 = 0.75$ and $\beta_1 = 0.80$

In addition, the maximum strain in concrete for HPC should be increased to 0.0035

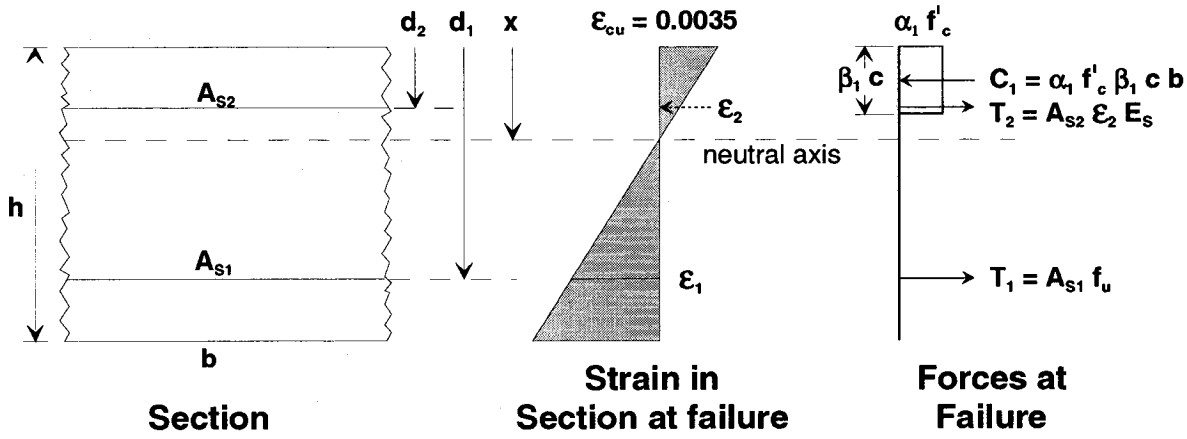

Using the diagram above the following stresses and strains can be computed:

f_{Se} = *effective prestress in the steel strands after prestress losses*

$$f_{se} = \frac{P_e}{A} = \frac{34 \times 150}{34 \times 140} = 1.07\ kN/mm^2$$

$f_{se} = 1{,}070\ MPa$

$$\varepsilon_{se} = \frac{f_{se}}{E_S} = \frac{1{,}070}{200{,}00} = 0.00535$$

$$\varepsilon_{SU} = \frac{f_{PU}}{E_S} = \frac{1860}{200{,}000} = 0.0093$$

From the placement of the strand within the slab (at midspan), the following can be determined:

$d_2 = 95\ mm\ (3.74\ in.)$

$d_1 = 180\ mm\ (7.09\ in.)$

Now assume the balanced case where the concrete ruptures as the prestressing steel starts to yield, set $c = x_{max}$, then solve for x_{max}, where:

$a = \beta_1\ x_{max} = 0.80\ x_{max}$ and

$$x_{\max} = \frac{\varepsilon_{cu}\ d_1}{\varepsilon_1 + \varepsilon_{cu}}$$

$$where: \varepsilon_1 = \varepsilon_{su} - \varepsilon_{se}$$

$$\varepsilon_1 = 0.0093 - 0.0053 = 0.0040$$

$$\varepsilon_{cu} = 0.0035$$

therefore:

$$x_{\max} = \frac{0.0035 \times 180}{0.004 + 0.0035}$$

$$x_{\max} = 84\ mm\ (3.31\ in.)$$

Now assume that the prestressing steel yields first.

$$\varepsilon_2 = \varepsilon_1\left(\frac{d_2 - x}{d_1 - x}\right) = 0.004\left(\frac{95 - x}{180 - x}\right)$$

$$T_1 = A_{S1} f_{pu} = 26 \times 140 \times 1860$$

$$T_1 = 6{,}770.4\ kN\ (1{,}523\ kips)$$

$$T_2 = 8 \times 140 \times 1860 \left(\frac{95 - x}{180 - x} \right)$$

$$T_2 = 2{,}083.2 \left(\frac{95 - x}{180 - x} \right)$$

$$C_1 = \alpha_1\ f'_c\ a\ b$$

where:

$$\alpha_1 = 0.75$$

$$a = \beta_1 x = 0.80x$$

$$b = 2135\ mm\ (84\ in.)$$

$f'_c = 70\ MPa$ (10,150 *psi*) based on design strength

$$C_1 = 89.7\ x\ kN\ (22.9\ x\ kips)$$

Collecting terms yields:

$$T_1 + T_2 = C_1$$

$$6{,}770.4 + 2{,}083.2 \left(\frac{95 - x}{180 - x} \right) = 89.7x$$

$$6{,}770.4\ (180 - x) + 2{,}083.2\ (95 - x) - 89.7x\ (180 - x) = 0$$

$$x^2 - 278.7x + 15{,}794 = 0$$

Solving by means of the quadratic equation yields:

x = 200 mm (7.87 in.) or x = 79 mm (3.11 in.)

Since x = 190 mm > x_{max} , therefore use x = 79 mm (3.11 in.).

Therefore:

$$\varepsilon_2 = \varepsilon_1\left(\frac{95-x}{180-x}\right) = 0.004\left(\frac{95-79}{180-79}\right)$$

$$\varepsilon_2 = 0.0006$$

Solving for T_1 and T_2 in terms of f_{s1} yields the following:

$$T_1 = A_{s1} f_{s1} = 26 \times 140 \times f_{s1}$$

$$T_1 = 3{,}640 f_{s1}$$

$$T_2 = A_{s2} f_{s1}\left(\frac{\varepsilon_2}{\varepsilon_1}\right) = 8 \times 140\ f_{s1}\left(\frac{0.0006}{0.0040}\right)$$

$$T_2 = 168 f_{s1}$$

Also:

$$C_1 = 0.75 f'_c\ a\ b$$

$$C_1 = 0.75 \times 70 \times (0.80 \times 79) \times 2135$$

$$C_1 = 7{,}083{,}930\ N\ (1{,}594\ kips)$$

$$C_1 = T_1 + T_2 = 3{,}640 f_{s1} + 168 f_{s1} = 3{,}808 f_{s1}$$

$$7{,}083{,}930 = 3{,}808 f_{s1}$$

$$f_{s1} = 1{,}860\ MPa\ (270\ ksi)$$

Therefore:

$$T_1 = 3{,}640 \times 1{,}860 = 6{,}770{,}400\ N\ (1{,}523\ kips)$$

$$T_2 = 168 \times 1{,}860 = 312{,}480\ N\ (70\ kips)$$

Taking moment about T_1 results in the following equation:

$$M_U = C_1\left(d_1 - \frac{a}{2}\right) - T_2\,(d_1 - d_2)$$

$$M_U = 7{,}083{,}930\left(180 - \frac{0.8 \times 79}{2}\right) - 312{,}480\ (180 - 95)$$

$$M_U = 1{,}024{,}694{,}412\,N - mm$$

$$M_U = 1{,}024.7\,kN - m\ (756\,kip - ft.)$$

For an applied load at midspan of the slab, supported on a 2.44 m (8 ft.) span, the following is the ultimate load:

$$M_u = \frac{P_u\,L}{4}$$

$$Therefore: P_u = \frac{4\,M_u}{L}$$

where:

$L = 2.44\ m$ (8 ft.)

$M_u = 1{,}024.7\,kN - m$

$$P_u = \frac{4 \times 1{,}024.7}{2.44}$$

$P_U = 1{,}680\,kN\ (378\,kips)$

For the load applied 0.92 m (3 ft.) from the support, the ultimate load is:

$$M_U = \frac{P_U\,ab}{L}$$

or:

$$P_U = \frac{M_U\,L}{ab}$$

where:

a = 0.92 m (3 ft.)

b = 1.52 m (5 ft.)

L = 2.44 m (8 ft.)

$M_U = 1{,}024.7\,kN - m$

therefore:

$P_U = 1{,}788\,kN\ (402\,kips)$

For a load applied 0.61 m (2 ft.) from the support, the ultimate load is:

$$P_U = \frac{M_U L}{ab}$$

where:

a = 0.61 m (2 ft.)

b = 1.83 m (6 ft.)

L = 2.44 m (8 ft.)

$M_U = 1{,}024.7\,kN - m$

therefore:

$P_U = 2{,}240\,kN\ (504\,kips)$

Similar calculations as above were performed using the actual f'c for each of the slabs, modifying the stress block factors according to the strength of concrete.

APPENDIX D

CRACKING MOMENT CAPACITY CALCULATIONS

Cracking Moment Capacity

The loading to cause first flexural cracking must overcome the compressive stress in the bottom fibre of the slab caused by prestressing plus the tensile stress capacity of the concrete in the bottom fibre of the slab. The compressive prestress at the bottom fibre is:

$$\sigma_b = \frac{P}{A} + \frac{Pe}{S_b}$$

where:

σ_b = stress at bottom of slab

P = effective prestressing force

A = area of concrete

e = eccentricity

S_b = section modulus of bottom of slab

First flexural cracking of concrete will occur when the tensile stress in the bottom fibre of the slab reaches a value of:

$$\sigma_{cr} = 0.5\sqrt{f_c'} \text{ (in MPa)}$$

where:

σ_{cr} = tensile cracking stress at bottom fibre

The total stress applied to the bottom fibre at first cracking is:

$$\sigma = \frac{P}{A} + \frac{Pe}{S_b} + 0.5\sqrt{f_c'}$$

The moment to cause this cracking is therefore:

$$M_{cr} = \{ \frac{P}{A} + \frac{Pe}{S_b} + 0.5\sqrt{f_c'} \} \times S_b$$

The cracking moment will change for each test location along the slab because the top of the slab is sloped and therefore the area and section modulus decrease towards the supports. The theoretical calculations for first flexural cracking of each slab are tabulated below.

Test Number	Slab Number	σ_b MPa	$0.5\sqrt{f_c'}$ MPa	S_b mm^3	M_{cr} kN-m
1	1	17.58	4.47	22.240×10^6	490.4
2	2	17.58	4.47	22.240×10^6	490.4
3	6	1.53	4.96	22.240×10^6	144.4
4	5	17.49	4.96	21.185×10^6	475.8
5a	4	17.37	4.73	20.156×10^6	445.6
5b	4	17.37	4.73	20.156×10^6	445.6
6	3	17.49	4.73	21.185×10^6	470.9

Table D.1 Summary of Predicted Cracking Moments

A similar calculation to the above was run for the specified strength of concrete at 70 MPa (10,150 psi).

APPENDIX E

SAMPLE PHOTOS DOCUMENTING

TEST PROGRESSION

TEST NO. 5B

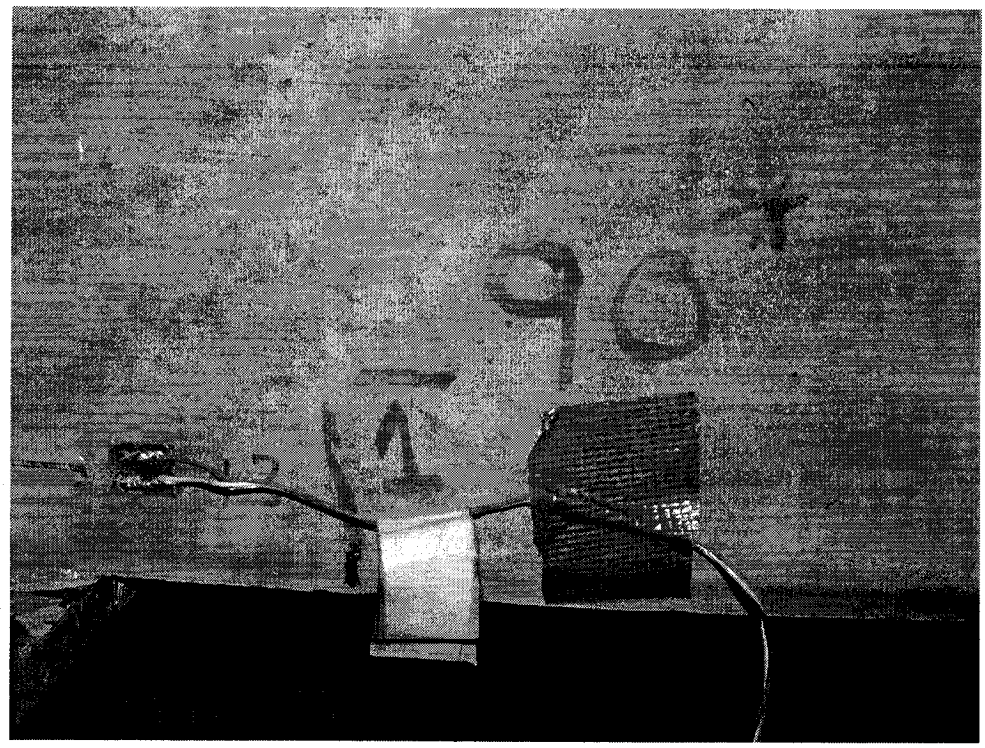

Figure E1 First Cracking at 90,000 kg loading

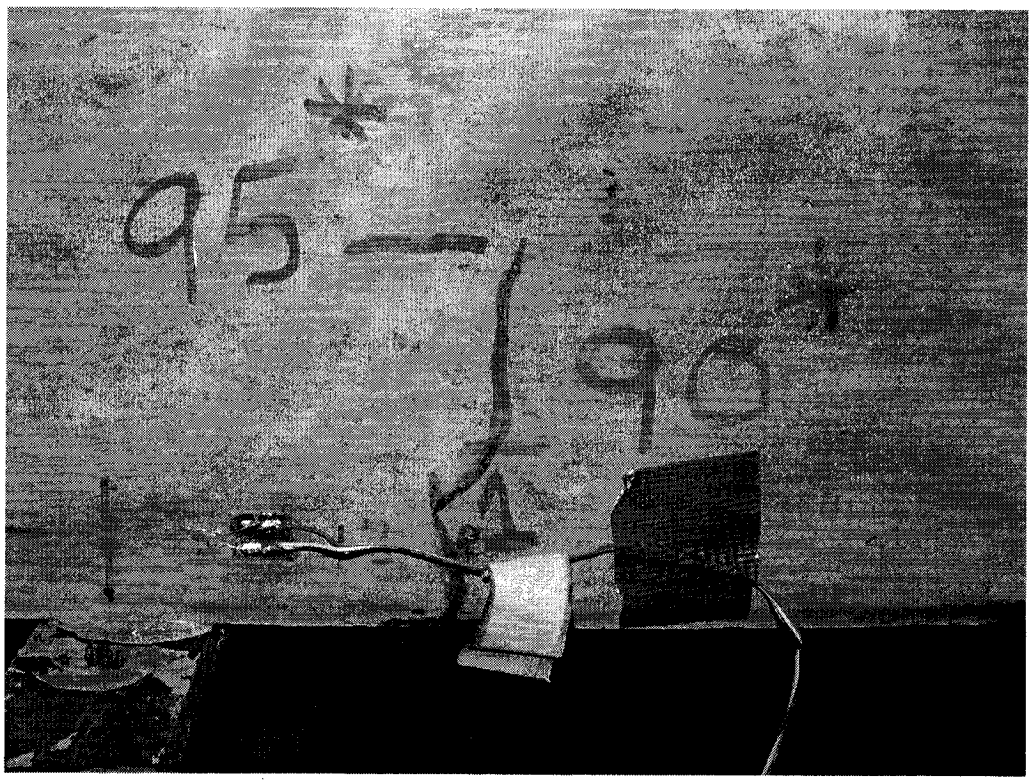

Figure E2 Large crack extension at 95,000 kg loading.

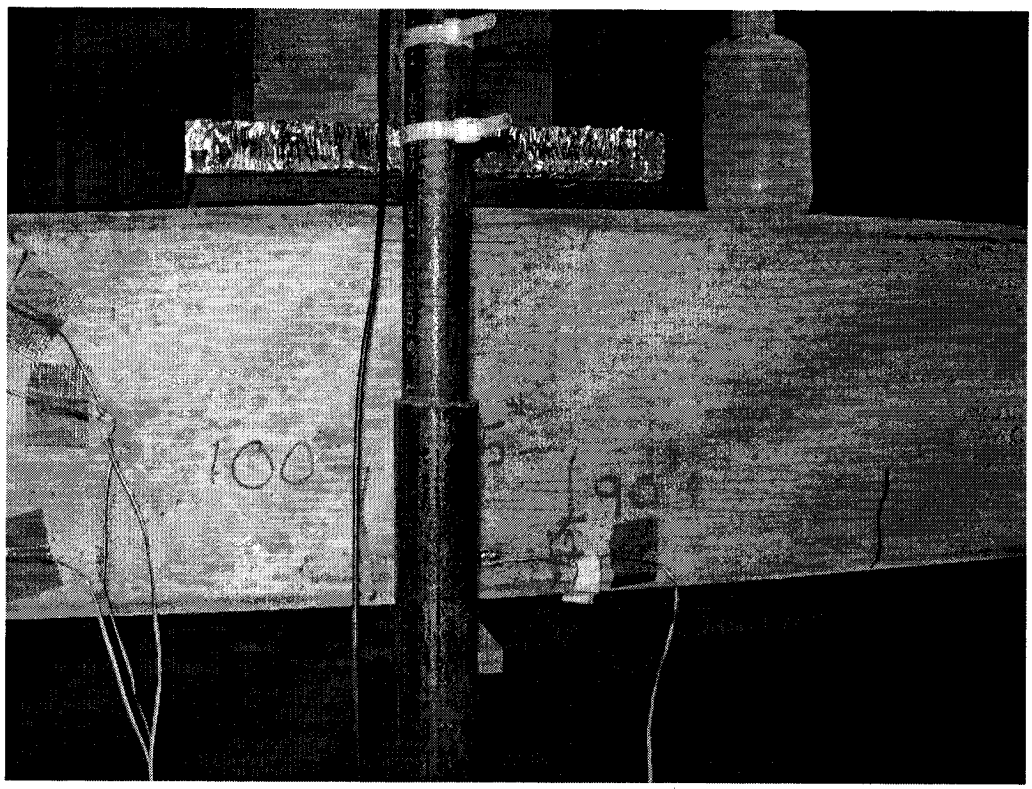

Figure E3 Crack progression at 100,000 kg loading.

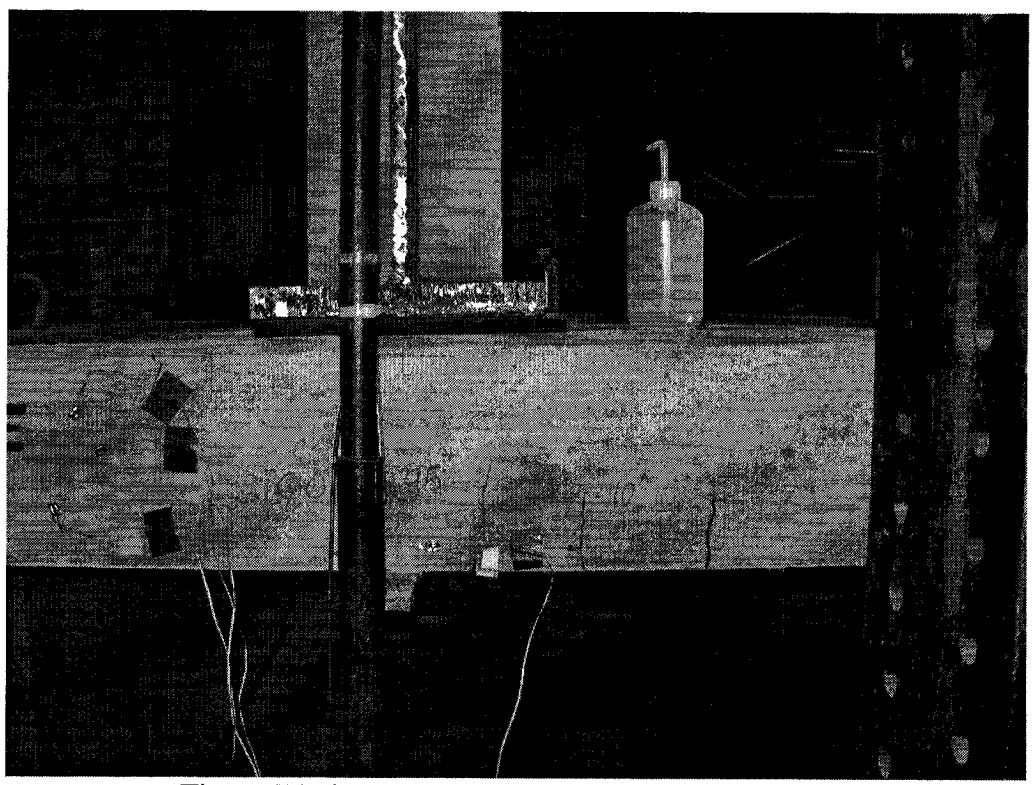

Figure E4 Crack progression at 110,000 kg loading.

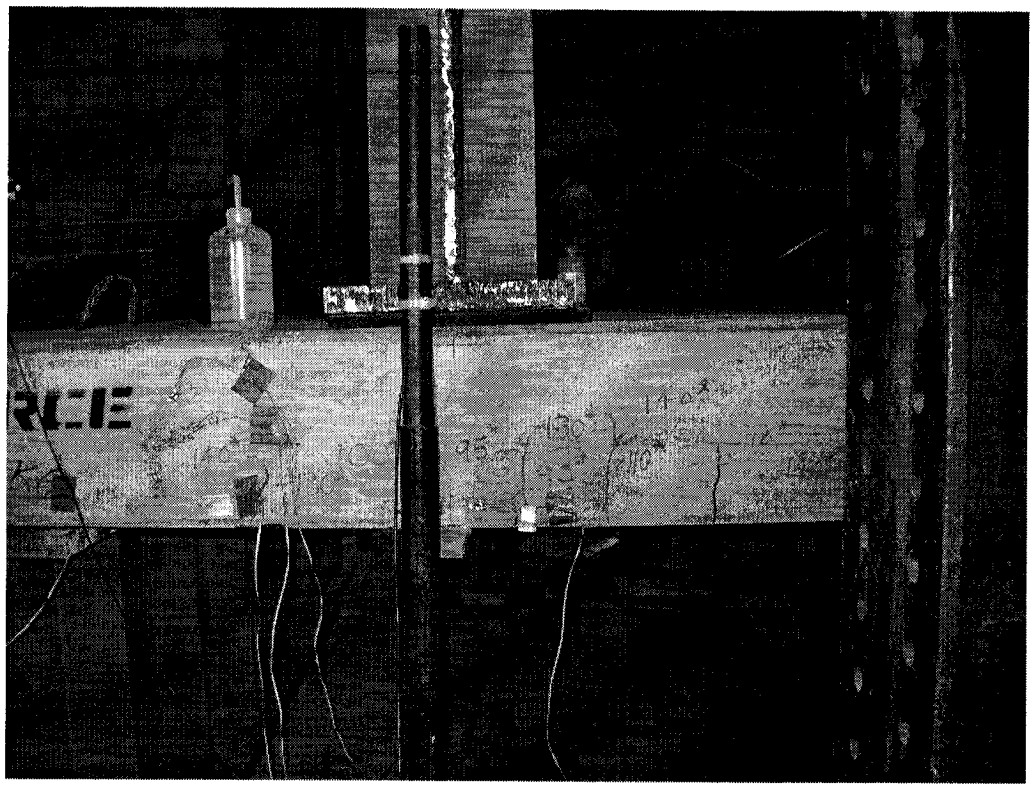

Figure E5 Crack progression at 140,000 kg loading.

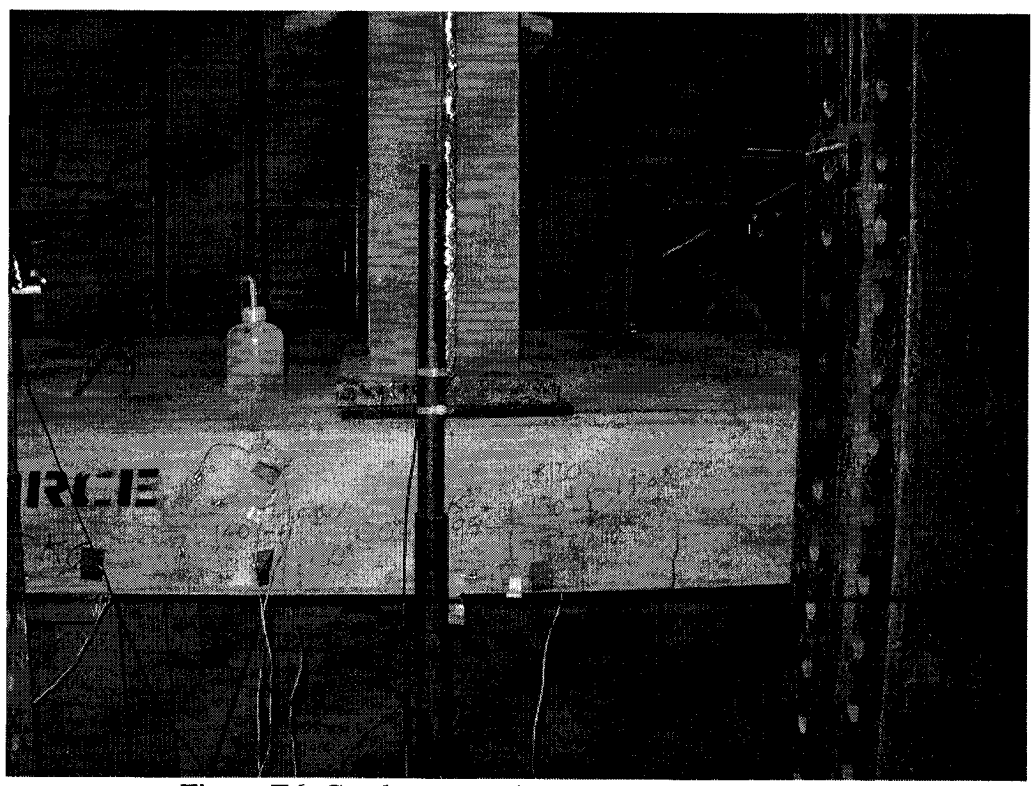

Figure E6 Crack progression to 150,000 kg loading.

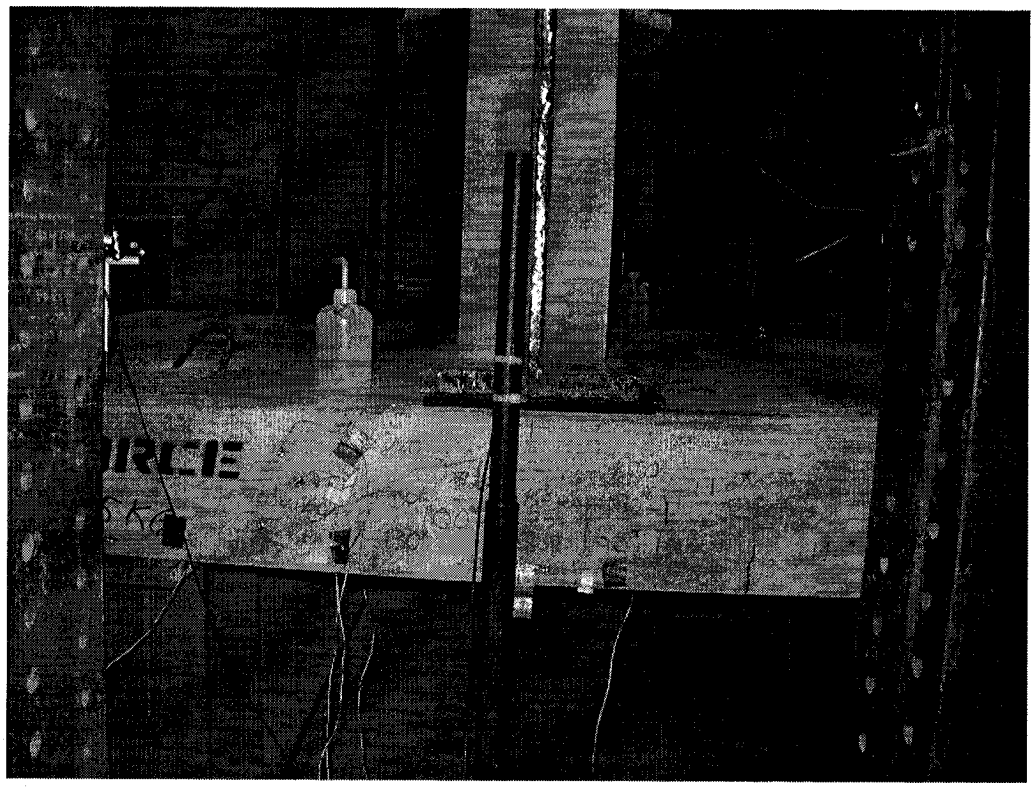

Figure E7 Crack progression to 160,000 kg loading

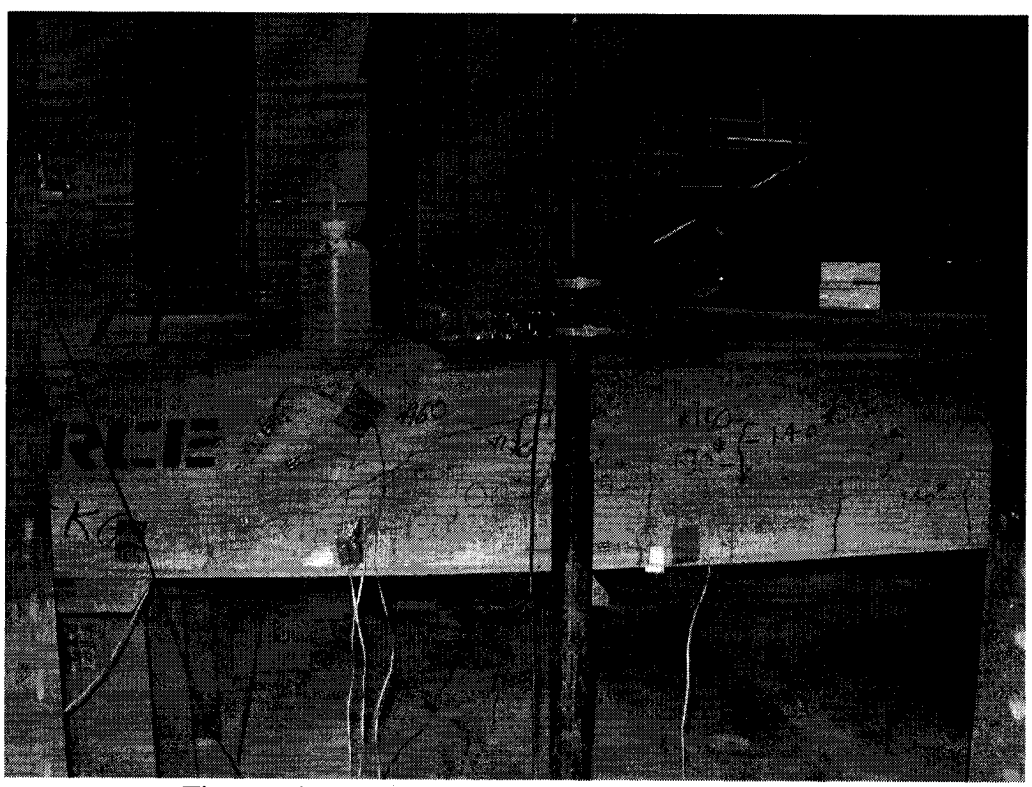

Figure E8 Crack progression to 180,000 kg loading.

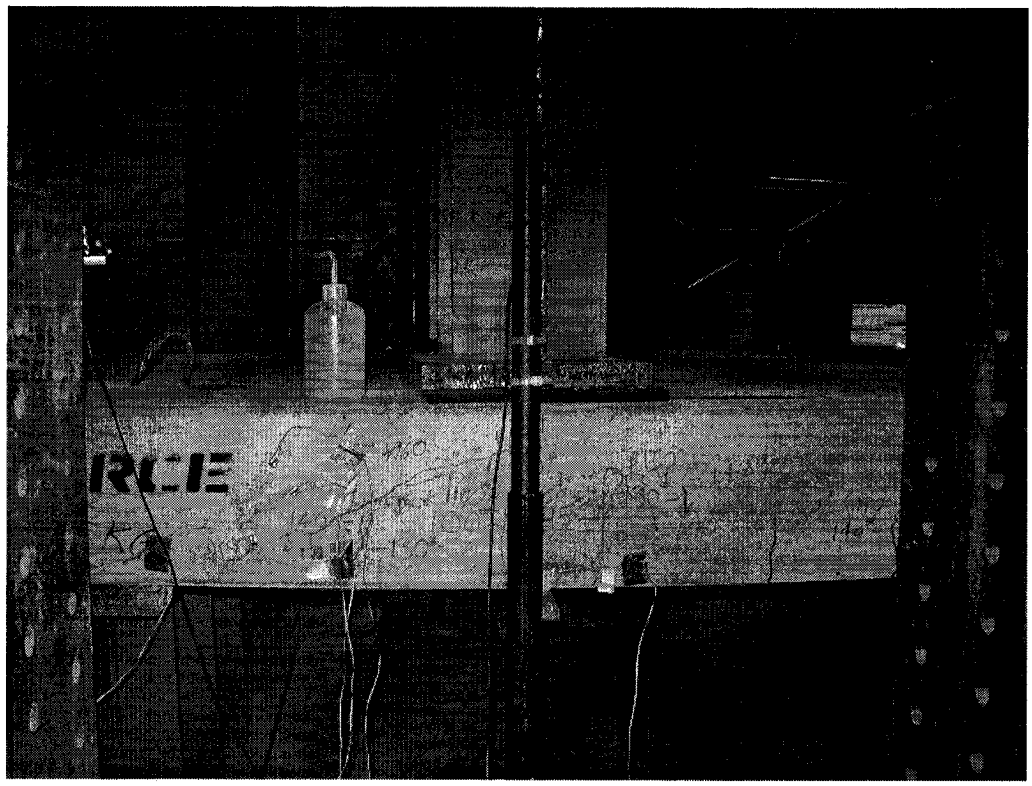

Figure E9 Crack progression to 190,000 kg loading.

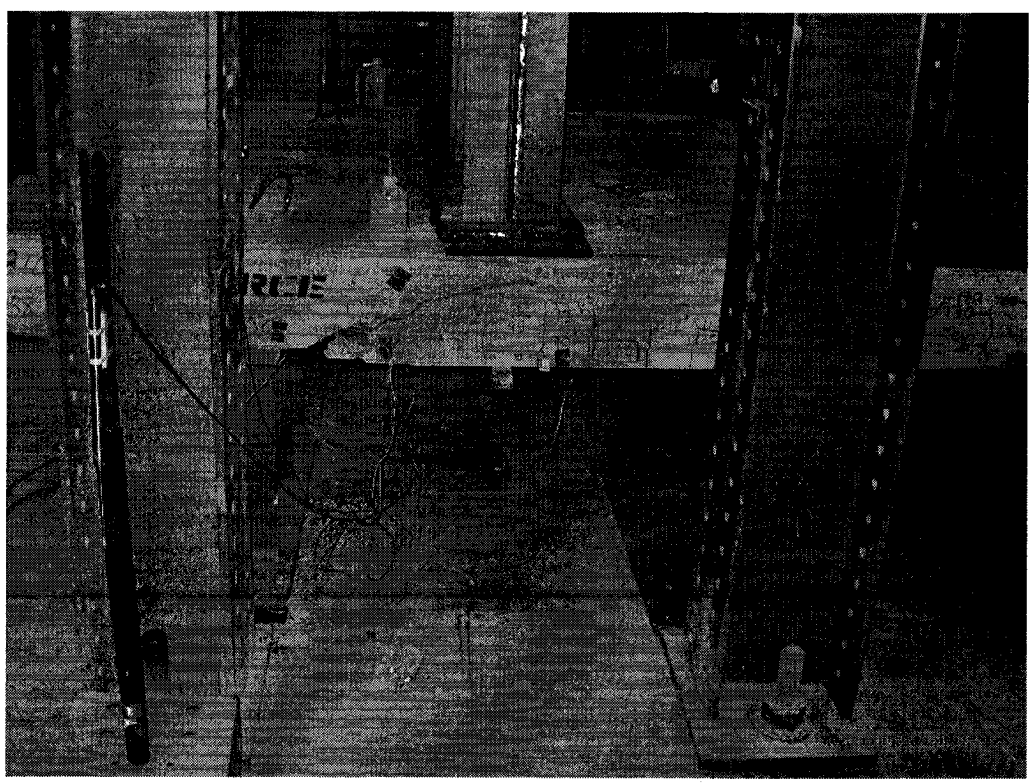

Figure E 10 Failure at 217,000 kg loading.

APPENDIX F

EXPERIMENTAL DATA

ALL TESTS

Data for Test Number 1, Slab Number 1

Date Tested June 14, 2002

Test #1 Load applied in center
Start Time: 14/06/2002 2:20:53 PM

Slab No. 1, Cast March 4, 2002

LOAD AND STRAIN VALUES

Assignment	Seconds Elapsed	1 LC Calibrated Values	1 LC Millivolts per volt	2 SG FLB Strain ue	3 SG FLD Strain ue	4 SG FCB Strain ue	5 SG FRD Strain ue	6 SG BRB Strain ue	7 SG BRD Strain ue	8 SG BCB Strain ue	9 SG BLD Strain ue
1	24.5	765	0	-1	0	1	1	0	0	-1	1
2	145.6	3983	0.0173	5	-2	32	-7	1	-3	42	-6
3	147.8	5475	0.0253	5	-3	44	-9	2	-4	59	-9
4	208.8	765	0	49	2	2	-1	0	0	-1	1
5	317	2117	0.0073	-43	0	18	-5	1	-1	19	-3
6	480.7	3983	0.0173	-131	-2	34	-8	2	-4	42	-7
7	504.6	4775	0.0215	-125	-2	40	-10	2	-4	53	-9
8	512	3749	0.016	-127	-1	32	-9	3	-2	35	-7
9	531.2	4775	0.0215	-126	-1	42	-10	2	-4	49	-8
10	680.9	6734	0.032	-108	-3	57	-12	2	-6	73	-11
11	688.2	9159	0.045	-106	-4	75	-16	2	-8	99	-15
12	751.3	11257	0.0563	-13	-6	93	-19	3	-12	122	-18
13	879.4	13449	0.068	-15	-9	110	-22	4	-13	142	-21
14	1095.6	15501	0.079	172	-9	128	-25	4	-15	163	-24
15	1111	18346	0.0943	175	-11	150	-29	5	-16	191	-28
16	1119.8	18905	0.0973	174	-11	158	-29	5	-17	198	-28
17	1137.7	20864	0.1077	175	-13	174	-33	6	-19	217	-31
18	1148.7	22776	0.118	177	-14	191	-36	7	-21	238	-32
19	1207.6	25107	0.1305	177	-16	214	-39	8	-23	265	-36
20	1288.1	26973	0.1405	178	-17	231	-41	8	-24	285	-38
21	1299.7	27579	0.1438	179	-18	237	-42	8	-24	290	-38
22	1360.6	30191	0.1578	179	-20	260	-45	8	-27	320	-40
23	1369.1	30004	0.1568	178	-20	260	-45	8	-26	321	-40
24	1430.8	33595	0.176	180	-22	290	-49	10	-29	361	-43
25	1458.6	35460	0.186	181	-23	311	-51	8	-31	395	-46
26	1545.6	37512	0.197	181	-24	335	-54	9	-34	435	-47

27	1547	37559	0.1973	181	-25	335	-53	10	-34	437	-48
28	1619.6	40123	0.211	182	-26	366	-56	10	-36	489	-51
29	1659.4	42455	0.2235	183	-28	368	-59	12	-37	485	-52
30	1661.3	42782	0.2253	184	-28	361	-60	11	-37	480	-53
31	1686.6	45160	0.238	184	-31	396	-63	11	-39	445	-55
32	1738.1	47585	0.251	186	-32	517	-65	11	-42	416	-58
33	1797.9	50010	0.264	186	-34	1155	-69	12	-44	389	-60
34	1800.8	50150	0.2647	186	-34	1201	-69	12	-44	388	-60
35	1845.3	53088	0.2805	187	-36	5357	-73	12	-46	373	-63
36	1881	55186	0.2918	187	-38	11948	-75	13	-49	361	-65
37	1958.7	60362	0.3195	189	-43	16754	-81	14	-53	310	-71
38	2046	64746	0.343	188	-47	167	-88	14	-57	273	-74
39	2048.4	65166	0.3453	188	-48	168	-89	14	-57	269	-74
40	2070.1	67591	0.3583	188	-49	166	-91	14	-59	252	-77
41	2071.1	68337	0.3623	188	-50	166	-92	13	-60	249	-77
42	2496.8	76264	0.4047	-49	-57	161	-100	14	-68	187	-84
43	2501.6	78549	0.417	-49	-59	158	-102	15	-70	177	-85
44	2512.9	80508	0.4275	-48	-61	155	-104	15	-71	164	-86
45	2542	85544	0.4545	-46	-65	149	-110	16	-74	133	-91
46	2560.3	90907	0.4833	-45	-68	160	-116	16	-78	104	-95
47	2577	97063	0.5162	-43	-73	246	-123	16	-83	71	-100
48	2590.4	100421	0.5343	-42	-77	551	-125	16	-86	55	-99
49	3285.2	110913	0.5905	280	-88	2352	-205	16	-84	27	-105
50	3433.5	122571	0.653	280	-83	238	-208	16	-85	2	-109
51	3445.9	126116	0.672	279	-82	229	-208	17	-85	-10	-109
52	3457.7	130686	0.6965	280	-73	248	-208	17	-82	-20	-110
53	3836.8	139919	0.746	281	-52	615	71	16	-81	109	-107
54	3864.2	142857	0.7618	280	-49	606	87	16	-81	113	-107
55	3876.9	145282	0.7748	280	-42	387	89	14	-80	130	-104
56	3892.8	150412	0.8023	279	-28	527	88	13	-100	133	-95
57	3905.5	153723	0.82	277	-30	529	77	12	-107	111	-87
58	3920.7	152370	0.8127	275	-35	544	79	11	-112	107	-88
59	4521	156008	0.8323	211	-165		-114	10	-156	98	-142

60	4528.4	160951	0.8588	210	-173		-116	9	-159	99	-144
61	4536.2	165428	0.8828	207	-189		-125	8	-166	112	-155
62	4867.1	160997	0.859	16	-200		391	5	-178	159	-166
63	4874.4	166220	0.887	15	-213		387	4	-182	344	-171
64	5095.8	-774	-0.0083	17	106	-117	81	334	150	348	

SLAB NO. 1

DEFLECTION VALUES

11 LVDT 150 mm FC Calibrated Values	Assignment	11 LVDT 150 mm FC Millivolts	12 LVDT 150 mm BC Calibrated Values	12 LVDT 150 mm BC Millivolts	13 LVDT 50 mm FLS Calibrated Values	13 LVDT 50 mm FLS Millivolts	14 LVDT 50 mm BLS Calibrated Values	14 LVDT 50 mm BLS Millivolts
0	1	0	0	-0.3	0	-0.3	0	-0.3
0	2	14.3	0	24.7	0	4.3	0	19.2
0	3	22.3	1	35.1	0	11.6	0	23.8
0	4	4.3	0	2.1	0	3.7	0	11
0	5	10.7	0	14.7	0	4.6	0	18
0	6	18.9	0	28.7	0	6.1	0	23.5
0	7	21.1	1	33.3	0	9.2	0	24.7
0	8	20.1	0	26.9	0	15.9	0	31.4
0	9	24.7	1	32.7	0	15.9	0	28.1
1	10	33.6	1	45.2	0	25	0	34.5
1	11	44.6	1	58	0	36.6	0	41.8
1	12	56.8	1	71.4	0	51.9	0	56.5
1	13	71.1	1	83.9	0	68.7	0	70.5
1	14	83	1	94	1	84.2	0	77.5
1	15	96.1	2	105.3	1	102.6	1	85.2
2	16	101	2	109.6	1	110.5	1	90.6
2	17	111.4	2	117.8	1	122.1	1	96.4
2	18	122.7	2	127	1	135.8	1	104.4
2	19	138.9	2	139.8	1	156	1	122.7
2	20	150.8	2	151.1	1	170.3	1	135.5
2	21	153.8	2	152.6	1	172.1	1	136.7
3	22	166	3	164.5	1	183.7	1	147.1
3	23	166.6	3	164.5	1	184.7	1	148.3
3	24	183.1	3	180.1	1	199.3	1	162.1
3	25	193.2	3	189.2	1	208.2	1	172.1

3	26	205.7	3	201.4	1	221.3	1	188.9
3	27	206.3	3	202.4	1	221	1	189.2
3	28	219.8	3	215.8	1	232.9	1	204.2
4	29	230.4	4	226.5	1	240.8	1	212.7
4	30	231.7	4	227.1	1	241.4	1	213.3
4	31	243.9	4	239.6	2	250.6	1	223.7
4	32	258.2	4	253.6	2	262.8	1	239
4	33	271.3	4	268.3	2	275.6	2	258.2
4	34	272.9	4	269.2	2	276.2	2	258.8
4	35	289.6	4	284.5	2	290	2	274.7
5	36	300	5	295.4	2	296.4	2	286
5	37	330.9	5	326.9	2	322	2	315
6	38	359.2	6	355.6	2	343.1	2	344.6
6	39	361.7	6	358.3	2	344.6	2	346.4
6	40	376.9	6	372.7	2	354.4	2	355.9
6	41	380.3	6	376.3	2	355	2	357.4
7	42	453.9	7	452	3	418.4	3	443.5
7	43	466.7	7	463.9	3	422.1	3	445
7	44	480.7	7	477	3	427.6	3	448.7
8	45	520.7	8	516.4	3	445.3	3	462.7
9	46	562.5	9	557.3	3	461.5	3	475.2
10	47	616.5	9	611.6	3	482.8	3	493.5
10	48	650.7	10	646.4	3	498.7	3	507.6
12	49	789.6	12	793.6	4	589.1	4	626
15	50	955	15	957.8	4	656.8	4	676
15	51	988.3	15	990.1	4	662	4	679.1
16	52	1048.7	16	1050.8	4	673.9	4	684.3
20	53	1276.7	20	1287.1	5	774	5	755.7
20	54	1310	20	1319.7	5	779.2	5	759.1
21	55	1354.8	21	1365.2	5	785	5	760.3
23	56	1471.7	23	1485.5	5	801.5	5	764.3
24	57	1575.2	25	1583.8	5	857.3	5	765.2
25	58	1595	25	1603	5	867.4	5	768.8

30	59	1914.6	29	1881.9	6	938.2	5	825.9
31	60	1989.1	30	1950.3	6	944.6	5	826.2
33	61	2124.6	32	2073	6	955.6	5	826.2
33	62	2139.5	32	2084	6	974.9	5	839
35	63	2247.3	34	2182.9	6	981.9	5	839.9
84	64	5427.9	86	5553.7	1	207.9	-5	-850

Data for Test Number 2, Slab Number 2

Date Tested July 12, 2002

Test #2 Test load applied at center
Start Time: 12/07/2002 8:39:38 AM

Deck Slab No. 2, Cast March 4, 2002

Strain Gauge Readings

Reading No.	Time Seconds	1 LC Calibrated Values kg	1 LC Millivolts per volt	2 SG#1 FLT Strain ue	3 SG#2 FLB Strain ue	4 SG#3 FLD Strain ue	5 SG#4 FCB Strain ue	6 SG#5 FRD Strain ue	7 SG#6 FRB Strain ue	8 SG#7 FRT Strain ue	9 SG#8 BRT Strain ue
1	37.4	0	0	1	0	0	-3	0	0	0	1
2	38.3	-48	-0.0003	1	0	1	-2	-1	0	-1	0
3	434.9	8157	0.0423	-7	6	-8	29	-6	6	-5	-5
4	738.8	11102	0.0575	-8	9	-11	43	-10	7	-4	-7
5	887.3	15011	0.0777	-9	11	-14	66	-13	8	-3	-8
6	1052.8	20031	0.1038	-12	15	-19	92	-19	11	-3	-9
7	1244.5	25003	0.1295	-13	16	-23	121	-22	14	-3	-10
8	1343.1	30071	0.1558	-16	18	-29	154	-26	16	-3	-11
9	1417.5	34994	0.1812	-18	22	-34	192	-35	16	-3	-10
10	1466.8	34994	0.1812	-17	21	-34	192	-35	17	-3	-9
11	1613.6	39966	0.207	-18	24	-38	226	-40	19	-2	-10
12	1671.6	41366	0.2142	-18	24	-39	234	-42	20	-1	-9
13	1684.4	45275	0.2345	-18	26	-43	262	-45	21	-2	-10
14	1783.8	50054	0.2592	-19	28	-47	432	-50	22	-1	-10
15	1885	54977	0.2848	-20	29	-52		-56	24	-2	-11
16	2049.4	60142	0.3115	-21	31	-58		-62	27	-2	-11
17	2365.1	65162	0.3375	-19	33	-63		-65	28	-2	-11
18	2511.3	70134	0.3633	-20	37	-67		-70	31	-2	-12
19	2671.6	71533	0.3705	-19	36	-71		-71	32	-3	-12
20	2681.5	76119	0.3942	-20	39	-75		-74	33	-4	-13
21	2976.5	80463	0.4168	-19	40	-80		-80	35	-6	-13
22	3962.7	80077	0.4148	-14	40	-78		-78	36	-5	-9
23	4171.5	85097	0.4408	-15	42	-83		-82	40	-9	-10

24	4281.8	90068	0.4665	-16	45	-88	-85	42	-10	-11
25	4587	95136	0.4928	-18	47	-93	-86	44	-12	-14
26	4696.7	100205	0.519	-19	50	-94	-87	46	-13	-13
27	4941.6	99867	0.5172	-19	50	-95	-85	45	-13	-14
28	4978.6	100494	0.5205	-20	50	-95	-86	46	-15	-14
29	5080.9	105852	0.5483	-21	51	-98	-88	46	-15	-14
30	5309.9	110003	0.5697	-23	53	-100	-89	47	-16	-15
31	5501.8	115168	0.5965	-25	56	-103	-91	48	-18	-17
32	5672.6	120139	0.6222	-27	58	-101	-86	50	-20	-19
33	5961.8	125208	0.6485	-31	61	-100	-81	51	-22	-19
34	6076.1	130276	0.6747	-33	61	-98	-79	52	-24	-22
35	6262.3	135296	0.7007	-37	63	-94	-68	53	-27	-24
36	6288.3	140122	0.7258	-38	63	-90	-60	53	-29	-25
37	6451.7	150403	0.779	-42	65	-77	-36	54	-36	-25
38	6653.2	159961	0.8285	-46	57	-49	-54	52	-48	-30
39	6814.2	164160	0.8503	-58	57	-122	-94	49	-50	-35
40	6821.1	165270	0.856	-57	57	-125	-113	49	-51	-35
41	6839.8	170145	0.8812	-60	56	-144	-137	49	-57	-35
42	6875.7	171738	0.8895	-66	49	-220	-154	45	-59	-39
43	6885.9	7433	0.0385		-3		100	12	-8	-86

Strain Gauge Readings

Reading No.	Time Seconds	1 LC Calibrated Values kg	1 LC Millivolts per volt	10 SG#9 BRB Strain ue	11 SG#10 BRD Strain ue	12 SG#11 BCB Strain ue	13 SG#12 BLD Strain ue	14 SG#13 BLB Strain ue	15 SG#14 BLT Strain ue	16 LVDT FC Calibrated Values mm
1	37.4	0	0	0	-1	1	-1	-1	2	0
2	38.3	-48	-0.0003	1	-1	1	0	-1	1	0
3	434.9	8157	0.0423	3	-8	61	-12	1	5	1
4	738.8	11102	0.0575	5	-11	81	-13	4	6	1
5	887.3	15011	0.0777	7	-12	108	-17	5	6	1
6	1052.8	20031	0.1038	9	-17	141	-22	9	7	2
7	1244.5	25003	0.1295	12	-21	175	-27	11	7	2
8	1343.1	30071	0.1558	14	-25	214	-31	13	8	3
9	1417.5	34994	0.1812	15	-29	259	-36	16	9	3
10	1466.8	34994	0.1812	15	-28	259	-35	15	9	3
11	1613.6	39966	0.207	18	-33	299	-41	16	10	3
12	1671.6	41366	0.2142	18	-33	309	-42	17	8	3
13	1684.4	45275	0.2345	20	-36	347	-45	18	9	4
14	1783.8	50054	0.2592	23	-41	412	-49	21	11	4
15	1885	54977	0.2848	23	-45	406	-54	21	9	4
16	2049.4	60142	0.3115	25	-49	326	-59	22	10	5
17	2365.1	65162	0.3375	29	-53	305	-64	24	11	5
18	2511.3	70134	0.3633	30	-57	290	-68	27	11	6
19	2671.6	71533	0.3705	32	-57	288	-68	27	12	6
20	2681.5	76119	0.3942	32	-61	281	-71	29	11	7
21	2976.5	80463	0.4168	34	-64	272	-75	31	11	7
22	3962.7	80077	0.4148	32	-62	247	-73	30	19	7
23	4171.5	85097	0.4408	34	-66	241	-77	34	13	8
24	4281.8	90068	0.4665	35	-70	227	-80	35	13	9
25	4587	95136	0.4928	36	-71	208	-84	36	10	9
26	4696.7	100205	0.519	36	-73	184	-86	36	10	10
27	4941.6	99867	0.5172	37	-73	175	-86	36	9	10

28	4978.6	100494	0.5205	37	-73	173	-86	38	8	10
29	5080.9	105852	0.5483	38	-75	156	-89	38	9	11
30	5309.9	110003	0.5697	39	-75	140	-86	38	8	12
31	5501.8	115168	0.5965	40	-74	123	-87	40	8	13
32	5672.6	120139	0.6222	40	-65	109	-87	40	7	14
33	5961.8	125208	0.6485	41	-61	91	-88	40	4	15
34	6076.1	130276	0.6747	41	-59	82	-88	40	7	16
35	6262.3	135296	0.7007	41	-57	86	-85	40	4	17
36	6288.3	140122	0.7258	42	-57	90	-85	39	2	18
37	6451.7	150403	0.779	40	-57		-90	37	-2	21
38	6653.2	159961	0.8285	33	-88		-124	30	-16	26
39	6814.2	164160	0.8503	31	-126		-154	26	-19	29
40	6821.1	165270	0.856	30	-128		-162	25	-19	29
41	6839.8	170145	0.8812	27	-141		-191	22	-21	31
42	6875.7	171738	0.8895	24	-162		-202	22	-23	34
43	6885.9	7433	0.0385	20			69	-21	41	52

Deflection Readings

Reading No.	Time Seconds	1 LC Calibrated Values kg	1 LC Millivolts per volt	16 LVDT FC Millivolts	17 LVDT BC Calibrated Values mm	17 LVDT BC Millivolts	18 LVDT FLS Calibrated Values mm	18 LVDT FLS Millivolts	19 LVDT BLS Calibrated Values mm	19 LVDT BLS Millivolts
1	37.4	0	0	0	0	0	0	0.3	0	0
2	38.3	-48	-0.0003	0	0	0	0	0.3	0	0
3	434.9	8157	0.0423	56.5	0	22.3	0	-0.9	0	49.4
4	738.8	11102	0.0575	76.6	1	38.5	0	0.9	0	63.2
5	887.3	15011	0.0777	96.8	1	60.1	0	23.8	0	80.3
6	1052.8	20031	0.1038	120.6	1	85.5	0	48.5	1	101.3
7	1244.5	25003	0.1295	143.1	2	112	0	77.2	1	119
8	1343.1	30071	0.1558	164.8	2	136.1	1	97.4	1	130
9	1417.5	34994	0.1812	187.4	3	162.7	1	123.3	1	142.8
10	1466.8	34994	0.1812	188	3	163.3	1	124.2	1	146.2
11	1613.6	39966	0.207	209.7	3	185	1	147.4	1	159
12	1671.6	41366	0.2142	215.2	3	190.8	1	151.7	1	161.5
13	1684.4	45275	0.2345	231.4	3	208.2	1	164.5	1	168.8
14	1783.8	50054	0.2592	258.2	4	228.6	1	190.8	1	190.5
15	1885	54977	0.2848	285.4	4	254.2	1	213	1	209.1
16	2049.4	60142	0.3115	316.8	4	283.2	1	235.9	1	233.2
17	2365.1	65162	0.3375	352.2	5	315.9	2	262.8	2	261.9
18	2511.3	70134	0.3633	384.6	5	346.7	2	280.8	2	276.8
19	2671.6	71533	0.3705	395.9	6	358	2	294.2	2	289.3
20	2681.5	76119	0.3942	423	6	385.8	2	304.3	2	294.2
21	2976.5	80463	0.4168	466.7	7	430.4	2	345.2	2	324.4
22	3962.7	80077	0.4148	460	7	431	2	330.2	2	303.1
23	4171.5	85097	0.4408	514.9	7	478.6	2	378.2	2	356.5
24	4281.8	90068	0.4665	550.3	8	514	2	392.8	2	366.9
25	4587	95136	0.4928	604	9	569.2	3	433.4	2	392.5

26	4696.7	100205	0.519	646.1	9	613.2	3	446.8	2	399.2
27	4941.6	99867	0.5172	664.1	10	633	3	470	3	411.1
28	4978.6	100494	0.5205	669	10	638.2	3	473.7	3	413.6
29	5080.9	105852	0.5483	709	11	680.9	3	485.6	3	418.8
30	5309.9	110003	0.5697	759.1	11	735.6	3	511.5	3	429.4
31	5501.8	115168	0.5965	815.5	12	796.6	3	533.5	3	438.6
32	5672.6	120139	0.6222	874.1	13	860.4	3	557.9	3	447.7
33	5961.8	125208	0.6485	974.2	15	942.2	4	593.6	3	460.9
34	6076.1	130276	0.6747	1033.8	16	1006.3	4	608.3	3	466.4
35	6262.3	135296	0.7007	1117.4	17	1094.5	4	639.4	3	477.4
36	6288.3	140122	0.7258	1183.6	18	1163.2	4	647.4	3	479.8
37	6451.7	150403	0.779	1361.6	21	1341.1	4	680.9	3	488.6
38	6653.2	159961	0.8285	1700.3	26	1680.2	5	738.9	3	499.6
39	6814.2	164160	0.8503	1861.8	29	1860.3	5	762.1	3	507.9
40	6821.1	165270	0.856	1886.8	29	1889	5	764.9	3	508.2
41	6839.8	170145	0.8812	2026	32	2039.1	5	774.3	3	509.1
42	6875.7	171738	0.8895	2199.7	35	2242.7	5	791.4	3	510.6
43	6885.9	7433	0.0385	3329.9	82	5307	2	372.7	3	452.6

Data for Test Number 3, Slab Number 6

Date Tested August 29, 2002

TEST # 3 (INVERTED SLAB), LOAD APPLIED AT CENTER

Start Time: 29/08/2002 2:05:07 PM

Deck slab No. 6, Cast Feb. 26, 2002

Strain Gauge Readings

Reading No.	Time Seconds	1 LC Calibrated Values [1 LC] kg	2 SG#1 FLT Strain ue	3SG#2FLD Strain ue	4 SG#3 FLP Strain ue	5 SG#4 FL45 Strain ue	6 SG#5 FCB Strain ue	7 SG#6 FRB Strain ue	8 SG#7 FRT Strain ue	9 SG#8 BRB Strain ue	10 SG#9 BRD Strain ue
3391	339.1	0	1	-1	-4	-34	-2	-1	-1	-2	-4
3789	378.9	2027	-2	1	-4	-27	-1	-2	-1	-4	-2
4541	454.1	4006	-5	4	-5	-10	-1	0	-1	-6	0
4817	481.7	6034	-8	6	-5	34	1	-1	-2	-7	1
5008	500.8	8061	-10	8	-6	478	2	-1	-2	-8	2
5252	525.2	10040	-12	9	-6	1770	2	-1	-1	-10	3
8980	898	12019	-14	10	-7	3082	3	2	1	-13	5
9158	915.8	14046	-16	14	-8	6518	6	2	1	-14	6
14879	1487.9	16073	-17	17	-9	4036	5	2	-1	-16	6
15034	1503.4	18101	-19	18	-9	5648	7	3	-1	-17	8
15288	1528.8	20031	-20	21	-9	13126	9	3	1	-19	11
18794	1879.4	25003	-26	25	-8		15	2	3	-22	16
20031	2003.1	30071	-30	31	-6		22	2	5	-26	20
20548	2054.8	35043	-32	35	3		29	2	4	-31	25
22418	2241.8	40063	-38	39	31		37	4	5	-35	29
22758	2275.8	45034	-43	44	53		43	5	3	-40	33
25652	2565.2	50006	-44	46	72		48	7	1	-42	37
29171	2917.1	55074	-45	50	92		44	8	-1	-44	40
29534	2953.4	60046	-45	50	113		52	10	-4	-46	40
33451	3345.1	65017	33	51	163		72	10	-5	-50	39
34017	3401.7	70037	30	50	174		87	12	-7	-51	39
37908	3790.8	75009	24	50	111		95	11	-10	-53	39
38649	3864.9	80029	23	51	67		110	13	-12	-54	39
40653	4065.3	82538	7	50	53		116	15	-12	-55	39
42413	4241.3	85000	5	49	33		119	16	-14	-55	38
42680	4268	87510	5	49	24		125	15	-14	-57	38
43748	4374.8	88041	4	45	5		134	17	-19	-51	31

Strain Gauge and Deflection Measurements

Reading No.	Time Seconds	1 LC Calibrated Values [1 LC] kg	11 SG#10 BRP Strain ue	13 SG#12 BCB Strain ue	14 SG#13 BLT Strain ue	15 SG#14 BLB Strain ue	16 LVDT FC Calibrated Values mm	17 LVDT BC Calibrated Values mm	18 LVDT FLS Calibrated Values mm	19 LVDT BRS Calibrated Values mm
3391	339.1	0	71	0	-2	-2	0	0	0	0
3789	378.9	2027	74	3	-3	1	0	0	0	0
4541	454.1	4006	79	6	-7	1	1	0	0	0
4817	481.7	6034	79	8	-7	2	1	0	-1	0
5008	500.8	8061	83	11	-7	4	1	0	-1	0
5252	525.2	10040	87	12	-8	4	2	0	-1	1
8980	898	12019	2509	16	-10	4	2	0	0	1
9158	915.8	14046	2516	19	-11	6	2	1	0	1
14879	1487.9	16073	2577	20	-14	6	3	1	0	1
15034	1503.4	18101	2579	24	-15	8	3	1	0	1
15288	1528.8	20031	2581	27	-15	8	3	1	0	1
18794	1879.4	25003	2530	32	-15	12	4	2	1	2
20031	2003.1	30071	2530	39	-16	15	4	3	1	2
20548	2054.8	35043	2539	48	-17	15	5	3	1	2
22418	2241.8	40063	2552	54	-17	15	5	4	2	2
22758	2275.8	45034	2592	63	-19	15	6	5	2	2
25652	2565.2	50006	2605	73	-17	15	7	6	2	2
29171	2917.1	55074	-7045	95	-15	15	9	7	2	3
29534	2953.4	60046	-6777	118	-14	12	10	8	2	3
33451	3345.1	65017	5413	186	-12	12	12	10	-1	3
34017	3401.7	70037	7333	313	-12	8	14	12	-1	3
37908	3790.8	75009		619	-11	7	16	14	0	3
38649	3864.9	80029		853	-10	4	19	17	0	3
40653	4065.3	82538		993	-9	3	20	19	0	3
42413	4241.3	85000			-10	0	23	22	0	3
42680	4268	87510			-9	-1	25	23	0	3
43748	4374.8	88041			-9	-5	31	29	0	3

Data for Test Number 4, Slab Number 5

Date Tested September 26, 2002

Test No. 4, Load applied 3 ft from support Slab No. 5, Cast Feb. 26, 2002
Start Time: 26/09/2002 9:52:19 AM

Reading No.	Time Seconds	1 LC Calibrated Values kg	2 SG#1 FLT Strain ue	3SG#2FCB Strain ue	4 SG#3 FRD Strain ue	5 SG#4 FRP Strain ue	6 SG#5 FR45 Strain ue	7 SG#6 FRB Strain ue	8 SG#7 FRT Strain ue	9 SG#8 BRB Strain ue	10 SG#9 BCB Strain ue
1	3058.8	2800	-1	10	-6	-11	-6	1	-9	-5	14
2	3065.9	4682	0	17	-5	-13	-8	3	-10	-4	24
3	3079.5	6323	2	22	-5	-14	-7	4	-11	-2	31
4	3097.1	10426	5	35	-5	-18	-9	6	-14	-1	52
5	3108.5	10040	4	34	-4	-17	-9	6	-12	-1	49
6	3120.6	15204	7	51	-4	-23	-10	8	-16	2	74
7	3131.7	19983	11	68	-3	-28	-10	9	-16	3	96
8	3140.5	26596	13	89	-2	-34	-12	13	-18	4	125
9	3162.5	31085	15	106	2	-41	-14	14	-20	7	144
10	3356.8	35332	18	85	-4	-52	-22	14	-21	8	161
11	3573.4	38856	18	72	-10	-63	-21	14	-21	8	168
12	3585.4	42186	20	86	-9	-68	-23	15	-22	9	183
13	3717.2	45131	21	93	-10	-76	-24	15	-23	11	196
14	3825.3	47930	23	100	-12	-81	-26	16	-23	11	209
15	3901.4	50295	22	108	-11	-87	-27	18	-24	12	221
16	4011.3	52709	22	116	-12	-92	-30	18	-24	13	235
17	4109.9	52130	23	112	-13	-92	-30	18	-24	12	234
18	4124.1	55508	24	127	-13	-98	-31	19	-25	13	252
19	4217.5	55991	24	128	-13	-101	-32	18	-25	13	255
20	4226.2	57873	25	136	-13	-104	-32	19	-26	13	265
21	4331.8	60046	26	147	-13	-109	-36	20	-26	15	278
22	4426.3	62652	26	161	-14	-115	-37	21	-26	15	292
23	4562.3	65162	27	180	-15	-123	-40	22	-27	16	313
24	4637	67865	28	198	-14	-126	-40	21	-28	16	337
25	4662.3	70327	28	219	-14	-131	-43	23	-29	17	365
26	4842.7	72692	29	243	-14	-139	-45	23	-29	17	390
27	4979.5	75781	29	259	-15	-146	-48	12	-37	19	353
28	5078.6	76602	29	246	-18	-151	-49	18	-34	18	340

29	5092.5	80222	31	214	-17	-157	-51	19	-35	18	327
30	5213	82442	31	203	-17	-163	-53	22	-34	19	320
31	5411.8	85242	31	199	-21	-172	-55	24	-34	19	319
32	5496	84469	30	193	-22	-172	-55	23	-33	19	314
33	5528.6	87462	31	194	-23	-178	-58	25	-34	20	316
34	5610.5	90117	31	170	-20	-180	-59	26	-35	21	315
35	5716.9	92530	31	159	-21	-185	-61	26	-35	20	309
36	5784	94847	33	145	-21	-189	-62	27	-35	20	301
37	5868.1	97453	32	140	-20	-193	-63	28	-37	21	300
38	6089.1	100108	32	127	-20	-199	-72	29	-37	21	300
39	6506.7	110003	32	121	-25	-217	-84	30	-42	20	160
40	6523.4	109762	31	121	-25	-217	-86	31	-42	20	159
41	6732.4	120043	31	90	-19	-239	-97	32	-48	20	129
42	7124.9	130276	31	47	4	-249	-102	34	-54	19	101
43	7402.6	150403	30	-37	-4	-281	-126	37	-67	16	46
44	7820.8	170242	32	-172	-56	-266	-115	33	-84	7	5
45	8072.9	180233	30	-196	-83	-323	-249	37	-98	0	-10
46	8229.1	190080	27	-224	-156	-363	-285	36	-108	-9	-43
47	8549.6	196403	27	-226	-213	-410	-284	23	-110	-15	-60

Strain Gauge and Deflection Measurements

Reading No.	Time Seconds	1 LC Calibrated Values kg	11 SG#10 BLD Strain ue	12 SG#11 BL45 Strain ue	13 SG#12 BLP Strain ue	14 SG#13 BLT Strain ue	15 SG#14 BLB Strain ue	16 LVDT FC Calibrated Values mm	17 LVDT BC Calibrated Values mm	18 LVDT FLS Calibrated Values mm	19 LVDT BLS Calibrated Values mm
1	3058.8	2800	-13	-12	-7	-7	-6	0	0	0	1
2	3065.9	4682	-12	-15	-7	-6	-6	0	0	0	1
3	3079.5	6323	-11	-18	-8	-5	-6	1	0	0	1
4	3097.1	10426	-9	-24	-10	-5	-7	1	0	0	1
5	3108.5	10040	-10	-23	-10	-6	-6	1	0	0	1
6	3120.6	15204	-7	-30	-12	-4	-7	1	1	0	-1
7	3131.7	19983	-6	-39	-13	-5	-7	1	1	0	-3
8	3140.5	26596	-2	-46	-16	-4	-7	2	1	1	-3
9	3162.5	31085	-1	-53	-17	-4	-7	2	1	1	-3
10	3356.8	35332	1	-60	-20	-3	-8	2	1	1	-3
11	3573.4	38856	2	-66	-22	-3	-9	2	2	1	-3
12	3585.4	42186	3	-70	-24	-3	-8	3	2	1	-3
13	3717.2	45131	4	-75	-24	-2	-8	3	2	1	-3
14	3825.3	47930	5	-80	-26	-3	-7	3	2	1	-3
15	3901.4	50295	6	-84	-27	-3	-7	3	2	1	-2
16	4011.3	52709	7	-87	-28	-4	-7	3	2	1	-2
17	4109.9	52130	7	-88	-28	-4	-8	3	2	1	-2
18	4124.1	55508	7	-92	-29	-3	-8	3	2	1	-2
19	4217.5	55991	8	-94	-29	-4	-8	3	2	1	-2
20	4226.2	57873	9	-96	-30	-4	-8	3	3	1	-2
21	4331.8	60046	8	-99	-31	-4	-7	4	3	1	-2
22	4426.3	62652	10	-103	-31	-4	-8	4	3	1	-2
23	4562.3	65162	11	-107	-33	-4	-7	4	3	2	-2
24	4637	67865	12	-110	-35	-5	-8	4	3	2	-2
25	4662.3	70327	14	-113	-35	-4	-7	4	3	2	-2
26	4842.7	72692	19	-118	-37	-4	-8	4	3	2	-2
27	4979.5	75781	10	-122	-38	-5	-7	5	4	2	-2

28	5078.6	76602	10	-124	-39	-6	-8	5	4	2	-2
29	5092.5	80222	10	-128	-40	-5	-7	5	4	2	-2
30	5213	82442	10	-131	-40	-6	-8	5	4	2	-2
31	5411.8	85242	57	-136	-43	-7	-7	5	4	2	-2
32	5496	84469	55	-134	-43	-6	-9	5	4	2	-2
33	5528.6	87462	55	-138	-44	-7	-9	5	4	2	-2
34	5610.5	90117	55	-141	-45	-7	-7	6	5	2	-2
35	5716.9	92530	68	-145	-45	-7	-7	6	5	2	-2
36	5784	94847	70	-147	-46	-8	-7	6	5	2	-2
37	5868.1	97453	73	-152	-48	-8	-7	6	5	2	-2
38	6089.1	100108	28	-157	-52	-10	-9	7	6	2	-2
39	6506.7	110003	77	-171	-55	-10	-8	8	7	2	-2
40	6523.4	109762	78	-171	-56	-10	-8	8	7	2	-2
41	6732.4	120043	102	-185	-67	-11	-8	9	8	3	-2
42	7124.9	130276	106	-202	-75	-12	-9	10	9	3	-1
43	7402.6	150403	126	-229	-100	-15	-10	13	12	3	-1
44	7820.8	170242	176	-263	-150	-16	-13	18	16	3	-1
45	8072.9	180233	387	-270	-160	-18	-15	21	18	4	-1
46	8229.1	190080	505	-263	-167	-21	-16	24	21	4	-1
47	8549.6	196403	199	-265	-277	-33	-23	30	27	4	0

Data for Test Number 5a, Slab Number 4

Date Tested October 28, 2002

Test No. 5a, Load applied 2 feet from Support Slab No. 4, Date cast Feb 28, 2002
Start Time: 28/10/2002 2:09:29 PM

Strain Gauge Readings

Reading No.	Time Seconds	1 LC Calibrated Values kg	2 SG#1 FLT Strain ue	3SG#2FCB Strain ue	4 SG#3 FRD Strain ue	5 SG#4 FRP Strain ue	6 SG#5 FR45 Strain ue	7 SG#6 FRB Strain ue	8 SG#7 FRT Strain ue	9 SG#8 BRB Strain ue	10 SG#9 BCB Strain ue	11 SG#10 BLD Strain ue
1	998.3	97	-3	-61	-5	-4	-5	-1	-4	-3	-39	-653
2	999.5	97	-4	-61	-5	-4	-5	-2	-4	-5	-39	-653
3	1046.2	5358	-11	-58	-6	0	-4	2	-6	-2	-2	-663
4	1078.3	10281	-17	-72	-7	2	-4	3	-6	0	23	-671
5	1184.9	15253	-22	-4	-8	5	-3	4	-8	2	45	-675
6	1253	20128	-27	23	-9	7	-5	6	-10	2	69	-681
7	1323.5	25292	-29	49	-10	8	-6	7	-12	4	91	-690
8	1399.5	30264	-33	74	-10	10	-6	8	-13	4	-66	-699
9	1467.3	35187	-35	86	-13	11	-8	10	-14	5	-5	-704
10	1543.6	40642	-37	113	-14	13	-9	11	-16	6	27	-710
11	1612.6	45613	-38	145	-15	15	-10	12	-18	5	58	-715
12	1722.4	50730	-38	176	-16	16	-12	13	-17	5	46	-731
13	1810.4	55219	-37	207	-18	17	-13	14	-19	5	70	-732
14	1930.4	60094	-36	238	-19	18	-16	16	-22	5	100	-740
15	2051.4	64631	-33	268	-19	17	-20	19	-26	2	141	-741
16	2113.9	70134	-34	311	-20	18	-20	20	-29	2	187	-743
17	2203.2	74960	-33	344	-22	19	-23	22	-31	1	239	-748
18	2308.9	79884	-34	348	-25	18	-26	21	-31	2	273	-752
19	2449.1	85000	-34	326	-25	20	-27	22	-32	2	267	-756
20	2554.1	89924	-35	245	-25	20	-28	23	-33	1	269	-761
21	2818.7	99963	-38	139	-28	22	-32	25	-33	2	155	-769
22	2958.7	110196	-42	11	-31	24	-36	27	-34	3	42	-778
23	3318.5	120767	-47	36	-33	25	-39	28	-34	3	5	-788
24	3412	130083	-51	18	-37	25	-44	30	-35	3	-9	-793
25	3815.6	140122	-57	-10	-39	22	-48	30	-37	3	-28	-807
26	4291.5	150066	-66	30	-40	17	-52	30	-38	4	-4	-824

27	4609.8	160009	-75	112	-40	7	-57	-40	3	15	-852
28	4903.7	170000	-85	237	-38	-6	-59	-42	2	131	-853
29	5370	179895	-97	378	-30	-17	-57	-44	-6	152	-836
30	6134.2	190080	-108	562	-22	-28	-51	-49	-13	122	-839
31	6465	195051	-115	612	-16	-33	-48	-47	-8	122	-860

Strain Gauge and Deflection Measurements

Reading No.	Time Seconds	1 LC Calibrated Values kg	12 SG#11 BL45 Strain ue	13 SG#12 BLP Strain ue	14 SG#13 BLT Strain ue	15 SG#14 BLB Strain ue	16 LVDT FC Calibrated Values mm	17 LVDT BC Calibrated Values mm	18 LVDT FLS Calibrated Values mm	19 LVDT BLS Calibrated Values mm
1	998.3	97	-17	-16	-4	-3	0	0	0	0
2	999.5	97	-16	-15	-5	-3	0	0	0	0
3	1046.2	5358	-13	-5	-2	-6	0	0	0	0
4	1078.3	10281	-13	1	-1	-6	1	1	0	0
5	1184.9	15253	-13	6	-2	-5	1	1	0	0
6	1253	20128	-13	10	-2	-5	1	1	0	0
7	1323.5	25292	-19	10	-3	-3	2	1	1	1
8	1399.5	30264	-23	11	-4	-1	2	2	1	1
9	1467.3	35187	-26	14	-7	2	2	2	1	1
10	1543.6	40642	-30	15	-9	4	3	2	1	1
11	1612.6	45613	-30	19	-11	5	3	2	1	1
12	1722.4	50730	-44	12	-14	6	3	3	2	1
13	1810.4	55219	-42	20	-15	9	3	3	2	1
14	1930.4	60094	-49	17	-19	11	4	3	2	2
15	2051.4	64631	-52	20	-23	15	4	4	2	2
16	2113.9	70134	-51	26	-25	17	4	4	2	2
17	2203.2	74960	-54	29	-26	18	5	4	2	2
18	2308.9	79884	-56	31	-27	20	5	4	3	2
19	2449.1	85000	-57	34	-29	21	5	5	3	2
20	2554.1	89924	-62	36	-30	21	6	5	3	3
21	2818.7	99963	-65	39	-35	18	6	6	3	3
22	2958.7	110196	-71	42	-41	16	7	6	3	3
23	3318.5	120767	-78	45	-42	17	8	7	4	4
24	3412	130083	-80	49	-45	16	9	8	4	4
25	3815.6	140122	-97	30	-50	14	10	9	4	4
26	4291.5	150066	-124	-11	-56	11	11	10	4	5
27	4609.8	160009	-169	-41	-62	7	12	12	5	5

28	4903.7	170000	-222	-105	-75	5	13	13	5	6
29	5370	179895	-224	-136	-84	2	15	14	5	6
30	6134.2	190080	-221	-140	-96	-6	16	16	5	6
31	6465	195051	-239	-153	-100	-11	17	17	5	7

Data for Test Number 5b, Slab Number 4

Date Tested October 30, 2002

Test No. 5(b), Load applied 2 feet from other support,
Start Time: 30/10/2002 9:56:12
AM

Slab No. 4, Cast Feb 28, 2002

Strain Gauge Readings

Reading No.	Time Seconds	1 LC Calibrated Values kg	2 SG#1 FLT Strain ue	3SG#2FLD Strain ue	4 SG#3 FLP Strain ue	5 SG#4 FL45 Strain ue	6 SG#5 FCB Strain ue	7 SG#6 FRB Strain ue	8 SG#7 FRT Strain ue	9 SG#8 BRB Strain ue	10 SG#9 BRD Strain ue	11 SG#10 BRP Strain ue
1	819.7	386	-4	-3	-2	-2	-9	-1	-3	-3	-8	-4
2	849.6	4923	-5	-5	-2	-7	7	4	-10	-3	-18	2
3	904.9	9991	-7	-7	0	-13	26	9	-17	-2	-27	7
4	1061.4	15542	-5	-12	1	-22	58	16	-27	-1	-41	9
5	1170.7	20031	-6	-17	-1	-30	81	20	-34	2	-51	12
6	1313.6	25099	-7	-20	1	-38	111	23	-41	3	-55	19
7	1549.9	30216	-8	-26	-3	-48	135	29	-47	7	-62	23
8	1703.4	34994	-9	-41	-14	-63	161	32	-51	9	-73	24
9	1792.8	39869	-11	-43	-12	-68	183	36	-56	11	-78	25
10	1929.6	45227	-15	-52	-21	-79	205	34	-62	15	-88	27
11	2094.3	50344	-16	-49	-14	-78	239	42	-62	19	-89	35
12	2278.3	55267	-18	-46	-13	-78	266	44	-64	21	-92	40
13	2406.9	60383	-20	-47	-12	-82	296	46	-69	24	-95	46
14	2508.7	65789	-21	-53	-17	-91	328	50	-74	25	-103	48
15	2652.6	70665	-22	-52	-16	-93	360	54	-76	27	-115	45
16	2806.4	75395	-25	-66	-31	-109	398	57	-82	29	-117	50
17	2926.5	80415	-25	-62	-29	-110	402	60	-88	29	-124	51
18	3124.8	85435	-27	-58	-25	-112	367	62	-94	33	-126	54
19	3447.1	90213	-27	-53	-23	-114	338	67	-99	34	-125	60
20	3833.4	95330	-28	-56	-28	-117	302	68	-106	36	-140	51
21	4182.3	100205	-29	-51	-26	-119	286	71	-112	37	-139	57
22	4525.5	110244	-33	-46	-30	-125	223	78	-125	42	-155	46

23	5010	120139	-34	-43	-44	-134	213	86	-138	44	-155	36
24	5287.7	129938	-36	-27	-41	-136	190	91	-152	44	206	16
25	5654.9	140364	-42	-12	-50	-136	169	98	-163	46	179	-3
26	6069.6	150162	-44	-6	-68	-147	125	101	-178	47	159	-20
27	6377.5	160105	-45	11	-79	-151	84	106	-190	42	154	-40
28	6633.7	170483	-46	25	-91	-155	37	110	-204	37	364	-50
29	6928.2	180185	-49	39	-104	-158	-18	110	-214	36	307	-74
30	7131.7	190273	-53	51	-119	-160	-41	88	-238	37	306	-134
31	7473.5	200458	-56	63	-133	-164	-82	9	-279	32	284	-221
32	7712.8	210063	-57	74	-147	-166	-124	-40	-300	15	238	-288
33	7919	214986	-60	79	-153	-169	-158	-84	-316	-22	183	-402
34	8118.1	214552	-61	70	-149	-173	-187	-137	-328	-85	104	-452
35	8161.2	216965	-61	69	-149	-178	-200	-168	-333	-97	88	-461
36	8163	216724	-61	68	-150	-178	-200	-172	-332	-97	87	-461
37	8179	216338	-62	67	-149	-178	-204	-200	-335	-104	81	-462
38	8199.3	216724	-63	64	-147	-180	-210	-220	-338	-112	73	-466
39	8217.9	215855	-62	61	-144	-180	-218	-236	-339	-120	62	-465

Strain Gauge and Deflection Measurements

Reading No.	Time Seconds	1 LC Calibrated Values kg	12 SG#11 BR45 Strain ue	13 SG#12 BCB Strain ue	14 SG#13 BLT Strain Ue	15 SG#14 BLB Strain ue	16 LVDT FC Calibrated Values mm	17 LVDT BC Calibrated Values mm	18 LVDT FLS Calibrated Values mm	19 LVDT BRS Calibrated Values mm
1	819.7	386	-4	1	-3	-2	0	0	0	0
2	849.6	4923	-18	26	-6	-1	0	0	0	0
3	904.9	9991	-31	52	-9	3	1	1	0	1
4	1061.4	15542	-48	82	-14	4	1	1	0	1
5	1170.7	20031	-59	108	-16	8	2	2	0	1
6	1313.6	25099	-67	129	-20	9	3	2	0	1
7	1549.9	30216	-77	161	-24	9	3	2	0	1
8	1703.4	34994	-90	190	-25	10	4	2	0	1
9	1792.8	39869	-99	221	-26	11	4	3	0	1
10	1929.6	45227	-111	252	-26	13	4	3	0	2
11	2094.3	50344	-114	283	-29	10	5	3	0	2
12	2278.3	55267	-122	316	-30	10	5	4	0	2
13	2406.9	60383	-126	355	-31	9	6	4	0	3
14	2508.7	65789	-138	397	-29	11	6	4	0	3
15	2652.6	70665	-153	420	-31	11	6	5	0	3
16	2806.4	75395	-157	396	-32	12	7	5	1	4
17	2926.5	80415	-165	383	-33	13	7	5	0	4
18	3124.8	85435	-170	367	-32	14	8	6	1	4
19	3447.1	90213	-170	260	-33	15	8	6	1	4
20	3833.4	95330	-186	231	-32	16	8	7	1	4
21	4182.3	100205	-189	189	-35	13	9	7	1	4
22	4525.5	110244	-211	170	-36	16	9	8	0	4
23	5010	120139	-225	144	-39	16	10	9	0	5
24	5287.7	129938	-243	118	-39	17	11	10	0	5
25	5654.9	140364	-266	94	-37	15	12	11	0	5
26	6069.6	150162	-276	68	-38	15	13	12	0	6
27	6377.5	160105	-271	47	-40	16	14	13	1	6

28	6633.7	170483	-261	24	-40	16	15	15	1	6
29	6928.2	180185	-246	13	-40	15	17	16	2	6
30	7131.7	190273	-251	1	-40	14	18	18	2	7
31	7473.5	200458	-287	-14	-40	10	20	19	3	7
32	7712.8	210063	-322	-30	-41	11	21	21	3	7
33	7919	214986	-344	-43	-41	9	22	23	3	7
34	8118.1	214552	-370	-59	-41	7	24	24	3	7
35	8161.2	216965	-377	-66	-42	7	24	24	3	7
36	8163	216724	-378	-66	-41	7	24	24	3	7
37	8179	216338	-380	-68	-41	6	24	25	3	7
38	8199.3	216724	-384	-70	-41	6	25	25	3	7
39	8217.9	215855	-385	-70	-43	6	25	25	3	7

Data for Test Number 6, Slab Number 3

Date Tested November 1, 2002

Test 6, Load applied 3 feet from support
Start Time: 01/11/2002 10:33:33 AM

Strain Gauge Readings

Reading No.	Time Seconds	1 LC Calibrated Values kg	2SG#1FLB Strain ue	3SG#2FLD Strain ue	4 SG#3 FLP Strain ue	5 SG#4 FL45 Strain ue	6 SG#5 FCB Strain ue	7 SG#6 FRT Strain ue	8 SG#7 FRB Strain ue	9 SG#8 BRB Strain ue	10 SG#9 BRD Strain ue
1	89.7	48	0	-2	-2	1	-2	12	2	-1	1
2	241.7	5020	4	-2	-2	-1	7	17	4	2	1
3	277	10329	9	-4	-2	-1	25	19	5	5	0
4	327.1	15156	13	-5	-1	-4	43	20	6	6	-1
5	374.6	20273	18	-7	-2	-9	64	22	6	10	-3
6	442.5	25389	21	-11	-1	-15	84	22	8	10	-4
7	506.5	30457	25	-13	1	-20	103	24	10	12	-6
8	604.6	35525	27	-20	0	-29	84	25	11	15	-8
9	664.6	41028	31	-19	3	-34	144	26	13	17	-10
10	815.6	45420	32	-22	5	-39	58	27	14	17	-12
11	926.8	50247	35	-25	6	-46	162	27	15	19	-13
12	1066.8	55219	38	-30	6	-54	185	28	16	21	-15
13	1439.8	60142	40	-30	10	-61	214	31	18	22	-17
14	1518	65065	41	-34	11	-67	218	30	19	22	-20
15	1664.6	70037	43	-38	11	-76	166	29	20	23	-22
16	1670.2	70085	43	-42	9	-80	169	30	21	24	-22
17	1832.5	75298	46	-41	14	-83	137	29	23	24	-25
18	2253.7	80173	46	-52	10	-100	96	29	24	24	-27
19	2520.9	90117	51	-64	5	-123	42	28	26	26	-29
20	2832.3	100012	53	-57	9	-133	28	27	29	27	-32
21	3177.5	110341	56	-70	-8	-165	-11	25	31	27	-32
22	3560.4	120091	59	-66	-3	-175	-25	24	33	27	-27
23	3878	130131	61	-96	-23	-214	-81	23	33	28	-17
24	4154.4	140219	64	-69	-31	-220	-96	21	35	29	-6

25	4566.3	150114	64	-49	-63	-239	-95	19	35	30	10
26	4981.2	160057	64	-38	-70	-213	-80	16	36	30	24
27	5310.1	170097	57	-142	-220	-312	-85	13	35	29	35
28	5639	179509	55	-210	-301	-379	8	4	37	25	34
29	5653.5	179895	55	-210	-300	-378	5	2	36	25	33
30	5655	179895	54	-211	-300	-376	4	1	36	26	33
31	5993.8	188197	53	-241	-326	-408	595	-4	32	25	-5
32	6035.7	190128	53	-248	-332	-416		-7	32	24	-15
33	6263.1	191287	47	-269	-335	-432		-9	30	24	-36

Strain Gauge Readings

Reading No.	Time Seconds	1 LC Calibrated Values kg	11 SG#10 BRP Strain ue	12 SG#11 BR45 Strain ue	13 SG#12 BCB Strain Ue	14 SG#13 BLT Strain ue	15 SG#14 BLB Strain ue
1	89.7	48	9	-2	2	-2	-4
2	241.7	5020	13	-5	25	2	-7
3	277	10329	13	-6	47	3	-7
4	327.1	15156	14	-9	66	3	-7
5	374.6	20273	15	-12	90	2	-7
6	442.5	25389	16	-15	112	0	-7
7	506.5	30457	17	-18	132	-1	-5
8	604.6	35525	17	-22	151	-3	-6
9	664.6	41028	18	-26	149	-5	-4
10	815.6	45420	19	-30	185	-5	-5
11	926.8	50247	19	-35	192	-7	-5
12	1066.8	55219	17	-39	226	-7	-4
13	1439.8	60142	12	-45	245	-8	-5
14	1518	65065	7	-50	319	-8	-4
15	1664.6	70037	1	-54	687	-10	-5
16	1670.2	70085	1	-55	707	-9	-6
17	1832.5	75298	-6	-61	829	-10	-4
18	2253.7	80173	-12	-66	901	-12	-6
19	2520.9	90117	-14	-77	1227	-14	-7
20	2832.3	100012	-19	-91		-18	-7
21	3177.5	110341	-25	-104		-22	-7
22	3560.4	120091	-38	-117		-24	-8
23	3878	130131	-63	-132		-28	-9
24	4154.4	140219	-81	-141		-33	-11
25	4566.3	150114	-101	-141		-35	-15
26	4981.2	160057	-120	-141		-50	-21
27	5310.1	170097	-132	-139		-56	-24
28	5639	179509	-134	-142		-61	-29
29	5653.5	179895	-132	-141		-62	-29
30	5655	179895	-133	-142		-61	-28
31	5993.8	188197	-259	-165		-64	-40
32	6035.7	190128	-286	-178		-67	-44
33	6263.1	191287	-349	-202		-68	-52

Deflection Measurements

Time	11 SG#10 BRP	1 LC Calibrated Values	16 LVDT FC Calibrated Values	17 LVDT BC	18 LVDT FLS Calibrated Values	19 LVDT BLS Calibrated Values
Seconds	Strain			Calibrated Values		
	ue	kg	mm	Mm	mm	mm
89.7	9	48	0	0	0	0
241.7	13	5020	0	0	0	0
277	13	10329	0	1	0	0
327.1	14	15156	1	1	1	1
374.6	15	20273	1	1	1	1
442.5	16	25389	1	2	1	1
506.5	17	30457	2	2	1	1
604.6	17	35525	2	2	1	1
664.6	18	41028	2	3	2	1
815.6	19	45420	3	3	2	1
926.8	19	50247	3	3	2	1
1066.8	17	55219	3	4	2	2
1439.8	12	60142	4	4	2	2
1518	7	65065	4	4	2	2
1664.6	1	70037	4	5	2	2
1670.2	1	70085	4	5	2	2
1832.5	-6	75298	5	5	3	2
2253.7	-12	80173	5	5	3	2
2520.9	-14	90117	6	6	3	3
2832.3	-19	100012	7	7	3	3
3177.5	-25	110341	8	9	3	3
3560.4	-38	120091	9	10	4	3
3878	-63	130131	10	11	4	4
4154.4	-81	140219	12	13	4	4
4566.3	-101	150114	14	15	4	4
4981.2	-120	160057	16	18	5	4
5310.1	-132	170097	19	21	5	4
5639	-134	179509	23	24	5	5
5653.5	-132	179895	23	25	5	5
5655	-133	179895	23	25	5	5
5993.8	-259	188197	27	29	5	5
6035.7	-286	190128	28	30	5	5
6263.1	-349	191287	30	32	5	5